Liquefaction of plant biomass for use in polymers – is it the right strategy?

J. Karger-Kocsis[*]

Polymer Technology, Faculty of Engineering and the Built Environment, Tshwane University of Technology, Pretoria 0001, Republic of South Africa, and Department of Polymer Engineering, Faculty of Mechanical Engineering, Budapest University of Technology and Economics, H-1111 Budapest, Hungary

Liquefaction is a widely practiced technology to convert gaseous and solid products into liquids. Biomass is considered as natural, renewable, combustible, high molecular weight material in which the energy of sunlight is stored – via photosynthesis – in the form of chemical bonds. From the viewpoint of chemical structure the plant biomass consists of cellulose, hemicelluloses and lignin which fall under the heading of lignocellulose. However, the term 'plant biomass' covers not only forestry products but also wastes from the agriculture, agroindustry and even municipal/domestic ones (e.g. waste paper). In the past great efforts were dedicated to the conversion of biomass into fuels. Recent developments target, however, is its conversion into raw materials for polymer synthesis and modification. This R&D direction is driven by the facts that biomass is permanently regenerated, it is carbon neutral (i.e. no extra CO_2 emission being the major cause of global warming), and it may compete with crude oil as suitable feedstock for polymer production. In order to break up the chemical backbone and functionalize the related 'fragments' various hydrolytic and solvolytic (solvents as phenol, di- and polyols, acetone etc.) techniques with and without additional catalysts (alkali or acidic types) are adapted. The resulting highly reactive 'black liquor' can be used as raw material to produce phenolic resins and polyurethanes due to its phenolic and alcoholic hydroxyl groups. It is, however, not an easy task to guarantee the quality of the decomposition products derived from a natural feedstock. This requires the development of an online process control of liquefaction. It can hardly be done without fundamental analytical studies on the liquefaction of suitable model compounds. Moreover, there is a need for value-added liquefied compounds allowing us their diversified use. Instead of costly separation afterwards, the liquefaction process should yield the target compound. The process is expected to be environmentally friendly and thus harmful solvents like phenol should be replaced by other ones. In this respect supercritical fluids and ionic liquids may have an important role. Possible value added products from the liquefaction of plant biomass are further thermosets, such as epoxy and unsaturated polyester resins. It would be of interest to check whether the partial decomposition of lignocellulosic materials (resulting in cellulose nanowhiskers) could be combined with an in situ polymerization molding to produce novel thermoset nanocomposites. It is obvious that the liquefied products are more costly raw materials for polymers than those from fossil feedstock. However, this may change, also by legislative actions, provided that the technical feasibility of thermochemical liquefaction of biomass and the straightforward use of the related products are confirmed. This is the task for the near future in order to give the right reply to the question posed in the title!

Prof. Dr.-Ing. Dr.hc. J. Karger-Kocsis, editor-in-chief

[*]Corresponding author, e-mail: karger@pt.bme.hu

Mechanical properties and structure development in poly(butylene succinate)/organo-montmorillonite nanocomposites under uniaxial cold rolling

Y. J. Phua, W. S. Chow, Z. A. Mohd Ishak

School of Materials and Mineral Resources Engineering, Engineering Campus, Universiti Sains Malaysia, 14300 Penang, Malaysia

Abstract. Polymer nanocomposites have potentially enhanced properties when the molecular orientations of the polymer chains can be controlled. In this study, the mechanical and structural properties of poly(butylene succinate) (PBS) and 2wt% organo-montmorillonite (OMMT) filled PBS nanocomposites were modified by uniaxial cold rolling. Cold rolling was carried out to different compression ratios. The mechanical properties of rolled samples were studied in both the machine direction (MD) and the transverse direction (TD). Along the MD, distinct improvements in tensile strength and elongation at break were observed. However, the tensile strength degraded along the TD. Wide angle X-ray diffraction (WAXD) and microwave molecular orientation analysis reported on the degree of molecular orientation after rolling. Further, degree of crystallinity was reduced after cold rolling.

Keywords: *nanocomposites, molecular orientation, cold rolling, poly(butylene succinate), organo-montmorillonite*

1. Introduction

Aliphatic polyesters have been recognized as environmentally friendly biodegradable polymers. Poly(butylene succinate) (PBS) is one of the most promising biodegradable aliphatic polyesters. PBS is commercially available with many desirable properties including biodegradability, melt processability, thermal and chemical resistance [1–7]. Addition of organo-montmorillonite (OMMT) has been reported to increase the strength and modulus of PBS [1–3]. However, the extent of these improvements is rather limited. As the structure of molecular orientation is an important factor in producing polymer materials with outstanding properties, orientating the polymer chains using various methods such as cold rolling should be able to further improve polymer strength and ductility [8, 9].

Cold rolling is a process by which a polymer sheet is introduced between two unheated rollers and then compressed and squeezed. It is usually carried out at temperature below the crystallization temperature of the polymer. The technical merits offered by cold rolling process are the controllability, energy-saving and better dimensional retention after rolling due to the lower operation temperature. Basically, the rolling conditions, including temperature, time, and final thickness, determine the properties of the rolled product. Understanding the relationship between the deformation characteristics and the induced microstructure is essential to enable prediction on the final properties of the product [8–12]. Although studies on polymer chain orientation are rather abundant, research on the deformation of polymer nanocomposites is rare. Abu-Zurayk *et al.*

[13] reported that biaxial hot stretching on the nanocomposites has caused the delamination of clay stacks and orientation of clay. However, there is no relevant work has been reported on the uniaxial cold rolling of polymer nanocomposites. It is an interesting field of study in order to further enhance the material properties by using a relatively simple process. During uniaxial cold rolling, the direction of the molecular orientation relative to the applied stress direction is of particular importance [14]. In this study, uniaxial cold rolling has been carried out on PBS and 2 wt% OMMT filled PBS nanocomposites. Sheets are reduced in thickness by 20–60% which defined by the compression ratio (λ). Uniaxial cold rolling is believed to improve the mechanical properties of nanocomposites. Generally, tensile strength of rigid polymers increases in the direction parallel to the rolling direction, which is known as the machine direction (MD). However, such strength decreases in the direction perpendicular to the rolling direction or known as the transverse direction (TD) [14, 15]. Vega-Baudrit *et al.* [15] have previously reported on the dramatic enhancement of strength and modulus of PBS along the MD after uniaxial rolling process.

In this research, the mechanical properties of the rolled samples were investigated both in the MD and in the TD. The mechanical properties are greatly influenced by the polymer chain orientation that develops during cold rolling. Birefringence generated by microwave molecular orientation analyzer provides a quantitative study on the molecular orientation of polymers at different λ. Moreover, it provides the information on the molecular orientation angle (MOA) and molecular orientation ratio (MOR) of polymer chains. Wide angle X-ray diffraction (WAXD) is another common method used to observe the molecular orientation of crystalline phase in PBS. The effects of cold rolling on the degree of crystallinity were studied using WAXD and differential scanning calorimetry (DSC).

2. Experimental details
2.1. Materials
PBS (Bionolle #1020) was supplied by Showa Highpolymer Co., Ltd., Japan with MFI value of 25 g/10 min (190°C, 2.16 kg), melting temperature

of 115°C and density of 1.26 g/cm³. OMMT (Nanomer® I.30TC, Nanocor Inc, USA) with cation exchange capacity (CEC) of 110 mequiv/100 g was used in this study.

2.2. Preparation of nanocomposites
In this research, PBS was incorporated with 2 wt% of OMMT to form a nanocomposite (PBS/2%OMMT). First, PBS pellets and OMMT were dried at 60°C for 24 hours. Melt-mixing of PBS with OMMT was performed using an internal mixer (Haake PolyDrive R600, Thermo Electron Cooperation, Germany). The mixing process was carried out for 5 minutes at a temperature of 135°C and a rotary speed of 50 rpm. The mixed compound was dried at 60°C for 24 hours. The dried compound was then molded on a compression molding machine (GT 7014-A30C, GOTECH Testing Machines Inc., Taiwan). The compound was pre-heated at 135°C for 7 minutes, followed by compression molding for 3 minutes. After that, the sample was cooled through a cold-pressing at 15°C for 5 minutes.

2.3. Uniaxial cold rolling
The two-roll mill machine (XK-160, Shanghai rubber-machine work, China) consists of two rotating rollers with diameter of 160 mm, length of 320 mm and rotating speed of 60 rpm. PBS and nanocomposite sheets with original thickness of 1 mm were rolled between the unheated rollers at room temperature. The sheets were rolled for several times in one direction to reduce the thickness to 20, 40 and 60% (~0.8, 0.6 and 0.4 mm, respectively) by controlling the gap between the two rollers. The sample thickness was measured after each rolling cycle to enable the control of final thickness. The compression ratio (λ) is defined by d_0/d where d_0 and d are the sample thickness before and after rolling. The relationship between the sample thickness and λ are shown in Table 1.

Table 1. Compression ratio with different thickness reduction

Thickness reduction [%]	d_0 [mm]	d [mm]	λ
20	1	0.8	1.25
40	1	0.6	1.67
60	1	0.4	2.50

2.4. Sample characterizations
2.4.1. Mechanical properties
Tensile properties were studied by using a universal testing machine (Instron 3366, Instron Co., Ltd., USA) at 23±2°C and 50±5% relative humidity. Tensile test was carried out according to the ASTM D638-03 (Type IV) standard with a gauge length of 50 mm and a cross-head speed of 5 mm/min. The tensile properties such as tensile strength, modulus and elongation at break were investigated in both the MD and TD. Five measurements were conducted on each sample.

2.4.2. Differential scanning calorimetry (DSC)
DSC analysis was carried out using Perkin-Elmer DSC-6 (PerkinElmer Inc., USA) under a nitrogen atmosphere. The sample was heated from 30 to 150°C at a heating rate of 10°C/min and followed by a cooling stage from 150 to 30°C at the same rate. The first heating is to eliminate the thermal history in the sample. A second heating was then performed from 30 to 150°C. Finally, samples were cooled to room temperature. The data was analyzed to determine the melting temperature, T_m, and crystallization temperature, T_c, of PBS. Degree of crystallinity (χ_c) was calculated by using Equation (1) for pure PBS:

$$\chi_c = \frac{\Delta H_c}{\Delta H_m^0} \cdot 100\,\% \qquad (1)$$

where ΔH_c – crystallization enthalpy of sample, ΔH_m^0 – melting enthalpy of 100% crystalline PBS (110.3 J/g) and using Equation (2) for polymer nanocomposites:

$$\chi_c = \frac{\Delta H_c}{\Delta H_m^0 (1 - W_f)} \cdot 100\,\% \qquad (2)$$

where W_f – weight fraction of fillers in the nanocomposite.

2.4.3. Microwave molecular orientation analysis
The effects of uniaxial cold rolling process on the development of polymer chain alignments were investigated by microwave molecular orientation analyzer (MOA-6015), Oji Scientific Instrument, Japan. This is a simple technique to determine the molecular orientation and dielectric anisotropy of sheet materials. Sample was inserted into the gap between a pair of rectangular waveguides of the cavity resonator system. Then, polarized microwaves were irradiated perpendicular to the sample [16, 17]. The sample was rotated around the central axis normal to the sheet plane at a speed of 6.0 s per turn. The transmitted wave intensity is measured at every 1° of rotation angles. The orientation patterns are obtained by detecting the transmitted microwave intensity at a fixed frequency. It provides the information on molecular orientation angle (MOA). The molecules in polymer sheets are aligned on average in the direction specified by the MOA. Molecular orientation ratio (MOR) can be measured to describe the extent of alignment of molecular chains with reference to the rolling direction. Besides that, birefringence (Δn) was determined as the difference between the refractive indices along the MD and TD [18].

2.4.4. Wide angle X-ray diffraction (WAXD)
The molecular orientation of rolled samples was investigated by using CuK$_\alpha$ radiation with a wavelength of 0.154 nm in a RINT2100FSL diffractometer (Rigakudenki Ltd, Japan). The samples were scanned in a scan range from 2–40° by using 2.0°/min scanning rate. WAXD patterns and diffractograms were recorded. The results were analyzed by using X'Pert HighScore Plus software. χ_c were calculated via the software on the basis of Equation (3):

$$\chi_c = \frac{A_c}{A_T} \cdot 100\,\% \qquad (3)$$

where A_c – area of the peak due to crystal diffraction of the sample, A_T – total area of the crystal and amorphous from the sample diffractograms.

3. Results and discussion
3.1. Mechanical properties
After uniaxial cold rolling, the PBS and PBS/2%OMMT nanocomposite were subjected to the tensile test in both the MD and TD, as illustrated in Figure 1.

Table 2 summarizes the tensile characteristics of PBS and PBS/2%OMMT before and after cold rolling. In the MD, distinct differences in the tensile strength and elongation at break could be seen on the PBS and PBS/2%OMMT after uniaxial cold rolling. As the λ increases, tensile strength and elongation at break improved significantly, with

Table 2. Tensile properties of PBS and PBS/2%OMMT nanocomposites along the MD and TD

Rolling direction	λ	Compound	Tensile strength [MPa]	Modulus [MPa]	Elongation at break [%]
Unrolled	–	PBS	32.6 ± 2.7	589 ± 6.8	10.9 ± 2.6
		PBS/2%OMMT	33.6 ± 1.2	632 ± 9.1	12.9 ± 2.4
MD	1.25	PBS	38.3 ± 3.4 (+17.5)	526 ± 10 (−10.7)	38.3 ± 16 (+251.4)
		PBS/2%OMMT	38.5 ± 0.86 (+14.7)	578 ± 23 (−8.6)	22.3 ± 1.8 (+72.9)
	1.67	PBS	57.4 ± 6.2 (+76.0)	563 ± 35 (−4.4)	119 ± 25 (+991.7)
		PBS/2%OMMT	58.8 ± 2.2 (+75.2)	599 ± 32 (−5.2)	113 ± 23 (+776.0)
	2.50	PBS	96.7 ± 2.2 (+196.5)	526 ± 50 (−10.7)	123 ± 7.0 (+1030.3)
		PBS/2%OMMT	98.1 ± 3.7 (+192.4)	568 ± 15 (−10.1)	116 ± 14 (+797.7)
TD	1.25	PBS	32.3 ± 0.40 (−1.0)	606 ± 33 (+2.94)	27.5 ± 3.0 (+152.3)
		PBS/2%OMMT	30.8 ± 0.58 (−8.1)	641 ± 20 (+1.4)	20.5 ± 8.6 (+58.9)
	1.67	PBS	31.0 ± 0.90 (−4.8)	688 ± 10 (+16.8)	17.8 ± 1.6 (+63.3)
		PBS/2%OMMT	30.4 ± 0.51 (−9.3)	748 ± 42 (+18.4)	17.0 ± 1.8 (+31.8)
	2.50	PBS	28.8 ± 0.33 (−11.6)	757 ± 21 (+28.6)	17.4 ± 0.06 (+59.6)
		PBS/2%OMMT	28.0 ± 0.68 (−16.6)	837 ± 6.6 (+32.5)	10.0 ± 0.06 (−22.5)

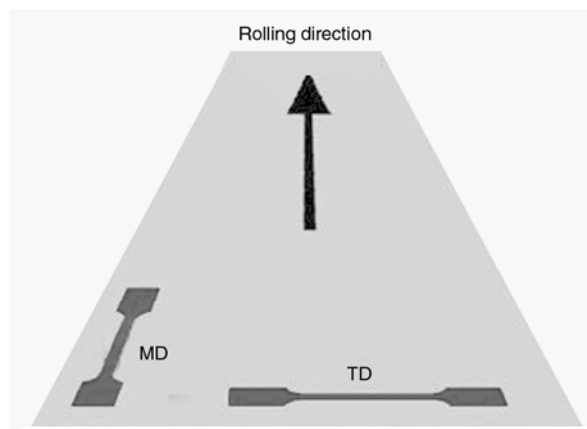( ) Percentage of changes in the tensile properties after cold rolling

Figure 1. Schematic diagram of sample preparation in the machine direction (MD) and transverse direction (TD) after uniaxial cold rolling process

Figure 2. Illustration of molecular orientation and clay alignment after uniaxial cold rolling

greatest improvement visible in samples with the highest $\lambda = 2.50$. Strength improved by 192–196%, and elongation at break improved by 700–1000%, respectively.

Generally, polymer chains will align along the rolling direction to form a more anisotropic material. Most commonly, enhanced properties have been observed along the direction parallel to the rolling direction (MD) in which the molecules are
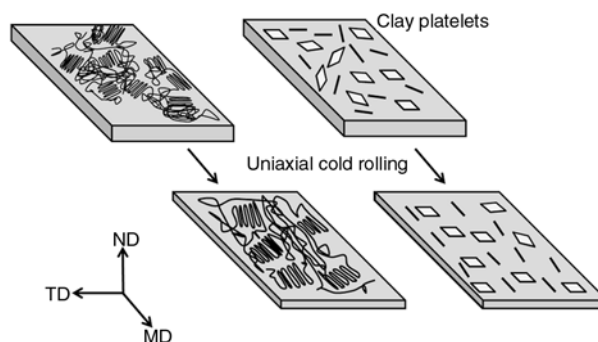
aligned/oriented, while poorer properties have been observed perpendicular to the molecular orientation (TD). The enhancement in strength along the MD could be due to increased molecular orientation and enhanced clay alignment after rolling [13], as illustrated in Figure 2.

Herewith, the anisotropy of the material can be derived from the ratio of strength along the MD to strength along the TD, as presented in Figure 3. It is found that the anisotropy improved with the increment of λ, indicates a better molecular orientation and clay alignment at high λ. Furthermore,
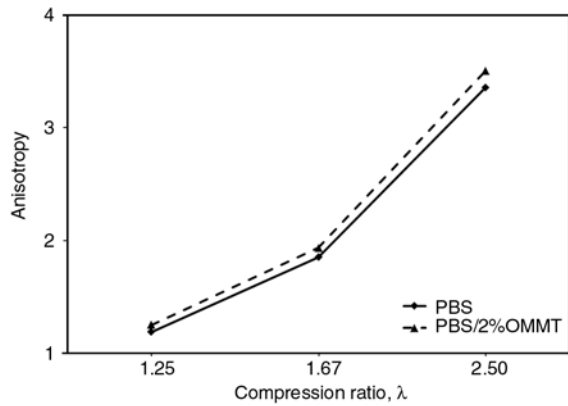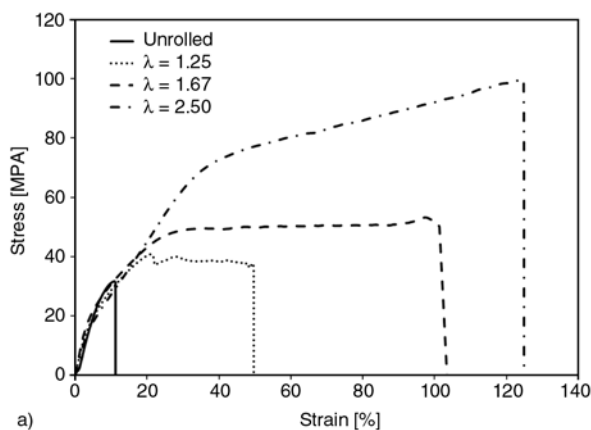
Figure 3. Anisotropy of PBS and PBS/2%OMMT at various compression ratios

PBS/2%OMMT nanocomposite exhibits higher anisotropy than pure PBS due to clay alignment. This indicates that the anisotropy derived from the enhancement of strength is influenced by both the anisotropy in polymer chains and the clay alignment, which differs from the determination via birefringence that will be discussed later.

Both of the tensile stress-strain curves of PBS and PBS/2%OMMT nanocomposite are showing a similar trend. The typical stress-strain curves of PBS and PBS/2%OMMT along the MD are presented in Figure 4. The unrolled PBS and PBS/2%OMMT nanocomposite fractured in a brittle mode. Upon uniaxial cold rolling, plastic deformation occurred on the rolled samples in the MD, which was manifested by the occurrence of yielding as observed in the stress-strain curves. Plastic deformation which involves both breaking of van der Waals bonds between molecules and also scission of some covalent bonds occurred [19]. The force required to break a covalent bond is relatively higher than that required for breaking van der Waals bonds. Orienta-

tion of the polymer chains along the MD results in the presence of a larger number of covalent bonds which must be overcome by a larger tensile force [18]. Thus, the tensile strength of the material increases. In addition, more rolling actions as measured by the λ will likely lead to higher molecular orientation, and commensurately to increased strength [8, 19]. Further, it is believed that uniaxial cold rolling could lead to the enhancement of the degree of clay alignment. Investigation on the effects of various rolling conditions to the clay alignment will be reported in our future publication. As observed in Figure 5, elongation at break increased drastically from unrolled sample to $\lambda =$ 2.50 in the MD, outlining the occurrence of the brittle-to-ductile transition. Parallel to the orientation direction, the polymer has become ductile and has a yield point and high elongation [20]. This is due to the more ordered polymer chains alignment in the MD, which reduces the chain entanglements and increases the chain flexibility and mobility to flow and slide [21]. The presence of 'necking' on the rolled samples after yield point indicates that plastic
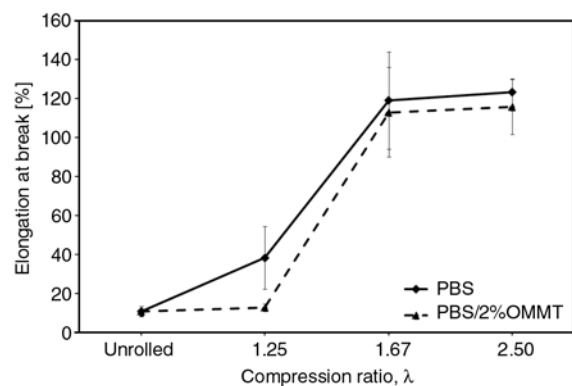

Figure 5. Elongation at break of PBS and PBS/2%OMMT at various compression ratios along the MD
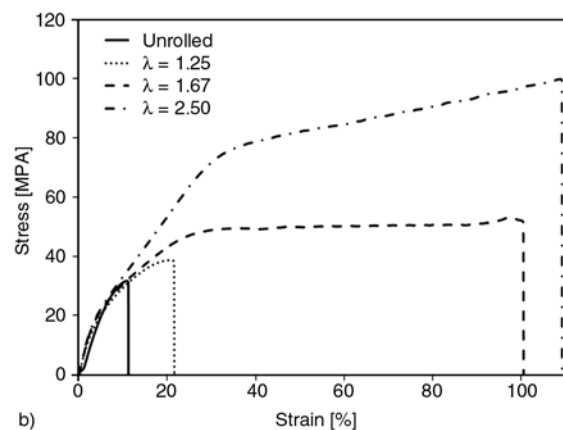

Figure 4. Typical tensile stress-strain curves of (a) PBS and (b) PBS/2%OMMT at various compression ratios along the MD

deformation occurred [22]. During plastic deformation, polymer chains slide among each other and thereby permit the polymer to be elongated more than it could otherwise [20]. A slight decrement in the modulus of PBS and PBS/2%OMMT nanocomposite in the MD is a result of brittle-to-ductile transition. The ductility after uniaxial cold rolling enables the polymer chains to flow and slide during stretching. Thereby, it would reduce the stiffness of the material and subsequently reduce the modulus along the MD.

When tested in the TD, however, opposite trends were observed. As the λ increased, tensile strength was reduced, whilst the modulus increased. Anisotropy generally weakens a polymer specimen perpendicular to the direction of orientation [14, 20, 23], which in this case corresponds to the TD of the cold rolling process. In the TD, loads are carried primarily by weak van der Waals bonds. Fracture in the TD only requires breakage of these much weaker bonds [23, 24]. Further, if there are small cracks or other imperfections in the polymer, they become oriented parallel to the rolling direction. These oriented cracks are strong stress concentrators for loads applied perpendicular to the orientation direction [20], leading to the fracture at a lower tensile force.

Table 2 shows that, even for the sheets with the lower λ (1.25 and 1.67), elongation at break increased in the TD. Stretching along the TD involves the disorientation and reorientation of the polymer molecules [23]. Upon stretching the previously oriented material in the TD, molecules will first disorient and then reorient themselves along the direction of the applied force [20]. The disorientation and reorientation processes lead to plastic deformation of the material and causes a slight increment in the elongation at break. For the PBS/2%OMMT nanocomposite, there is a slight decrease in the elongation at break for the highest λ. This is due to the high clay orientation and exfoliation, which limited the disorientation and reorientation processes. Moreover, the materials become rigid with an increasing modulus with λ along the TD. Unlike uniaxial stretching, uniaxial rolling process could induce a biaxial orientation since the rolling will result in the expansion of samples both in the MD and TD direction. However, the orientation along the TD is relatively lower than that of along

the MD [24]. Thus, it could only be traced from the modulus which obtained at the low strain level. Further research to ascertain this phenomenon is in progress by using a higher λ up to 4.0 in order to investigate the changes in modulus along the TD at high λ. It will be reported in our future publication.

3.2. Microwave molecular orientation analysis

Generally, the polymer chains tend to orient parallel to the MD with uniaxial rolling process, leading to the enhancement of the mechanical properties [8–10, 12–15] as discussed above. Therefore, the investigation upon the orientation of polymer chains is essential to understand the effects of uniaxial cold rolling on the anisotropy of polymers. Microwave molecular orientation analysis by using polarized microwaves is able to provide information on the birefringence of a material [25]. Birefringence is a measurement of the total molecular orientation of both crystalline and amorphous region in a semicrystalline polymer such as PBS [26–28]. It is able to provide a quantitative measurement on the overall molecular orientation by detecting the differences in polarizability of molecular chains at two perpendicular directions [29].

Figure 6 shows the birefringence, Δn as a function of λ. The value of Δn is often taken as a measure of molecular orientation. Both of the PBS and PBS/2%OMMT are showing a similar trend. The Δn for unrolled samples is very low, which is 0.0001 and 0.0003 for PBS and PBS/2%OMMT, respectively. After subjected to uniaxial cold rolling, Δn increases with the λ. This indicates that higher λ during uniaxial cold rolling is able to induce higher molecular orientation to the polymer chains. The Δn of PBS is higher than that of PBS/2%OMMT, which con-
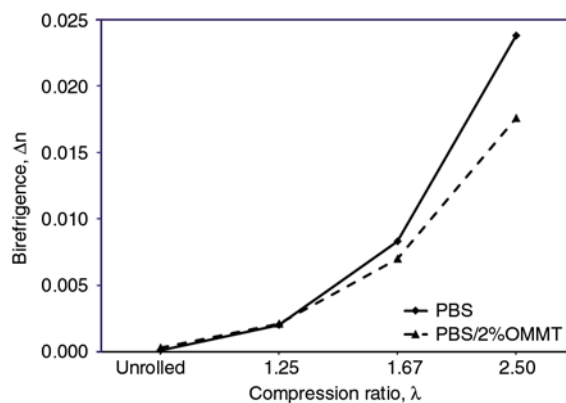

Figure 6. Birefringence of PBS and PBS/2%OMMT at various compression ratios

forms to the WAXD results. Δn may arise from the molecular anisotropy but also from the ordered alignment of similar particles such as OMMT. However, as reported by Yalcin *et al.* [12], the formation of Δn due to the ordered alignments of OMMT is negligible. The nanometer size OMMT has similar refractive index as the polymer matrix and will not influence the Δn. Thus in this case, the effect of clay alignment is neglected in the determination of anisotropy. As mentioned above, anisotropy derived from Δn and WAXD show a different trend than that of derived from strength.

Besides that, the microwave molecular orientation analysis can provide the study on molecular orientation angle (MOA) and molecular orientation ratio (MOR) of the polymer chains. MOA represents the magnitude of the chain alignment angle diverted from the MD. MOA is approximately zero when the polymer chains are aligned parallel to the MD. The MOR value reveals the relative number of polymer chains orientating to the direction specified by MOA [30]. Typical orientation patterns of PBS and PBS/2%OMMT are presented in Figure 7. The vertical axis is corresponding to the MD; whilst the horizontal axis is corresponding to the TD.

Figure 8 shows a comparison of the MOA and MOR according to their respective λ. Both PBS and PBS/2%OMMT are showing a similar trend. After subjected to uniaxial cold rolling, MOA decreased significantly. This indicates that the polymer chains tend to align in the direction more parallel to the MD as compared with the unrolled samples. Generally, the MOA reduces with the increment of λ due to a more parallel orientation with the MD [30]. The polymer chains aligned most parallel to the MD at $\lambda = 2.50$, which is manifested by the lowest MOA. At the $\lambda = 2.50$, higher rolling actions has contributed to a better molecular orientation, leading to a better enhancement of the mechanical properties. The MOA of the samples which rolled at $\lambda = 1.67$ is slightly higher than that at the $\lambda = 1.25$. However, the difference is insignificant, which is 3 and 4° for PBS and PBS/2%OMMT, respectively.

Another important indication of molecular orientation in a sample is the MOR. For both PBS and PBS/2%OMMT, MOR increased with the increment of λ. The highest MOR is observed at $\lambda = 2.50$, reveals a higher quantity of polymer chains aligned close to the MD with the angle defined by MOA [25]. The relationship between MOA and
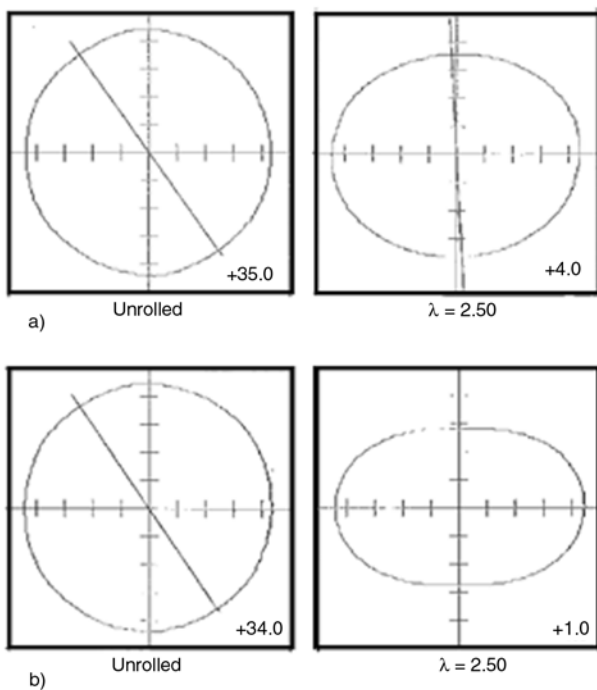

Figure 7. Typical orientation patterns of (a) PBS and (b) PBS/2%OMMT obtained at various compression ratios
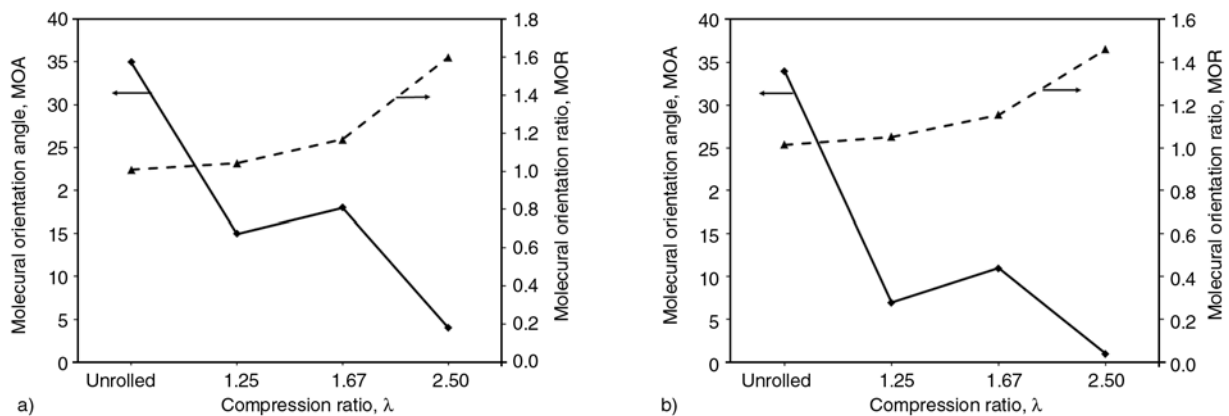

Figure 8. Molecular orientation angle and molecular orientation ratio as a function of compression ratio for (a) PBS and (b) PBS/2%OMMT

MOR determines the molecular orientation of the polymers. The polymer chains are oriented slightly close to the MD at $\lambda = 1.25$, comparing with the $\lambda = 1.67$ as verified by MOA. However, a better molecular orientation can be observed at the $\lambda = 1.67$ with better properties enhancement is attributed to the relatively higher MOR. The higher MOR at $\lambda = 1.67$ has compensated the slight increment in MOA, leading to a better molecular orientation. Thus, it can be concluded that the degree of molecular orientation along the MD increased when subjected to greater rolling action (or higher λ). The results are conforming to the mechanical properties and WAXD.

3.3. Wide angle X-ray diffraction (WAXD)

Details of the molecular orientation and degree of crystallinity of PBS and PBS/2%OMMT were obtained by WAXD. WAXD is a common technique to evaluate the molecular orientation of crystalline region in a semicrystalline polymer, such as PBS. Figures 9 and 10 show the WAXD patterns for PBS and PBS/2%OMMT at different λ, where the uniaxial rolling direction is vertical. The Debye rings indicate that PBS is an isotropic material, which becomes orientated as the thickness is reduced by uniaxial cold rolling. For unrolled PBS and PBS/2%OMMT, the azimuthal intensity distri-
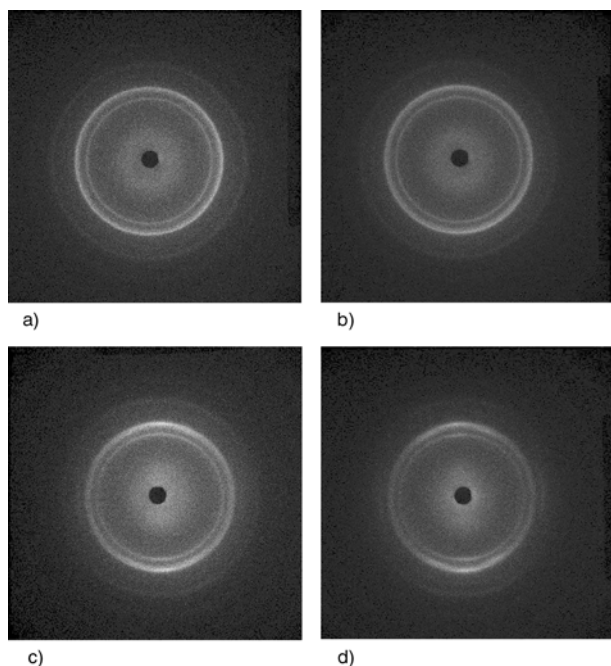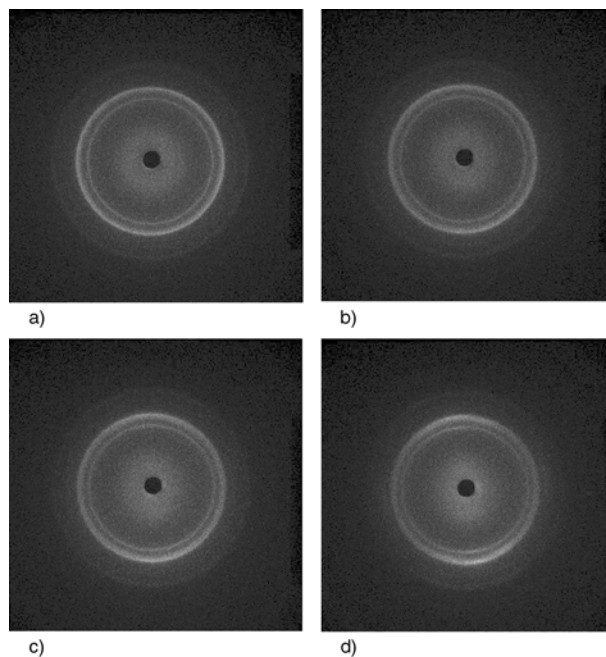

Figure 10. WAXD patterns of rolled PBS/2%OMMT sheets at various compression ratios: (a) unrolled, (b) $\lambda = 1.25$, (c) $\lambda = 1.67$, (d) $\lambda = 2.50$

bution for each reflection is uniform, confirming that PBS is an isotropic material. Upon uniaxial cold rolling to a higher λ, gradual intensification of the amorphous halo in the equator has been observed. At $\lambda = 2.50$, a clear intensity difference between meridian and equator indicates the development of molecular orientation [10, 12, 31, 32]. Moreover, rolled PBS has higher molecular orientation than does rolled PBS/2%OMMT. This appears in the WAXD patterns as a more dramatic intensity change in PBS after rolling. This result can be correlated with the anisotropy determined by microwave molecular orientation analysis.
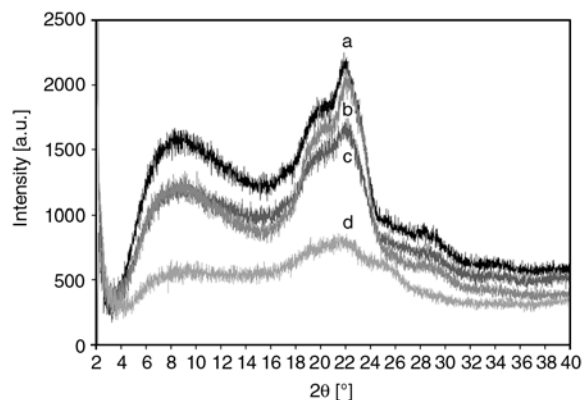

Figure 9. WAXD patterns of rolled PBS sheets at various compression ratios: (a) unrolled, (b) $\lambda = 1.25$, (c) $\lambda = 1.67$, (d) $\lambda = 2.50$

Figure 11. WAXD diffractograms of PBS at various compression ratios: (a) unrolled, (b) $\lambda = 1.25$, (c) $\lambda = 1.67$, (d) $\lambda = 2.50$
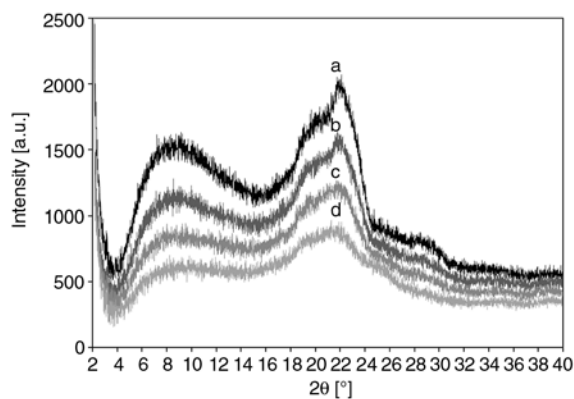
Figure 12. WAXD diffractograms of PBS/2%OMMT at various compression ratios: (a) unrolled, (b) λ = 1.25, (c) λ = 1.67, (d) λ = 2.50

Table 3. Degree of crystallinity verified by WAXD at various compression ratios

Compound	λ	χ_c [%]
PBS	unrolled	49.37
	1.25	46.98
	1.67	46.75
	2.50	40.74
PBS/2%OMMT	unrolled	40.87
	1.25	39.52
	1.67	39.31
	2.50	38.07

Figures 11 and 12 show the WAXD diffractograms of PBS and PBS/2%OMMT at different λ. Degree of crystallinity, χ_c, are identified from the diffractograms, as presented in Table 3. Cold rolling action decreased the χ_c due to the destruction of crystalline regions as large lamellae (folded chain structures) were subjected to rolling to form microfibrils (extended chain structures). The transition from folded chain structures to extended chain structures after cold rolling resulted in thinner lamellae and lower crystallinity [33].

3.4. Differential scanning calorimetry (DSC)

Uniaxial cold rolling does not show significant effect on the melting and crystallization behaviour of PBS and PBS/2%OMMT nanocomposites, as observed in Figure 13 and Table 4. Figure 13a shows that there are no distinct differences in DSC patterns as well as in the melting peaks for rolled and unrolled samples. The presence of two melting peaks corresponds to the two different types of crystalline lamellae present in PBS [6]. Vega-Baudrit *et al.* (2005) [15] suggested that the low endotherm, '*y*' is corresponds to the melting of the original crystallites; and the high endotherm, '*x*' corresponds to the melting of the recrystallized one. As presented in Table 4, no notable changes in melting temperatures, $T_{m,x}$ or $T_{m,y}$ were observed after the cold rolling process.

Table 4 shows that rolling and clay addition do not significantly impact the crystallization temperature, T_c. No shifting of the crystallization peaks was observed in Figure 13b. However, the degree of crystallinity, χ_c decreased after clay addition and uniaxial cold rolling process as discussed previ-
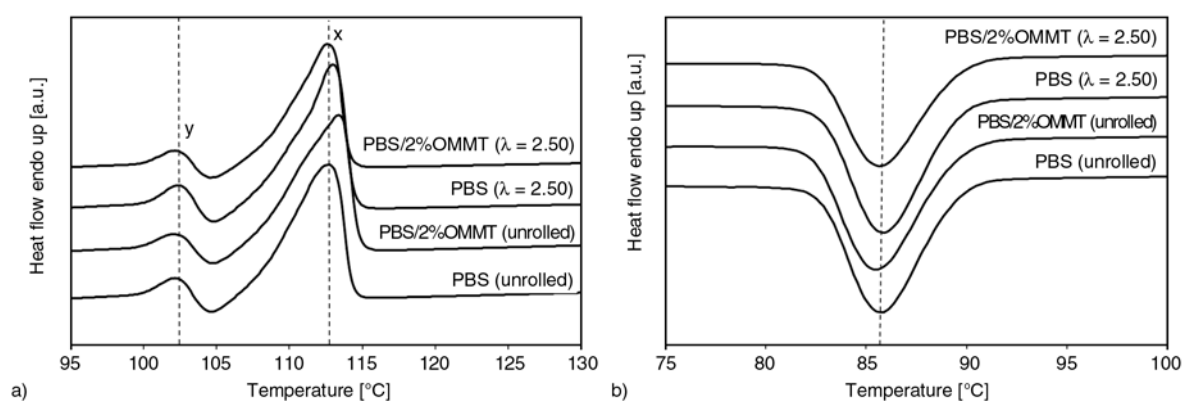

Figure 13. DSC thermograms at (a) melting and (b) crystallization

Table 4. DSC results of rolled and unrolled PBS and PBS/2%OMMT nanocomposite

Compound	$T_{m,x}$ [°C]	$T_{m,y}$ [°C]	ΔH_m [J/g]	T_c [°C]	χ_c [%]
PBS (unrolled)	112.4	102.2	63.6	85.9	57.6
PBS (λ = 2.50)	112.9	102.4	59.8	85.9	54.2
PBS/2%OMMT (unrolled)	113.4	102.1	60.3	85.6	55.7
PBS/2%OMMT (λ = 2.50)	112.6	102.2	50.9	85.7	47.1

ously. According to Dubnikova *et al.* [34], the crystallization of polymer chains decreases as a result of their confinement between the intercalated and exfoliated clay layers. χ_c is also most reduced for samples with the highest λ. The χ_c values of DSC are slightly different from that of obtained from WAXD, however, the trend appears to be the same. The variation is believed to be a result of errors between different characterization methods and equipments. The DSC results show that any enhancement in mechanical properties after cold rolling is not a result of crystallinity enhancement.

4. Conclusions

The addition of 2 wt% OMMT to PBS via melt mixing slightly improved both the strength and the elongation at break of the nanocomposites. When PBS and PBS/2%OMMT sheets were subjected to uniaxial cold rolling, tensile strength along the MD increased substantially. This is mainly due to the increased molecular orientation after cold rolling, which is verifiable by microwave molecular orientation analysis and WAXD. A brittle-to-ductile transition was also observed along the MD, identifiable by a substantial increase in elongation at break and a reduction of the modulus. The strength of the rolled samples degraded along the TD. However, the modulus and elongation at break increased along the TD. Thus, it is concluded that PBS is an isotropic material, whose properties are greatly reliant on molecular chain alignment. WAXD and DSC demonstrated a decrease in crystallinity after cold rolling. This reduction is due to the destruction of crystalline regions during cold rolling. Hence, it indicates that any enhancement in mechanical properties observed is not a result of crystallinity enhancement. Moreover, according to DSC thermograms, no notable changes in T_m and T_c were observed after cold rolling. As a conclusion, uniaxial cold rolling does not influence the thermal properties of PBS or of its nanocomposites.

References

[1] Chieng B. W., Ibrahim N. A., Wan Yunus W. M. Z.: Effect of organo-modified montmorillonite on poly (butylene succinate)/poly(butylene adipate-co-terephthalate) nanocomposites. Express Polymer Letters, **4**, 404–414 (2010).
DOI: 10.3144/expresspolymlett.2010.51

[2] Okamoto K., Ray S. S., Okamoto M.: New poly(butylene succinate)/layered silicate nanocomposites. II. Effect of organically modified layered silicates on structure, properties, melt rheology, and biodegradability. Journal of Polymer Science Part B: Polymer Physics, **41**, 3160–3172 (2003).
DOI: 10.1002/polb.10708

[3] Someya Y., Nakazato T., Teramoto N., Shibata M.: Thermal and mechanical properties of poly(butylene succinate) nanocomposites with various organo-modified montmorillonites. Journal of Applied Polymer Science, **91**, 1463–1475 (2003).
DOI: 10.1002/app.13366

[4] Chen G-X., Kim E-S., Yoon J-S.: Poly(butylene succinate)/twice functionalized organoclay nanocomposites: Preparation, characterization, and properties. Journal of Applied Polymer Science, **98**, 1727–1732 (2005).
DOI: 10.1002/app.22264

[5] Utracki L. A.: Clay-containing polymeric nanocomposites. Rapra Technology, Shropshire (2004).

[6] Ray S. S., Bousmina M., Okamoto K.: Structure and properties of nanocomposites based on poly(butylene succinate-co-adipate) and organically modified montmorillonite. Macromolecular Materials and Engineering, **290**, 759–768 (2005).
DOI: 10.1002/mame.200500203

[7] Okada K., Mitsunaga T., Nagase Y.: Properties and particles dispersion of biodegradable resin/clay nanocomposites. Korea-Australia Rheology Journal, **15**, 43–50 (2003).

[8] Lee W. B., Wu S. Z., Song M. S.: Characterization of the orientation structure and distribution in rolled polypropylene. Journal of Materials Engineering and Performance, **5**, 637–645 (1996).
DOI: 10.1007/BF02646094

[9] Wu S. Z., Lee W. B.: Modeling of the elastic properties of cold-rolled polypropylene sheets. Scripta Materialia, **46**, 587–592 (2002).
DOI: 10.1016/S1359-6462(02)00035-0

[10] Wong Y. S., Stachurski Z. H., Venkatraman S. S.: Orientation and structure development in poly(lactide) under uniaxial deformation. Acta Materialia, **56**, 5083–5090 (2008).
DOI: 10.1016/j.actamat.2008.06.027

[11] Fasce L. A., Costamagna V., Pettarin V., Strumia M., Frontini P. M.: Poly(acrylic acid) surface grafted polypropylene films: Near surface and bulk mechanical response. Express Polymer Letters, **2**, 779–790 (2008).
DOI: 10.3144/expresspolymlett.2008.91

[12] Yalcin B., Ergungor Z., Konishi Y., Cakmak M., Batur C.: Molecular origins of toughening mechanism in uniaxially stretched nylon 6 films with clay nanoparticles. Polymer, **49**, 1635–1650 (2008).
DOI: 10.1016/j.polymer.2008.01.046

[13] Abu-Zurayk R., Harkin-Jones E., McNally T., Menary G., Martin P., Armstrong C.: Biaxial deformation behavior and mechanical properties of a polypropylene/clay nanocomposite. Composites Science and Technology, **69**, 1644–1652 (2009).
DOI: 10.1016/j.compscitech.2009.03.014

[14] Miller E.: Introduction to plastics and composites: Mechanical properties and engineering applications. Marcel Dekker, New York (1996).

[15] Vega-Baudrit J., Sibaja M., Martin-Martinez J. M., Nakayama K., Masuda T., Cao A.: New developments in polymer analysis, stabilization and degradation. Nova Science, New York (2005).

[16] Osaki S.: A new method for the determination of polymer optical anisotropy. Journal of Applied Physics, **76**, 4323–4326 (1994).
DOI: 10.1063/1.358494

[17] Osaki S.: Explanation of orientation patterns determined for sheet materials by means of microwaves. Journal of Applied Physics, **67**, 6513–6519 (1990).
DOI: 10.1063/1.345127

[18] Kurose T., Urman K., Otaigbe J. U., Lochhead R. Y., Thmes S. F.: Effect of uniaxial drawing of soy protein isolate biopolymer film on structure and mechanical properties. Polymer Engineering and Science, **47**, 374–380 (2007).
DOI: 10.1002/pen.20716

[19] Fakirov S.: Oriented polymer materials. Hüthig and Wepf, Basel (1996).

[20] Nielsen L. E., Landel R. F.: Mechanical properties of polymers and composites. Marcel Dekker, New York (1994).

[21] Karger-Kocsis J., Fakirov S.: Nano- and micromechanics of polymer blends and composites. Hanser Verlag, Munich (2009).

[22] Mouzakis D. E.: Study of the stress oscillation phenomenon in syndiotactic polypropylene/montmorillonite nanocomposites. Express Polymer Letters, **4**, 244–251 (2010).
DOI: 10.3144/expresspolymlett.2010.31

[23] Bicerano J.: Prediction of polymer properties. Marcel Dekker, New York (2002).

[24] Poh B. T.: Mechanical properties of oriented polypropylene. Plastics and Rubber Processing and Applications, **7**, 215–219 (1987).

[25] Osaki S., Tashiro K.: Molecular orientation and dielectric anisotropy in polyimide films as determined by the microwave method. Macromolecules, **31**, 1661–1664 (1998).
DOI: 10.1021/ma961713y

[26] Cheremisinoff N. P.: Handbook of polymer science and technology. Marcel Dekker, New York (1989).

[27] Fujimoto F., Yamaguchi K., Ikeda H., Kishida H., Arai T.: Behavior of nylon 6 filaments in cold drawing (molecular orientation and physical propertie). Journal of the Textile Machinery Society of Japan, **25**, 1–6 (1972).

[28] Golik A. Z., Kuchinka M. Y., Fridman A. Ya.: Relation between molecular orientation characteristics determined from birefringence and acoustic data and the effect of orientation on the strength of polycaprolactam fibers. Polymer Mechanics, **3**, 3–7 (1967).
DOI: 10.1007/BF00859263

[29] Kim K. H., Isayev A. I., Kwon K., Sweden C. V.: Modeling and experimental study of birefringence in injection molding of semicrystalline polymers. Polymer, **46**, 4183–4203 (2005).
DOI: 10.1016/j.polymer.2005.02.057

[30] Tetsuya T., Hashimoto Y., Ishiaku U. S., Mizoguchi M., Leong Y. W., Hamada H.: Effect of heat-sealing temperature on the properties of OPP/CPP heat seals. Part II. Crystallinity and thermomechanical properties. Journal of Applied Polymer Science, **99**, 513–519 (2006).
DOI: 10.1002/app.22443

[31] Dean D. M., Rebenfeld L., Register R. A., Hsiao B. S.: Matrix molecular orientation in fiber-reinforced polypropylene composites. Journal of Materials Science, **33**, 4797–4812 (1998).
DOI: 10.1023/A:1004474128452

[32] Nogales A., Hsiao B. S., Somani R. H., Srinivas S., Tsou A. H., Balta-Calleja F. J., Ezquerra T. A.: Shear-induced crystallization of isotactic polypropylene with different molecular weight distributions: In situ small- and wide-angle X-ray scattering studies. Polymer, **42**, 5247–5256 (2001).
DOI: 10.1016/S0032-3861(00)00919-8

[33] Tiaw K. S., Teoh S. H., Chen R., Hong M. H.: Processing methods of ultrathin poly(ε-caprolactone) films for tissue engineering applications. Biomacromolecules, **8**, 807–816 (2007).
DOI: 10.1021/bm060832a

[34] Dubnikova I. L., Berezina S. M., Korolev Yu. M., Kim G-M., Lomakina S. M.: Morphology, deformation behavior and thermomechanical properties of polypropylene/maleic anhydride grafted polypropylene/layered silicate nanocomposites. Journal of Applied Polymer Science, **105**, 3834–3850 (2007).
DOI: 10.1002/app.26665

Morphology-properties relationship on nanocomposite films based on poly(styrene-*block*-diene-*block*-styrene) copolymers and silver nanoparticles

L. Peponi[1*]*, A. Tercjak*[2]*, L. Martin*[2]*, I. Mondragon*[2]*, J. M. Kenny*[1]

[1]Materials Engineering Centre, University of Perugia, Loc. Pentima Bassa, 21, 05100 Terni, Italy
[2]'Materials + Technologies' Group, Dpto. Ingeniería Química y M. Ambiente, Escuela Politécnica, Universidad País
 Vasco/Euskal Herriko Unibertsitatea, Pza. Europa 1, 20018 Donostia-San Sebastián, Spain

Abstract. A comparative study on the self-assembled nanostructured morphology and the rheological and mechanical properties of four different triblock copolymers, based on poly(styrene-*block*-butadiene-*block*-styrene) and poly(styrene-*block*-isoprene-*block*-styrene) matrices, and of their respective nanocomposites with 1 wt% silver nanoparticles, is reported in this work. In order to obtain well-dispersed nanoparticles in the block copolymer matrix, dodecanethiol was used as surfactant, showing good affinity with both nanoparticles and the polystyrene phase of the matrices as predicted by the solubility parameters calculated based on Hoftyzer and Van Krevelen theory. The block copolymer with the highest PS content shows the highest tensile modulus and tensile strength, but also the smallest elongation at break. When silver nanoparticles treated with surfactant were added to the block copolymer matrices, each system studied shows higher mechanical properties due to the good dispersion and the good interface of Ag nanoparticles in the matrices. Furthermore, it has been shown that semi-empirical models such as Guth and Gold equation and Halpin-Tsai model can be used to predict the tensile modulus of the analyzed nanocomposites.

Keywords: nanocomposites, block copolymer, atomic force microscopy, rheology, mechanical properties

1. Introduction

Metal-polymer nanocomposites (MNC) consisting of metallic nanoparticles incorporated into polymers are receiving immense attention in today's research for their potential applications in the fields of catalysis, bioengineering, photonics and electronics [1–3]. The salient features of these nanostructures, the material composition, as well as morphology, dimensions, spacing, and order are of primary significance for the chemical, mechanical, optical and electromagnetic properties they exhibit. Not only nanoparticles give rise to nanocomposite with exceptional properties, but also the nano-organization of the matrix is an important factor to take into account when working with nanocomposite materials. So, the spontaneous formation of nanostructured materials via molecular self-assembly has attracted increasing interest throughout the last decades. Block copolymers, BC, are a prominent example of this class of material as they form a large variety of well-ordered microdomain structures of molecular dimensions [4–7]. BC are long-chain molecules built up from different types of monomers, which are grouped in blocks covalently linked to each other. Depending on length, connectivity, the degree of polymerization, mutual interac-

tions of the different blocks and solvent used, the microdomains can form spheres, cylinders, lamellae, or more complex shapes [8, 9].

The molecular packing and the thermodynamically stable microdomain patterns of block copolymers are governed by the positive mixing enthalpy and the low mixing entropy of block segments. Since the covalent bonding between the segments, the systems can not macroscopically phase separate and, in order to minimize the interfacial energy, they adjust themselves in well-defined microdomain patterns [10, 11]. When the blocks mix endothermically the origin of microphase separation can be attributed to enthalpic effects [12, 13]. Evidently, the microphase separation of block copolymers affects their rheological behaviour [14–16] and mechanical behavior [16–18]. Unusual melt rheological properties of block copolymers such as very high viscosity and elasticity, very high sensitivity to the molecular weight and highly non-Newtonian behaviour even at very low shear rates and high temperature, (i.e. non-terminal behaviour) have been reported in literature [19]. The order-disorder transition Temperature (T_{ODT}), also referred to as the microphase separation transition Temperature (T_{MST}), which indicates the temperature at which the BC changes from a homogeneous material to a microphase separated state, is found in literature to be accompanied by gross changes in the rheological properties at low frequencies [19–21].

The unique properties of BC can be further improved and enlarged, introducing nanosized objects into their mesostructure opening the way to many innovative applications. Combination of both nanosized particles and nanostructured templates can lead to increased quantities of unique and complex nanocomposite materials [22–24].

Nevertheless, the main drawback of nanoparticles, which still limits their wide applications, is related to their high surface energy which implies a high tendency to self-aggregation. Their stabilization in different polymeric matrices has been proven to be one of the most promising strategies to prevent their aggregation and to design and control the properties of the resulting nanocomposites [25].

Surfactants are, usually, amphiphilic organic compounds, which contain both hydrophobic groups (their tails compatible with the polymer) and hydrophilic groups (their heads tethered to the nanoparti-

cles) that can lower the surface energy of nanoparticles to prevent their aggregation and to well-disperse them into the polymeric matrix [26]. Moreover, when working with block copolymer matrices, an adequate surfactant should be able to selectively disperse nanoparticles in only one of the blocks through physical or chemical interactions, without altering the chemical structure of the block copolymer matrix. This selectivity is exploited to design the properties of nanoparticle/block copolymer hybrid systems containing well-dispersed nanoparticles [27]. As previously published by our research group [28, 29], when surfactant modified silver nanoparticles are added to poly(styrene-*b*-isoprene-*b*-styrene) as well as to poly(styrene-*b*-butadiene-*b*-styrene), morphological changes can be obtained due to the enlargement of the polystyrene phase. Consequently, the thermal, mechanical and rheological behaviour of the nanocomposites would change with respect to the same properties shown by neat BC. Property enhancement is strongly dependent on the morphology and on the degree of dispersion of the inorganic phase in the polymeric matrix [30].

The main aim of this work is to analyze novel metal-polymer nanocomposites that combine phase-separated block copolymer domains ordered at nanoscale and nanosized silver particles dispersed with the aid of dodecanethiol (DT) used as surfactant. In particular four different poly(styrene-*block*-diene(butadiene or isoprene)-*block*-styrene) block copolymer matrices (two SBS and two SIS) with different amounts of polystyrene (PS), are compared. Above all, this study focuses on the influence of the addition of 1 wt% Ag nanoparticles on the morphology, rheological and mechanical properties of block copolymers. Moreover, two models, Guth and Gold equation [31, 32] and Halpin-Tsai model [33, 35] have been used to predict the tensile modulus of the obtained nanocomposites.

2. Experimental
2.1. Materials
Four different block copolymers, two poly(styrene-*b*-butadiene-*b*-styrene) block copolymers and two poly(styrene-*b*-isoprene-*b*-styrene) block copolymers with different amounts of PS block, kindly provided by Kraton Polymers, Kraton Performance Polymers Inc., Amsterdam, Europe, were selected. Values of specific volume of 0.95 cm^3·g^{-1} were

used for PS, of 1.1 cm$^3 \cdot$g^{-1} for PB and 1.25 cm$^3 \cdot$g^{-1} for PI [36].

Silver nanopowder, P203, was supplied by Cima Nano Tech, Cima NanoTech Inc., Caesarea, Israel. It has a specific surface area of 4.9 m^2/g and particle size distribution varying from 20 to 70 nm with evident particle agglomeration. Prior to use it was subjected to thermal treatment to purify the nanoparticles. In fact, the data sheet of the nanoparticles indicates residual processing solvent and impurities and from thermal gravimetric analysis (TGA) (data not shown) 3 wt% of impurities have been detected; so a thermal treatment at 700°C for 1 h has been performed in air conditions. After this treatment no more impurities were detected by TGA analysis and no evident agglomeration was observed. We consider an elastic modulus of about 80 GPa for the silver nanoparticles. We took as reference the elastic modulus of bulk material considering that the value is closed to the average elastic modulus calculated by Greer *et al*. [37] for nanoparticles silver thin films.

Previously, we have studied the behavior of nanostructured copolymers when different amounts of silver nanoparticles (from 0 to 7 wt%) have been added focusing the attention on the morphological changes of the self-assembled nanostructures [27]. Following these results we have selected 1 wt%, corresponding to 0.10 vol%, as this concentration of silver nanoparticles showed a better dispersion behaviour. Following previous research results on the efficiency of different surfactants on the dispersion of Ag nanoparticles in polymer matrices [29] we have selected dodecanethiol, DT, from Sigma-Aldrich®, Spain, as surfactant in this research. Pure toluene was used as solvent.

2.2. Sample preparation

Metallic-organic hybrid films have been obtained sonicating silver nanoparticles in toluene solution for 1.5 h with a microprocessor sonicator 750 W, Vibracell 75043 from Bioblock Scientific, Fisher Scientific SAS, France, with amplitude of 25%. Another 1 h of sonication was necessary, when

dodecanethiol was added to the Ag solution (optimized weight ratio of 1:1 respect to Ag nanoparticles [18]) in order to obtain Ag/DT well dispersed suspension. Finally nanocomposites were obtained, after the addition of the BC at the suspension and sonicating for further 3 h. The final solution was cast on a glass support. The solvent was evaporated for 24 h at room temperature.

Solution processing is the typical route to obtain and study the morphologies of nanostructured block copolymers. This processing route can lead to the formation of pores on the film surface that can alter or destroy the nanostructuration. Sometimes it is also possible to obtain solvent tracks on the surface due to a wrong evaporation process. For this reason we have optimized the solution processing of these materials in our long and well documented research on block copolymers. In particular we have chosen an adequate solvent with relatively low vapour pressure such as toluene, and adequate processing conditions (such as to cover the film cast with an aluminium foil and evaporating the solvent slowly under ambient conditions for 24 h) to avoid pores in the surface. No pores were observed by visual and microscopic inspection on the films produced.

The self-organization of the block copolymer matrices did not require special annealing conditions (similar nanostructured morphologies have been obtained at room temperature and after annealing at 110°C). Samples of different thickness have been prepared for the AFM analysis (about 300 nm) and for rheological and mechanical analysis (300 μm). The same procedure was used to obtain neat block copolymers thin films, which were labelled as L1, L2, L3 and L4, respectively, in Table 1. Nanocomposites with 0.10 vol% Ag nanoparticles treated with dodecanethiol are named N1, N2, N3 and N4, respectively. As reported on Table 3, L(1/4)+DT represents the block copolymer with 1 wt% DT, which is the same weight concentration of surfactant added in the nanocomposite formulations. The last sample, N(1/4)ws, indicates the nanocomposite obtained without surfactant.

Table 1. Main characteristics of the different BC studied

Materials	M$_n$	PD	PS [wt%]	T$_g$ [°C]	T$_{ODT}$ [°C]
SBS D1493 – L1	60 000	1.8	75	110	200
SBS D1101 – L2	56 500	1.6	31	95	149
SIS D1161 – L3	81 200	1.7	15	90	132
SIS D1165 – L4	58 200	1.5	30	95	152

2.3. Physico-chemical analysis

Gel permeation chromatography, GPC, tests were performed in Perkin-Elmer LC-235, Perkin Elmer Inc. Spain, equipment with a UV detector set at 245 nm and a refractive index detector LC-30 RI. The mobile phase was tetrahydrofuran at a flow rate of 1 ml/min. Number average molecular weights (M_n) and the polydispersity index (PD) were calculated using a universal calibration method with polystyrene standards. A Milton Roy Spectronic Genesys 5 UV spectrophotometer, Spectronic Genesys 5 spectrophotometer, Spain, was used to calculate the critical surfactant concentration necessary to optimally cover the external surface of Ag nanoparticles that, as reported elsewhere [18], corresponds to an Ag/DT wt ratio of 1.

2.4. Morphological analysis

The morphological features of both neat BC and the respective nanocomposite films were investigated using atomic force microscopy (AFM) operating in tapping mode with a scanning probe microscope (Nanoscope IIIa, Multimode TM from Digital Instruments, Santa Barbara, USA) equipped with an integrated silicon tip/cantilever having a resonance frequency ~300 kHz, from the same manufacturer. Height and phase images were obtained under ambient conditions with typical scan speed of 0.5–1 line/s, using a scan head with a maximum range of 16 μm×16 μm. Field Emission Scanning Electron Microscopy, FE-SEM, ZEISS SUPRA 25, Carl Zeiss SMT AG, Germany has been used also for the morphological characterization.

2.5. Thermal analysis

Differential Scanning Calorimetry, DSC, measurements were performed with a Mettler Toledo DSC-822 calorimeter, (Mettler Toledo Int. Inc., Spain) calibrated with high purity indium. All experiments were conducted under a nitrogen flow of 20 ml·min^{-1}, using 7–10 mg samples in closed aluminium pans, in a temperature range from 30 to 150°C with a rate of 10°C/min, using the cycle heating-cooling-heating. The second heating scan is taken into account to calculate the glass transition temperature (T_g) of the matrices.
Thermogravimetric analysis (TGA) was performed using a Seiko Exstar 6000 TGA (Seiko Instruments Inc, Japan) quartz rod microbalance in nitrogen and

air atmosphere at a heating rate of 10°C/min. Thermograms were recorder from room temperature to 900°C. Sample of about 10 mg were used in order to verify the purity of the silver nanoparticles.

2.6. Rheological tests

An Advanced Rheometrics Expansion System, Ares, Rheometric Scientific Inc., USA with parallel plates of 25 mm diameter was used with a gap between the plates around 1 mm. Three different types of experiments were performed: dynamic temperature ramps, dynamic strain sweeps and dynamic frequency sweeps. For the viscoelastic measurements, the samples were tested at 110°C, which is above the T_g of both blocks of the block copolymer. Moreover, dynamic strain sweep tests at a constant frequency were used to find the linear viscoelastic region in which storage modulus G' and loss modulus G'' were independent of the strain amplitude. In particular, after the strain sweep tests at 110°C, the linear viscoelastic regime was obtained when the strain amplitude was 0.8. Consequently, isochronal dynamic temperature ramp tests were performed from 110 to 200°C at a heating rate of 5°C·min^{-1} and at a frequency of 6.28 rad·s^{-1}. Data were collected and analyzed using the equipment software. Taking the sensibility of the rheometer into account, the error of the value of the storage and loss moduli in each data point was ±3%. The transducer operating range was set to 0.2–200 or 0.2–2000 g·cm depending on the measured torque values. The measurements were performed on 5 samples for each different system. It should be pointed out that there was not difference among the morphologies generated at room temperature and at 110°. In fact, although the polymer was above the T_g of both block copolymers, the morphology remained constant for different annealing times for all the investigated systems. This behaviour was deeply analyzed in previous research [28, 29] and attributed to the strong segregation regime of the system under these conditions.

2.7. Mechanical tests

In order to study the tensile modulus of the metallic-organic hybrid films, tensile tests were carried out at room temperature using a Minimat 2000 Miniature Materials Tester, Rheometric Scientific Inc., USA. The measurements were performed on

10 dog-bone shaped samples for each different system. The specimens have been prepared cutting the cast film with a gauge length of 5 mm by using an Abrasive Cutting Labut 1010 of Benetec Ltd (UK). The tensile modulus was calculated at a cross-head rate of 0.5 mm/min. Data were collected and analyzed using Rheometric Scientific Minimat Main software. On the other hand, to calculate tensile strength and elongation at break, tensile testing of dog-bone shaped specimens was performed using a universal tensile machine Instron, model 4206, Instron, USA, at a cross-head rate of 50 mm/min at room temperature. These two different tests were necessary, because of the high elongation at break of thermoplastic elastomers, which could not be measured by the Minimat alone. Metallic-organic hybrid films with a gauge length of 5 mm were tested.

3. Results and discussion

Four different block copolymers have been analyzed in this work. Table 1 shows their main characteristics in terms of PS content (indicated by Kraton Polymer), the number average molecular weight (M_n) and the polydispersity index (PI) of each BC, measured by GPC and the T_g of the PS block obtained by DSC. Taking into account the density values for the PS and the PI reported in literature, [38], the solubility parameters calculated based on the Hoftyzer and Van Krevelen theory [39] for each block of the four BC have been reported on Table 2. Due to the high surface energy of the silver nanoparticles, and to their tendency to form aggregates, in order to obtain well-dispersed silver nanoparticles in the BC matrix, dodecanethiol was used as surfactant to obtain well-disperse 1 wt% Ag/DT nanocomposites corresponding to 0.10 vol% Ag. The DT solubility parameter, also calculated based on the Hoftyzer and Van Krevelen theory, is 19.10 very close to the PS one. This fact indicates the good affinity between the dodecanethiol and the PS phase. It is worth to note that the solubility parameters shown in Table 2 confirm that dodecanethiol-treated silver nanoparticles are dispersed in the PS block of the block copolymer matrix, for each BC. Rheological results allow to emphasize two main aspects. First, though not shown, the linear viscoelastic response of both SIS and SBS block copolymer matrices in Ag/DT/SIS or Ag/DT/SBS

Table 2. Solubility parameters calculated for the four different block copolymers

Materials	δ (PS)	δ (PB/PI)
SBS D1493	18.99	17.49
SBS D1101	19.08	17.42
SIS D1161	18.99	17.62
SIS D1165	18.90	17.50

nanocomposites was identified using low-frequency values. Thereafter, the temperature dependency of both storage and loss moduli above the T_g of PS-block for the Ag/DT/SIS and Ag/DT/SBS nanocomposite materials was evaluated.

Basically, homogeneous polymer melts follow typical terminal behaviour, that is, $G'\sim\omega_2$ and $G''\sim\omega_1$, as the frequency approaches very small values [18, 28]. When a transition, such as a phase separation occurs, a deviation from the terminal behaviour, typically the exponents of frequency in their relation with moduli become smaller. According to the thermal analysis for neat L4 SIS block copolymer, the first transition, around 95°C, indicates the T_g of PS block while the second one, around 135°C, can be attributed to an order-disorder transition temperature (T_{ODT}). This fact is confirmed by the theoretical value of T_{ODT} calculated by iteration among the empirical Equation (1) for the interaction parameter φ determined by references [18, 36]:

$$\varphi = -900 + \frac{750\,000}{T_{ODT}} \qquad (1)$$

and Equation (2) for χN, being χ the Flory-Huggins interaction parameter and N the polymerization degree [36], through:

$$\chi N = \varphi \left(M_{w,PS} \nu_{PS} + M_{w,PI/PB} \nu_{PI/PB} \right) \qquad (2)$$

where $M_{w,PS}$ and $M_{w,PI/PB}$ corresponds to the molecular weight of the PS and PI/PB blocks, ν_{PS} and $\nu_{PI/PB}$ are the specific volumes of PS and PI/PB respectively. Table 1 reports T_{ODT} values obtained for the different block copolymers studied. Moreover, in order to confirm these transitions, a morphological AFM analysis of the neat BC annealed at different temperatures has been previously reported [28, 29]. In fact, it is worth to note that self-assembled nanostructures of the block copolymer matrix retain its cylindrical structure for different annealing times and temperatures. The BC nanostructure starts to lose its order after the sample has been annealed for 8 h at 135°C. These results are con-
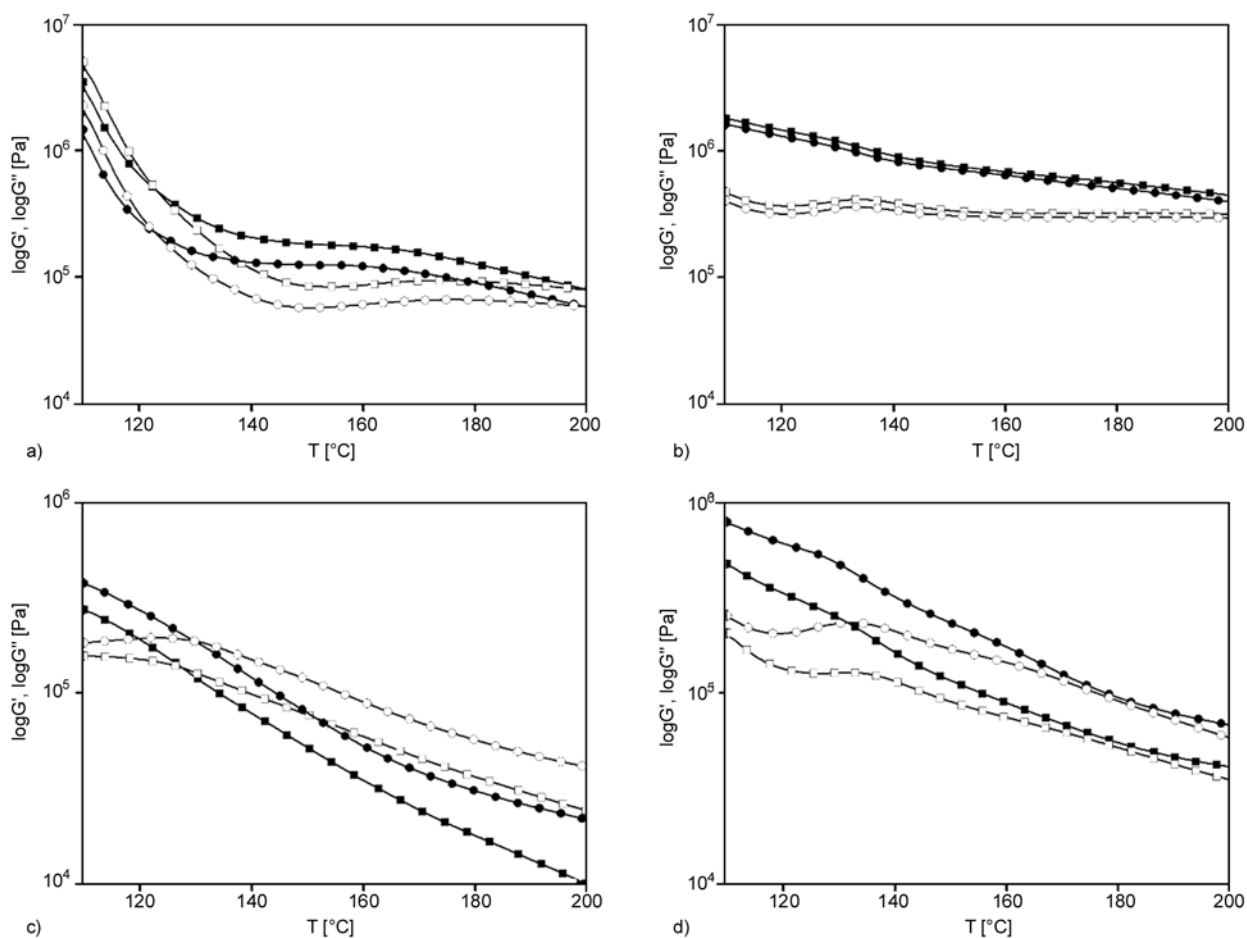
Figure 1. Isochronal dynamic temperature ramps for block copolymers (○) and their respective nanocomposites (□) in terms of *G′*(filled) and *G″* (unfilled): (a) L1, N1, (b) L2, N2, (c) L3, N3, (d) L4, N4

firmed by rheological tests, reported in Figure 1. In particular, Figure 1a reports isochronal dynamic temperature ramps of storage and loss moduli for neat L1 and N1. L1 shows a different behaviour with respect to the other BC systems. The curve of L1 is the steepest because of the higher value of T_g of PS block of the four block copolymers, as emerged also from thermal analysis. According with the highest T_{ODT} of the SBS matrix theoretically calculated, also the second transition, referred to the order-disorder transition, takes place at higher temperature respect to the other block copolymers studied. In Figures 1b–1d the isochronal dynamic temperature ramps for L2 and N2, L3 and N3, L4 and N4, respectively, are reported. The transition obtained in the rheological tests around 135°C for L4, abrupt fall of *G′* plot and a maximum in *G″* plot, can be attributed to an order-disorder transition, which has been already reported in literature for a diblock poly(styrene-*b*-isoprene) copolymer [40, 41]. While L2 and L4 show very similar rheological

behaviour, for L3, a SIS block copolymer with smaller content of PS than the others, the order-disorder transition takes place at temperature lower than 135°C, where the fall of *G′* plot and the *G″* maximum are obtained. The obtained results are in good agreement with the chemical compositions of the BC matrix. Higher amount of PS leads to higher values of the storage and loss moduli. In the case of L1 and N1 the shear thinning allows discrimination between the samples, thus confirming the different behaviour with the increase of PS in the BC matrix. Moreover, taking into account the behaviour of all nanocomposites, it is worth to note a small transition at about 125°C, which can be attributed to the decomposition temperature of the silver/dodecyl mercaptide, as reported elsewhere [42].

Due to the dramatic differences in viscoelastic response between the ordered phases in BC melts, rheological measurements have become a valuable tool to probe morphological changes. Figures 2a–2d reports the dynamic frequency sweeps for neat
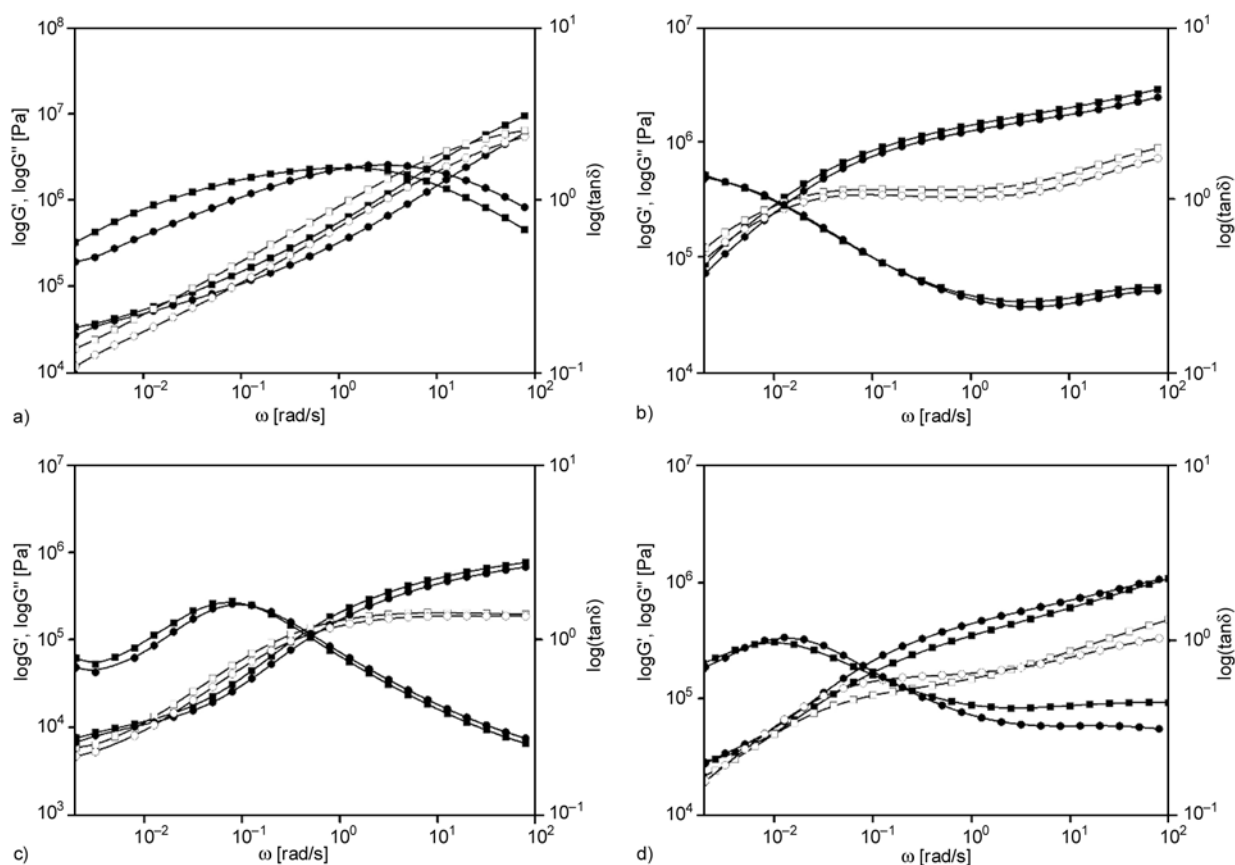
Figure 2. Frequency dependence of storage modulus (●), loss modulus (■) and tanδ for block copolymers (○) and their respective nanocomposites (□). (a) L1, N1, (b) L2, N2, (c) L3, N3, and (d) L4, N4. Neat block copolymers are characterized (●), while nanocomposites (■).

BC and their corresponding nanocomposites. A crossover of $G'(\omega)$ and $G''(\omega)$ is evident at different characteristic frequencies for each system. In case of L2-N2 and L4-N4, where the PS content in BC matrix is around 30 wt%, no second crossover of $G'(\omega)$ and $G''(\omega)$ has been detected. Moreover, only for L4-N4 system, a variation in the power law of BC with respect to the NC is observed, which reflects a morphological change. In fact, the power law behaviour, changes from 0.3 in the case of neat BC, consistent with the viscoelastic response of hexagonally closely packed cylindrically ordered structure, to 0.5 that corresponds to a lamellar structure [43]. This morphological change can be confirmed by AFM images, reported in Figure 3d. In fact, in order to get further information on phase separation and on the successful dispersion of Ag/DT nanoparticles in the PS phase of the block copolymer, transparent hybrid metal/polymer thin films obtained from the sonicated mercaptide/polymer solutions were analyzed by AFM. Figures 3a–3d shows TM-AFM height and phase images,

obtained in moderate tapping conditions, for the four neat copolymers and their respective nanocomposites with 0.10 vol% Ag nanoparticles. Two main aspects can be evidenced from this analysis. First, it is possible to obtain ordered nanostructures when Ag/DT nanoparticles are added to the BC matrix, and second, morphological changes on the self-assembled nanostructures of the BC matrix can occur in the respective nanocomposites. For the system L1-N1, reported in Figure 3a, the TM-AFM images show that, although a well defined ordered nanostructure was not detected for the neat BC, the addition of Ag/DT nanoparticles does not produce morphological changes (island-like) on the microstructure of BC matrix and the nanocomposite maintains a similar morphology to that for neat BC. A different situation can be observed for the system L2-N2, reported in Figure 3b. First it can be pointed out that neat L2 shows an ordered cylindrical morphology parallel to the free surface with dimensions of about 20 nm. When DT coated silver nanoparticles are added to the matrix, the ability of this nano-
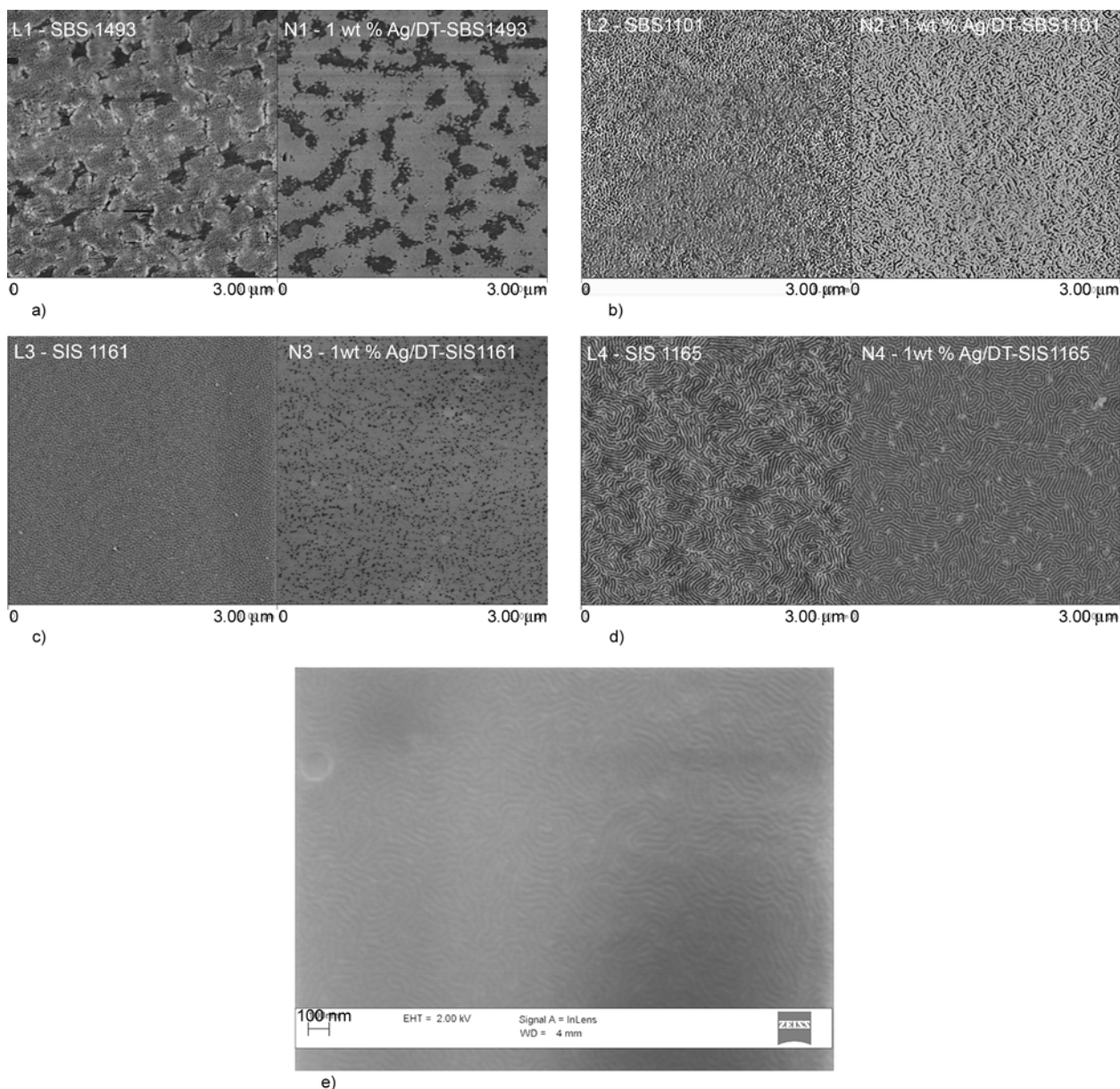
Figure 3. TM-AFM phase images for block copolymers and their respective nanocomposites: (a) L1, N1, (b) L2, N2, (c) L3, N3, (d) L4, N4, (e) L4 FE-SEM micrograph

structured heterogeneous polymer to self-assemble into cylindrical ordered nanostructure is retained. Also in N2 most of the PS cylindrical domains appear oriented parallel to the free surface. But, in this case, the addition of Ag/DT nanoparticles leads to an increase of the dimensions of the PS cylinders (about 30 nm). This fact confirms that the addition of Ag/DT nanoparticles in the block copolymer matrix enlarges the PS phase, in agreement to the solubility parameters values, and to the interactions noted by thermal analysis between Ag/DT mercaptide and the PS block of the block copolymer. In Figure 3c, for L3 and N3 films a different behaviour is observed. While L3 shows spherical ordered

nanostructures, when 0.10 vol% Ag nanoparticles treated with DT are added to the block copolymer matrix, disordered morphology is obtained. Moreover, in the N3 TM-AFM height and phase images, small aggregations of silver nanoparticles can be detected. These facts can be explained taking into account the PS content in the L3 matrix. In fact, L3 is the block copolymer that has the lowest content of PS respect to the other BC used in this work. It only contains 15 wt% of PS, thus demonstrating that the small PS microphase of the copolymer, cannot host all the Ag nanoparticles which correspond to 0.10 vol% of the total amount of copolymer.

A deeper morphological study of the last system, L4-N4 (Figure 3d), has been reported in a previous publication [29]. Here, it is worth noting that for L4, a cylindrical nanostructure is detected, confirming the microphase separation of PS blocks. Most PS cylindrical domains seem to be oriented parallel to the free surface with a period of about 20 nm. When 0.10 vol% Ag nanoparticles treated with DT are added, the nanostructure switches from ordered cylinders for neat BC to a lamellar structure characterized by a interlamellar periodicity of both polymeric phases of about 24–28 nm. The morphological change confirms the enlargement of the PS phase as a consequence of the good confinement of Ag/DT nanoparticles on this phase. The same morphological change has been detected previously by rheological tests at low frequencies. In order to compare the self-assembled nanostructures obtained with different techniques Figure 3e shows the FE-SEM analysis of L4. The AFM and FE-SEM images are comparable and even if in the FE-SEM image it is not possible to distinguish the typical AFM phase contrast (soft-dark contrast in the AFM phase images depending on the different phase of the block copolymer) it is possible to detect the same cylindrical nanostructured morphology. In particular, it is well known that homogeneous polymer melts follow a typical terminal behaviour, that is, G' is proportional to ω^2 and G'' is proportional to ω, as the frequency approaches very small values. When a transition in a material, such as a phase separation, occurs, a deviation from the terminal behaviour is observed. Typically a smaller exponent in the frequency appears in the relationship G-ω. So, in ordered systems like our nanostructured block

copolymers, the slope of the G'-ω and G''-ω curves at low frequency indicates the different morphologies of the self-assembled nanostructure. So, a slope of 0.3 for both curves corresponds to cylindrical morphologies, while a slope of 0.5 corresponds to lamellar morphologies.

So summarizing the morphological analysis, we must distinguish two different facts. The first one relates to the different morphologies of the four block copolymers studied (Figures 3a–3d, left side). The first one (Figure 3a) shows a poor nanostructuration, the second one (Figure 3b) shows a typical cylindrical structure [40, 41], the third one (Figure 3c) shows a typical spherical structure and, probably, the less clear morphology is shown by Figure 3d. Following our experience and previous publications by the main research groups working on this topic [12, 13], Figure 3d corresponds to a cylindrical structure parallel to the free surface. After the addition of the silver nanoparticles (see right side of Figures 3a–3d) all the samples show some little morphological changes with no nanostructure transition except for the L4-N4 system (Figure 3d). By comparison of the left and right sides of Figure 3d a slight enlargement of the domains – in length and width – can be detected. The longer domains are compatible with the change to a lamellar structure while the larger domains of the PS phase depend on the interaction of the nanoparticles with the neat matrix as already reported.

It is interesting to note that the morphology of BC and the good dispersion of nanoparticles in their nanocomposites affect not only the rheological behavior but also their mechanical properties. In Figures 4a, 4b the stress-strain curves are reported
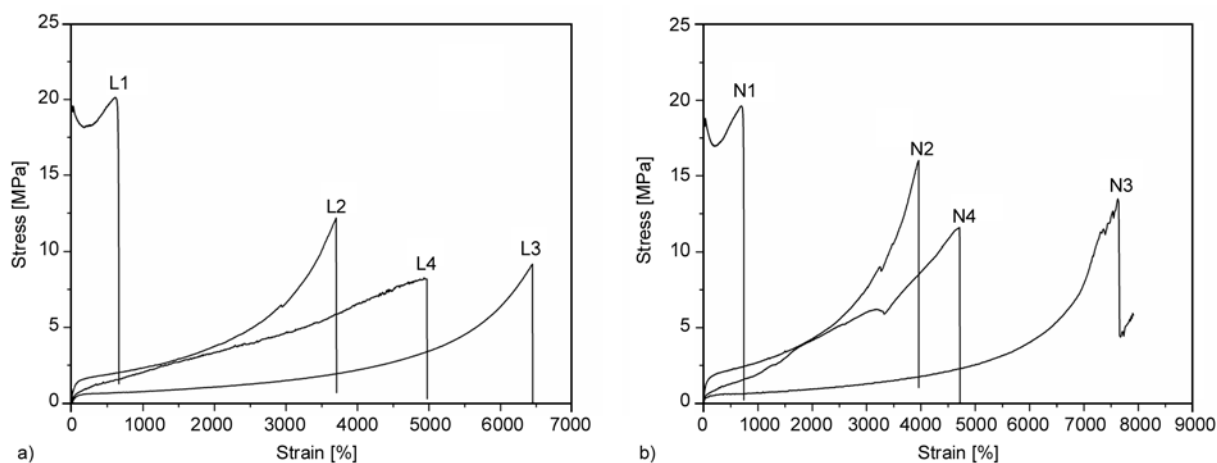

Figure 4. Stress-strain diagrams for: (a) the four BC and (b) the four NC

for the four BC and their NC, respectively. From the mechanical point of view, it is not possible to compare the results obtained with the four copolymers as they show completely different nanostructuration behavior. The scope here is only to analyze the effects of the dispersion of 1 wt% (0.10 vol%) of nano-silver particles on each one of the polymeric materials used. According to different volume fractions of the hard and soft phases and resulting morphologies, the block copolymers and their nanocomposites show a variety of mechanical properties. As expected, due to the high content of PS in the L1 matrix (75 wt%), this block copolymer shows the highest tensile properties in term of modulus and strength, thus indicating its high resistance to plastic deformation. For L1 and N1, after reaching the yield point, strain softening prevails, leading to fracture. A macroscopic stress whitening of the specimen was observed during the tensile testing, which indicates the formation of microvoids in the sample thus confirming that, as reported in literature for SB diblock copolymers [44, 45], cavitation of the dispersed PB phase is followed by plastic deformation of the PS matrix via necking and drawing. However in L1 triblock copolymers, crazing of the PS matrix has been found thus indicating the preferential cavitation of the PS matrix. Cavitation in the PS phase is favored by termination of the copolymer chain ends in the styrene matrix [46]. Both SIS copolymers show higher elongation at break than the SBS ones. A first analysis of the mechanical tests indicates that the PI block is the main responsible of this behavior. In fact, the L3 SIS block copolymer, having the highest content of PI, was the one that showed the highest elongation at break.

The content of PS as also expected influences the mechanical properties. L1, the BC with the higher PS content, showed the highest elastic modulus but the smaller elongation at break. Even though the contents of PS in L2 and L4 block copolymers were very similar to each other, even L4, SIS, showed higher elongation at break due to the presence of PI block.

For each block copolymer-nanocomposite system studied the tensile modulus E, tensile strength, σ, and elongation at break, ε, are shown in Table 3, also including the influence of surfactant on the tensile properties.

As expected, due to the high content of PS in the L1 matrix (75 wt%), the block copolymer showed high modulus and strength, thus indicating the high resistance to plastic deformation. Nanocomposite N1, with 0.10 vol% Ag nanoparticles treated with DT (Ag/DT weight ratio = 1), showed higher modulus, strength and elongation at break than the corresponding neat BC, thus confirming that addition of adequate amount of surfactant leads to well-dispersed silver nanoparticles in the PS phase of the BC matrix. The influence of surfactant in the L1 matrix and the mechanical properties of nanocomposite without surfactant have also been analyzed. Comparing the results, the addition of surfactant to the neat matrix decreases the mechanical performance, as expected, as well as the nanocomposite obtained without surfactant shows mechanical properties lower than Ag/DT nanocomposite.

Higher values of the mechanical properties were also obtained for the other systems when Ag/DT nanoparticles were added to the BC matrix. The behavior of L2-N2 system in terms of tensile modu-

Table 3. Tensile properties of the different studied systems

Materials	PS [wt%]	E [MPa]	σ [MPa]	ε [%]	G-G equation E [MPa]	H-T model E [MPa]
L1		394 ± 90	20.6 ± 2.0	772 ± 135		
L1+DT	75	333 ± 95	23.8 ± 2.0	805 ± 105	514	498
N1ws		372 ± 90	23.6 ± 1.6	980 ± 110		
N1		440 ± 98	24.6 ± 1.8	1021 ± 128		
L2		13.6 ± 2.2	13.5 ± 2.2	3507 ± 108		
L2+DT	31	13.5 ± 2.1	14.0 ± 2.8	3590 ± 364	18.6	16.2
N2ws		13.0 ± 1.8	14.2 ± 2.1	3695 ± 305		
N2		23.4 ± 2.0	15.5 ± 1.8	3818 ± 87		
L3	15	1.3 ± 0.2	9.4 ± 1.4	6562 ± 146	–	–
N3		2.0 ± 0.6	11.7 ± 1.6	7567 ± 152		
L4		3.4 ± 0.4	8.7 ± 0.9	3756 ± 651		
L4+DT	30	2.8 ± 0.8	7.6 ± 0.9	3891 ± 453	4.7	4.5
N4ws		4.0 ± 0.5	4.6 ± 0.9	3788 ± 756		
N4		4.5 ± 0.3	9.7 ± 0.7	4718 ± 400		

lus, strength and elongation at break is also reported in Table 3. The Ag/DT/L2 nanocomposite showed the higher value for each mechanical property. N2 presented double tensile modulus and higher tensile strength with respect to neat L2 and also high elongation at break, around 3800%. It is worth to note that in this case even for the nanocomposite obtained without surfactant it was possible to obtain higher mechanical properties with respect to neat L2, due to the well-ordered morphology that can be obtained, as reported below.

The mechanical response of L3-N3 system is shown in Table 3. In this case the influence of surfactant has not been reported since a very low value of tensile modulus was obtained. It is worth to note that, even the L3 material showed very low modulus, the elongation at break was the largest of the materials studied, around 6500%, due to the high content of PI. In the case of the nanocomposite, the characteristic elongation at break increased up to a value of more than 7000%, indicating a good interfacial adhesion between the nanoparticles and the matrix.

Finally the mechanical properties for L4-N4 are reported also on Table 3. Also in this case, higher mechanical properties were obtained for the nanocomposite based on BC matrix and coated Ag/DT nanoparticles. Furthermore, it can be pointed out that in the case of nanocomposite without surfactant, the mechanical properties were lower, thus indicating agglomeration of nanoparticles. Basically, taking into account the lower tensile strength obtained for the nanocomposite without surfactant with respect to neat L4, agglomerated Ag nanoparticles act as 'defects', thus worsening the mechanical performance of the nanocomposites.

Moreover, comparing the SIS block copolymer L4, with the SBS containing similar amount of PS, that is L2, it can be noted that the tensile strength of the Ag/SBS nanocomposite is not lower than the tensile strength obtained for neat BC matrix, as occurred in case of L4-N4. This fact can be explained taking into account the morphology of the NC obtained without surfactant, as shown below. Figure 5a presents in fact, the morphology obtained for uncoated Ag/L1 nanocomposites. No aggregation was observed due to good dispersion of Ag nanoparticles in the SBS matrix. For Ag/L2 nanocomposite a cylindrical morphology can be still detected (Figure 5b). The good confinement of Ag nanoparticles in the SBS matrix

justifies the higher value in terms of tensile properties obtained respect to neat L2. On the contrary, for Ag/L4 system, (Figure 5c) when untreated Ag nanoparticles were added to the matrix, no self-assembly of the BC matrix was obtained. Taking into account the agglomeration observed in Ag/DT/L3 samples, it was decided to neglect the analysis of the morphology of the L3 nanocomposite, without surfactant.

Finally, the tensile properties of the different studied systems have been summarized and compared with the theoretical values obtained from the empirical models represented by the Guth and Gold (G-G) equation [31–32] and the Halpin-Tsai (H-T) model [33–35] for the tensile modulus of composite materials. Guth and Gold introduced a quadratic term on the Smallwood-Einstein equation to explain the reinforcing effect of fillers on elastomeric matrices taking into account the interactions between fillers, as shown in Equation (3):

$$E_c = E_m[1 + 2.5\phi_f + 14.1\phi_f^2] \tag{3}$$

where E_c is the tensile modulus of the composite, E_m is the tensile modulus of the matrix and ϕ_f is the volume fraction of filler. This equation is only applicable to elastomers filled with an amount of spherical filler lower than 10 vol%. Besides, the Halpin-Tsai model, based on the properties of the pure components and the morphology of the final composite, is also widely used to estimate reinforcement effects of fillers in composites. This model, that also shows good results when applied to nanocomposites [45], is expressed by Equation (4):

$$E = E_m \cdot \frac{1 + \zeta\eta\phi_f}{1 - \eta\phi_f} \tag{4}$$

where ζ is a shape factor parameter dependent upon filler geometry and loading direction (ζ can be considered equal to 2 for spherical nanoparticles [46]) and η is given by Equation (5):

$$\eta = \frac{\dfrac{E_f}{E_m} - 1}{\dfrac{E_f}{E_m} + \zeta} \tag{5}$$

An assumption inherent in all of these theories is that each component acts independently of the other. In our case it is worth to consider also the surfactant effect. So, to calculate the theoretical tensile modu-
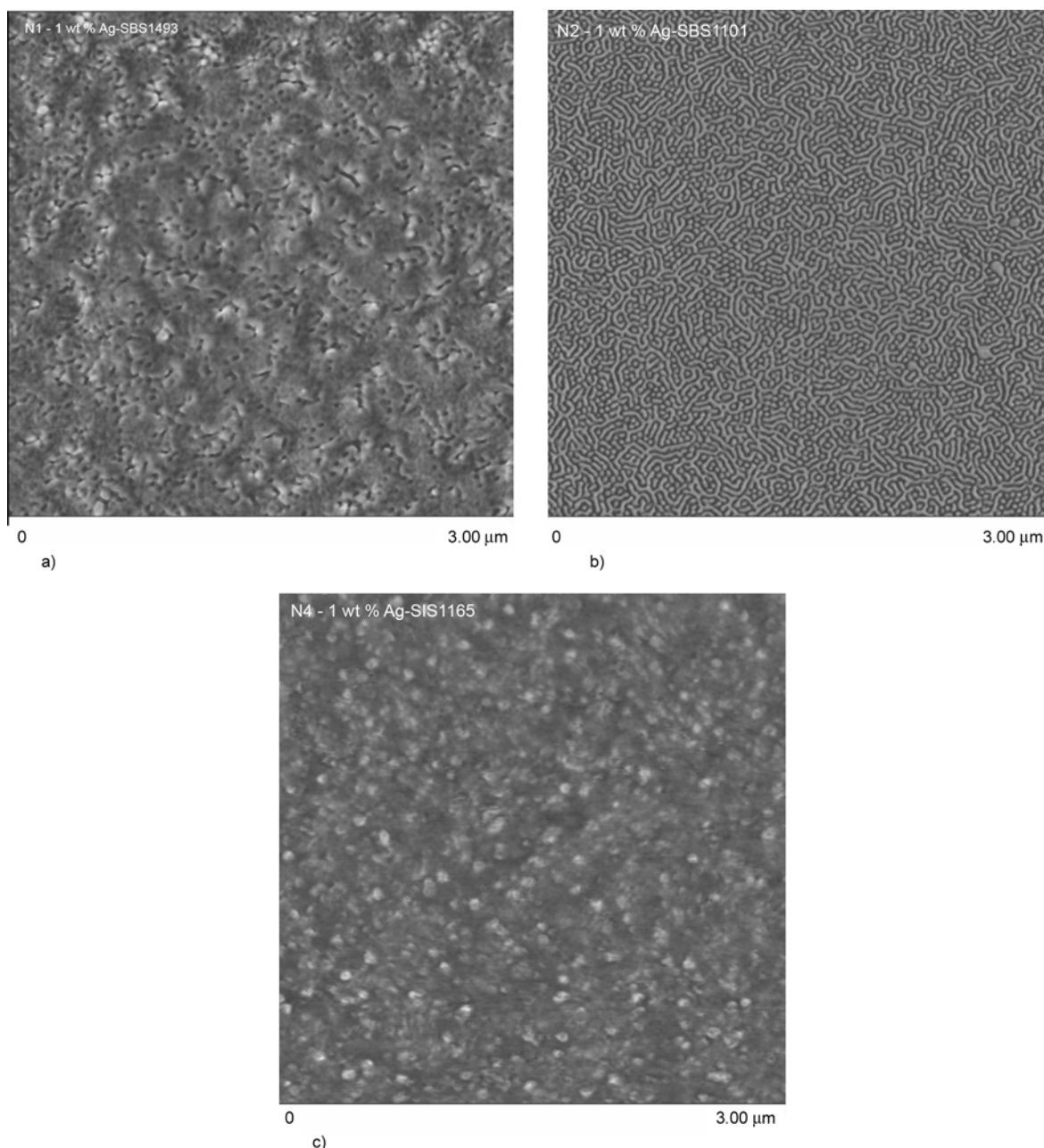
Figure 5. TM-AFM height and phase images for: (a) Ag/L1, (b) Ag/L2, and (c) Ag/L4 films

lus of the final nanocomposite, first, the rule of mixtures has been taken into account to calculate the effect of surfactant on the matrix tensile modulus [46], as shown in Equation (6):

$$E_{DT/BC} = \phi_{DT}E_{DT} + (1 - \phi_{DT})E_{BC} \qquad (6)$$

Thus the value obtained for tensile modulus, $E_{DT/BC}$, can be considered as the matrix tensile modulus in the Guth and Gold and Halpin-Tsai models to calculate the nanocomposite tensile modulus reported in Table 3. The highest value of tensile modulus and tensile strength was found for the first block copolymer, L1, confirming that the higher amount of PS

influences the mechanical properties. Furthermore, this BC is the only one star block copolymer, and, as reported in literature, star block copolymers show higher mechanical properties than linear ones. Additionally, for the same wt% of PS, SBS block copolymers showed higher tensile properties than the SIS ones in terms of tensile modulus and tensile strength. On the other hand, SIS block copolymers showed higher elongation at break than SBS ones. The lower was the content of PS in the BC matrix the higher was the value of elongation at break. Interesting is to note that, even for L3, characterized by the lowest tensile modulus, the tensile strength

values were comparable with those obtained for the other systems, such as L2 or L3, thus confirming the well confinement of the Ag nanoparticles in the PS block of the block copolymer matrix and their good adhesion.

Regarding the theoretical tensile modulus, it is worth to note that in case of L3, due to its low value, the empirical model is not applicable. Whereas for the other systems the Guth and Gold and Halpin-Tsai models have shown to be able to predict the tensile modulus of the studied nanocomposites. In fact, the theoretical values are quite similar to the experimental ones, even considering the effects of many factors not considered by the simple Guth and Gold model and the no ideality of Halpin-Tsai hypothesis.

4. Conclusions

The macroscopic response in terms of mechanical properties of metallopolymer films based on BC matrix and silver nanoparticles has been analyzed. To obtain well dispersed silver nanoparticles in SBS or SIS matrices dodecanethiol was used as surfactant with a weight ratio Ag/DT of 1. From the mechanical point of view, the good confinement of Ag nanoparticles in the PS phase leads to higher tensile properties in terms of tensile modulus, tensile strength and elongation at break than neat BC matrices. When surfactant was not used, the increase in the mechanical properties values was not so significant, thus indicating that aggregation of Ag nanoparticles can act as defects into the BC matrix. As expected, the amount of PS influences the mechanical response of the nanocomposites as well as the rheological one. Indeed L1-N1, the system with higher content of PS showed the highest tensile strength and tensile modulus and, on the other hand, this system presented the lowest elongation at break. Finally, it should be pointed out that L3-N3 showed an interesting behavior when compared to the others. Even if this BC is characterized by the lowest content of PS and its tensile modulus is very low, the obtained tensile strength was comparable with that for the other systems while the elongation at break was the highest, thus confirming that the soft block of this BC, isoprene, is responsible of the peculiar elastic behavior to this material and of its nanocomposite.

References

[1] Krausch G., Magerle R.: Nanostructured thin films via self-assembly of block copolymers. Advanced Materials, **14**, 1579–1583 (2002).
DOI: 10.1002/1521-4095(20021104)14:21<1579::AID-ADMA1579>3.0.CO;2-6

[2] Hamley I. W.: Nanostructure fabrication using block copolymers. Nanotechnology, **14**, R39–R54 (2003).
DOI: 10.1088/0957-4484/14/10/201

[3] Sangermano M., Priola A., Kortaberria G., Jimeno A., Garcia I., Mondragon I. Rizza G.: Photopolymerization of epoxy coatings containing iron-oxide nanoparticles. Macromolecular Materials and Engineering, **292**, 956–961 (2007).
DOI: 10.1002/mame.200700093

[4] Lazzari M., López-Quintela A.: Block copolymers as a tool for nanomaterial fabrication. Advanced Materials, **15**, 1583–1594 (2003).
DOI: 10.1002/adma.200300382

[5] Serrano E., Tercjak A., Kortaberria G., Pomposo J. A., Mecerreyes D., Zafeiropoulos N. E., Stamm M., Mondragon I.: Nanostructured thermosetting systems by modification with epoxidized styrene-butadiene star block copolymers. Effect of epoxidation degree. Macromolecules, **39**, 2254–2261 (2006).
DOI: 10.1021/ma0515477

[6] Bates F. S., Fredrickson G. H.: Block copolymer thermodynamics: Theory and experiment. Annual Review of Physical Chemistry, **41**, 525–557 (1990).
DOI: 10.1146/annurev.pc.41.100190.002521

[7] Huang C-I., Lodge T. P.: Self-consistent calculations of block copolymer solution phase behavior. Macromolecules, **31**, 3556–3565 (1998).
DOI: 10.1021/ma980007p

[8] Matsen M. W., Bates F. S.: Unifying weak- and strong-segregation block copolymer theories. Macromolecules, **29**, 1091–1098 (1996).
DOI: 10.1021/ma951138i

[9] Matsen M. W., Bates F. S.: Conformationally asymmetric block copolymers. Journal of Polymer Science Part B: Polymer Physics, **35**, 945–952 (1997).
DOI: 10.1002/(SICI)1099-0488(19970430)35:6<945::AID-POLB9>3.0.CO;2-G

[10] Tercjak A., Gutierrez J., Peponi L., Rueda L., Mondragon I.: Arrangement of conductive TiO_2 nanoparticles in hybrid inorganic/organic thermosetting materials using liquid crystal. Macromolecules, **42**, 3386–3390 (2009).
DOI: 10.1021/ma8022553

[11] Park C., Yoon J., Thomas E. L.: Enabling nanotechnology with self assembled block copolymer patterns. Polymer, **44**, 6725–6760 (2003).
DOI: 10.1016/j.polymer.2003.08.011

[12] Bates F. S., Fredrickson G. H.: Block copolymers – Designer soft materials. Physics Today, **52**, 32–38 (1999).
DOI: 10.1063/1.882522

[13] Ott H., Abetz V., Alstadt V.: Morphological studies of poly(styrene)-*block*-poly(ethylene-*co*-butylene)-*block*-poly(methyl methacrylate) in the composition region of the 'knitting pattern' morphology. Macromolecules, **34**, 2121–2128 (2001).
DOI: 10.1021/ma0017079

[14] Jeson H. S., Rameshwaram J. K., Kim G., Weinkauf D. H.: Characterization of polyisoprene-clay nanocomposites prepared by solution blending. Polymer, **44**, 5749–5758 (2003).
DOI: 10.1016/S0032-3861(03)00466-X

[15] Incarnato L., Scarfato P., Scatteia L., Acierno D.: Rheological behavior of new melt compounded copolyamide nanocomposites. Polymer, **45**, 3487–3496 (2004).
DOI: 10.1016/j.polymer.2004.03.005

[16] Raghu P., Nere C. K., Jagtap R. N.: Effect of styrene-isoprene-styrene, styrene-butadiene-styrene, and styrene-butadiene-rubber on the mechanical, thermal, rheological, and morphological properties of polypropylene/polystyrene blends. Journal of Applied Polymer Science, **88**, 266–277 (2003).
DOI: 10.1002/app.11677

[17] Buzdugan E., Ghioca P., Stribeck N., Badea E. G., Serban S., Iovu M. C.: Mechanical properties of some brominated styrene-diene block copolymers. European Polymer Journal, **34**, 1531–1537 (1998).
DOI: 10.1016/S0014-3057(98)00004-4

[18] Peponi L., Tercjak A., Torre L., Kenny J. M., Mondragon I.: Surfactant effects on morphology-properties relationships of silver-poly(styrene-*b*-isoprene-*b*-styrene) block copolymer nanocomposites. Journal of Nanoscience and Nanotechnology, **9**, 2128–2139 (2009).
DOI: 10.1166/jnn.2009.437

[19] Fan F. R. F., Bard A. J.: Chemical, electrochemical, gravimetric, and microscopic studies on antimicrobial silver films. Journal of Physical Chemistry B, **106**, 279–287 (2002).
DOI: 10.1021/jp012548d

[20] Hutter E., Fendler J. H.: Exploitation of localized surface plasmon resonance. Advanced Materials, **16**, 1685–1706 (2004).
DOI: 10.1002/adma.200400271

[21] Bockstaller M. R., Mickiewicz R. A., Thomas E. L.: Block copolymer nanocomposites: Perspectives for tailored functional materials. Advanced Materials, **17**, 1331–1349 (2005).
DOI: 10.1002/adma.200500167

[22] Thompson R. B., Ginzburg V. V., Matsen M. W., Balazs A. C.: Predicting the mesophases of copolymer-nanoparticle composites. Science, **292**, 2469–2472 (2001).
DOI: 10.1126/science.1060585

[23] Niu S. J., Saraf R. F.: Selective assembly of nanoparticles on block copolymer by surface modification. Nanotechnology, **18**, 125607/1–125607/4 (2007).
DOI: 10.1088/0957-4484/18/12/125607

[24] Bockstaller M. R., Lapetnikov Y., Margel S., Thomas E. L.: Size-selective organization of enthalpic compatibilized nanocrystals in ternary block copolymer/particle mixtures. Journal of the American Chemical Society, **125**, 5276–5277 (2003).
DOI: 10.1021/ja034523t

[25] Darling S. B., Yufa N. A., Cisse A. L., Bader S. D., Sibener S. J.: Self-organization of FePt nanoparticles on photochemically modified diblock copolymer templates. Advanced Materials, **17**, 2446–2450 (2005).
DOI: 10.1002/adma.200500960

[26] Huh J., Ginzburg V. V., Balazs A. C.: Thermodynamic behavior of particle/diblock copolymer mixtures: Simulation and theory. Macromolecules, **33**, 8085–8096 (2000).
DOI: 10.1021/ma000708y

[27] Peponi L., Tercjak A., Gutierrez J., Stadler H., Torre L., Kenny J. M., Mondragon I.: Self-assembling of SBS block copolymers as templates for conductive silver nanocomposites. Macromolecular Materials and Engineering, **293**, 568–573 (2008).
DOI: 10.1002/mame.200800033

[28] Peponi L., Tercjak A., Torre L., Kenny J. M., Mondragon I.: Influence of the amount of silver nanoparticles in the properties of nanocomposites based on poly(styrene-*b*-isoprene-*b*-styrene) and poly(styrene-*b*-butadiene-*b*-styrene) block copolymer matrix. Journal of Nanostructured Polymer Nanocomposites, **4**, 76–83 (2008).

[29] Peponi L., Tercjak A., Torre L., Kenny J. M., Mondragon I.: Morphological analysis of self-assembled SIS block copolymer matrices containing silver nanoparticles. Composite Science and Technology, **68**, 1631–1638 (2008).
DOI: 10.1016/j.compscitech.2008.02.032

[30] Lee J. Y., Thompson R. B., Jasnow D., Balazs A. C.: Effect of nanoscopic particles on the mesophase structure of diblock copolymers. Macromolecules, **35**, 4855–4858 (2002).
DOI: 10.1021/ma0200266

[31] Wu Y-P., Jia Q-X., Yu D-S., Zhang L-Q.: Modeling Young's modulus of rubber-clay nanocomposites using composite theories. Polymer Testing, **23**, 903–909 (2004).
DOI: 10.1016/j.polymertesting.2004.05.004

[32] Guth E., Gold O.: On the hydrodynamic theory of the viscosity of suspensions. Physical Review, **53**, 322 (1938).

[33] Halpin Affdl J. C., Kardos J. L.: The Halpin-Tsai equations: A review. Polymer Engineering and Science, **16**, 344–352 (1976).
DOI: 10.1002/pen.760160512

[34] Camacho C. W., Tucker III C. L., Yalvaç S., McGee R. L.: Stiffness and thermal expansion predictions for hybrid short fiber composites. Polymer Composites, **11**, 229–239 (1990).
DOI: 10.1002/pc.750110406

[35] Miyagawa H., Mase T., Sato C., Drown E., Drzal L. T., Ikegami K.: Comparison of experimental and theoretical transverse elastic modulus of carbon fibers. Carbon, **44**, 2002–2008 (2006).
DOI: 10.1016/j.carbon.2006.01.026

[36] Han C. D., Kim J., Kim J. K.: Determination of the order-disorder transition temperature of block copolymers. Macromolecules, **22**, 383–394 (1989).
DOI: 10.1021/ma00191a071

[37] Greer J. R., Street R. A.: Mechanical characterization of solution-derived nanoparticle silver ink thin films. Journal of Applied Physics, **101**, 103529/1–103529/5 (2007).
DOI: 10.1063/1.2735404

[38] Brandrup J., Immergut E. H.: Polymer handbook. Wiley, New York (1989).

[39] Van Krevelen D. W.: Properties of polymers. Elsevier, Amsterdam (1990).

[40] Floudas G., Steffen W., Hadjichristidis N.: Order-disorder transition in a poly(styrene-*b*-isoprene) diblock copolymer at hypersonic frequencies. Europhysics Letters, **44**, 37–43 (1998).
DOI: 10.1209/epl/i1998-00431-5

[41] Hamersky M. W., Tirell M., Lodge T. P.: Self-diffusion of a polystyrene-polyisoprene block copolymer. Journal of Polymer Science Part B: Polymer Physics, **34**, 2899–2909 (1996).
DOI: 10.1002/(SICI)1099-0488(199612)34:17<2899::AID-POLB4>3.0.CO;2-M

[42] Lee K. M., Han C. D.: Linear dynamic viscoelastic properties of functionalized block copolymer/organoclay nanocomposites. Macromolecules, **36**, 804–815 (2003).
DOI: 10.1021/ma020816f

[43] García I., Tercjak A., Rueda L., Mondragon I.: Self-assembled nanomaterials using magnetic nanoparticles modified with polystyrene brushes and poly (styrene-*b*-butadiene-*b*-styrene). Macromolecules, **41**, 9295–9298 (2008).
DOI: 10.1021/ma801701k

[44] Weidisch R., Michler G. H., Arnold M., Fischer H.: Mechanical properties of weakly segregated block copolymers – Part IV – Influence of chain architecture and miscibility on tensile properties of block copolymers. Journal of Materials Science, **35**, 1257–1268 (2000).
DOI: 10.1023/A:1004757008254

[45] Miller A. C., Bennet R. D., Hammond P. T., Irvine D. J., Cohen R. E.: Functional nanocavity arrays via amphiphilic block copolymer thin films. Macromolecules, **41**, 1739–1744 (2008).
DOI: 10.1021/ma7019418

[46] Fornes T. D., Paul D. R.: Modeling properties of nylon 6/clay nanocomposites using composite theories. Polymer, **44**, 4993–5013 (2003).
DOI: 10.1016/S0032-3861(03)00471-3

Characterization of hydrolytic degradation of polylactic acid/rice hulls composites in water at different temperatures

B. S. Ndazi[1,2*], *S. Karlsson*[1]

[1]Department of Fibre and Polymer Technology, Royal Institute of Technology (KTH), 100 44, Stockholm, Sweden
[2]Permanent address: Department of Mechanical and Industrial Engineering, College of Engineering and Technology,
 University of Dar es Salaam, P.O. Box 35131, Dar es Salaam, Tanzania

Abstract. Hydrolytic degradations of polylactic acid/rice hulls (PLA/RH) composites with various rice hulls contents due to water absorptions at 23, 51 and 69°C were investigated by studying the thermal properties, chemical composition, molecular weight, and morphology of the degraded products. The results have attested that the stability of PLA/RH composites in water depends slightly on rice hulls contents but it is significantly influenced by water temperature. Water absorption in 30 days at 23°C was between 0.87 and 9.25% depending on rice hull contents. However, at thermophilic temperatures, the water absorption and degradation of these products were increased significantly. Saturations were achieved in less than 25 and 9 days at 51°C and 69°C, respectively, while hydrolytic degradation was demonstrated by an increase in fragility and development of crystallinity. At 69°C, there were significant reductions of the decomposition and glass transition temperatures of the polymer by 13°C. These changes were associated with the reduction of the molecular weight of PLA from 153.1 kDa to ~10.7 kDa due to hydrolysis of its ester group.

Keywords: biodegradable polymers, polylactic acid, rice hulls, hydrolytic degradation, molecular weight

1. Introduction

There has been a growing interest in the development of environmentally benign composites based on biodegradable poly(lactic acid) (PLA) polymer and various lignocellulosic materials such as kenaf [1, 2], flax [3], hemp [4], bamboo [5, 6], wood fibers [7], and reed fibers [8]. Addition of lignocellulosic materials in PLA is intended to improve the properties of this polymer without compromising its biodegradability. Although there has been very little work in the development of biodegradable polymer composites using rice hulls [1], several studies have demonstrated the potential of rice hulls in polymer composites [9–13]. Rice hulls are siliceous lignocellulosic residues, which have moderate water resistance and stability against degradation. It may

be interesting therefore to find out how these properties can affect the biodegradability of PLA.
PLA is a biodegradable polymer, which is naturally hydrophilic due to its polar oxygen linkages. It contains a methyl side group, which confers hydrophobic properties to this polymer [14]. The natural hydrophilic characteristic of PLA is responsible for its moderate decomposition in accordance with the surrounding moisture and temperature. The first stage of PLA degradation is usually the reduction of its molecular weight by hydrolysis to <10 kDa before it becomes biodegradable. The hydrolysis of PLA occurs by random cleavage of the –C–O– ester bond by water molecules. The hydrolysis products, which may contain fragments of lactic acid, oligomers and other water soluble products, can then be con-

---

sumed by microorganisms to produce carbon dioxide (CO_2), water (H_2O) and solid biomass [15]. This reaction can be increased under acidic or basic conditions or in the presence of high moisture and high temperature [16, 17]. Previous studies have shown that PLA is moderately stable in water at mesophilic temperatures (15–40°C). It can absorb between 0.7 and 1% of water in 30 days [18] or slightly higher at longer immersion periods [2] at these temperatures. The absorption of water by PLA biocomposites at these temperatures can lead to moderate change in their properties depending on filler contents [2, 18]. Since hydrolysis of PLA is influenced by ambient moisture and temperature, it is possible to accelerate the diffusion of water and hence increase the hydrolysis or degradation of this polymer by subjecting it to thermophilic temperatures above 50°C. In this report, the degradation of PLA/RH composites due to water absorption at 23, 51 and 69°C was investigated. The tests were carried out by immersing the PLA products in water until they were completely saturated. Their degradation was studied by thermal analysis, infrared spectroscopy, molecular weight analysis, and surface morphology analysis.

2. Materials and methods
2.1. Materials and preparations
Rice hulls were obtained from rice mills in Tanzania. A commercial grade PLA (Ingeo 3051D) in pellets form with a melt flow index of 1–2.5 g/min, from RESINEX Nordic AB Sweden, was used as a resin. The resin had the following specifications: specific gravity 1.24; melting temperature between 145 and 155°C, crystallization temperature from 95 to 120°C and the glass transition temperature ranging from 55 to 58°C. Dicumyl peroxide (DCP)-98% (Aldrich) and maleic anhydride (MA) briquettes M188-99% (Aldrich), purchased from Sigma Aldrich Sweden AB, were used as free radical initiator and coupling agent, respectively.

The PLA polymer and MA were prepared separately by grinding though a 1 mm sieve. The rice hulls (RH) were also ground though a 1-mm sieve and were dried overnight in an oven at 102°C to remove residual moisture. The ground rice hulls were designated as untreated rice hulls (URH).

2.2. Preparation of the composites
The composites were prepared by mixing different ratios of ground PLA resin and dry rice hulls. The amount of MA in the composites was controlled by the proportion of RH (i.e. 7% RH) while DCP was fixed at 7% MA. The mixture was tumbled in a mechanical mixer that rotates in three axes for about 30 minutes. This was followed by vacuum drying the mixture at 80°C for about 6 hours and then pressing under vacuum in a 400 kN compression moulding machine (Fontune Presses) at 190°C and 10 MPa for 5 minutes to produce 140 mm × 52 mm × 2 mm PLA composites with various contents of rice hulls. The PLA without rice hulls was designated as PLA-100 and those which contained the rice hulls were designated as PLA/URH 80/20, PLA/URH 70/30 and PLA/URH 60/40 where the digits refer to the proportion of PLA and RH in the composites, respectively.

2.3. Water absorption test
Water absorption tests were carried out in accordance with ASTM D570-98 guideline by submerging five rectangular test specimens with 20 × 50 × 2 mm³ dimensions into water at 23±1°C, 51±0.5°C and 69±1°C until they were completely saturated. All test specimens were dried in a conventional oven at 51±0.5°C for 24 hours prior to immersion in water. The test specimens were periodically removed from water and dried thoroughly with tissue papers before recording their weight gains. After saturation, all the test specimens were re-dried to constant weights at 51±0.5°C for 24 hours at the end of the test.

Absorption of water into the polymer composite is controlled by diffusion. If the diffusion follows Fickian behavior, an increase in weight can be described in terms of the diffusion coefficient, D, and the maximum moisture content, M_m as shown by Equation (1) [5, 18].

$$\frac{M_t}{M_m} = \frac{4}{h}\left(\frac{D}{\pi}\right)^{\frac{1}{2}} \cdot t^{\frac{1}{2}} \tag{1}$$

where M_t is the degree of water-sorption at time t; M_m is the water-sorption amount at equilibrium sorption time; h is the thickness of the specimen; and t is the water-sorption time.

The diffusion coefficient, D, may be given by Equation (2) from the slope (k) of the initial linear portion of the absorption curve M_t against $t^{1/2}$.

$$D = \pi \left(\frac{kh}{4M_m} \right)^2 \qquad (2)$$

2.4. Visual inspection of physical changes

Changes in the physical appearance such as color and flexibility of the test specimens were also monitored during the test.

2.5. Infrared spectroscopy analysis

Hydrolytic degradations of PLA and PLA/RH composites with different contents of rice hulls were also studied by infrared spectroscopy using a Fourier Transform Infrared (FTIR)-spectrometer 2000 system (Perkin Elmer). Each sample was run in duplicate and the results presented are the average of two runs. Samples were dried at 51±0.5°C for 24 hours before the analysis.

2.6. Thermal analysis

The influence of hydrolytic degradation on the thermal transitions and thermal stability of PLA and PLA/RH composites was determined by scanning calorimetry 1 (DSC1) and thermal gravimetric analysis (TGA) TGA/SDTA851 systems (Mettler Toledo AB, Sweden). The DSC1 system was calibrated using the melting temperature and enthalpy of indium as standard. The control samples from the non-immersed PLA and PLA/RH composites were ground through 1 mm test sieve while those from water soaked PLA and the PLA/RH composites were cut or crushed by hand. All test samples were accurately weighed into 100 μl aluminium pans to within 8.50 mg. An empty pan was used as a reference and each test sample was run in duplicate. The test was started by holding the samples at 25°C for 5 minutes and then raising the temperature to 200°C at 10°C/min under 50 ml/min of N_2 gas. The samples were isothermally heated at 200°C for 3 minutes and subsequently cooled back to 25°C at –10°C/min and held at that temperature for 3 minutes before heating again at the same rate to 200°C. All DSC measurements were taken from the second heat cycle in order to eliminate the influence of sample history.

Crystallinity of the PLA polymer was calculated from the DSC results using the melting enthalpy (ΔH_m^*) of a pure crystalline PLA. The ΔH_m^* value used to estimate the crystallinity is either 135 J/g suggested by Mitaya and Masuko [19] or 93.7 J/g calculated by Fischer *et al.* [20]. In this study, Mitaya and Masuko's value was used in conjunction with the Equation (3), which has been used elsewhere [21].

$$\chi_c = \frac{\Delta H_m}{\Delta H_m} \cdot 100\% \qquad (3)$$

where ΔH_m is the melting enthalpy of PLA in the composite.

Thermal stability measurements of the PLA and PLA/RH composites were carried out between 25°C and 700°C at 10°C/min under N_2 environment at 50 ml/min using TGA technique. The sample weight was maintained within 12.0±0.5 mg. The samples were initially dried at 51±0.5°C for 24 hours before the analysis.

2.7. Molecular weight analysis

Molecular weights reduction of PLA due to water absorptions were measured by TripleSEC Size Exclusion Chromatography (SEC) system using THF (1.0 ml/min) as the mobile phase was performed at 35ºC using a Viscotek TDA model 301 equipped with two T5000 columns with porous styrene divinylbenzene copolymer (300 mm $L \times$ 7.8 mm ID, exclusion limit MW polystyrene: 400 000 kDa) from Malvern (UK), a VE 2500 GPC autosampler, a VE 1121 GPC solvent pump, and a VE 5710 GPC degasser from Viscotek Corp. (the Netherlands). The samples were prepared by dissolving ~20 mg of PLA into 10 ml of THF. After filtration, the samples were transferred into 2 ml vials for analysis.

2.8. Morphological analysis

The influence of hydrolytic degradation on the fracture surfaces of PLA and PLA/RH composites was examined by Hitachi Field Emission SEM S-4800 system (Spectral Solutions AB, Sweden). The observations were made on the cross sections of the fracture surfaces of gold sputtered samples and also on the surfaces of these samples, which were in contact with water. All samples were prepared by breaking

with hand except those that were immersed at 23°C, which required freeze-drying in liquid nitrogen prior to breaking.

3. Results and discussion
3.1. Water absorption and physical changes

Figures 1a to 1c show the results of water absorption by PLA and PLA/RH composites at 23, 51 and 69°C, respectively. The diffusion of water into these products was higher during the first periods and decreased gradually until they were saturated suggesting a classical Fickian diffusion phenomenon. A mixed diffusion behavior has been reported previously in other PLA products [5, 18, 2]. However, it is shown that most of the PLA products that were immersed at 69°C (Figure 1c) did not reveal consistent saturations and therefore failed to exhibit Fickian diffusion phenomenon. At 51 and 69°C temper-
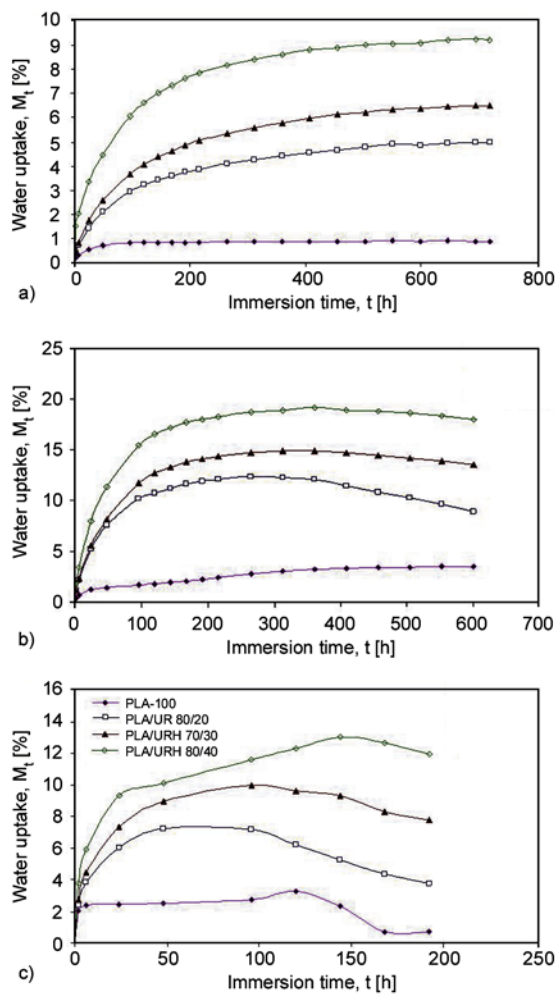
Figure 1. Moisture absorption in PLA/RH composites immersed in water at (a) 23°C, (b) 51°C and (c) 69°C

atures, the PLA/RH composites did not stabilize long at the saturation points and the time to reach that saturation was also significantly reduced. This was probably due to increased hydrolysis and leaching of the rice hulls and water soluble polymer products from the composites. Visual observations revealed that PLA products, which were immersed at 69°C, lost the transparency and became fragile from the third day. The composites that were immersed at 51 and 69°C became fragile during the testing period. On the contrary, the PLA products that were immersed at 51°C developed hardness while undergoing hydrolysis. This physical anomaly was examined by studying the morphologies of the fracture surfaces of all PLA and PLA/RH composites. PLA products are generally stable against hydrolysis at mesophilic temperatures [15] and absorb little amount of water [2, 18]. However, the results have attested that the hydrolysis and water absorption of these products can be accelerated significantly by simply subjecting them above the softening temperature of PLA.

By using the classical Fickian diffusion phenomenon, it was possible to estimate the diffusion parameters of some of the composites, which exhibited this behavior. The results shown in Table 1 generally corroborate the proposition that the rate of water diffusion into the composites increases at higher immersion temperatures with the exception of PLA and PLA/RH composites with 40% rice hulls content (PLA/URH 60/40) which were immersed at 51°C. The results show further that weight losses occurred only in the composites that were immersed at 51 and 69°C. This loss is attributed to the leaching of rice hulls and water soluble products mainly lactic acid and probably low molecular weight oligomers from the composite during the degradation of PLA in water. The weight gains shown by all the products, which were immersed at 23°C, attests further the stability of PLA in water at mesophilic temperatures. On the contrary, the weight gain revealed by PLA that was immersed at 51°C may be explained by different phenomena. However, it is worthy to note that this product hardened while undergoing water absorption. This could be attributed to aging of the product and hydrolysis of the amorphous domains. As expected, the diffusion of water into the composites increased with the increase of rice hulls content. This agrees with the

Table 1. Diffusion parameters of PLA and PLA/RH composites

Product	Temp [°C]	M_m [%]	$D \cdot 10^{-5}$ [mm²/s]	Weight gain of re-dried product [%]
PLA-100	23	0.87	0.665	–0.07
	51	3.57	0.223	–0.21
	69	–	–	3.16
PLA/URH 80/20	23	4.98	0.120	–3.15
	51	12.35	0.172	8.85
	69	7.19	1.676	12.10
PLA/URH 70/30	23	6.49	0.113	–0.25
	51	14.95	0.148	4.40
	69	9.96	1.164	10.31
PLA/URH 60/40	23	9.25	0.303	–1.46
	51	19.14	0.195	3.63
	69	1.00	–	9.89

previous studies [5,18] by demonstrating the role of rice hulls as hydrophilic fillers in the composite.

3.2. Thermal properties

The influence of hydrolytic degradations on the thermal properties of PLA/RH composites as measured by DSC1 system, are shown in Figure 2 and the summary is given in Table 2. As shown in Figure 2a, peaks ascribed to crystallization and melting of neat PLA did not appear during the re-heating cycle. Absence of the crystallization peak implies that the pellets were more amorphous. It is shown further that the crystallinity of PLA was slightly reduced during immersion of the PLA products in water at 23°C for 30 days. This is explained by a decrease of the crystallization and melting peaks

observed on the thermogram of this sample compared with the control PLA (PLA 100). The results show that the crystallization peaks of the composites were somewhat enhanced after addition of rice hulls in PLA (Figures 2b to 2d). These peaks increased considerably due to hydrolysis at higher temperatures. They were much stronger in the composites than in PLA at 51°C and increased substantially at 69°C in PLA ad well as in the composites. The large melt crystallizations shown in these products are evidence of enormous transformation of amorphous PLA into crystalline phases as the polymer was undergoing hydrolysis in water at 51 and 69°C temperatures. The results also seem to suggest further that the presence of rice hulls somehow enhanced the crystallization of PLA during water
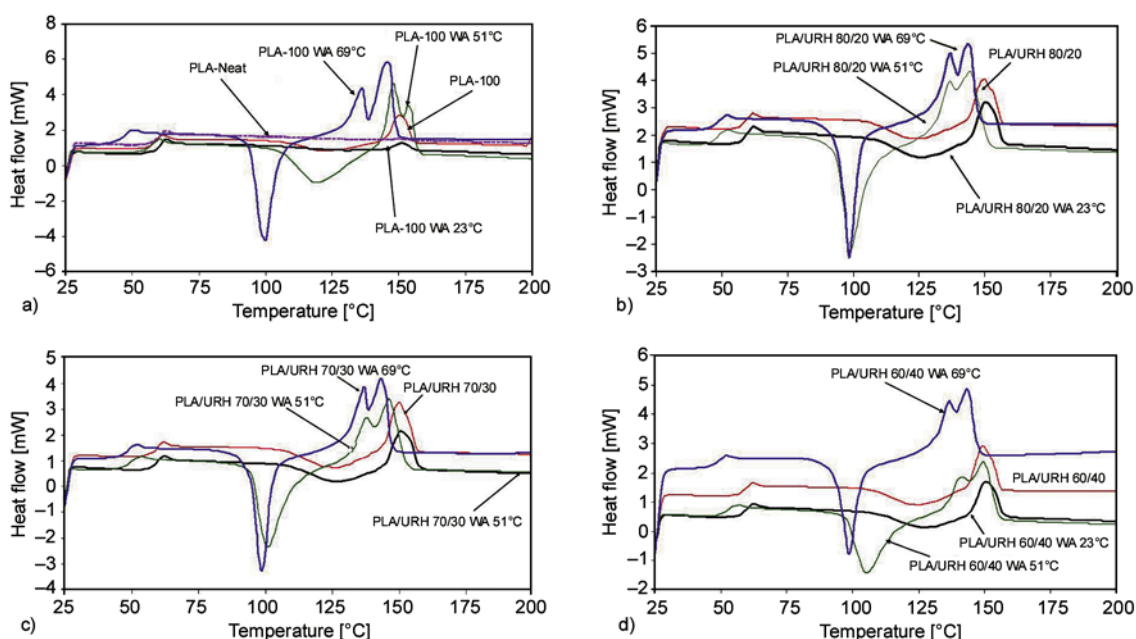
Figure 2. DSC thermograms of (a) PLA, (b) PLA/URH 80/20 composites, (c) PLA/URH 70/30 composites, and (d) PLA/URH 60/40 composites before and after water absorption

Table 2. Thermal properties of PLA/RH composites due to water absorption at different temperatures

Product	Immersion temp [°C]	T_g [°C]	T_c [°C]	*T_m [°C]	ΔH_m [J/g]	χ_c [%]
PLA-100	–	59.0	122.5	150.0	8.6	6.4
	23	59.1	126.5	151.1	1.9	1.4
	51	56.2	119.6	148.0	26.1	19.3
	69	46.4	99.8	145.6	41.6	30.8
PLA/URH 80/20	–	57.9	123.4	149.3	10.6	6.3
	23	58.1	125.8	150.5	8.9	5.3
	51	49.0	99.0	144.6	29.9	17.7
	69	47.9	98.6	143.8	28.5	16.9
PLA/URH 70/30	–	58.1	125.1	149.4	11.7	6.1
	23	58.4	126.3	150.7	8.9	4.6
	51	48.8	101.4	146.4	27.8	14.4
	69	47.6	98.7	143.1	28.4	14.7
PLA/URH 60/40	–	58.4	124.1	149.4	9.0	4.0
	23	58.5	126.9	150.7	7.0	3.1
	51	51.7	105.3	149.5	19.6	8.7
	69	48.3	98.9	143.4	22.1	9.8

*Two fusion peaks observed in PLA and PLA/RH composites immersed at 51 and 69°C

absorption at 51°C. However, this may be subjected to further scrutiny. Intensities of the melting peaks also increased slightly at higher temperatures. However, two melting peaks were observed in the products that had been hydrolyzed in water at 51 and 69°C. Neither of these peaks could be associated with thermal transitions of rice hulls as this biomass does not melt or crystallize and also on the fact that two peaks appeared in PLA, which did not contain rice hulls. It is therefore permissible to associate these peaks to the melting of hydrolytic degradation products of PLA since they were only visible in the products that had been subjected to hydrolysis at higher temperatures.

The summary of DSC results presented in Table 2 show very small increase in the glass transition temperature (T_g) of PLA by 0.4°C at the immersion temperature of 23°C. This small increase could be associated with minor changes in the polymer that might have influenced a slight increase of its high molecular weight fractions. It is shown further that T_g, the crystallization temperatures (T_c) and melting temperatures (T_m) also decreased probably due to hydrolysis of the polymer at higher water temperatures. Kale *et al.* [16] applied Fox-Flory equation to demonstrate the reduction of the T_g with the decrease of the number average molecular weight ($\overline{M}_n$) of commercial PLA products during degradation in a compost. Based on this relation, which has also been applied a couple of years earlier [22], we can associate the decrease of the T_g of PLA with the

reduction of its molecular weight due to hydrolysis. Perhaps there was a molecular weight degradation during water absorption that would be associated with the cleavage of the chain at –C–O– ester group by water molecules due to hydrolysis. To verify whether these changes are related to the molecular weight degradation of PLA or not, a molecular weight analysis was conducted by SEC. The results are shown in the corresponding section. Nevertheless, we cannot fully associate the physical changes of PLA products that were immersed at 23°C with any cross-linking or recombination reactions of the polymer under water at that temperature.

Change of crystallinity (χ_c) and fusion enthalpies (ΔH_m) due to hydrolysis of PLA were also examined. It is shown in Table 2 that the crystallinity and enthalpies of fusion of PLA decreased slightly at 23°C. However, it is shown further that there was a remarkable transformation of the amorphous region of PLA into crystalline phases at higher hydrolysis temperatures as shown by an increase of crystallinity. The largest transformation of the PLA to crystalline domains was achieved at 69°C, which was accompanied with maximum reduction of the T_g and T_m. Hydrolysis of the semi-crystalline PLA starts in the amorphous region transforming these domains to crystalline phases and it increases with the hydrolysis temperature [23]. The crystallinity can decrease if hydrolysis is extended in the crystalline domains once the hydrolysis of the amorphous region is over. The decrease of the T_g can be

related to molecular weight degradation as demonstrated previously using Fox-Flory equation [16]. It can thus be suggested that the development of crystalline phases in this polymer during hydrolysis at higher temperatures was accompanied with the reduction of its molecular weight. This proposition can also be verified by studying the molecular weight degradation of this polymer.

The representative results of the influence of hydrolytic degradations on the thermal stability of PLA and its composites as determined by TGA are shown at Figure 3. It is shown that all PLA products degraded in one major stage between 220 and 389°C. A secondary stage for the PLA/RH composites, which is shown between 370 and 530°C, was associated with the degradation of lignin and cellulose products in rice hulls. Additionally, there are two degradation stages between 220 and 333°C and from 333 to 389°C for the PLA product that was immersed at 69°C (PLA-100 WA69°C). These stages could be ascribed to thermal degradation of two hydrolytic degradation products of PLA with distinct thermal stabilities. Since these changes resulted from the hydrolysis of the polymer, it may be plausible to ascribe the two degradation stages to the decomposition of hydrolytic products with distinct molecular weights. By relating the decomposition temperature to the molecular weights as proposed by Kale *et al.* [16] using an expression similar to Fox-Flory equation, a higher molecular weight product decomposes at higher temperature and vice-versa. This implies that the first decomposition stage of this product could be attributed to the degradation of low molecular weight fractions of the polymer while the second stage involved hydrolytic degradation products with slightly higher molecular weight fractions. However, the legitimacy of this

assertion relies on the agreement with the molecular weight degradations results. It can also be shown further that peaks of maximum degradation zones for PLA and the composites that were immersed at 23°C generally occurred at higher temperatures. The high thermal stability of PLA was probably due to an increase of higher molecular weight fractions in the polymer during hydrolysis at this temperature. These products also lost large weights in the main degradation zones compared with similar products that were immersed at higher temperatures as indicated by stronger DTG curves peaks.

The influence hydrolytic degradations on the kinetics of thermal degradation of PLA were also studied using Horowitz and Metzeger [24] model shown in Equation (4).

$$\ln\frac{1 - C^{1-n}}{1 - n} = \frac{E(\Delta T)}{RT_{max}^2} \tag{4}$$

where $C = (w - w_f)/(w_0 - w_f)$ is the fraction of the sample lost, E is the activation energy, T_{max} is the temperature at maximum weight loss obtained from the peaks of DTG curves, R is the universal gas constant, $\Delta T = T - T_{max}$ and n is the order of reaction.

The reaction orders, n, estimated from $C_{max} = n^{1/(1-n)}$ were found to range from 0.6 to ∼1.0. The kinetics of thermal degradation of PLA was approximated using the first order reaction of this model. The left term of Equation (4) was reduced to $\ln[\ln\alpha]$ and E was obtained from the slope of the linear relation $\ln[\ln(w_0 - w_f)/(w - w_f)]$ versus ΔT. The results shown in Table 3 suggest that the thermal stability of PLA was slightly reduced due to processing. After hydrolysis of PLA in water at higher temperatures, the activation energy of thermal degradation generally decreased except at the immersion temperature of 23°C, where it slightly increased. In
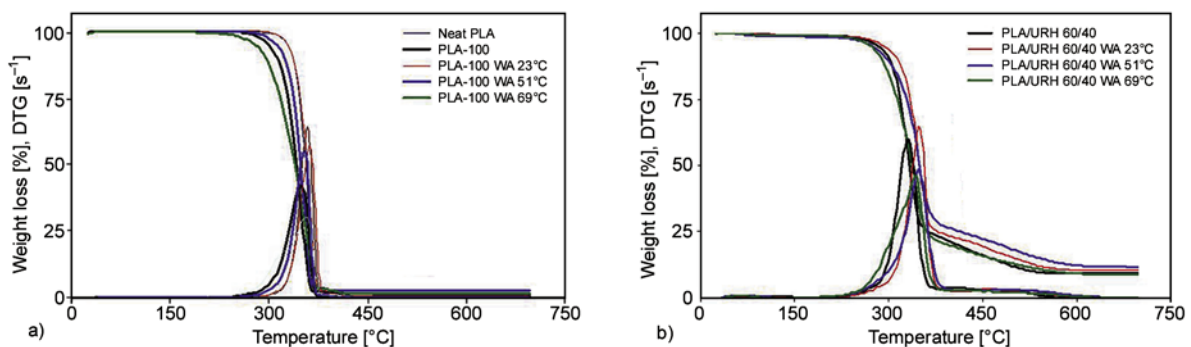

Figure 3. Thermograms of (a) PLA and (b) PLA/URH 60/40 composites products before and after water absorption at different temperatures

Table 3. Kinetic parameters of thermal and hydrolytic degradation of PLA and its rice hulls composites

Product	Decomposition step [°C]		T_{max} [K]		E [kJ/mol]		Estimated reaction order, n	
PLA-Neat	291–375		357.5		332.5		1.2	
PLA-100 (control)	266–371		350.5		224.0		0.6	
PLA-100WA23°C	291–375		361.0		305.8		1.0	
PLA-100WA51°C	266–371		354.0		250.7		0.7	
PLA-100WA69°C	231–378		357.5		161.6		overall	
PLA-100WA69°C	231–336	336–378	326	357.5	170.0	359.9	0.4	1.9

conjunction with SEC results, it may be possible to explain clearly and relate the changes to the molecular weight of the polymer. However, with the fact that higher molecular weight products require more energy to decompose and vice versa, the decrease in the activation energy can be related to molecular weight degradations. Concurrently, a slight increase in the activation energy observed at 23°C attests the proposition of the increase of high molecular weight fractions in the polymer at this temperature.

3.3. Infrared spectroscopy analysis

The results of infrared spectroscopy of PLA and PLA/RH composites, which were subjected to water absorption at 23, 51 and 69°C, are shown in Figures 4a to 4d. In this analysis the region of interest is between 1800 and 800 cm^{-1} where active ester and methyl groups of PLA are located. The results show strong absorption between ~1747 and ~1080 cm^{-1}, which is ascribed to symmetrical stretching of C=O and –C–O– groups of ester bonds, respectively. Unexpectedly, the vibration of rice hulls functional groups (Si, OH and C=C, etc) could not be shown on the spectra suggesting that the rice hulls might have been completely dispersed into the matrix and therefore were not available for surface spectroscopic analysis. Hydrolysis due to hydrogen bonding or nucleophilic attack by water molecules
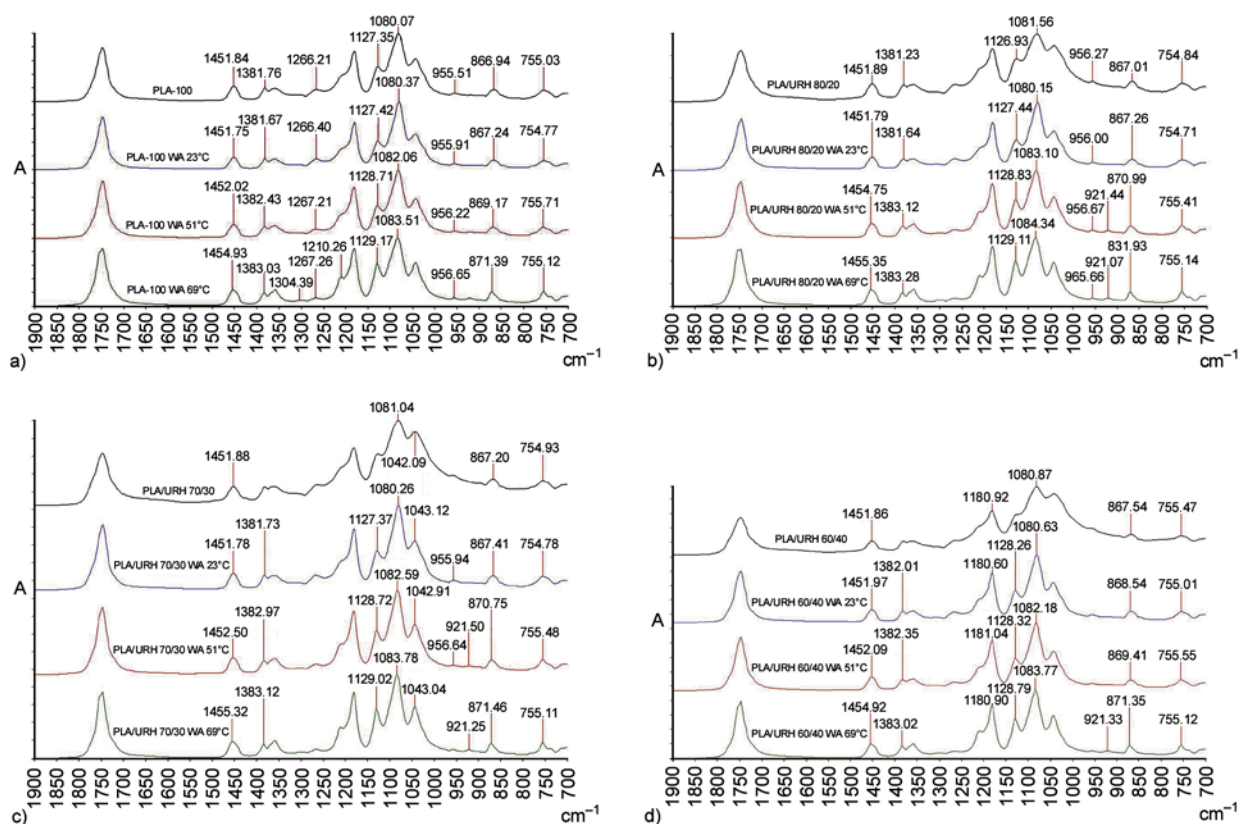
Figure 4. a) Infrared spectra of PLA products due to hydrolysis at different temperatures, b) Infrared spectra of PLA/URH 80/20 composites due to hydrolysis at different temperatures, c) Infrared spectra of PLA/URH 70/30 composites due to hydrolysis at different temperatures, d) Infrared spectra of PLA/URH 60/40 composites due to hydrolysis at different temperatures

at the –C–O– ester bond tends to shift ester bands to lower frequencies. The results show that the carbonyl group C=O band ascribed to ester bond did not shift. The only notable change shown on this band is a slight increase in intensity by 1.03, 1.23 and 1.14 relative to control PLA products. This change may be associated with stretching vibration that favored the hydrolysis of the polymer chains. Although a fraction of MA was used as a grafting agent between the polymer and the rice hulls, its presence could not be detected by an infrared spectroscopy in the composites between 1700 and 1600 cm^{-1}. This could be attributed to inadequate dispersion of the little proportion of MA used in the preparation of the PLA/RH composites.

Further changes in the structure of PLA due to hydrolysis and water absorption were noted in the regions of 1451–1454 cm^{-1}, 1381–1383 cm^{-1}, 1264–1267 cm^{-1}, 1210 cm^{-1}, 1180–1181 cm^{-1}, 1127–1129 cm^{-1}, 1080–1083 cm^{-1}, 955–956 cm^{-1}, 921 cm^{-1} absorptions. The 1451 cm^{-1} band, which is attributed to asymmetric stretching of methyl –CH$_3$ group, shifted slightly to higher frequency by 3 cm^{-1} at higher hydrolysis temperatures. This is associated with changes of the hydrophobic properties of the PLA, which is conferred by the –CH$_3$ group, during hydrolysis. The band at 1375 cm^{-1} assigned to symmetric deformation of methyl –CH$_3$ group occurred at 1381 cm^{-1} and also shifted slightly to higher frequencies by 2 cm^{-1} with the increase of hydrolysis temperatures. A similar trend associated with this group can be observed at ~1264 cm^{-1}. However, their intensities decreased slightly at higher water absorption temperatures. The 1080 cm^{-1} ascribed to symmetric stretching of –C–O– band of ester groups also shifted slightly to higher frequencies by 3 or 4 cm^{-1} due to hydrolysis at higher temperatures. This change can be attributed to strengthening of the ester bond against hydrolysis.

3.4. Molecular weight degradation analysis

Table 4 shows the results of molecular weights ($\overline{M}_w$, $\overline{M}_n$) analysis of PLA that had been subjected to water absorptions at 23, 51 and 69°C. It is shown that the weight average molecular weight ($\overline{M}_w$) and the number average molecular weight ($\overline{M}_n$) of control PLA were around 153.1 and 93.9 kDa, respectively. After 30 days of water absorption at 23°C,

Table 4. Molecular weights degradation of PLA due to water absorption at different temperatures

Product	Temperature [°C]	$\overline{M}_w$ [kDa]	$\overline{M}_n$ [kDa]	$\overline{M}_w/\overline{M}_n$
PLA-100 (control)	–	153.13	93.89	1.631
PLA-100WA23°C	23	156.89	82.80	1.895
PLA-100WA51°C	51	42.12	20.38	2.067
*PLA-100WA69°C	69	10.70	5.31	2.016
	Low MW peak	4.62	3.14	1.471

*Two peaks observed

increased slightly by 3.8 kDa while $\overline{M}_w/\overline{M}_n$ also increased. The increase of $\overline{M}_w/\overline{M}_n$ implies that the molecular weight distribution was broadened due to the increase of high molecular weight fractions. Hydrolysis and cleavage of ester bonds of PLA is said to occur randomly where longer chains of the polymer become more susceptible to cleavage than the shorter chains [16]. The reduction in $\overline{M}_n$ observed with a subsequent increase of $\overline{M}_w$ could be ascribed to partial cleavage of some high molecular weight chains and recombination reactions leading to addition of high molecular weight fractions in the polymer. Kale *et al.* [17] ascribed a similar change during their study on composting of commercial PLA products to the cross-linking or recombination reactions. However, we cannot ascertain if there was any cross-linking reaction in these products at this condition. It is shown further that as the polymer was subjected to hydrolysis at higher temperatures, both $\overline{M}_w$ and $\overline{M}_n$ decreased significantly. This was attributed to an increase of low molecular fragments in the polymer with subsequent broadening of molecular distributions as shown by an increase of $\overline{M}_w/\overline{M}_n$. This change was associated with more hydrolysis of ester bonds and more cleavage of the chains as the polymer was heated in water at higher temperatures. The cleavage was more significant at 69°C where the $\overline{M}_w$ of the polymer was reduced to 10.7 kDa in less than 9 days compared to 42.1 kDa at 51°C in 25 days. Despite exhibiting abnormal hardness and slight increase in the weight after re-drying, the PLA that was immersed at 51°C only showed the reduction of molecular weights and broadening of the molecular weight distribution peak. These changes are also related to the cleavage of the molecular weight chains with subsequent increase of low molecular weight fractions in the polymer.

3.5. Morphological analysis

SEM results for the morphological analysis of fracture surfaces of PLA and PLA/RH composites after water absorption at 23, 51 and 69°C are shown in Figures 5–8. It can be shown in Figures 5a to 5b that PLA was not substantially affected physically during water absorption at 23 and 51°C for 30 and 25 days, respectively. However, this polymer was seriously deteriorated and shattered only in 9 days after being subjected to hydrolysis in water at 69°C. This is explained by random shattering of the polymer matrix as shown in Figure 5c, which indicates that the polymer was fragile. It is shown further that the deterioration of the matrix in the composites was influenced by the immersion temperature as well as the contents of rice hulls. At 23°C, the matrix did not indicate any physical deterioration as shown on the fracture surface. Fractures in these products were due to breaking of the rice hulls (RH) and the matrix (M) or due to partial debonding (Figures 6 to 8). However, significant development of embrittlement in the polymer matrix (M) especially at higher immersion temperatures was observed. The matrix was made fragile while most of the rice hulls (RH) remained intact as shown in Figures 6b and 6c, 7b and 7c, and 8b and 8c. Figures 9a and 9b suggest that the rice hulls in some way enhanced the deterioration of the matrix. This is shown by the develop-

Figure 5. SEM image of the fracture surface of PLA after water absorption at (a) 23°C-30 days, (b) 51°C-25 days and (c) 69°C-9 days
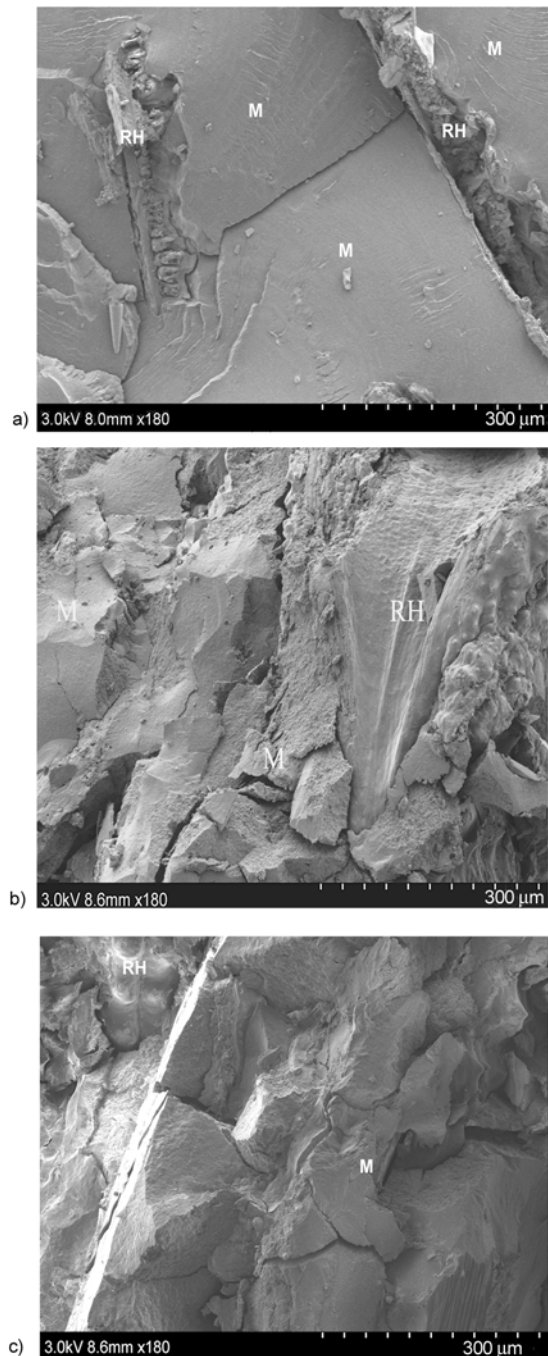
Figure 6. SEM image of the fracture surface of PLA/URH 80/20 composite after water absorption at (a) 23°C-30 days, (b) 51°C-25 days and (c) 69°C-9 days
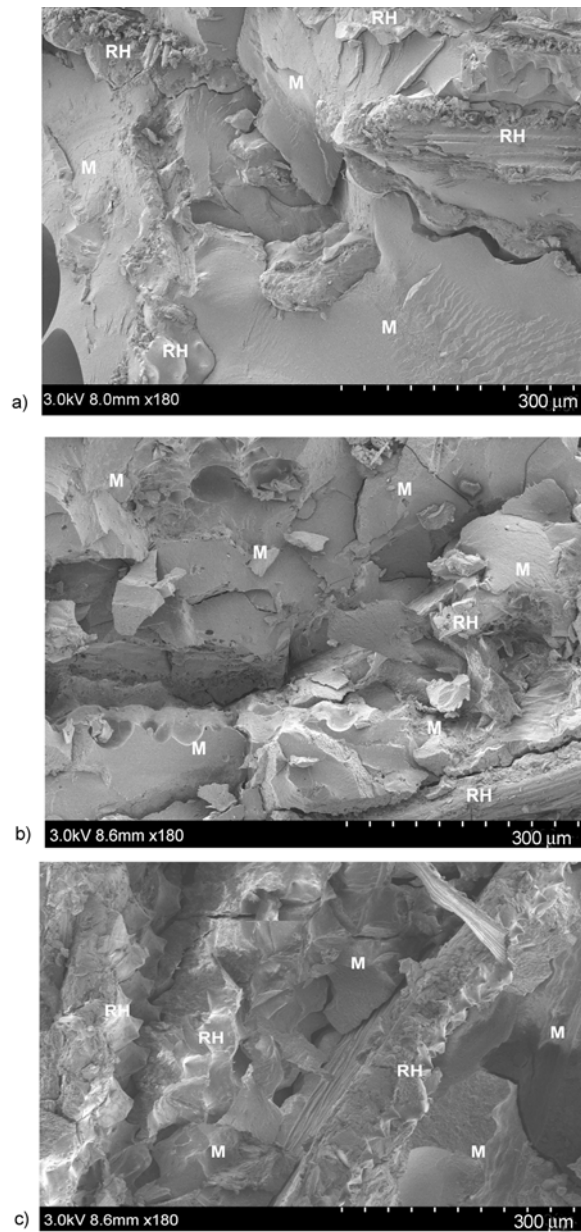
Figure 7. SEM image of the fracture surface of PLA/URH 70/30 composite after water absorption at (a) 23°C-30 days, (b) 51°C-25 days and (c) 69°C-9 days
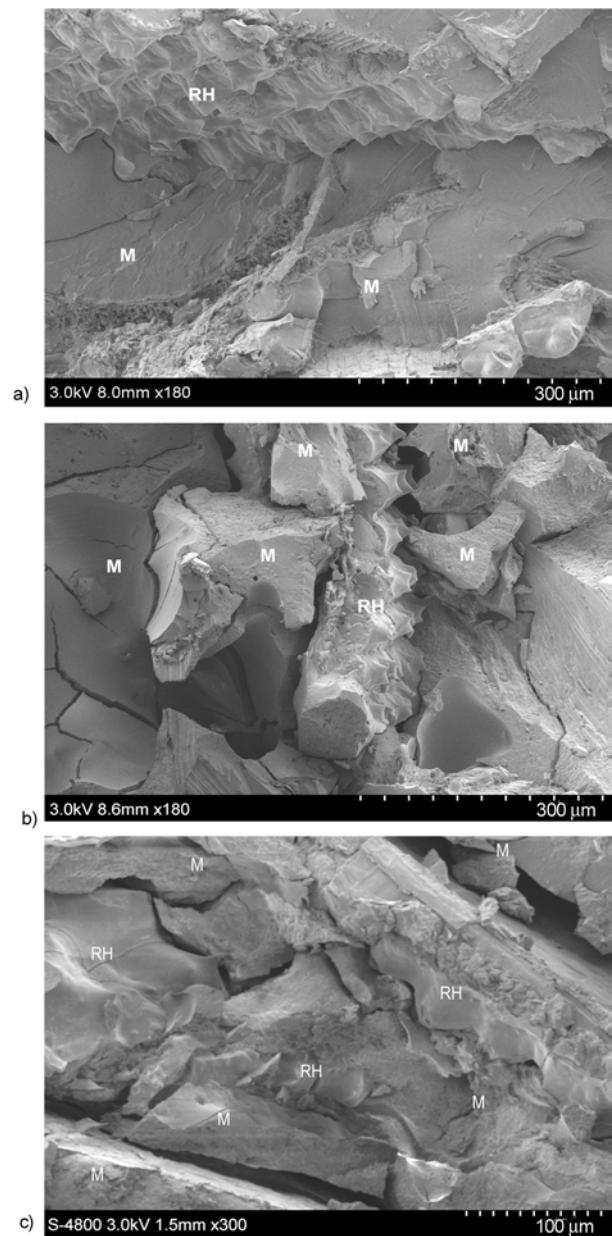
Figure 8. SEM image of the fracture surface of PLA/URH 60/40 composite after water absorption at (a) 23°C-30 days, (b) 51°C-25 days and (c) 69°C-9 days
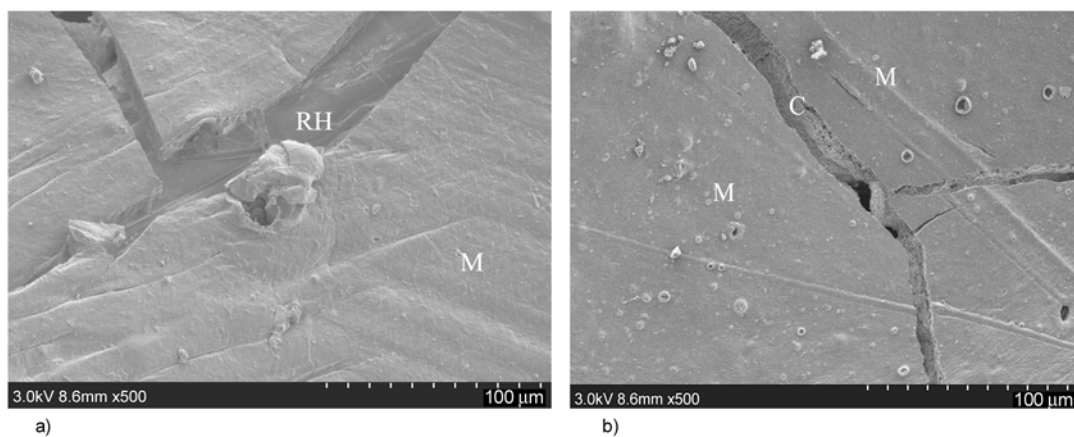
Figure 9. Surface of (a) PLA/URH 60/40 and (b) PLA/URH 70/30 composites after water absorption at 51°C-25 days

ment of cracks (C) on the surface of the composite, which were most probably attributed to the swelling of the rice hulls (RH) as shown in Figure 9a. It might have been the swelling of the rice hulls during water absorption that accelerated the fragmentation of the weakened matrix.

4. Conclusions

Degradation of PLA and PLA/RH composites due to hydrolysis in water was influenced significantly by the temperature of water. At the mesophilic temperature~23°C, these products were fairly stable. They absorbed between 0.87 and 9.2% water in 30 days with no appreciable physical and chemical changes as revealed by SEM, infrared spectroscopy and SEC, respectively. However, close to the glass transition temperature (T_g) of PLA at 51°C, PLA started to show remarkable physical and chemical deteriorations. The rate of water diffusion and degradation in the composites increased significantly above the T_g (69°C) leading to saturation in less than 9 days. This was accompanied with the development of fragility in the material as revealed by SEM and an increase in crystallinity by 24%. The T_g also reduced significantly by 13°C whereas the average molecular weight of the polymer decreased to ~42 100 and ~10 700 Da at 51 and 69°C, respectively. These changes were associated with the hydrolytic degradation of PLA. Rice hulls in some way enhanced indirectly the disintegration of the matrix during their water absorption and swelling as was suggested by SEM. The degradation of PLA due to hydrolysis in water was also demonstrated by the reduction of the thermal stability of its products.

Acknowledgements

References

[1] García M., Garmendia I., García J.: Influence of natural fiber type in eco-composites. Journal of Applied Polymer Science, **107**, 2994–3004 (2008).
DOI: 10.1002/app.27519

[2] Taib R. M., Ramarad S., Mohd Ishak Z. A., Todo M.: Properties of kenaf fiber/polylactic acid biocomposites plasticized with polyethylene glycol. Polymer Composites, **31**, 1213–1222 (2009).
DOI: 10.1002/pc.20908

[3] Bax B., Müssig J.: Impact and tensile properties of PLA/cordenka and PLA/flax composites. Composites Science and Technology, **68**, 1601–1607 (2008).
DOI: 10.1016/j.compscitech.2008.01.004

[4] Hu R., Lim J-K.: Fabrication and mechanical properties of completely biodegradable hemp fiber reinforced polylactic acid composites. Journal of Composites Materials, **41**, 1655–1669 (2007).
DOI: 10.1177/0021998306069878

[5] Lee S-H., Ohkita T., Kitagawa K.: Eco-composite from poly(lactic acid) and bamboo fiber. Holzforschung, **58**, 529–536 (2004).
DOI: 10.1515/HF.2004.080

[6] Tokoro R., Vu D. M., Okubo K., Tanaka T., Fujii T., Fujiura T.: How to improve mechanical properties of polylactic acid with bamboo fibers. Journal of Materials Science, **43**, 775–787 (2008).
DOI: 10.1007/s10853-007-1994-y

[7] Huda M. S., Drzal L. T., Misra M., Mohanty A. K.: Wood-fiber-reinforced poly(lactic acid) composites: Evaluation of the physicomechanical and morphological properties. Journal of Applied Polymer Science, **102**, 4856–4869 (2006).
DOI: 10.1002/app.24829

[8] Ganster J., Fink H-P.: Novel cellulose fibre reinforced thermoplastic materials. Cellulose, **13**, 271–280 (2006).
DOI: 10.1007/s10570-005-9045-9

[9] Ahmad I., Abu Bakar D. R., Mokhilas S. N., Ram A.: Direct usage of products of poly(ethylene terephthalate) glycolysis for manufacturing of rice hull/unsaturated polyester composite. Iranian Polymer Journal, **16**, 233–239 (2007).

[10] Gerardi V., Minelli F., Viggiano D.: Steam treated rice industry residues as an alternative feedstock for the wood based particleboard industry in Italy. Biomass and Bioenergy, **14**, 295–299 (1998).
DOI: 10.1016/S0961-9534(97)10042-3

[11] Ndazi B. S., Karlsson S., Tesha J. V., Nyahumwa C. W.: Chemical and physical modifications of rice husks for use as composite panels. Composites Part A: Applied Science and Manufacturing, **38**, 925–935 (2007).
DOI: 10.1016/j.compositesa.2006.07.004

[12] Rozman H. D., Musa L., Abubakar A.: Rice husk–polyester composites: The effect of chemical modification of rice husk on the mechanical and dimensional stability properties. Journal of Applied Polymer Science, **97**, 1237–1247 (2005).
DOI: 10.1002/app.21268

[13] Shukla B. D., Ojha T. P., Gupta C. P.: Mechanical and physical properties of huskboards. Agricultural Mechanization in Asia, Africa and Latin America, **16**, 53–60 (1985).

[14] Vroman I., Tighzert L.: Biodegradable polymers. Materials, **2**, 307–344 (2009).
DOI: 10.3390/ma2020307

[15] Kale G., Auras R., Singh S. P.: Comparison of the degradability of poly(lactide) packages in composting and ambient exposure conditions. Packaging Technology and Science, **20**, 49–70 (2007).
DOI: 10.1002/pts.742

[16] Kale G., Auras R., Singh S. P.: Degradation of commercial biodegradable packages under real composting and ambient exposure conditions. Journal of Polymer and Environments, **14**, 317–334 (2006).
DOI: 10.1007/s10924-006-0015-6

[17] Kale G., Auras R., Singh S. P., Narayan R.: Biodegradability of polylactide bottles in real and simulated composting conditions. Polymer Testing, **26**, 1049–1061 (2007).
DOI: 10.1016/j.polymertesting.2007.07.006

[18] Yew G. H., Mohd Yusof A. M., Mohd Ishak Z. A., Ishiaku U. S.: Water absorption and enzymatic degradation of poly(lactic acid)/rice starch composites. Polymer Degradation and Stability, **90**, 488–500 (2005).
DOI: 10.1016/j.polymdegradstab.2005.04.006

[19] Mitaya T., Masuko T.: Crystallization behaviour of poly(L-lactide). Polymer, **39**, 5515–5521 (1998).
DOI: 10.1016/S0032-3861(97)10203-8

[20] Fischer E. W., Sterzel H. J., Wegner G.: Investigation of the structure of solution grown crystals of lactide copolymers by means of chemical reactions. Colloid and Polymer Science, **251**, 980–990 (1973).
DOI: 10.1007/BF01498927

[21] Jang W. Y., Shin B. Y., Lee T. J., Narayan R.: Thermal properties and morphology of biodegradable PLA/starch compatibilized blends. Journal of Industrial Engineering and Chemistry, **13**, 457–464 (2007).

[22] Jamshidi K., Hyon S-H., Ikada Y.: Thermal characterization of polylactides. Polymer, **29**, 2229–2234 (1988).
DOI: 10.1016/0032-3861(88)90116-4

[23] Hakkarainen M., Albertsson A-C., Karlsson S.: Weight losses and molecular weight changes correlated with the evolution of hydroxyacids in simulated *in vivo* degradation of homo- and copolymers of PLA and PGA. Polymer Degradation and Stability, **52**, 283–291 (1996).
DOI: 10.1016/0141-3910(96)00009-2

[24] Horowitz H., Metzger G.: A new analysis of thermogravimetric traces. Analytical Chemistry, **35**, 1464–1468 (1963).

Influence of nano-AlN particles on thermal conductivity, thermal stability and cure behavior of cycloaliphatic epoxy/trimethacrylate system

*J. H. Yu, J. K. Duan, W. Y. Peng, L. C. Wang, P. Peng, P. K. Jiang**

Department of Polymer Science and Engineering and Shanghai Key Lab of Electrical Insulation and Thermal Aging, Shanghai Jiao Tong University, Shanghai 200240, People's Republic of China

Abstract. We have prepared a series of nano-sized aluminium nitride (nano-AlN)/cycloaliphatic epoxy/trimethacrylate (TMPTMA) systems and investigated their morphology, thermal conductivity, thermal stability and curing behavior. Experimental results show that the thermal conductivity of composites increases with the nano-AlN filler content, the maximum value is up to 0.47 W/(m·K). Incorporation of a small amount of the nano-AlN filler into the epoxy/TMPTMA system improves the thermal stability. For instance, the thermal degradation temperature at 5% weight loss of nano-AlN/epoxy/TMPTMA system with only 1 wt% nano-AlN was improved by ~8ºC over the neat epoxy/TMPTMA system. The effect of nano-AlN particles on the cure behavior of epoxy/TMPTMA systems was studied by dynamic differential scanning calorimetry. The results showed that the addition of silane treated nano-AlN particles does not change the curing reaction mechanism and silane treated nano-AlN particles could bring positive effect on the processing of composite since it needs shorter pre-cure time and lower pre-temperature, meanwhile the increase of glass transition temperature of the nanocomposite improves the heat resistance.

1. Introduction

In recent years, polymer composite materials with excellent thermal conductivity have attracted increasing attention because the amount of heat generated in electronic devices is getting larger and larger, leading manufactures to seek for new composites that can remove the heat efficiently form the devices [1, 2]. Epoxy resins are widely used as matrices in the manufacturing process of reinforced composites, adhesives and surface coatings, high voltage electrical insulation materials, electronic components and packaging because of their high strength, stiffness, good thermal stability, and excellent adhesion and electrical insulating properties [3–5]. As the thermal conductivity of epoxy systems is very low (about 0.2 W/(m·K)), thermally conductive fillers are added to these composites in order to dissipate the heat generated in electronic devices [6]. Various kinds of fillers, such as metals and metal oxides [7, 8], aluminum nitride (AlN) [9-11], boron nitride (BN) [12], and silicon carbide (SiC) [13] have been applied to prepare thermally conductive polymer composites. Among them, AlN is a nontoxic, low cost substance, readily available as high purity powder. On the one hand, because of the low coefficient of thermal expansion (CTE) and the high thermal conductivity (150–300 W/(m·K)) of AlN, AlN filled composite materials have attracted much attention in an attempt to reduce the CTE and thermal resistivity of polymer composites [14].

*Corresponding author, e-mail: pkjiang@sjtu.edu.cn

In a previous paper, our research group have reported the preparation and characterization of epoxy/trimethylol-1,1,1-propane trimethacrylate (TMPTMA) system [15, 16]. In this study, nano-AlN particles with an average particle size of 50 nm were used with epoxy/TMPTMA system as the base system. Nano-AlN particles were pretreated with a silane coupling agent, which was employed to enhance the compatibility between the nano-AlN particles and the epoxy/TMPTMA system, as well as to prevent the agglomeration of the nano-AlN particles. By studying thermal conductivity, thermal stability, and curing behavior of nano-AlN/epoxy/ TMPTMA system, we expect to learn comprehensive and in-depth understanding of the thermophysical properties and curing behavior of this system.

2. Experimental
2.1. Materials
The raw materials and corresponding specifications of epoxy resin, curing agent, latent accelerator, modifier agent, initiator and filler are given in Table 1.

2.2. Surface modification of nano-AlN particles
The nano-AlN particles were dried in a vacuum oven at 180ºC for 24 h and appropriate amount of the silane (0.5–1 wt% based on the weight of AlN

particles) was added into a 500 ml three-necked flask, equipped with a mechanical stirrer and a reflux condenser, and mixed in high purity acetone (5 wt% based on the weight of silane) by stirring at 110–120ºC for at least 4 h. After filtration, the silane treated powders were dried in a vacuum oven at 120ºC for 2 h to remove the solvent and the silane molecules that were not well bonded and thus would not significantly contribute to the joint strength. The probable schematic reaction between nano-AlN particles and GPTMS is indicated in Figure 1.

2.3. Sample preparation
Firstly, epoxy resin (100 parts by weight [pbw]) and latent accelerator (0.5 pbw) were weighing and mixed vigorously at 160ºC for about 10 min until the latent accelerator was dissolved completely in the epoxy resin. Then, the blends of epoxy resin and accelerator were rapidly cooled to the ambient temperature; this was followed by the addition of 90 pbw curing agent and suitable amounts of the initiator and modifier agent mixing for about 30 min. At last a specified quantity of silane treated nano-AlN particles were added into the blend and the mixture was dispersed by sonication for 1 hour at ambient temperature. The specimens with the compositions listed in Table 2 in detail.
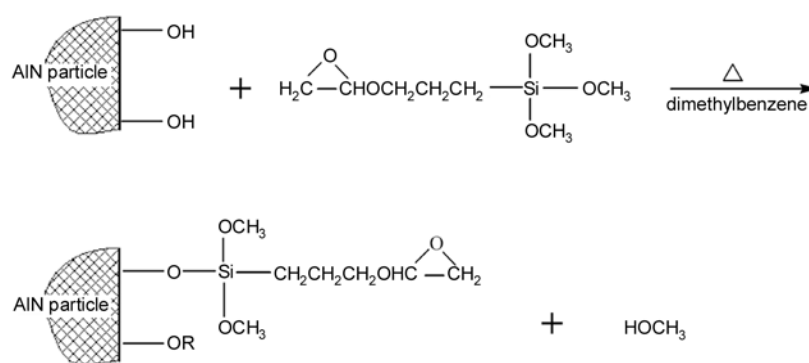

Figure 1. The schematic reactions of AlN particles and GPTMS

Table 1. The detailed raw materials

Materials	Abbreviation	Purity	Supplier
3, 4-epoxycyclohexylmethy-(3′, 4′-epoxy)cyclohexane carboxylate	CER	>98%	DOW Chemical, USA
methyl-hexahydrophthalic anhydride	MeHHPA	>98%	Shanghai Li Yi Science & Technology Development Co. Ltd., China
neodymium (III) acetylacetonate	Nd(III)acac	>99%	Qinyang Tianyi Chemical Co., Ltd., China
trimethylolpropane trimethacrylate	TMPTMA	>98%	Jinshi Tech-development Co., Ltd., China
dicumyl peroxide	DCP	>99%	Qinyang Tianyi Chemical Co., Ltd., China
3-glycidoxypropyltrimethoxy silane	GPTMS	>98%	Dow Corning Company, USA
aluminum nitride	AlN	>99%	Hefei Kaier Nanometer Technology Development Co., Ltd., China

Table 2. Formulation of experiment (parts by weight [pbw])

System	CER	MeHHPA	Nd(III)AcAc	TMPTMA	DCP	nano-AlN
A1	100	90	0.5	20	0.2	0
A2	100	90	0.5	20	0.2	1
A3	100	90	0.5	20	0.2	3
A4	100	90	0.5	20	0.2	5
A5	100	90	0.5	20	0.2	10
A6	100	90	0.5	20	0.2	15
A7	100	90	0.5	20	0.2	20

2.4. Characterizations and measurements

Field emission scanning electron microscope (FE-SEM, JEOL JEM-7401, Tokyo, Japan) was used to observe the dispersion of the nanoparticles in the composite samples. Samples were sputtered with thin layers of gold to avoid the accumulation of charge.

Transmission electron microscopy (TEM, JEOL JEM-2100, Tokyo, Japan) was utilized to analyze the morphology of the silane treated AlN particles at 120 kV under low-dose conditions. The AlN/acetone solution was dropped on a copper grid and subsequently the solvent was evaporated in an oven.

FTIR spectrum was recorded in KBr pellets on a Paragon 1000 (Perkin Elmer, Inc.,USA) using a resolution of 4 cm^{-1}, and transmission measurements was employed.

LFA 447 Nanoflash (NETZSCH, Germany) was employed to automatically determine the thermal conductivity according to ASTM E1461, using the measured heat capacity and thermal diffusivity, with separately entered density data. Samples were prepared in cylindrical shape of 12.7 mm in diameter and 1.0–2.0 mm in thickness.

TGA (NETZSCH TG 209 F3, Germany) was used to investigate the thermal stability of the composites. The weight samples was approximately 10 mg and all the measurements were carried out under nitrogen atmosphere. Dynamic runs were carried out from 50 to 700ºC at a heating rate of 10ºC/min. Dynamic DSC (NETZSCH DSC 200 F3, Germany) measurements were performed at different heating rates of 5, 10, 15, and 20 K/min over a temperature range of 30–300ºC. The reaction was considered to be complete when the rate curve leveled off to a baseline. The exotherm was measured under a nitrogen flow rate of 10 ml/min. The exotherm baseline was corrected via data in chamber. The cured sample was left in the DSC cell and cooled to 30ºC, and then the cured sample was scanned at 20 K/min to determine the glass transition temperature (T_g) of the reacted product. The initial temperature of the heat flow step of the second diagram was taken to be the T_g. The total area under the exotherm curve, based on the extrapolated baseline at the end of the reaction, was used to calculate the heat of reaction, ΔH [J/g].

3. Results and discussion
3.1. AlN characterization

In this study, to enhance the dispersion and interfacial adhesion between the AlN nanoparticles and epoxy matrix, a silane monomer, 3-glycidoxypropyl trimethoxy silane (GPTMS) has been chosen as a coupling agent to functionalize AlN nanoparticles. The chosen silane has two different functional groups, one of which is reactive with the epoxy resin and the other reacts with the surface of AlN nanoparticles. GPTMS can hydrolyze in aqueous solution (e.g. the acetone as used in the present study, where a small amount of water is present) and its methoxy groups will transform into hydroxyl groups. Afterwards these hydroxyl groups react with those on the surface of AlN nanoparticles, then the active coating of nano-AlN particles are obtained. The possible reaction scheme between GPTMS and nano-AlN particles can be seen in Figure 1. The epoxide groups at the other ends of silane can react with the epoxy during the curing process. The dispersion of AlN nanoparticles is thus enhanced by the silane coating. Thus, the interacting force between the AlN nanoparticles and epoxy matrix is improved because the chemical bonding between the AlN nanofillers and the epoxy matrix is enhanced.

Microscopy is very useful for the characterization of generated filler structures. The TEM images obtained for the as received nano-AlN and silane treated nano-AlN powders are compared in Figure 2. Comparison of TEM images (a) and (b) shows that silane treated nano-AlN particles display that
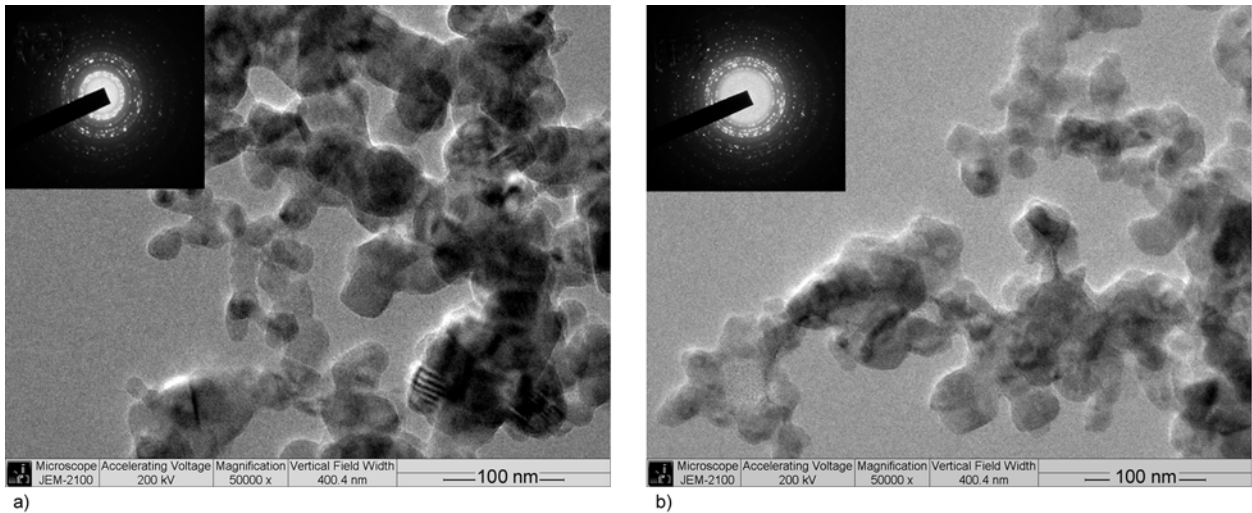
Figure 2. TEM micrograph and corresponding SAED patterns (insets) of (a) as received nano-AlN and (b) silane treated nano-AlN

the surface modification dramatically affects the aggregate particle size. The inset in Figure 2 illustrates the identical selected area electron diffraction (SAED) patterns for both AlN powders, which indicates that the silane treatment has modified only the nano-AlN particle surface leaving the particle core structure intact.

As shown in Figure 3a, the as received nano-AlN particles show a much strong absorption at $v = 3200–3500$ cm^{-1}, which may be attributed to hydroxyl group (–OH) peak stretching. The band at $v = 1641$ cm^{-1} is attributed to –NH– group vibration, which indicates that nano-AlN particles have the higher affinity and reactivity to moisture and water. Therefore, the surface treatment has been undertaken to prevent the nano-AlN particles from hydrolyzing. The spectra of silane-modified AlN nanoparticles are very similar to those of raw nano-

AlN particles, but some differences can still be detected. From Figure 3b, the stretching vibration band of ether group is found in the region 1050–1150 cm^{-1}. The band at 2990 cm^{-1}, attributed to methylene groups, is stronger than that of the raw nano-AlN particles. The absorption bands of epoxy groups at $v_{as}(CH_2) = 3003$ cm^{-1}, $v_b(CH_2) = 1479$ cm^{-1}, $v(C–O) = 1225$ cm^{-1} can be also observed. In addition, the absorption intensity of the bands at $v = 3200–3500$ cm^{-1} and $v = 1641$ cm^{-1}, which are assigned to hydroxyl group and amine group, respectively, can be found to apparently decrease. These changes of characteristic peaks indicate that GPTMS has already been grafted successfully on the surface of nano-AlN particles.

The morphology of the fractured surfaces for A1 and A4 are shown in Figures 4a and 4b, respectively. In the case of the neat epoxy/TMPTMA system, the fractured paths of river-like patterns can be observed, indicating brittle fracture. The nanocomposite fails in brittle manner and silane treated nano-AlN particles are seen to be separated and uniformly embedded in the matrix. The inset in Figure 4b shows that no obvious naked particles and inorganic clusters are present, indicating good interfacial adhesion between the particles and polymer matrix after silane pretreatment. The scheme for epoxy/TMPTMA system filled with silane treated nano-AlN is shown in Figure 4c. It represents that the covalent bridge bonds are formed between silane treated nano-AlN fillers and the epoxy resin.
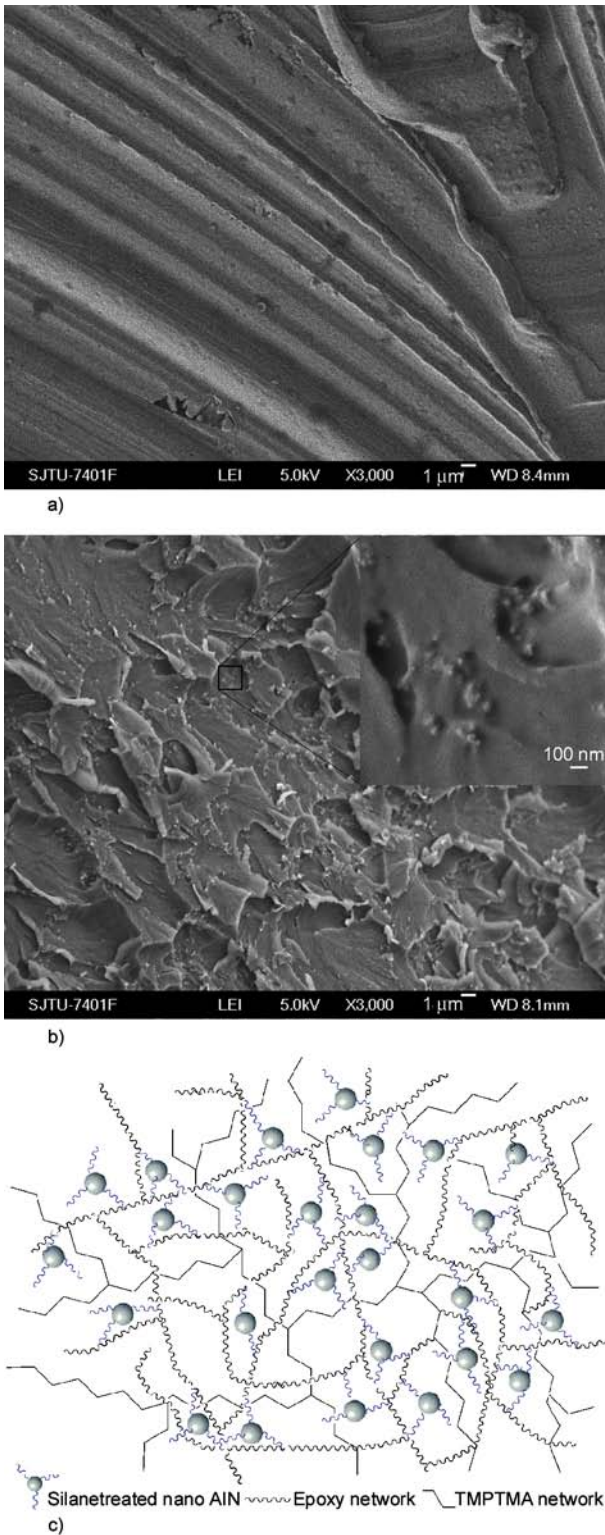

Figure 3. FT-IR spectrum of as received nano-AlN (a) and silane treated nano-AlN (b)

a)

b)

Silanetreated nano AlN ~~~~~ Epoxy network ___ TMPTMA network

c)

Figure 4. FE-SEM micrograph of fracture surface of (a) A1, (b) A4, and (c) scheme for epoxy/TMPTMA system filled with silane treated nano-AlN. The inset in (b) is a magnificent showing the draw part.

3.2. Thermal conductivity

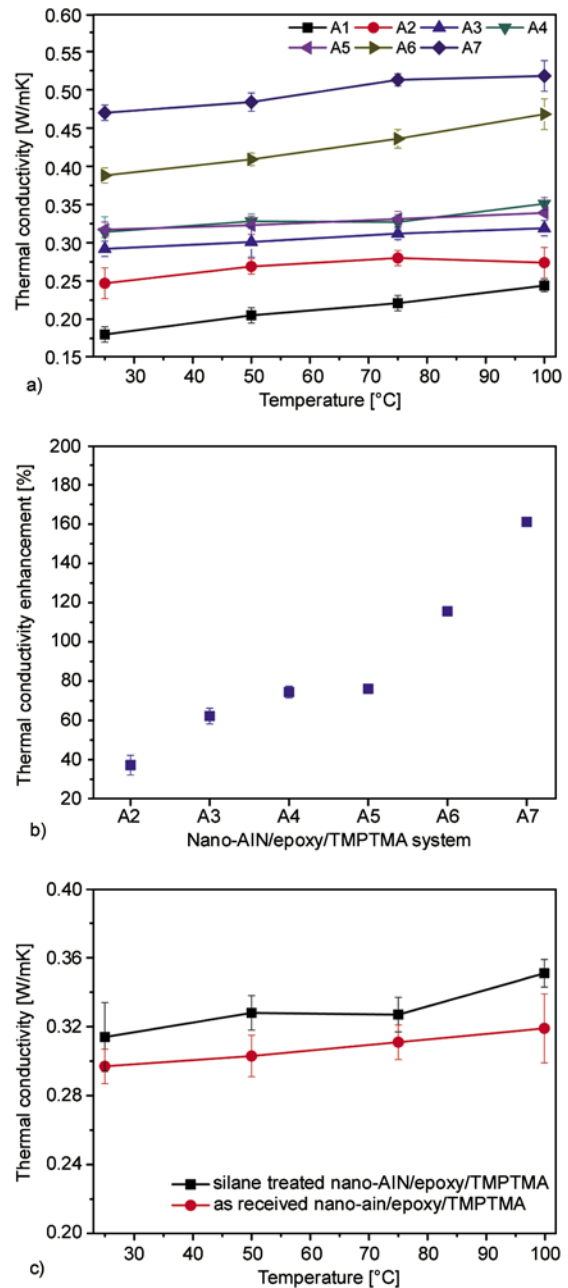Figure 5a shows the variation of thermal conductivity of nano-AlN/epoxy/TMPTMA system as a func-

a)

b)

c)

Figure 5. (a) thermal conductivity of nano-AlN/epoxy/ TMPTMA system. (b) thermal conductivity enhancement of nano-AlN/epoxy/TMPTMA system comparison with neat epoxy/TMPTMA system at 25ºC. (c) thermal conductivity of silane treated nano-AlN/epoxy/TMPTMA system and as received nano-AlN/epoxy/TMPTMA system with 5 wt% AlN loading.

tion of temperature. In the range from 25 to 100ºC, the absolute thermal conductivity of the nano-AlN/ epoxy/TMPTMA system increases, which is similar to the conclusion of Timofeeva *et al.* [8]. The experimental data also display that the thermal conductivity of nano-AlN/epoxy/TMPTMA system increased

with increasing the nano-AlN filler loading. The thermal conductivity enhancement for nano-AlN/ epoxy/TMPTMA system containing different content nano-AlN filler is presented in Figure 5b. Here, λ enhancement (%) = $(\lambda_1 - \lambda_0)/\lambda_0$, where λ_0 is the thermal conductivity of the neat epoxy/ TMPTMA system (0.18 W/(m·K)) and λ_1 is the thermal conductivity of the nanocomposites due to the addition of nano-AlN filler at 25ºC. The results show that there is a 161% enhancement in thermal conductivity for A7. For the lower nano-AlN filler content (less than the percolation threshold), the main reason is attributed to that the covalent bridges minimize the interfacial phonon scattering and decrease the interface heat resistance by surface modification particles/epoxy resin. Various mechanisms have been presented to explain the increase of the effective thermal conductivity of composites containing different nanoparticles, such as interface interaction at the particle/resin interface [17], the nature of heat transport in the nanoparticles and the effects of nanoparticle clustering [18]. Based on our experimental results, it was concluded that the three dimensional network formed by the silane treated nano-AlN/epoxy dominates the thermal conduction mechanism, which leads to the nanocomposite with excellent thermal conductivity. Meanwhile, thermal conduction chains, the prevailing means to conduct thermal diffusion in the large-size filler/resin, are the secondary means to conduct thermal diffusion in the nanocomposites [13]. Figure 5c shows the detailed information for comparing the thermal conductivity of as received nano-AlN/epoxy/TMPTMA system and silane treated nano-AlN/epoxy/ TMPTMA system with 5 wt% AlN loading. We can see that the thermal conductivity of silane treated

nano-AlN/epoxy/TMPTMA system is higher than that of as received nano-AlN/epoxy/TMPTMA system. It can be inferred that silane treatment is an effective approach to increase the thermal conductivity of nano-AlN/epoxy/TMPTMA system. The understanding of interface structure between nano-AlN fillers and the resin enables us to understand the thermal conduction mechanisms, therefore guides us to choose proper filler surface treatment approaches to gain excellent thermal conductivity. Furthermore, it also leads us to design the novel nanocomposites with high thermal conductivity.

3.3. Thermal stability

Thermal stability is very important for polymeric materials. In present study, the thermal stability of epoxy/TMPTMA system incorporated with the silane treated nano-AlN filler has been investigated by TGA by using heating rate of 10ºC/min. Figure 6 shows the TG and DTG thermograms of the nano-AlN/epoxy/TMPTMA system. The weight loss of the system due to degradation is monitored as a function of temperature. The characteristic thermal parameters selected were the temperature for 5% and 10% weight loss and maximum degradation temperature, which is the highest thermal degradation rate temperature. The results are summarized in the Table 3. In case of neat epoxy/TMPTMA system, there is almost no weight loss up to 250ºC, but the degradation rate becomes very quick beyond that temperature, the main decomposition is degraded abruptly between 250ºC and 410ºC. There exists a second decomposition reaction between 410 and 500ºC, which could be assigned to the decomposition reaction of TMPTMA network. The first decomposition reaction could be attributed to the decom-
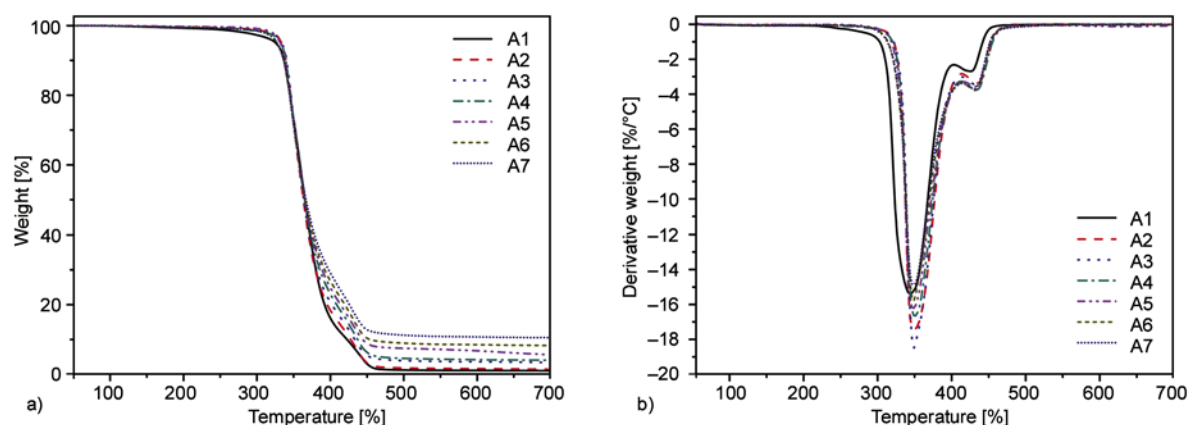

Figure 6. TGA (a) and DTG (b) curves of the nano-AlN/epoxy/TMPTMA system

Table 3. Degradation properties of nano-AlN/epoxy/ TMPTMA system

Sample	Weight loss temperature [ºC]			Residue [%]
	$T_{5\%}$	$T_{10\%}$	T_{max}	
A1	326	336	340	0.9
A2	334	340	349	1.5
A3	334	340	349	3.4
A4	331	339	350	4.1
A5	331	339	348	5.7
A6	328	337	348	8.3
A7	329	337	349	10.5

position reaction of epoxy network. This was in good agreement with the results from our previous study [15, 16]. In the case of A2, incorporation of this small amount of the nano-AlN filler into the epoxy/TMPTMA system slightly improves the thermal stability because it increase the temperature at 5% weight loss by about 8ºC. The maximum degradation temperature (T_{max}) also increased by addition of the nano-AlN filler. However, higher loading of the nano-AlN filler does not lead to any further improvement of the thermal stability. The experimental results also show that the residual weight percent at 700ºC of the nano-AlN/epoxy/ TMPTMA system increases upon addition of increasing amount of nano-AlN filler.

3.4. Curing behavior

In order to understand the influence of the silane treated nano-AlN filler on the epoxy/TMPTMA system in-depth, the curing behavior of all systems were investigated. The curing curves of A1 and A4 systems are shown in Figure 7. Shift of the DSC exothermic peaks to lower temperatures is observed in the presence of silane treated nano-AlN particles, illuminating that silane treated nano-AlN particles filled epoxy is obviously faster in reaching the

exothermic peak than neat epoxy/TMPTMA system. The curing mechanism of epoxy/TMPTMA system involves three stages consisting of radical reaction of TMPTMA, the adduct, and etherification reactions of epoxy/MeHHPA. The third stage (i.e., the etherification reaction) dominates the cure process and is discussed mainly in this study.

The exothermic peak temperatures (T_p) and the heats of the reaction (ΔH) for A1-A7 systems are summarized in Table 4. From Table 4, it is clear that silane treated nano-AlN particles act as catalyst and facilitate the curing at the initial curing stage by lowering T_p. For the development of the composites, the cure acceleration effect caused by silane treated nano-AlN particles could bring positive effect on the processing of composite since it needs shorter pre-cure time or lower pre-temperature. In this study, this accelerating effect might also be partially attributed to the remaining hydroxyl groups (–OH) and amino groups (–NH$_2$) on the surface of nano-AlN particles since the epoxy/TMPTMA system was used as the martrix. The total heats of reaction (ΔH) of all the studies systems which are calculated by the total area under the exothermic peaks are reported in Table 4. The result indicate that the inclusion of silane treated nano-AlN parti-

Table 4. Curing kinetic parameters of the nano-AlN/epoxy/ TMPTMA system and glass transition temperatures (T_g) of the cured systems

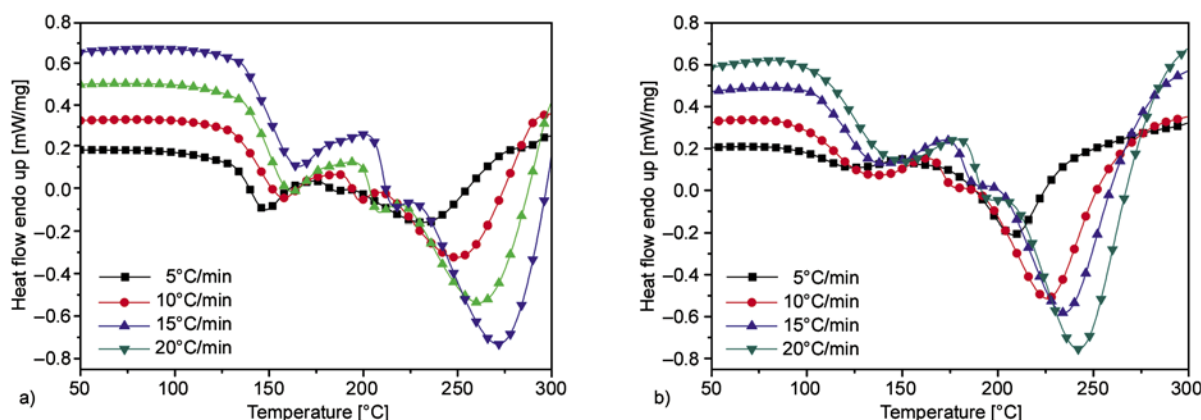| System	T_p [ºC]	ΔH [J/g]	E_a [kJ/mol]	T_g [ºC]
A1	249.8	130.4	83.28	176.4
A2	227.6	137.3	71.27	180.0
A3	222.7	139.9	53.13	180.1
A4	222.7	139.6	68.85	181.4
A5	216.2	154.0	64.54	177.9
A6	222.3	132.1	77.20	181.8
A7	222.0	137.8	73.81	186.7

Figure 7. Dynamic DSC curves with different heating rates of (a) A1 and (b) A4

cles increases the ΔH, possibly due to the addition of epoxy concentration in the composite.

From a dynamic DSC run, the total area S of the exothermal peak (the region between the exotherm and the baseline) is in direct proportion to the ΔH release during the whole cure reaction. The fraction extent of conversion α at any temperature T can be expressed by Equation (1):

$$\alpha = \frac{\Delta H_T}{\Delta H} = \frac{S_T}{S}, \quad 0 \leq \alpha \leq 1 \quad (1)$$

where ΔH_T is the heat of reaction of partially cured samples heated up to the temperature T. A comparison of the curing process, at 10ºC/min heating rates, among the neat epoxy/TMPTMA system and the silane treated nano-AlN particles filled epoxy/TMPTMA systems is shown in Figure 8. It confirms that the silane treated nano-AlN particles act as catalyst at the initial curing stage again. Furthermore, a sigmoidal form of the curves, which is indicative of an autocatalytic kinetics of all the studies systems, is observed. That is to say, the addition of the silane treated nano-AlN particles does not change the autocatalytic cure reaction mechanism of the epoxy/TMPTMA system. It can be seen that all α values increased very slowly at the beginning. When the temperature is high enough, the α values are raise rapidly over 90%, and then they are leveled off.

Ozawa Equation (2), which was concluded to be independent of the order of reaction, is used to calculate the cure reaction activation energy E_a [19, 20].

$$\frac{d(-\ln\beta)}{d\left(\frac{1}{T_p}\right)} = 1.052 \frac{E_a}{R} \quad (2)$$

The value of E_a can be determined from the slope of the plot of $-\ln\beta$ versus $1/T_p$. Furthermore, the influence of the silane treated nano-AlN particles on the E_a parameters of A1–A7 systems was also studied. The calculated values of E_a of A1–A7 systems are reported in Table 4. The decreased of values of E_a for the filled system also implied that the nano-AlN particles facilitate the curing process. Since the effect of increased concentration of the silane coupling agent was equal to the effect of increase the crosslinking density in the curing system, it is understandable of the decrease values of E_a when the
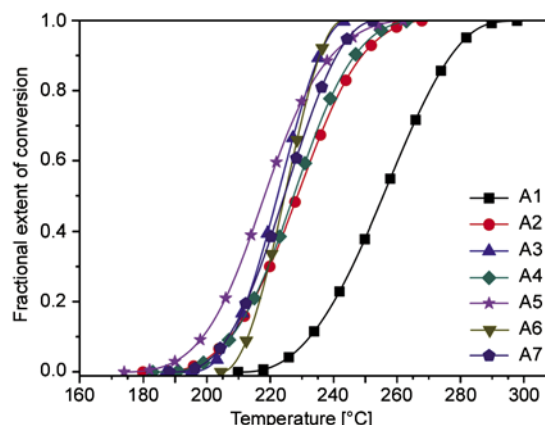
Figure 8. Conversion versus temperature plot at 10ºC/min heating rates of the A1–A7 systems

nano-AlN particles coupled with higher concentration of the silane coupling agent. But the E_a does not show any trend on increasing the amount of the nano-AlN particles.

During the cure reaction, the system undergoes gelation (liquid-to-rubber) and vitrification (rubber-to-glass) transitions. As the cure reaction proceeds, it is the possible that the glass transition temperature (T_g) increases over the curing temperature (T_c), this phenomenon is called vitrification. [21] From Table 4, the T_gs of the silane treated nano-AlN particles filled epoxy/TMPTMA systems are found to higher than that of the neat epoxy/TMPTMA system. Meanwhile, the T_gs of the silane treated nano-AlN particles filled epoxy/TMPTMA systems were improved with increasing content of the silane treated nano-AlN particles, although A5 system deviates from this trend. The glass transition in polymers in a complex phenomenon that in influenced by many factors including free volume, molecular mobility, molecular weigh, and crosslink density [22, 23]. When the silane treated nano-AlN particles are introduced into systems, there would result in increased T_g. There could be the main reason that the epoxide groups is the end group of silane coupling agent which wound result in a higher crosslinking density in epoxy/TMPTMA system.

4. Conclusions

The influences of nano-AlN particles on the thermal conductivity, thermal stability and the curing reaction of CER/TMPTMA systems have been investigated. The thermal conductivity of A7 system was up to 0.47 W/(m·K), which is 161%

increase when compared with the neat epoxy/ TMPTMA system. Incorporation of a small amount of the nano-AlN filler into the epoxy/TMPTMA system improves the thermal stability. However, higher loading of the nano-AlN filler does not lead to any further improvement of the thermal stability. For instance, the thermal degradation temperature at 5% weight loss for A2 system was improved by ～8ºC over the neat epoxy/TMPTMA system.

The resulting fractional extent of conversion versus temperature curves of all the systems considered present the same sigmoidal functional form which is indicative of an autocatalytic kinetics, that is to say, the addition of silane treated nano-AlN particles does not change the cure reaction mechanism. For the development of the nanocomposite, the cure acceleration effect caused by silane treated nano-AlN particles could bring positive effect on the processing of composite since it needs shorter pre-cure time and lower pre-temperature, meanwhile the increase of glass transition temperature of nanocomposite would bring the positive effect to improve the heat resistance.

References

[1] Yu A. P., Ramesh P., Sun X. B., Bekyarova E., Itkis M. E., Haddon R. C.: Enhanced thermal conductivity in a hybrid graphite nanoplatelet – Carbon nanotube filler for epoxy composites. Advanced Materials, **20**, 4740–4744 (2008).
DOI: 10.1002/adma.200800401

[2] Veca L. M., Meziani M. J., Wang W., Wang X., Lu F., Zhang P., Lin Y., Fee R., Connell J. W., Sun Y-P.: Carbon nanosheets for polymeric nanocomposites with high thermal conductivity. Advanced Materials, **21**, 2088–2092 (2009).
DOI: 10.1002/adma.200802317

[3] Cheng J., Li J., Zhang J. Y.: Curing behavior and thermal properties of trifunctional epoxy resin cured by 4,4′-diaminodiphenyl sulfone. Express Polymer Letters, **3**, 501–509 (2009).
DOI: 10.3144/expresspolymlett.2009.62

[4] Zhang J., Xu Y. C., Huang P.: Effect of cure cycle on curing process and hardness for epoxy resin. Express Polymer Letters, **3**, 534–541 (2009).
DOI: 10.3144/expresspolymlett.2009.67

[5] Philipp M., Gervais P. C., Sanctuary R., Müller U., Baller J., Wetzel B., Wetzel B., Krüger J. K.: Effect of mixing sequence on the curing of amine-hardened epoxy/alumina nanocomposites as assessed by optical refractometry. Express Polymer Letters, **2**, 546–552 (2008).
DOI: 10.3144/expresspolymlett.2008.66

[6] Procter P., Solc J.: Improved thermal conductivity in microelectronic encapsulants. IEEE Transactions on Components Hybrids and Manufacturing Technology, **14**, 708–713 (1991).
DOI: 10.1109/33.105121

[7] Huang X. Y., Jiang P. K., Xie L. Y.: Ferroelectric polymer/silver nanocomposites with high dielectric constant and high thermal conductivity. Applied Physics Letters, **95**, 242901/1–242901/3 (2009).
DOI: 10.1063/1.3273368

[8] Timofeeva E. V., Gavrilov A. N., McCloskey J. M., Tolmachev Y. V., Sprunt S., Lopatina L. M., Selinger J. V.: Thermal conductivity and particle agglomeration in alumina nanofluids: Experiment and theory. Physical Review E, **76**, 061203/1–061203/16 (2007).
DOI: 10.1103/PhysRevE.76.061203

[9] Xu Y., Chung D. D. L., Mroz C.: Thermally conducting aluminum nitride polymer-matrix composites. Composites Part A: Applied Science and Manufacturing, **32**, 1749–1757 (2001).
DOI: 10.1016/S1359-835X(01)00023-9

[10] Wang W., Yang X., Fang Y., Ding J., Yan J.: Enhanced thermal conductivity and thermal performance of form-stable composite phase change materials by using β-aluminum nitride. Applied Energy, **86**, 1196–1200 (2009).
DOI: 10.1016/j.apenergy.2008.10.020

[11] Pezzotti G., Kamada I., Miki S.: Thermal conductivity of AlN/polystyrene interpenetrating networks. Journal of the European Ceramic Society, **20**, 1197–1203 (2000).
DOI: 10.1016/S0955-2219(99)00282-4

[12] Li T-L., Hsu S. L-C.: Enhanced thermal conductivity of polyimide films via a hybrid of micro- and nano-sized boron nitride. Journal of Physical Chemistry B, **114**, 6825–6829 (2010).
DOI: 10.1021/jp101857w

[13] Zhou T. L., Wang X., Gu M. Y., Liu X. H.: Study of the thermal conduction mechanism of nano-SiC/DGEBA/ EMI-2,4 composites. Polymer, **49**, 4666–4672 (2008).
DOI: 10.1016/j.polymer.2008.08.023

[14] Michael M., Nguyen L.: Effect of mold compound thermal-conductivity on IC package thermal performance. in 'InterSociety Conference on Thermal Phenomena in Electronic Systems, 1992. I-THERM III, Austin, USA' 246–252 (1992).
DOI: 10.1109/ITHERM.1992.187769

[15] Duan J., Kim C., Jiang P. K.: On-line monitoring of cycloaliphatic epoxy/acrylate interpenetrating polymer networks formation and characterization of their mechanical properties. Journal of Polymer Research, **16**, 45–54 (2009).
DOI: 10.1007/s10965-008-9201-7

[16] Duan J., Kim C., Zheng Y., Jiang P. K.: Morphology and thermal and dielectric behavior of cycloaliphatic epoxy/trimethacrylate interpenetrating polymer networks for vacuum-pressure-impregnation electrical insulation. Journal of Applied Polymer Science, **110**, 566–576 (2008).
DOI: 10.1002/app.28835

[17] Yu W., Choi S. U. S.: The role of interfacial layers in the enhanced thermal conductivity of nanofluids: A renovated Maxwell model. Journal of Nanoparticle Research, **5**, 167–171 (2003).
DOI: 10.1023/A:1024438603801

[18] Chen H., Ding Y., He Y., Tan C.: Rheological behaviour of ethylene glycol based titania nanofluids. Chemical Physics Letters, **444**, 333–337 (2007).
DOI: 10.1016/j.cplett.2007.07.046

[19] Ozawa T.: Estimation of activation energy by isoconversion methods. Thermochimica Acta, **203**, 159–165 (1992).
DOI: 10.1016/0040-6031(92)85192-X

[20] Ozawa T.: A new method of analyzing thermogravimetric data. Bulletin of the Chemical Society of Japan, **38**, 1881–1886 (1965).
DOI: 10.1246/bcsj.38.1881

[21] Zhou T., Wang X., Liu X., Xiong D.: Influence of multi-walled carbon nanotubes on the cure behavior of epoxy-imidazole system. Carbon, **47**, 1112–1118 (2009).
DOI: 10.1016/j.carbon.2008.12.039

[22] White S. R., Mather P. T., Smith M. J.: Characterization of the cure-state of DGEBA-DDS epoxy using ultrasonic, dynamic mechanical, and thermal probes. Polymer Engineering and Science, **42**, 51–67 (2002).
DOI: 10.1002/pen.10927

[23] Allaoui A., El Bounia N.: How carbon nanotubes affect the cure kinetics and glass transition temperature of their epoxy composites? – A review. Express Polymer Letters, **3**, 588–594 (2009).
DOI: 10.3144/expresspolymlett.2009.73

Advances in synthetic optically active condensation polymers – A review

S. Mallakpour[*1,2], *A. Zadehnazari*[1]

[1]Organic Polymer Chemistry Research Laboratory, Department of Chemistry, Isfahan University of Technology, Isfahan, 84156-83111, I. R. Iran
[2]Nanotechnology and Advanced Materials Institute, Isfahan University of Technology, Isfahan, 84156-83111, I. R. Iran

Abstract. The study of optically active polymers is a very active research field, and these materials have exhibited a number of interesting properties. Much of the attention in chiral polymers results from the potential of these materials for several specialized utilizations that are chiral matrices for asymmetric synthesis, chiral stationary phases for the separation of racemic mixtures, synthetic molecular receptors and chiral liquid crystals for ferroelectric and nonlinear optical applications. Recently, highly efficient methodologies and catalysts have been developed to synthesize various kinds of optically active compounds. Some of them can be applied to chiral polymer synthesis. In a few synthetic approaches for optically active polymers, chiral monomer polymerization has essential advantages in applicability of monomer, apart from both asymmetric polymerization of achiral or prochiral monomers and enantioselective polymerization of a racemic monomer mixture. The following are the up to date successful approaches to the chiral synthetic polymers by condensation polymerization reaction of chiral monomers.

Keywords: *biodegradable polymers, optically active polymers, polycondensation reaction, amino acids, chiral monomer*

1. Introduction

Chiral phenomena play significant roles in nature. The synthesis and application of optically active polymers are topics currently attracting much consideration in recent times, due to the wealthy and multifaceted architecture of macromolecular chirality as compared to that of small molecules. Because of unique chiral arrays, nature produces numerous smaller chiral, optically active compounds. Most of the naturally occurring molecules/macromolecules, such as nucleic acids, proteins, and polysaccharides are chiral and optically active. Chirality is essential for life. This situation can be very obviously seen if we look at the chirality of nearly 800 drugs (about 97%) derived from natural sources. Only 2% are racemates and only 1% is achiral. In the past 30 years, the development of chiral drugs with a single enantiomer (optical isomer) has attracted great attention in drug industries, and the market for chiral drugs has tremendously grown. We are undoubtedly living in a chiral world, because of this fact that our life results from homochiral biosubstances [1–3]. Deoxyribonucleic acid (DNA) is a typical example of a homochiral biopolymer whose chirality derives from two features: (i) the incorporation of enantiopure chiral sugars connecting the achiral chromophoric bases such as adenine, guanine, cytosine and thymine and (ii) the double-stranded, stiff helical conformation arising from complementary base pairing and base stacking in water [4]. Optically active polymers often play important functions as key basic materials for well-

---

defined high-performance polymers [5]. Recent advances in asymmetric reactions and catalysis as well as in chiral separations have afforded a rapid increase in the number of commercially available optically active compounds and reagents. Both naturally occurring and synthetic chiral polymers and supramolecules have found prosperous applications in chiral chromatographic separations and shown potential uses in chiral catalytic systems, liquid crystals in ferroelectric and nonlinear optical (NLO) devices, electrodes for enantioselective recognition for performing bioelectro synthesis, microwave absorbents, membrane separation technology, optical switches, biomedical equipments and optoelectronics application. A direct and efficient approach for synthesizing chiral polymers is to introduce chiral elements into the macromolecule backbone or the side chains [6–14].

In the history of synthetic polymer chemistry, it seems that one of the most challenging tasks is to construct functional polymeric systems and optically active synthetic polymers that will be as effective as those in living systems [15–18]. Specially, the synthesis of chiral polymers containing amino acids is a subject of much interest, since a high degree of amino acid functionality can lead to polymers with increased solubility and the ability to form secondary structures. The synthetic chiral polymers that have been reported may be categorized into two parts: the first category represents polymers that adopt helical conformations. Such polymers do not contain any chiral center in the main chain or side chain. If a right-handed or left-handed helical conformation is generated in excess, the polymer can show chiroptical properties. However, the helical conformation is responsible for their optical activity. Helical polymers existing in genes, proteins (α-helix), DNA (double helices), collagen (triple helices), enzymes, and polypeptides are frequently found in nature. They are easily denaturalized by certain physical factors such as heat, ultraviolet irradiation, and high pressure and by other chemical factors such as organic solvents. In contrast, synthetic polymers represent much better stability. Various helical polymers have been synthesized, which include polyisocyanates, polyisocyanides, polychloral, polymethacrylates, polysilanes, polythiophenes, poly(p-phenylene)s, poly(1-methylpropargyl-ester)s, poly(phenylacetylene)s

and poly(α,β-unsaturated ketone) [19–30]. The second one is polymers whose optical activity is derived from main chain or side chain chirality such as: amino-acid-based polymers. Because the amino acids are naturally occurring compounds, synthetic polymers based on amino acids are anticipated to be nontoxic, biocompatible, and biodegradable. On the other hand, synthetic polymers containing amino acid residues in the main chain or in the side chain can be employed for biomedical applications. Possible applications include dentistry, temporary artificial skin substrates, polymer carriers for protein conjugates, drug delivery, gene therapy, tissue engineering, chiral recognition stationary phases, asymmetric catalysts, metal ion absorbents, and biomaterials [31–33]. Chiral recognition of optically active polymers has been utilized in various forms of catalytic and separation chemistry. For example, one of the generally function of chiral polymers is the use as chiral stationary phase in high-performance liquid chromatography (HPLC) for the separation of racemic mixtures [2, 34–38].

Optically active polymers were divided to three types: biopolymers, polymers prepared by almost completely isotactic polymerization by modification of naturally occurring polymer backbones such as polysaccharides and synthetic polymers [2]. Chiral synthetic polymers can be classified as: addition polymers, condensation polymers and cross-linked gels. Addition polymers are including vinyl, aldehyde, isocyanide and acetylene polymers that were prepared via addition polymerization reaction such as poly(acryl amide)s, polyolephynes, polystyrene derivatives, polyazulenes, poly(vinyl ether)s, polymethacrylate, polymethacryloylamine, polychloral, polyisocyanides, polyisocyanates, polyacethylene and polyethers [39–45]. Condensation polymerization continues to receive intense academic and industrial attention for the preparation of polymeric materials used in a vast array of applications [46]. One of application is synthesis of chiral polymers. For this purpose, monomer must be optically active. Cross-linked gels possessing chiral cavities have been prepared and their chiral recognition ability has been studied. The synthesis of gels is based on molecular imprinting technique. Two distinctive methods have been independently developed, that is, (i) polymerizing a monomer having a removable chiral template moiety with a cross-linking agent

and removing the template groups from the products or (ii) polymerizing a monomer with a cross-linking agent in the presence of a non-polymerizable template molecule and removing the template [2]. This article reviews the synthesis of optically active polymers via polycondensation reaction of chiral monomers.

2. Synthetic optically active condensation polymers
2.1. Polyamides
Historically, the first study of optically active polymers has been of those available i.e. natural polymers such as proteins, polypeptides, polynucleotides and so on. These polymers are remarkable for their high structural regularity, their ability to take on secondary ordered structures, even in solution, and to undergo order disorder conformational transitions by changes in external conditions (solvent, temperature, pH, etc.). Progress in polymer chemistry has allowed the synthesis of entirely different condensation polymers which one of them is optically active polyamides (PA)s [47].

Many studies concerned with the synthesis and characterization of optically active PAs have been undertaken [48–55], mainly polypeptides and proteins which have been extensively investigated. Synthesis and optical properties of asymmetric PAs derived from composed of optically active cyclic dicarboxylic acids, (+)-(S)- and (–)-(R)-trans-1,2-cyclopropanedicarboxylic acids, (–)-(R)-trans-1,2-cyclobutanedicarboxylic acids, (+)-and (–)-trans-1,3-cyclopentanedicarboxylic acids and secondary diamines such as trans-2,5-piperazine, piperazine or N,N′-dimethylethylenediamine was reported by Overberger and Shimokawa [56]. Overberger *et al*. [57] also prepared optically active PAs by interfacial polycondensation reactions of (+)-(S)-trans-2-

methylcyclopropanedicarboxylic acid or (+)-and (–)-trans-1,2-cyclohexanedicarboxylic acids with rigid spirodiamine, 2,6-diazaspiro[3,3]heptane. They prepared several model compounds, too. These model compounds were (±)-trans-1,2-cyclopropanecarboxylic acid azetidide, (+)-trans-2-methylcyclopropanedicarboxylic acid diazetidide, 2,6-di[(±)-trans-2-methylcyclopropanecarboxyl]-2,6-diazaspiro[3,3] heptane and (+)-trans-1,2-cyclohexanedicarboxylic acid dipiperidide for studying the conformation of the polymers. The conformations of the polymers and the model compounds were investigated by means of optical rotatory dispersion, circular dichroism (CD) and by hydrodynamic methods.

A series of chiral PAs containing optically active thymine groups as pendants were synthesized from N-acylation of an active diester of N-hydroxy-5-norborene-2,3-dicarboxamide, N,N′-(isophthaloyl-dioxy)-bis(5-norbornene-2,3-dicarboximide), with 1,3-diamino-2-hydroxypropane by Overberger's group [58]. Overberger *et al*. [59] prepared optically active PAs based on the polycondensation of two new active diesters: the active diesters of 4-chloro-1 hydroxybenzotriazole, such as 1,1′-(terephthaloyldioxy)bis(4-chloro-benzotriazole), and 1,1′-(isophthaloyldioxy)bis(4-chlorobenzotriazole), with optically active isomers of 2,4-diaminopentane. Dipolar aprotic solvents such as N,N-dimethylformamide (DMF) and dimethyl sulfoxide (DMSO) were used as reaction solvents. The solution polycondensation carried out in solution at room temperature afforded optically active PAs. The aminolysis of the two active diesters was carried out as a model reaction study.

Synthesis of optically active PAs derived from L or D-tartaric acid have been also reported in some cases [60–65] (Figure 1).
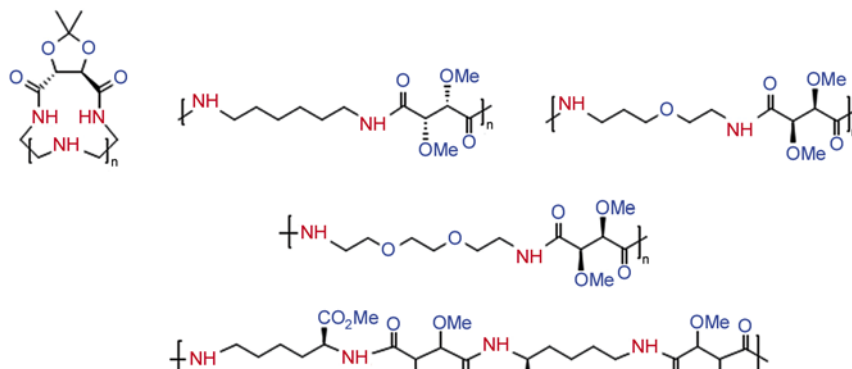

Figure 1. Chemical structures of PAs derived from tartaric acid [60–65]

A number of optically active PAs containing *α*-amino acids have been prepared. In the case of the synthetic PAs, only those containing the naturally occurring (L)-*α*-amino acids, being structurally close to the natural polypeptides, possess potentially degradable linkages that make them suitable as biomaterials [66–70].

A new polyamidation reaction between N,N′-bistrimethylsilylated diamines and 2,2′-p-phenylenebisazalactones in N,N-dimethylacetamide (DMAc) was investigated by Katsarava *et al*. [71]. By the interaction of bisazalactones with N$^{\alpha}$,N$^{\epsilon}$-bistrimethylsilylated L-lysin alkyl ester, PAs were obtained containing dipeptide links in the main chain. It was shown that these can be transformed into water-soluble polyacids upon saponification of ester side groups.

PAs derived from carbohydrates are the object of current attention, because they are not only optically active, but also for its potential as biodegradable and biocompatible materials [72–77].

Mallakpour and coworkers [78–80] have investigated the synthesis of PAs from the polycondensation reaction of chiral 5-(4-methyl-2-phthalimidyl-pentanoylamino)isophthalic acid, (2S)-5-(3-phenyl-2-phthalimidylpro-panoylamino)iso-phthalic acid and 5-(3-methyl-2-phthalimidylpentanoylamino) isophthalic acid with several aromatic and aliphatic diisocyanates such as 4,4′-diphenylmethane diisocyanate (MDI), toluylene-2,4-diisocyanate (TDI), isophorone diisocyanate (IPDI) and hexamethylene diisocyanate (HDI) under microwave irradiation as well as conventional technique (Figure 2). The resulting aromatic PAs were optically active and soluble in various organic solvents and have good
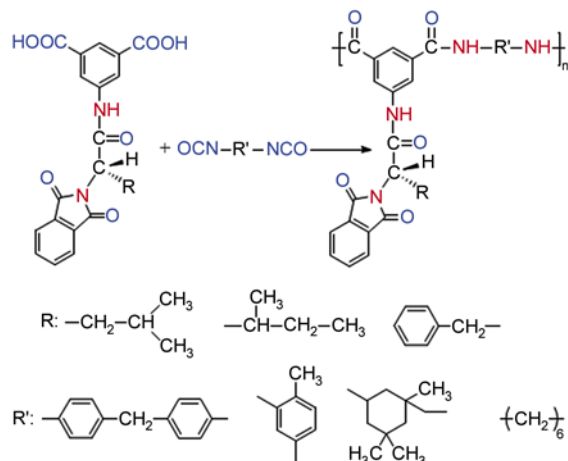
thermal stability. Microwave-assisted step-growth polymerization reactions proceeded rapidly compared to conventional solution polycondensation and it was almost complete within a short period of time. The reactions were carried out in the presence of a small amount of dibutyltin dilaurate (DBTDL), pyridine (Py) or triethylamine (TEA) as catalysts and/or under no catalyst conditions. The use of such an organic medium was necessary to induce effective homogeneous heating of the monomers. They obtained comparable results from the viewpoint of yield and inherent viscosity of the polymers with lower reaction time by several orders of magnitude under microwave conditions and straightforward procedure. The polymerization reactions were also carried out in the presence of tetrabutylammonium bromide (TBAB) as a molten ionic liquid (IL) or traditional solvent like1-methyl-2-pyrrolidone (NMP) under microwave irradiation as well as conventional heating conditions by Mallakpour and coworkers[81–83]. In recent years, Mallakpour and coworkers reported on the synthesis and characterization of a new class of wholly aromatic and optically active PAs containing phthalimide and L-leucine pendant groups by condensation polymerization of a bulky diacid, (2S)-5-[4-(4-methyl-2-phthalimidylpentanoyl-amino)benzoylamino] isophthalic acid, and several diisocyanates (Figure 3) [84]. Polymerization reactions were performed in the presence of DBTDL as a catalyst and without catalyst in molten TBAB as a green solvent and were compared with polymerization in NMP as a conventional solvent. The resulting polymers were obtained in good yields and inherent viscosities ranging between 0.26 and 0.96 dL·g^{-1}. Amalgamation of the bulky side chain in the PAs, cause an

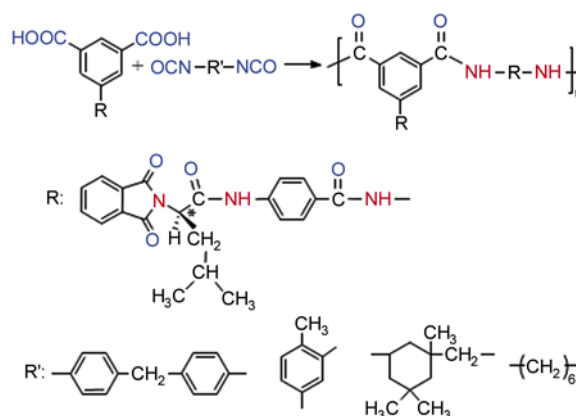**Figure 2.** Synthesis of optically active and thermally stable PAs [78–80]

Figure 3. Synthesis of optically active PAs containing phthalimide and L-leucine pendant groups [84]

increase in the solubility, while maintaining good thermal stability.

The same researchers also synthesized novel thermally stable and optically active PAs with flame retardant properties which were prepared via an oil bath heating method using a mixture of 1,3-dipropylimidazolium bromide (as IL) and triphenyl phosphite (TPP) both as reaction media and activator [85]. The main advantage of this polycondensation reaction is that this procedure is a one-pot reaction and use of diacid chloride is not needed. These polymers presented high thermal stability, with the decomposition temperature being above 400ºC, although slightly diminished compared with those of related aromatic PAs which do not contain any pendant groups (Figure 4). The reaction proceeded efficiently with IL/TPP as condensing agent without the need of any additional promoters, which are necessary upon utilizing of traditional organic solvents like NMP. The incorporation of tetrabromophthalimide, and L-phenylalanine groups into PAs backbone gave polymers with good solubility in common organic solvents.

In another study, Mallakpour and Rafiee [86] synthesized novel optically active aromatic PAs from the reaction of new diacid monomer, 5-[3-phenyl-2-(9,10-dihydro-9,10-ethanoanthracene-11,12-dicarboximido) propanoylamino]isophthalic acid that was successfully synthesized starting from cis-9,10-dihydro-9,10-ethanoanthracene-11,12-dicarboxylic acid anhydride and L-phenylalanine and different aromatic diamines by two diverse methods such as: microwave-assisted and conventional heating polyamidation (Figure 5). A highly effective, very fast microwave method was described to synthesize optically active aromatic PAs under microwave heating for only 3 min. Generally, better yields are obtained under faster and cleaner reactions when compared to those from conventional heating. All of these polymers having bulky anthracenic and amino acid functionality in the side chain showed excellent solubility and readily dissolved in various organic solvents. PAs were thermally stable, with 10% weight loss recorded at 385°C in the nitrogen atmosphere, and char yields at 800°C higher than 50% and glass transition temperature (T_g) above 180°C.

Because of importance of optically active materials and polymers with amino acid, Mallakpour and Taghavi [87] prepared a series of novel optically active PAs by direct polycondensation of novel chiral dicarboxylic acid, containing a rigid naphthalimide and flexible S-valine pendant group, 5-[3-methyl-2-(1,8-naphthalimidyl)-butanoylamino]isophthalic acid with different diisocyanates in the
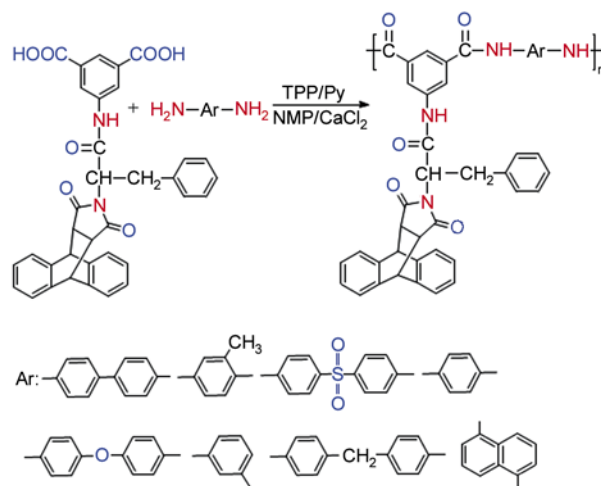
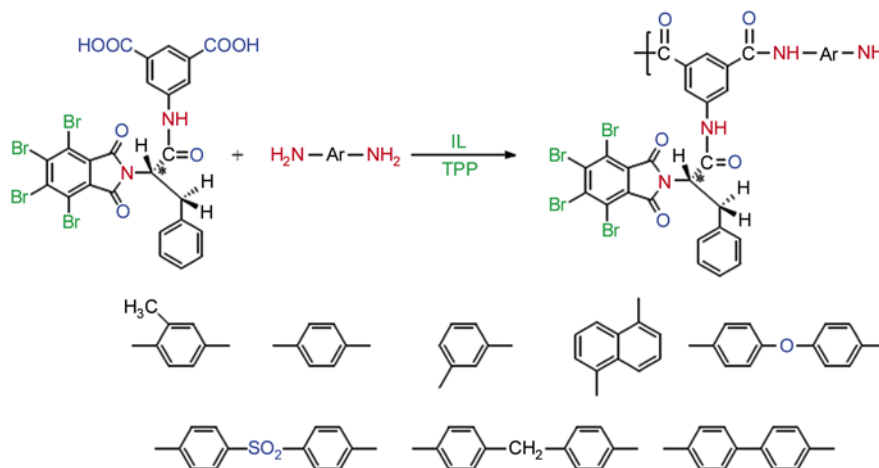**Figure 5.** Polycondensation reactions of chiral monomer with aromatic diamines [86]

Figure 4. Synthesis of optically active flame retardant PAs [85]
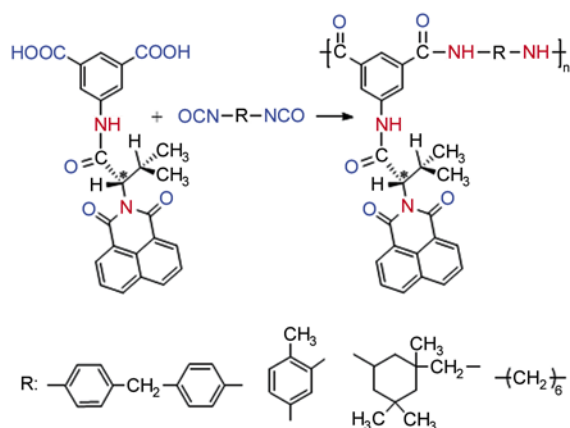
Figure 6. Synthesis of optically active flame retardant PAs [87]

presence of a small amount of ILs that act as a primary microwave absorber as well as conventional heating was carried out (Figure 6). Incorporation of the naphthalimide group into the polymer side chain as well as combination of the aromatic backbone and aliphatic pendant group in the presence of several functional groups remarkably enhanced the solubility while maintaining good thermal stability of the new polymers. The choice of 1,8-naphthalenedicarboxylic anhydride was due to the many derivatives of l,8-naphthalic anhydride exhibit strong fluorescence emission and serve for this reason as fluorescent dyes and fluorescent whitening agents. They reported for the first time an electrochemical oxidation method based on the adsorptive stripping cyclic voltammetry technique on the multi-walled carbon nanotube-modified glassy carbon electrode for the investigation of electrochemical stability of the resulting polymers in aqueous solution at various pH values. The resulting polymers have many applications as photoactive materials which can be used in solar energy collectors as electro-optically sensitive materials and for laser activity.

Optically active PAs with asymmetric structure and dipole groups can easily form strong hydrogen bonds between amide groups along the molecular chain and hence can yield crystalline structures with asymmetric modality; as such, they should possess considerable ferroelectric properties. Liu *et al.* [88] synthesized a series of optically active PAs by polycondensation of various diamines and diacetyl chlorides and studied the dielectric properties of the resulting polymers. They found that these polymers formed a chiral tilted smectic phase and

therefore should have ferroelectric properties. This implies that the polymers have asymmetric liquid crystalline structures. Chen *et al.* [89] reported on the synthesis of a variety of optically active PAs and o-methylated PAs, derived from (–)-anti head-to-head coumarin dimer component. Polymers were absorbed on macroporous silica gel particles and used as chiral stationary phases for direct resolution of racemates having aromatic moiety by HPLC. Preparation and properties of aromatic PAs from 2,2′-bis(p-carboxyphenoxy) biphenyl or 2,2′-bis(p-carboxyphenoxy)-1,1′-binaphthyl and aromatic diamines was investigated by Liou *et al.* [90]. 2,2′-bis(p-aminophenoxy)biphenyl and 2,2′-bis(p-aminophenoxy)-1,1′-binaphthyl, were synthesized by the reaction of p-fluoronitrobenzene with biphenyl-2,2′-diol and 2,2′-dihydroxy-1,1′-binaphthyl, respectively, followed by catalytic reduction. Biphenyl-2,2′-diyl- and 1,1′-binaphthyl-2,2′-diyl-containing aromatic PAs having inherent viscosities of 0.44–1.18 and 0.26–0.88 dl/g, respectively, were obtained either by the direct polycondensation or low-temperature solution polycondensation of the diamines with aromatic dicarboxylic acids (or diacid chlorides). These aromatic PAs containing biphenyl and binaphthyl units had T_gs in the range of 215–255 and 266–303°C, respectively. This group also prepared [91] new aromatic dicarboxylic acids having 2,2′-bis(p-carboxyphenoxy) biphenyl and 2,2′-bis(p-carboxyphenoxy)-1,1′-binaphthyl by the reaction of p-fluorobenzonitrile with biphenyl-2,2′-diol and 2,2′-dihydroxy-1,1′-binaphthyl, respectively, followed by hydrolysis. Biphenyl-2,2′-diyl- and 1,1′-binaphthyl-2,2′-diyl containing aromatic PAs were obtained with inherent viscosities in the range of 0.58–1.46 and 0.63–1.30 dl/g, respectively via solution polycondensation of the corresponding diacid chlorides with aromatic diamines. Nozaki *et al.* [92] prepared two cyclic PAs from glycine and 1,1′-binaphthyls, and their structures were determined by single-crystal X-ray analysis. Conformations of these two cyclic PAs in organic solvents and their interaction with other organic molecules were also studied. Hsiao *et al.* [93] synthesized two series of novel fluorinated aromatic PAs from 2,2′-bis(4-amino-2-trifluoromethylphenoxy) biphenyl and 2,2′-bis(4-amino-2-trifluoromethylphenoxy)-1,1′-binaphthyl with various aromatic dicarboxylic acids via phosphorylation polycondensation tech-

nique and using TPP and Py as condensing agents in the NMP solution containing dissolved calcium chloride (CaCl$_2$). All polymerization reactions proceeded homogeneously throughout the reaction and gave clear and viscous polymer solutions. All of the resulting PAs could be cast to transparent, light-colored, and flexible films with moderately high T_gs and thermal stability. A series of optically active helical PAs were synthesized by Agata *et al*. [94] via polycondensation of (R)- or (S)-6,6′-diamino-2,2′-dimethylbiphenyl with various aromatic dicarbonyl chlorides with an optically active axially dissymmetric diaminobiphenyl compound. The molecular weights of the PAs obtained with the same type of (R)- or (S)-linkages were similar to each other, and also had very similar specific rotation values, with opposite signs. The resulting wholly aromatic PAs were soluble in common organic solvents, and excellent conformational stability of their helical structures was observed at higher temperatures. Liou *et al*. [95] prepared a series of novel aromatic PAs having noncoplanar biphenylene units in the main chain and bulky naphthyl or phenyl pendant group at 2,2′-disubstituted position from phenyl and naphthyl-substituted rigid-rod aromatic dicarboxylic acids, 2,2′-diphenylbiphenyl-4,4′-dicarboxylic acid and 2,2′-dinaphthylbiphenyl-4,4′-dicarboxylic acid, and various aromatic diamines via direct phosphorylation polycondensation (Figure 7). The introduction of the bulky phenyl and naphthyl-substituted group could increase the solubility and disrupt the copolanarity of aromatic units in chain packing and exhibited excellent thin-film-forming ability and thermal stability.

Among PAs there is a large group of polymers which differ from other PAs in their properties and methods of preparation. This group, called polypeptides or Poly(amino acid)s (PAA)s, is very close in its composition and structure to one of the most important classes of polymeric substances-proteins [96]. PAAs are of substantial commercial interest. As biodegradable polyanionic materials their applications range from slow release agents in agriculture, to detergents, surfactant, metal adsorbents, and cosmetics [97]. PAAs may offer numerous advantages in biomedical applications such as in diagnos-
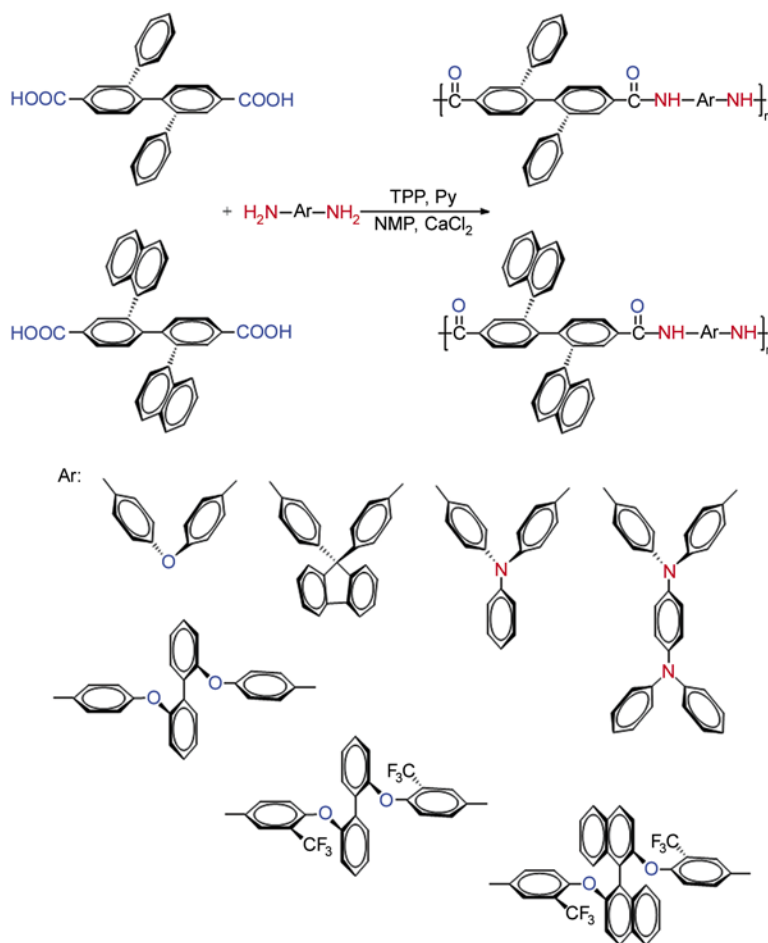
Figure 7. Synthesis of noncoplanar aromatic PAs [95]

tics, sustained release matrices, microencapsulation, for plasma membrane isolation and chromosomal preparations, carriers for therapeutic protein conjugates and drug delivery systems [98, 99]. PAAs are obtained by the polymerization of amino acids or their suitable derivatives, serving as monomers, and like other synthetic polymers they represent a mixture of macromolecules of varying chain lengths. Recent refinements in the chemical technique of polymerization and the development of new physical methods in polymer chemistry have led to a renewal of interest in the polymers of amino acids. Most of the polymers described in the literature are composed of a single amino acid. A number of copolymers have also been prepared [100]. Many attempts were made to prepare PAAs and much considerable progress has been achieved in the synthesis and study of them. Several studies were carried out in polycondensation of *α*-amino acid derivatives by Frankel and coworkers [101–105]. Fasman and Blout [106] studied the synthesis and the conformation of poly-L-serine and poly-o-acetyl-L-serine. These materials were synthesized with degrees of polymerization (DP) slightly above 100. Novel derivatives of poly(aspartic acid) conjugated with various amino acids such as *γ*-amino butyric acid, leucine, serine, valine, glycine and *β*-alanine and their amphiphilic copolymers were synthesized and characterized by Kim *et al*. [107]. The resulting polymers exhibited biocompatibility by in-vitro cytotoxicity test. These amino acid-conjugated biocompatible polymers had potential applications in pharmaceutical and cosmetic fields as base materials for drug-carrier systems. Yuki *et al*. [108] prepared a series of poly(*β*-amino acid)s, poly[(RS)-*β*-proline] and poly[(R)-*β*-proline], by the polycondensation reaction of the p-nitrophenyl esters. They studied conformational properties of polymers.

2.2. Polyimides

As polyimides (PI)s possess many desirable attributes, so this class of materials has found applications in many technologies. They have inherently high mechanical properties, good chemical resistance, low dielectric constant and high thermal stability. The high processing temperature of these materials requires dopant molecules to have high thermal decomposition temperatures. Currently,

high performance PIs are being widely used for several primary applications in the electronics area as: (1) Fabrication aids such as photoresists, planarization layers and in implant masks; (2) Passivation overcoats and interlevel insulators; (3) Adhesives and underfill materials for micro BGA (*μ*BGA) packaging and flip chip technology; (4) Substrate components. Some of other applications include aerospace, automotive and general engineering. In the aerospace and automotive industry they are used in structural composites and as high temperature adhesives. General engineering applications include high temperature bearings and seals [109, 110].

More recently, optically active PIs have been developed. The synthesis of optically active PIs derived from binaphthyl compounds and dianhydrides was reported [111–113]. Binaphthyls are very important chiral compounds which have been used in polymer systems. The chirality of them is arising from the restricted rotation along the carbon-carbon single bond of the two naphthalene rings. The resulting polymers showed good chiral recognition ability when used as a chiral packing material for HPLC. In 1996 Mi *et al*. [114] reported on the first synthesis of a type of thermally stable and optically active aromatic PIs possessing (R)-(+)- or (S)-(–)-1,1′-bi-2-naphthalene units in the main chain, along with some of their important properties. The key monomers, optically active (R)-(+)- or (S)-(–)-2,2′-bis(3,4-dicarboxyphenoxy)-1,1′-binaphthalene dianhydrides (5R and 5S), were prepared by the reactions of optically active (R)-(+)- or (S)-(amic acid)s and subsequent chemical imidization with acetic anhydride-triethylamine (Figure 8). The solubility of resulting PIs was greatly improved by the incorporation of noncoplanarity in axially dissymmetric 1,1′-bi-2-naphthalene units into the polymer backbone. The optical stability at high temperatures could be expected because the racemization resulting from the rotation around the axis of the two binaphthalene rings would be highly hindered by the long chain stretching out on both sides. This group [115] also prepared new optically active aromatic PIs from (R)-(+)-2,2′-bis(2-trifluoro-4-aminophenoxy)-1,1′-binaphthyl monomer with 4,4′-oxydianhydride by one step method. The same researchers [116] performed the similar reaction for the preparation of thermally stable chiral PIs. They
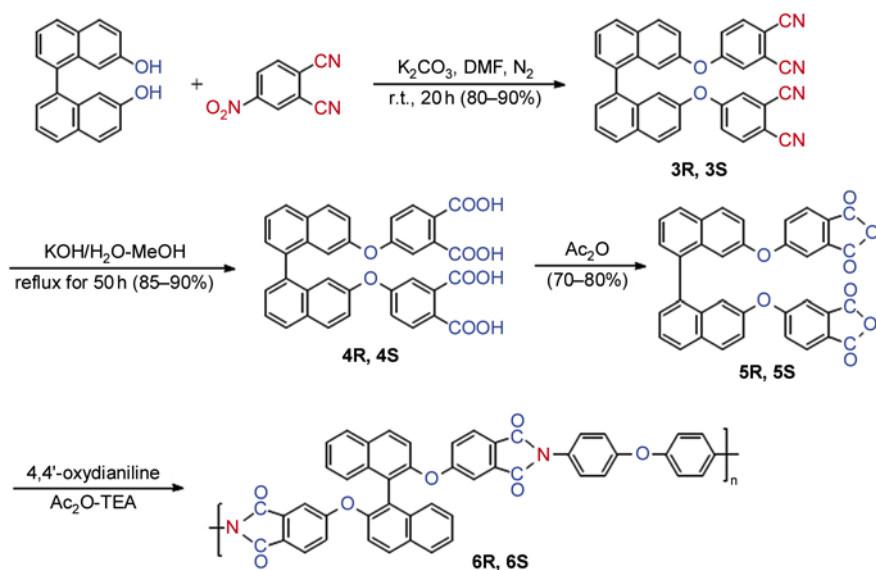
Figure 8. Synthesis of optically active twisted PIs containing 1,1′-bi-2-naphthalene unit [114]

synthesized polymers from condensation of afore-mentioned monomer with various dianhydrides by using the one-step method. These polymers had glass-transition temperatures of 256~278°C and were optically active with specific rotations ranged from 167~258° and their chiroptical properties also were studied.

Liou [117] reported on the synthesis of organosoluble aromatic chiral PIs from 2,2′-bis (3,4-dicarboxyphenoxy)-1,1′-binaphthyl dianhydride. The dianhydride monomer was subjected to the one-step polycondensation with various aromatic diamines, giving moderate molecular weight PIs with inherent viscosities up to 0.67 dl/g. The introduction of bulky, cranked, and twisted noncoplanar binaphthyl-2,2′-diyl unit into the polymer backbone highly improved solubility of the PIs in organic solvents. All the PIs showed typical amorphous diffraction patterns and had T_gs in the range of 280–350°C, depending on the nature of the diamine moiety. All polymers were stable up to 400°C, with 10% weight loss being recorded above 485°C in air.

Yigit *et al.* [118] described chiral synthetic functionalized PIs containing a chiral (R,R) or (S,S) 1,3-bis(p-N,N′-dimethylaminobenzyl)-perhydrobenzimidazol-2-thion unit in the backbone. The reactions were performed between an optically active aromatic dimethylamine and various dianhydrides such as: pyromellitic dianhydride (PMDA), 3,3′,4,4′-benzophenonetetracarboxylic dianhydride (BPDA), 4,4′-oxydiphthalic anhydride (ODPA) and 3,3′,4,4′-biphenyltetracarboxylic dianhydride (BTDA) in the
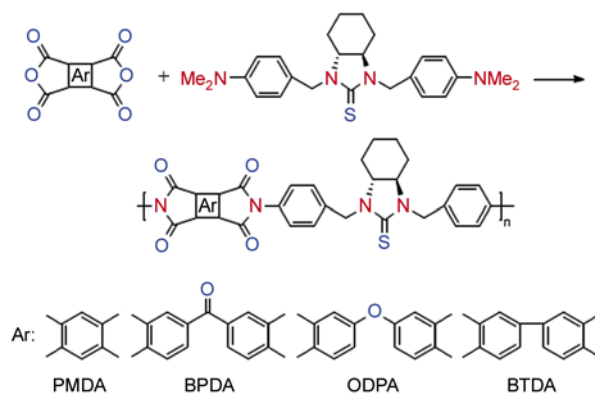
Figure 9. Synthesis route for PIs [118]

presence of the solvent NMP (Figure 9). PIs were soluble in some polar aprotic solvents such as NMP, DMF, DMAc and DMSO and insoluble in apolar solvents such as ether and hexane. The inclusion of chiral groups containing perhydrobenzimidazole groups in the polymer backbone makes the polymer thermally stable with increased solubility. The improved solubility may be attributed to the bulky structure of the monomers, which decreases the interchain interaction owing to the rigid aromatic repeating units. The PIs prepared exhibit excellent properties, with a high potential for optically active polymers.

Kudo and coworkers [119] have reported on the synthesis of constitutionally isomeric head-to-head, head-to-tail and random PIs using an unsyrnmetric alicyclic tetracarboxylic dianhydride. They reported on a first example for the structurally isomeric PIs that show a different physical property (Figure 10). They also prepared optically active alicyclic PIs via
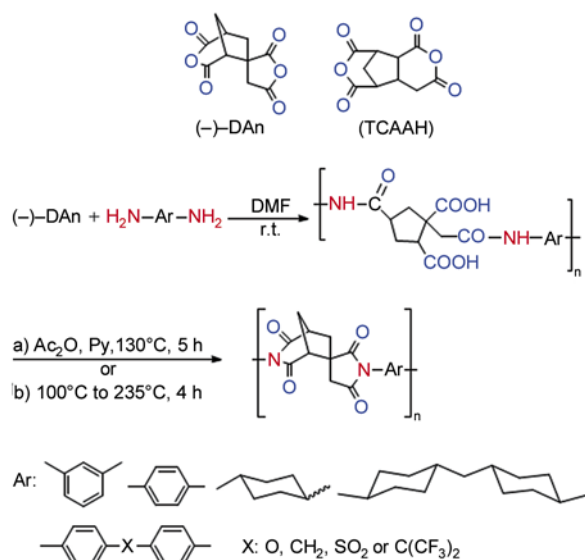
Figure 10. Synthesis of optically active coPIs derived from DAn [119–123]

polycondensation of (–)-[1S*,5R*,6S*]-3-oxabicy-clo[3.2.1]octane-2,4-dione-6-spiro-3′-(tetrahydrofu-ran-2′,5′-dione) [(–)-DAn] with diamines and subsequent chemical or thermal imidization (Figure 10). The dianhydride (–)-DAn was synthesized by an asymmetric Diels-Alder reaction of a chiral itaconic acid derivative as a key step. Colorless or slightly yellow flexible films were obtained for the (–)-DAn-derived PIs. The resulting polymers showed good solubility toward dipolar aprotic solvents and Py [120]. Kudo's group also successfully synthesized a series of optically active and soluble PIs having a spiro alicyclic unit in the main chain by the reactions of DAn with several diamines through a general two-step polymerization method [121–122]. In another research, they reported on a systematic investigation of the physical properties of coPIs of DAn [123]. The comonomer used in their study was c-3-carboxymethyl-r-1,c-2,c-4-cyclopentane tricarboxylic acid 1,4:2,3-dianhydride (TCAAH), a structural isomer of DAn, which is unsymmetric but does not have a spiro unit (see Figure 10). The refractive indices of coPIs were also studied. They showed the DAn content in the backbone affects various properties of coPI, which might be attributed to its unsymmetric spiro-alicyclic structure. The structure property relationships found here should be universal in principle, and might be applicable to the design and modification of other polymers.

Barikani *et al.* [124] investigated a new optically active diisocyanate containing methylene groups and a preformed imide ring using the Curtius rearrangement of corresponding diacylazides. The diisocyanate was polycondensed with PMDA, benzophenone tetracarboxylic dianhydride, and hexafluoroisopropylidene diphthalic anhydride to provide three optically active PIs. The introduction of methylene moieties as well as the presence of a preformed imide ring in the polymer backbone improved the solubility of the polymers without too much thermal stability being sacrificed. Synthesis and characterization of new optically active PIs containing L-leucine amino acid residue are reported by Yeganeh *et al.* [125]. They prepared a new optically active diisocyanate from the reaction of L-leucine and PMDA and subsequent transformation of intermediate imide-containing diacid to diisocyanate via Weinstock modification of Curtius rearrangement using TEA, ethylchloroformate and sodium azide reagents. The solution polycondensation using DMF solvent and appropriate duration and temperature programming which optimized via study of model compound was applied successfully for preparation of PIs from this diisocyanate and three different dianhydrides such as PMDA, 3,3,4,4-benzophenonetetracarboxylic dianhydride, and hexafluoroisopropylidene 2,2-bis(phthalic anhydride). Two different optically active dianhydrides were also prepared by them [126] from the reaction of L-aspartic acid with either PMDA or benzophenone tetracarboxylic dianhydride and subsequent transformation of tetraacids to dianhydrides using thionyl chloride. Twelve novel optically active and soluble PIs having inherent viscosities of 0.18–0.55 dl/g were synthesized from the reaction of optically active dianhydrides with different aromatic and aliphatic diisocyanates. These polymers showed acceptable physical properties as well as optical activity.

2.3. Polyesters

Recently, Mallakpour and coworkers [127–131] synthesized optically active thermally stable aromatic polyesters (PE)s containing phthalimide group from the reaction of two different diacid monomer with several aromatic diols via direct polyesterification with tosyl chloride (TsCl)/Py/

DMF system as condensing agent. The resulting polymers were obtained in good yields with inherent viscosities ranging between 0.21 and 0.61 dL/g. Thermal gravimetric analysis (TGA) showed that the 10% weight loss temperature in a nitrogen atmosphere was more than 360ºC, which indicates that the resulting PEs have a good thermal stability. From the chemical point of view the ester group imparts to the polymer's structure increased sensibility to hydrolysis that can cause chain breaking. In addition because of the existence of amino acids in the polymer pendant group these polymers were expected to be biodegradable and were therefore classified under environmentally friendly polymers. More recently this group also synthesized optically active and photoactive aromatic PEs by step-growth polymerization of a chiral diacid containing naphthalimidyl and flexible chiral groups with different diols via direct polyesterification reaction. The resulting polymers show excellent solubility due to bulky pendant groups, good thermal stability with glasstransition temperature around 200ºC, and fluorescence emission phenomena [132].

A series of coPEs based on 2-[(S)-(+)-methyl-l-butoxylhydroquinone as the chiral monomer with several nonchiral hydroquinones was synthesized by Fujishiro and Lenz [133] to form a new family of main-chain cholesteric liquid crystalline polymers containing a flexible spacer. Copolymers containing unsubstituted hydroquinone units formed two liquid crystalline phases, one of which was a cholesteric phase, but the other may have been a cybotactic nematic phase. Copolymers with nonchiral substituted hydroquinone units formed only a cholesteric phase. Schwartz *et al*. [134] reported on the polycondensation of silylated 2,3-isopropylidene D-threitol with a dicarboxylic acid dichloride in o-dichlorobenzene or 1-chloronaphthalene at 180–230°C and ten cholesteric coPEs were prepared by polycondensation of mixtures of silylated methylhydroquinone and cis- or trans-1,4:3,6-dianhydro-D-sorbitol (trans: isosorbide, cis: isomannide), or 2,3-isopropylidene threitol with the dichloride of l,l0-bis(4′-carboxyphenoxy)decane. The polymers containing isosorbide units are optically active. The resulting coPEs form a broad cholesteric phase above 200°C. This approach is also useful for the synthesis of coPEs from diols and diphenols, and thus, allows the preparation of cholesteric

PEs with interesting optical properties. For the first time, Kricheldorf's group [135] investigated a process for the production of optically active PEs based on the polycondensation of 4-carboxycinnamic acid in the form of its acid chloride with chiral spacers in the presence of Py. Difunctional cinnamic acids such as 4-hydroxy- or 4-aminocinnamic acid are useful and interesting components of photoreactive polycondensation. Chiral spacer was synthesized from (R)-3-bromo-2-methyl-l-propanol and 4-mercaptophenol. Three homoPEs were also prepared via polycondensation of 4,4′-dihydroxybiphenyl and 2,5-bis(n-octyloxy)-2,5-bis(dodecyloxy)- or 2,5-(hexadecyloxy) terephthaloyl-chloride by this group [136]. Furthermore, several coPEs were synthesized from 4,4′-dihydroxybiphenyl and mixtures of 2,5-bis-(hexadecyloxy) terephthaloylchloride and 2,5-bis((S)isopentyloxy)terephthaloylchloride. All PEs were characterized by inherent viscosities, elemental analyses, ^{1}H NMR spectroscopy, differential scanning calorimetry (DSC) measurements, dynamic mechanical analyses (DMA), wide-angle X-ray diffraction (WAXD)s powder patterns at various temperatures and optical microscopy. Two liquid crystalline phases were detected for the homoPEs and most coPEs: a viscous sanidic (biaxial nematic) phase and, at higher temperatures, a mobile nematic phase. Sanidic PEs are PEs forming a layered supramolecular structure with the layer planes parallel to the main chain in contrast to the smectic systems where the layer planes are more or less perpendicular. Kricheldorf and coworkers [137] also synthesized a series of chiral PEs by polycondensation of silylated 4,4′-dihydroxybiphenyl and mixtures of 2,5-bis(dodecylthio)terephthaloyl chloride and 2,5-bis((S)-2-methylbutylthio)terephthaloyl chloride. The resulting coPEs were characterized by elemental analyses, viscosity, DSC and X-ray measurements, and optical microscopy. Depending on the reaction conditions low and high molecular weights were obtained. Bahulayan and Sreekumar [138] investigated chiral PEs with azobenzene moieties in the main chain by the polycondensation of terephthaloyl chloride with isosorbide, which acts as the chiral building unit, and an azobiphenol, bis(4-hydroxyphenylazo)-2,2′-dinitrodiphenylmethane or bis(4-hydroxyphenylazo)-2,2′-dinitro-3,5,3′,5′-tetramethyldiphenylmethane in a solvent mixture of DMAc and 1,2-

dichlorobenzene (1:4 v/v). These polymers exhibited good thermal properties, had high T_g values and TGA studied showed they were stable up to 400°C. The polymer chains characterized by helical structures were non-centrosymmetric at the molecular level. But in randomly oriented polymer films obtained by solvent evaporation, non-centrosymmetry may be lost. This group [139] prepared a series of optically active PEs with π-conjugated donor-acceptor segments was synthesized by the condensation of azobenzene-4,4′-dicarbonylchloride with 1,4:3,6-dianhydro-D-sorbitol ($[\alpha]_D^{25}$ = 42.5°) and biphenolic chromophores, bis(4-hydroxyphenylazo)-2,2′-dinitrodiphenylmethane and bis(4-hydroxyphenylazo)-2,2′-dinitrodiphenylsulfone. The second-harmonic generation (SHG) efficiency of the polymers was experimentally verified by a powder-reflection technique with 2-methyl-4-nitroaniline as a reference. The SHG efficiencies of the polymers were compared to those of the chromophores and explained as a function of the percentage of chiral composition. WAXD scans showed that with the increase in the percentage of the chiral unit, the packing order in the polymers increased. They also synthesized [140] several chiral PEs containing donor-acceptor substituted π-conjugated segments in the main chain by high-temperature polycondensation of biphenolic chromophores, bis(4-hydroxyphenylazo)-2,2′-dinitrodiphenylmethane and bis(4-hydroxyphenylazo)-2,2′-dinitrodiphenylsulfone with (2R,3R)-(+)-diethyl tartrate and terephthaloyl chloride. Results showed that the optical rotation increased with the increase in the composition of diethyl tartrate units. The temporal stability showed that the chiral organization and, hence, the dipole orientation are stable in these systems. The high T_g value of the polymers also supported the thermal stability of the orientation. Thus, chiral polymers incorporating donor-acceptor substituted π-conjugated segments can offer themselves as promising materials in the field of nonlinear optics. The same researchers reported on [141] the synthesis, characterization and solvatochromic behavior of a new series of optically active PEs. These polymers were prepared from polycondensation of diacid chlorides with biphenolic azo chromophores such as bis(4-hydroxyphenylazo)-2,2′-dinitrodiphenylmethane and bis(4-hydroxyphenylazo)-2,2′-dinitrodiphenylsulphone with Λ-shaped

conformation and isosorbide compound. The polymerizations were carried in different highly polar solvents like DMF and DMAc with Py as acid acceptor. The PEs were obtained with higher dipole moment in excited state than in ground state so that they were stabilized more in the excited state by an increase in solvent polarity. This shows that in all respects these PEs are suitable for NLO studies.
Nemoto *et al.* [142] prepared new types of PEs containing containing second-order NLO active chromophores with high density by the condensation polymerization between the isophthalic acid derivatives and the N-substituted diethanolamines using TPP and diethyl azodicarboxylate as the condensing agents in DMSO or NMP. The obtained amorphous PEs exhibited good solubility in common organic solvents and provided optical-quality films by spin-coating. The weight average molecular weights of PEs estimated from gel permeation chromatography (GPC) were the magnitude of thousand, which indicates the DP was ca. 10–15. Mehl *et al.* [143] investigated a series of optically active PEs containing chiral groups in the main chain by polycondensation of chiral diol with several aromatic diacids. The DP for all the polymers lay between 13 and 15 repeat units. The polydispersity of the samples was more or less similar, and therefore comparisons between different polymers were possible. The comparatively low polydispersity was a result of the good solubility of the monomers and low molar mass oligomers in methanol. Synthesis and characterization of novel optically active biodegradable network PEs from L- and D-malic acid and various glycols with different number of methylene groups ($HO(CH_2)_nOH$, nG, n = 2–6, 8–10, and 12) was studied by Nagata *et al.* [144]. The biodegradation experiments for the network PE films were carried out in enzymatic solution with *Rhizopus delemar* lipase and in an activated sludge. The stereochemistry between the L- and D-isomer of network PE films gave rise to the small differences in biodegradation rate: the rate of biodegradation for the network PE with L-isomer is higher than that with D-isomer. Bai *et al.* [145] synthesized a series of new liquid-crystalline PEs having the chiral centers and dipolar groups isoregically arranged along the polymer backbones. The physical properties such as molecular weights, intrinsic viscosities, elemental analyses, and thermal analy-

ses of polymers were studied. The thermal stability for polymers was similar regardless the difference in spacer length and molecular weight, because they have same functional groups and linkages. Srinivasan and Radhakrishnan [146] reported on the synthesis, characterization, and examination of liquid-crystalline properties of thermotropic main-chain random coPEs based on 4,4′-biphenol using twin spacers-chiral and achiral-revealed that chiral spacers were able to transmit the twist direction and a tilt angle to the molecule (their ferroelectric properties were investigated). The number average molecular weights measured by GPC were between 6000 and 8000 with polydispersities ranging from 1 to 1.1. Liquid-crystalline PEs based on hexanediol or butanediol, dimethyl 4,4′-biphenyldicarboxylate, and a sugar-based diol, and and various levels of isosorbide or isomanide (Figure 11), were organized with conventional melt polycondensation by Lin *et al*. [147]. Modest molecular weights were obtained, although they were typically lower than those of PE analogues that did not include sugar-based diols. TGA confirmed that the insertion of isosorbide or isomanide units did not reduce the thermal stability in a nitrogen atmosphere.

Hilker *et al*. [148] reported on the examination of a novel concept for the synthesis of chiral PEs (Figure 12), a lipase-catalyzed dynamic kinetic resolution (DKR) polymerization of racemic monomers. In their investigation, a mixture of stereoisomers of a secondarydiol is enzymatically polymerized with a difunctional acyl donor (dicarboxylic acid derivative) in the presence the Noyori-type ruthenium catalyst A and an immobilized Candida Antarctica Lipase B (Novozym 435). Because of its enantioselectivity the Lipase B converts only the hydroxy
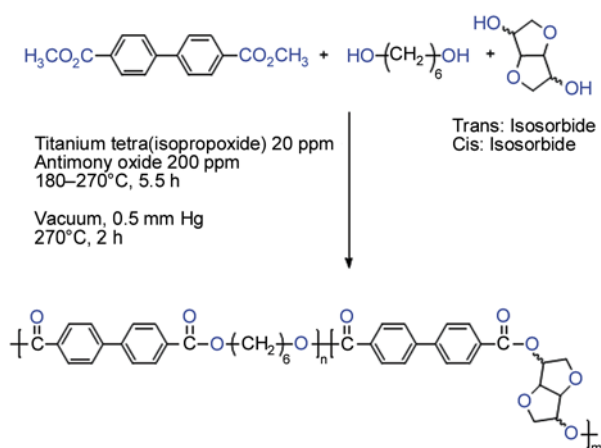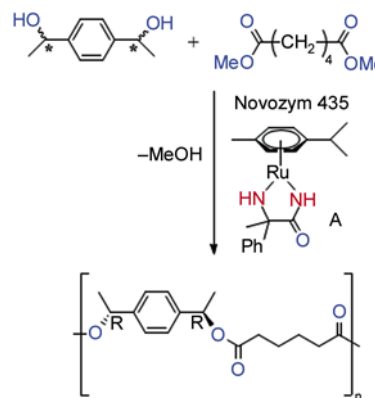
Figure 12. Reaction sequence for the one-pot DKR polymerization [148]

groups at the R-configured centers. In situ racemization of the hydroxysubstituted stereocenters from the S to the R configuration allows the polymerization to proceed to high conversion. They showed that DKR can be combined with enzymatic polymerization for the preparation of chiral PEs from racemic secondary diols. This notion offers an efficient method for the one-pot synthesis of chiral polymers from nonnatural monomers.

Under similar conditions DKR of secondary alcohols and esters was extended to secondary diols and diesters to afford chiral PEs by Van As *et al*. [149]. With these conditions, chiral polymers were obtained with peak molecular weights up to 15 kDa, enantiomeric excess (ee) values up to 99%. At most, an ee of 46% was obtained with low molecular weights in the range of 3.3–3.7 kDa. This process is an example of iterative tandem catalysis, an effective method for synthesis of chiral polymers from a variety of optically inactive monomers. Gómez *et al*. [150] reported on the first synthesis of optically active PE containing 11,11,12,12-tetra-cyano-9,10-anthraquinodimethane (TCAQ) as an efficient electron acceptor in the main chain by polycondensation reaction of (S)-2,2′-bis(dodecyloxy)-1,1′-binaphthyl-6,6′-dicarboxylic acid chloride with 2,6-dihydroxy-TCAQ. The reaction was carried out at moderate temperature in an aprotic solvent and in the presence of TEA. Cyclic voltammetry investigations showed that TCAQ preserved its acceptor ability in the polymer system and preliminary photophysical investigations showed fluorescence quenching in mixtures containing the acceptor polymer and fluorescent conjugated polymers.

Figure 11. Synthesis of chiral liquid-crystalline PEs [147]

2.4. Poly(amide-imide)s

Synthesis and characterization of a number of optically active poly(amide-imide)s (PAIs) were investigated by Mallakpour's group [151–154]. The polymerization reactions were carried out via polycondensation reaction of N-trimellitylimidoleucine, N-trimellitylimidoisoleucine, N-trimellitylimidophenylalanine and N-trimellitylimido-DL and L-alanine with several diamines in the presence of TPP, NMP, Py, and CaCl₂ under various conditions for different periods of time, and in another method (Figure 13). These aromatic PAIs showed optical rotations, were readily soluble in various organic solvents, and had moderate thermal stability. This could be due to the formation of some cyclic polymers instead of linear polymers.

Mallakpour and coworkers [155, 156] reported on some of preparation of chiral PAIs via direct solution polycondensation of different aliphatic and aromatic diisocyanates with a chiral diacid monomer. The optically active N-trimellitylimido-L-isoleuceine as a monomer was reacted with some aromatic as well as aliphatic diisocyanates according to isocyanate route. This method was a convenient technique for the preparation of novel optically active PAIs. In addition, in this method use of diamines was eliminated and there was no need to activate diacid monomer. Mallakpour *et al*. [157–159] have also investigated the synthesis of PAIs from the polycondensation reaction of N,N′-

(pyromellitoyl)-bis-L-*α*-amino diacid chloride such as: L-leucine, L-isoleucine and L-valine with different aromatic diamines under microwave heating in a porcelain dish and the results were compare with those polymers obtained by conventional heating (Figure 14). The obtained aromatic PAIs were optically active and soluble in various organic solvents and have good thermal stability. Microwave-assisted step-growth polymerization reactions preceded rapidly compared to conventional solution polycondensation and it was almost completed within a short period of time. Several types of optically active PAIs were prepared by Mallakpour *et al*. [160–163] from polycondensation reaction of N,N′-(4,4′-carbonyldiphthaloyl)-bis *α*-amino diacid chloride such as: L-phenylalanine, L-alanine and L-leucine with several aromatic diamines in o-cresol or DMAc (Figure 15). Polymerization reactions were carried out using microwave irradiation and conventional solution polycondensation. The polycondensation proceeded rapidly, compared with the conventional melt polycondensation and solution polycondensation giving a series of PAIs with inherent viscosities about 0.22–0.85 dl/g. All aromatic PAIs were optically active and readily soluble in various organic solvents and had good thermal stability. The inherent viscosities obtained from microwave assisted polycondensation reactions are much higher than those polymers obtained from solution polymerization. Furthermore, the above
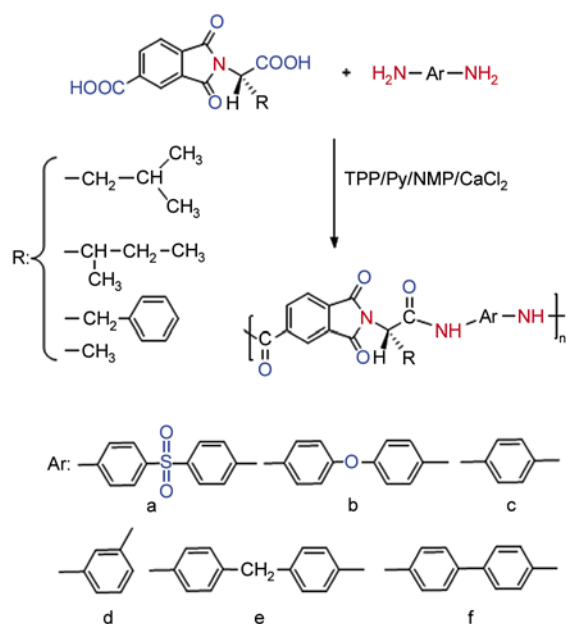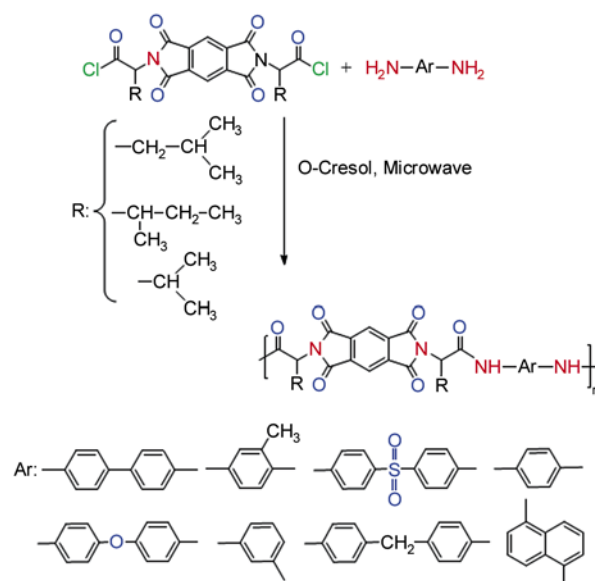

Figure 13. Synthesis route for optically active PAIs [151–154]

Figure 14. Synthesis of chiral PAIs by reaction of different N,N′-(pyromellitoyl)-bis-L-*α*-amino diacid chloride with aromatic diamines [157–159]

Figure 15. Reaction of several optically active diacid chlorides with different aromatic diamines [160–172, 176–179]

results demonstrate that microwave heating is an efficient method (shorter reaction time and high efficiency of energy) for the polycondensation reactions. Polymerization reaction of several diamines with 4,4′-(hexafluoroisopropylidene)-N,N′-bis-(phthaloylmethionine) diacid chloride and 4,4′-(hexafluoroisopropylidene)-bis-(phthaloylleucine) diacid chloride were performed in polar aprotic solvents by Mallakpour's group [164, 165] (Figure 15). By applying different solution polycondensation methods, fluorine containing PAIs having inherent viscosities in a range of 0.09–0.45 dL/g (molecular weight ranging 15 000–25 000 dalton) were synthesized. These polymers exhibit a higher thermal stability than non-fluorine bearing polymers with comparable structures. The presence of both amide and chiral imide groups into the polymer backbone, gives a good balance of properties with chiral centers; and introducing two CF$_3$ groups into the monomer unit, giving a good solubility in comparison to the other PAIs.

This group have also investigated direct polycondensation of 4,4′-(hexafluoroiso-propylidene)-N,N′-bis(phthaloylleucine-p-amidobenzoic acid) and N,N′-(4,4′-hexafluo-roisopropylidendiph-thaloyl)-bisisoleucine with aromatic diamines in a medium consisting of TPP, NMP, Py, and CaCl$_2$ or via Vilsmeier adduct derived from TsCl and DMF

[166, 167] (Figure 15). The resulting PAIs were obtained in high yield and are optically active and thermally stable. Furthermore, the resulting optically active PAIs contain amino acid linkages, could be biocompatible and biodegradable. Mallakpour's group [168–172] studied the microwave-promoted as well as conventional heating polycondensation of N,N′-(4,4′-oxydiphthaloyl)-bis-methionine diacid chloride or diacid chlorides contain amino acids of (S)-valine, L-isoleucine or L-leucine with several aromatic diamines (Figure 15). They also investigated a series of optically active PAIs via step-growth polymerization reactions of bis (p-amidobenzoic acid)-N-trimellitylimidoleucine monomer with different diisocyanates via direct step-growth polymerization under microwave irradiation, solution polymerization under gradual heating and reflux conditions in the presence of Py, DBTDL, and TEA as a catalyst and without a catalyst [173]. The optically active PAIs were obtained after a short time of 3 min in good yields (53–95%) and inherent viscosities in the range of 0.17 to 0.61 dL/g.

Moreover, this group [174, 175] studied the direct polyamidation of above monomer with different aromatic diamines in order to prepare another series of optically active PAIs with inherent viscosities of 0.22–0.52 dL/g, based on L-leucine and L-methionine amino acids. Because of combination of aromatic backbone and aliphatic side chain in the presence of several functional groups, the solubility of these polymers was improved without significant loss in their thermal properties. In addition, because of the existence of amino acid in the polymer backbone, these polymers are expected to be biodegradable and therefore are classified under environmentally friendly polymers. Synthesis of optically active PAIs by the reactions of chiral diacid chlorides containing 3,3′,4,4′-diphenylsulphonetetracarboxylic dianhydride and α-amino acids (S-valine, L-phenylalanine, L-leucine or L-isoleucine) moieties with several aromatic diamines was reported by Mallakpour and coworkers [176–179] (Figure 15). The polymerization reactions were carried out in the presence of a small amount of o-cresol and polymers with high yields and moderate inherent viscosities were obtained within 6 min with 100% of radiation power. In order to compare this method with conventional solution polycondensation, PAIs

were also synthesized by both low and high temperature solution step-growth polymerization reaction. The polyamidation reaction of 4,4′-carbonyl-bis(phthaloylalanine) diacid chloride with six different derivatives of tetrahydropyrimidinone and tetrahydro-2-thioxopyrimidine compounds were discussed earlier in the work of Mallakpour *et al.* [180] in the presence of a small amount of o-cresol. Under microwave irradiation power of 900 W, a
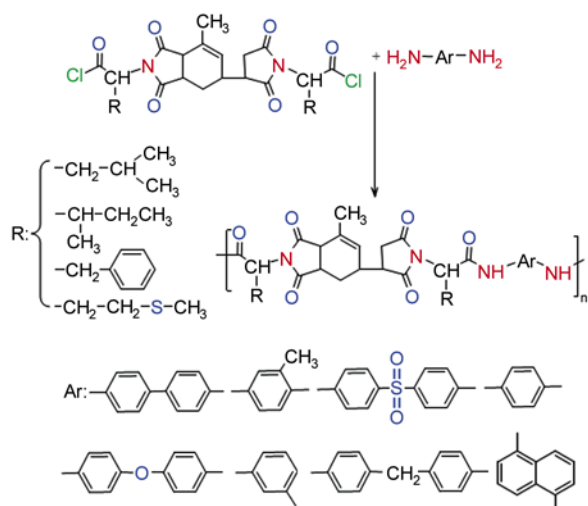
Figure 16. Synthesis of optically active PAIs containing epiclon and several amino acids [181–185]
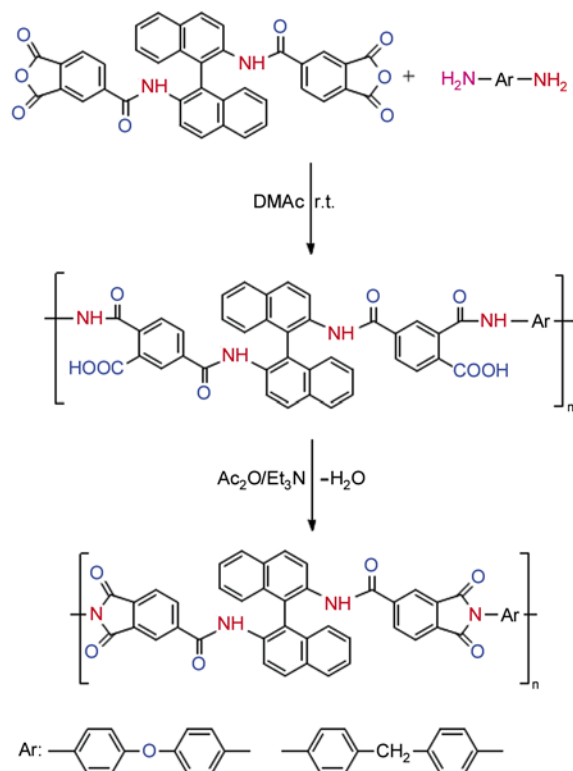
Figure 17. Synthesis of optically active PAIs derived from new chiral dianhydride and diamines [189]

series of optically active and thermally stable PAIs were produced within 10 min with inherent viscosities in the range of about 0.25–0.45 dL/g and high yields. The syntheses and characterization of optically active PAIs derived from diacid chloride containing epiclon and several amino acids such as L-phenylalanine, L-isoleucine, L-methionine, L-valine or L-Leucine with different aromatic diamines in the presence of a small amount of a polar organic medium such as NMP under microwave irradiation (Figure 16) was studied by Mallakpour and coworkers [181–185]. To compare microwave irradiation polymerization with solution polymerization methods PAIs were also synthesized by both low temperature and high temperature classical solution polymerization. The results of these methods were comparable with the microwave method. But the microwave heating is a more efficient method for these step-growth polymerization reactions.

Faghihi *et al.* [186–188] studied synthesis and characterization of optically active PAIs with hydantoin and thiohydantoin derivatives in the main chain via polycondensation reaction of N,N′-(pyromellitoyl)-bis-l-phenylalanine diacid chloride and six different derivatives of 5,5-disubstituted hydantoin compounds in the presence of a small amount of o-cresol as a polar organic media. Polymers were synthesized via two different methods: Classical heating and microwave irradiation method. The results showed that microwave heating is an efficient method for the polycondensation reactions. These PAIs exhibited excellent solubility in the organic solvents at room temperature.

Song *et al.* [189] prepared newly optically active aromatic PAIs from polycondensation reaction of 2,2′-bis(3,4-dicarboxybenzamido)-1,1′-binaphthyl dianhydride and different diamines in DMAc (Figure 17). Polymers with different ee% were investigated with respect to their structures and chiroptical properties. The results suggested that optically active PAIs posseed regular chiral conformations. They showed high glass transition temperatures of 287–290°C and 5% weight loss temperatures of 450–465°C in nitrogen.

2.5. Poly(ester-amide)s

Poly(ester-amide)s (PEA)s are emerging as promising materials for a wide range of biomedical applications due to their potential for both hydrolytic and

enzymatic degradation as well as the ease with which their properties can be tuned by the choice of monomers. The architecture of the PEA polymers is a blend of PA and PE polymer character. This leads to a blend of the characteristic behavior and properties of these two distinct polymers as well. The thermal properties of PEAs include higher melt transitions and increased thermal stability versus PEs. Conversely, the characteristic thermal properties are lower for PEAs than for PAs. PAs tend to be high melting and thermally stable. These characteristics make PAs difficult to process. PAs also generally display better mechanical endurance than the corresponding PEs, thanks to the formation of strong hydrogen bonding between the amide linkages of individual chains. PEs, on the other hand, is generally superior in flexibility, solubility, and hydrolytic susceptibility, and can thus be designed to degrade within a reasonable time-scale. PEAs represent a mixture of PE and PA character and therefore the corresponding thermal properties are a blend of the two homopolymers. The lower melt transitions versus PAs mean that molding, shaping and extruding are all possible. As a consequence, it is preferentially cleaved by enzymes. In PEAs, the combination of the bonding from two parent polymer families can be used to tailor the final thermal and enzymatic properties of the synthesized PEA polymer. The blend of characteristics is accomplished by varying the ratio of amide to ester bonds in the final polymer. This can be accomplished via co-polymerization of monomers containing both types of bonds, but more frequently by the condensation of monomers with terminal amines and terminal acids. The biological degradation behavior for PEAs is generally less complete than for PEs but much more complete than PAs. This is due to the ester bond being more readily hydrolyzed than the corresponding amide bond. The structure of the PEA polymer backbone, in particular, provides a straightforward route to biodegradable materials because of the possibility of incorporating biologically related molecules. The incorporation of pendant functional handles along the PEA backbone has the potential to further expand their applications by allowing the charge and hydrophilicity of the polymers to be altered, and facilitating the conjugation of active molecules such as drugs, targeting groups, and cell signaling molecules [190–193].

Atkins *et al*. [190] described a simple and versatile approach based on orthogonal protecting groups, by which L-lysine and L-aspartic acid could be incorporated into several families of PEAs based on monomers including the diacids succinic and terephthalic acid, the diols 1,4-butanediol and 1,8-octanediol, and the amino acids L-alanine and L-phenylalanine. Molina Pinilla *et al*. [194] reported on the synthesis and stereoregular high intrinsic viscosity chiral PEA derived from L-arabinose and succinic anhydride by using the active ester polycondensation method. The polymerization reaction was carried out in different polar solvents. The TGA thermogram indicated that this PEA was stable up to 250°C under nitrogen. Fan *et a*l. [195] prepared several optically active PEAs derived from L-isoleucine. Polymers were synthesized from the p-toluenesulfonic acid salt of o,o′-bis(leucyl)-hexanediol (TS-+LHD+TS-) and p-phthaloyl chloride and styrene-2,5-dicarbonyl chloride styrene by interfacial polymerization. The resulting polymers were soluble in strong acids (formic, dichloroacetic and trifluoroacetic acid) and chlorinated polar solvents such as chloroform and dichloromethane. The synthesis of PEAs from the reaction of p-nitrophenyl esters of sebacic or adipic acids and diamines containing α-amino acid ester groups was studied by Fan *et al*. [196] (Figure 18). The biodegradability of the resulting polymers was investigated by in vitro hydrolysis with proteases and a lipase as catalysts in borate buffer solutions. The results indicated that the polymers containing L-phenylalanine were hydrolyzed most effectively by α-chymotrypsin (α-CT), subtilisin Carlsberg, and subtilisin BPN′. The PEAs containing other amino acid residues also underwent hydrolysis to different extents, reflecting the substrate specificity of the proteases. Lipase had almost no effect on the hydrolytic degradation of these PEAs. The polymers containing glycine residues were hardly decomposed by any of the enzymes used.

Several optically active PEAs were synthesized by interfacial polycondensation of the mixture of 1,6-hexanediol diester of L- and D-alanine with sebacoyl chloride or terephthaloyl chloride by Nagata [197]. The enzymatic degradation of the PEAs was followed by the weight loss in a buffer solution (pH 7.2) of proteolytic enzymes (proteinase-K, papain and α-CT) and lipase enzymes (R. delemar, P. cepa-
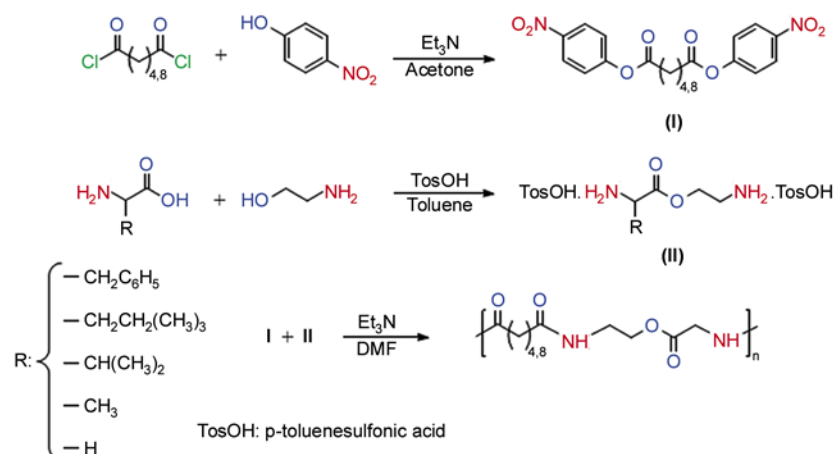
Figure 18. Synthesis of the optically active and biodegradable PEAs from amino acids, 2-aminoethanol, and dicarboxylic acid [196]

cia and C. rugosa) at 37°C. It was found that the degradation with the proteolytic enzymes is not caused by hydrolysis of the semi-peptide linkage but of the ester linkage. The synthesis and characterization of a new series of chiral PEAs was reported by Philip and Sreekumar [198]. These PEAs were prepared by solution polycondensation of diacid chlorides of bismaleamic acid with biphenolic azo chromophores and optically active isosorbide in DMAc at 100°C. The resulting polymers showed T_g between 100 and 190°C and were stable up to 400°C.

Asín *et al*. [199] synthesized sequential chiral PEAs derived from glycine by a two-steps method, involving a final thermal polyesterification. They compared this method in detail with their previous reported on the basis of interfacial polymerization. Thermal synthesis of the indicated glycine derivatives was carried out with high yield and generally provided polymers with the right molecular weight (M_W) to render fiber- and film-forming properties. Thermal synthesis seems to be useful for preparing polymers derived from diacid chlorides such as oxaloyl or succinoyl chlorides and diols such as 1,4-butanediol because the interfacial synthesis of these polymers is highly deficient. Furthermore, the intrinsic viscosities of the other studied polymers with aliphatic or aromatic components were generally higher when thermal synthesis was used. The resulting PEAs appear to be susceptible to the proteolytic enzymatic attack with papain as a result of the presence of glycine units. Degradable polymers may still be obtained when oxaloyl or terephthaloyl units were incorporated. In another study by Pare-

des *et al*. [200], a new kind of PEA derived from L-alanine was synthesized and the biodegradation and biocompatibility of the resulted polymer were investigated by them. The obtained polymer had good fiber and film-forming properties, as well as other characteristics like thermal stability and solubility in chloroform, which enhanced its processing facilities. Degradation studies showed that both pH and temperature influenced in the hydrolysis rate that took mainly place through the ester linkages. Degradation was also studied using different enzymes. Results indicated that papain was the most efficient of these, and that the hydrolysis to water-soluble products could be attained in a few days. The biocompatibility of the obtained polymer was investigated using cell culture techniques, because in vitro assessment of biocompatibility with permanent cell lines is a good screening method for detecting adverse effects.

Amino alcohols are easily obtained by the reduction of amino acids, which serve as useful chiral building blocks in organic synthesis. Step-growth polymerization of dicarboxylic acids with diols having amide moieties derived from optically active amino alcohols were carried out by Koyama *et al*. [201]. Polymers were obtained by the polycondensations using of 1-ethyl-3-(3-dimethylaminopropyl) carbodiimide hydrochloride in DMF at room temperature for 8 h in satisfactory yields. The T_g of the polymer rose with decrease of the methylene chain length of the dicarboxylic acid. Currently available synthetic biodegradable elastomers are primarily composed of crosslinked aliphatic PEs, which suffer from deficiencies including (1) high crosslink
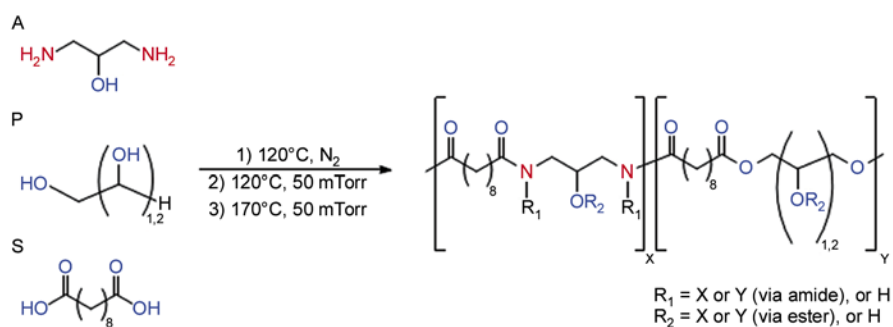
Figure 19. Synthesis scheme of APS polymers [202].

densities, which results in exceedingly high stiffness, (2) rapid degradation upon implantation, or (3) limited chemical moieties for chemical modification. Bettinger *et al*. [202] developed a new class of synthetic, biodegradable and chiral elastomeric PEAs, poly(1,3-diamino-2-hydroxypropane-co-polyol sebacate)s, composed of crosslinked networks based on an amino alcohol (Figure 19). These crosslinked networks featured tensile Young's modulus on the order of 1 MPa and reversable elongations up to 92%. These polymers showed in vitro and in vivo biocompatibility and were projected degradation half-lives up to 20 months in vivo.

Kobayashi *et al*. [203] prepared several optically active PEAs from polycondensation of ester-containing chiral dicarboxylic acid and different aromatic diamines in the presence of TPP, Py, and CaCl$_2$ in NMP. The resulting optically active polymers were obtained with inherent viscosities of 0.44–0.79 dl/g, and specific rotations from –43.6 to –78.5°. The T_gs of the polymers were in the range from 129 to 169°C, and their decomposition started at a temperature from 231 to 249°C to afford bis-crotonamide and terephthalic acid.

A new class of optically active and biodegradable PEAs was prepared by Gomurashvili *et al*. [204]. Polymers were synthesized by two step method. At first isosorbide or isomannide were esterified with *α*-amino acids in the presence of p-toluenesulfonic acid, and the resulting esters bisammonium tosylates were isolated. Second, the amino groups were liberated and polycondensed with p-nitrophenyl esters of aliphatic dicarboxylic acids. Biodegradation of resulting polymers was studied by chymotrypsin or lipase.

Poly(lactic acid) (PLA) and its copolymers have received great interest in industrial and medical applications. It can be used in plastic and fiber grade. Some of applications of PLA are resorbable sutures, drug delivery systems, artificial skin, implants for orthopedics, surgical materials, thermoforms, injection-molded or blow-molded containers, oriented and blown films, nonwovens, scaffold for tissue engineering and renewable plastics [205, 206]. To extend the use of LA-based polymers, functional group such as amide was introduced in the main chain. Most of the reports focus on the linear polymer, because they are easy to process, shape and manufacture. On the other hand, the attention was paid to the cross-linked polymers for enhancing the mechanical and thermal properties. A novel LA-based cross-linked PEA (LCPEA) with different cross-linking density was synthesized via polycondensation reaction of a dicarboxylic-terminated oligoester ELDA, a diacid derived from LA, TDI by Yue Ying *et al*. [205]. The tensile strength, elastic modulus and bend strength of the LCPEA of 65% gel fraction were 4.65, 136.55 and 39.63 MPa, respectively. The thermal decomposition temperature (50 wt%) of the LCPEA was around 410°C.

Although a number of PEAs of different compositions have been reported, there is a significant need for the incorporation of amino acids with functional side chains. This will allow for the conjugation of drugs or cell signaling molecules in tissue engineering scaffolds, thus expanding the potential applications of these materials. De Wit *et al*. [207] studied the synthesis, characterization and functionalization of novel PEAs. They reported on the incorporation of L-lysine into PEAs comprised of succinic acid, 1,4-butandiol, and L-phenylalanine to provide pendant amine functional groups for the first time in PEAs. The degradation of thin films of polymers was studied using scanning electron microscopy and the incorporation of lysine was found to signif-

icantly accelerate both the hydrolytic and enzy-matic degradation.

2.6. Poly(ester-imide)s

A series of optically active Poly(ester-imide)s (PEI)s were prepared through a facile and rapid polycondensation reaction of chiral N,N-(pyromel-litoyl)-bis-L-leucine diacid chloride and N,N-(pyromellitoyl)-bis-L-phenylalanine diacid chlo-ride with several aromatic diols such as phenol phthalein, bisphenol-A, 4,4′-hydroquinone, 1,8-dihydroxyanthraquinone, 1,5-dihydroxy naphtha-lene, 4,4′-dihydroxy biphenyl, and 2,4-dihydroxy-acetophenone using a domestic microwave oven in the presence of a small amount of a polar organic medium such as o-cresol by Mallakpour *et al*. [208, 209] (Figure 20). The polymerization reactions pro-ceeded rapidly and were completed within 10–20 min, producing a series of optically active PEIs with good yield and moderate inherent viscosity of 0.10–0.27 dl/g and were compare with polymeriza-tion reaction under solution condition but the result-ing materials were soluble in methanol probably due to formation of oligomers. Therefore microwave technique in this case was superior to the conven-tional solution method. These aromatic PEIs showed optical rotation and were readily soluble in various organic solvents and had good thermal stability. Fluorine containing PEIs having different α-amino acid such as: L-leucine, L-isoleucine and L-methio-

nine in main chain were also prepared by Mal-lakpour and coworkers [210–213] (Figure 21). The reactions with TsCl were significantly pro-moted by controlling alcoholysis with diols in the presence of the catalytic amounts of DMF to give a series of optically active PEIs with good yield, moderate to high inherent viscosity ranging 0.35–1.12 dL/g and also showed optical rotation. Ther-mal stability of the PEIs with fluorine containing linkage was higher than a related polymer having non-fluorinated. Furthermore, the resulting opti-cally active PEIs containing amino acid linkages so could be biocompatible and biodegradable. Mallakpour's group reported on the direct polycon-densation reactions of N,N′-(4,4′-oxydiphthaloyl)-bis-leucine diacid and N,N′-(4,4′-oxydiphthaloyl)-bis-methionine diacid with several aromatic diols in a system of TsCl, Py and DMF (method I) or thionyl chloride/Py (method II) [214–216] (Fig-ure 21). The influence of aging time, amount of DMF, concentration of monomers and condensing agents and reaction time on the physical properties of the resulting polymers was investigated by this group. Direct polyestrification in method II showed a series of advantages including improved reaction yield and higher M_W of the resulting PEIs and is very efficient in terms of cost and energy. The

Figure 20. Polycondensation reaction of chiral N,N-(pyromellitoyl)-bis-L-amino acid chloride with several aromatic diols [208, 209]
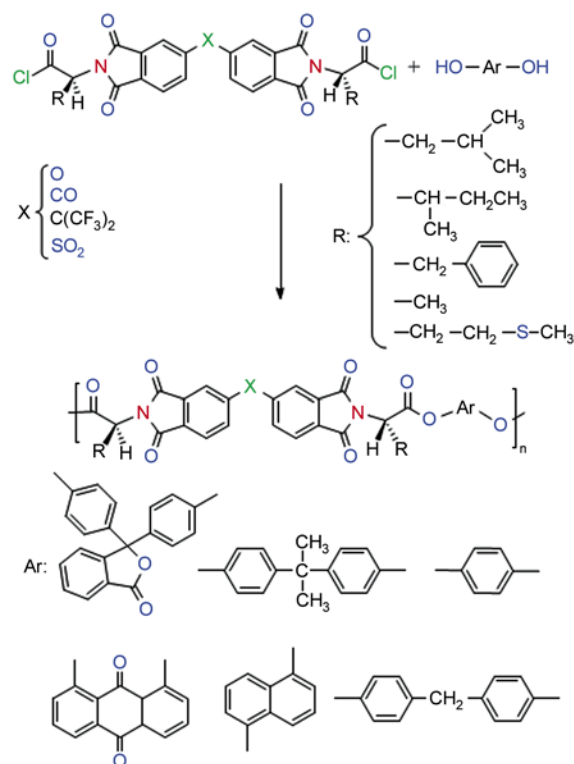
Figure 21. Preparation of different PEIs by reaction of sev-eral imide dicarboxylic acid and diols [210–219]

resulting PEIs had good yield and moderate inherent viscosity. The obtained polymers were thermally stable and were readily soluble in common organic solvents. Optically active PEIs containing benzophenone tetracarboxylic and L-phenylalanine or L-alanine moieties were synthesized from N,N′-(4,4′-carbonyldiphthaloyl)-bisphenylalanine or L-alanine diacid chloride with several aromatic diols by low-temperature solution polycondensation in CHCl₃/Et₃N solution and under microwave irradiation in the presence of a small amount of a polar organic medium such as o-cresol [217, 218] (Figure 21). These PEIs showed optical rotation and were readily soluble in various organic solvents and had moderate thermal stability. The same researchers also used L-isoleucine amino acid as a biocompatible material as well as optically active pure and chemical functional group in the polymer backbone for the formation of a series of new PEIs by direct polyesterification from aromatic diols and imide dicarboxylic acid which was prepared from trimellitic anhydride and L-isoleucine amino acid in a system of TsCl/Py/DMF [219] (Figure 21). Mallakpour's group also reported on [220] the synthesis of optically active PEIs via direct polycondensation of N-trimellitylimido-L-methionine with various aromatic diols such as bisphenol A, phenolphthalein, 1,5-naphthalendiol, 2,6-dihydroxytoluene, hydroquinone, biphenyl-2,2′-diol, 1,4-dihydroxyanthraquinone. The resulting PEIs were obtained in good yields and exhibited low to moderate inherent viscosities ranging from 0.15 to 0.40 dL/g. All of the PEIs showed good solubility and readily dissolved in aprotic polar solvents. Recently, this group [221] synthesized several novel chiral and potentially biodegradable PEIs bearing natural amino acids in the main chain as well as in the side chain via direct polyesterification of N,N′-(pyromellitoyl)-bis-(L-tyrosine dimethyl ester) as a biodegradable optically active phenolic diol and synthesized diacids containing different amino acids and phthalimide group in the side chain in TsCl/Py/DMF system as a condensing agent under conventional heating condition.

A series of axially chiral PEIs were prepared by the polycondensation reactions of new axially asymmetric dianhydrides, (R)-2,2′-bis(3,4-dicarboxybenzoyloxy)-1,1′-binaphthyl dianhydride and (S)-2,2′-bis(3,4-dicarboxybenzoyloxy)-1,1′-binaphthyl

dianhydride, and various diamines with aromatic, semiaromatic, and aliphatic structures by Song *et al.* [222]. The film-forming ability of PEIs was tested by the casting of 10% (w/v) solutions in DMAc onto a glass slide. All the polymers were able to form tough, flexible, and transparent films with 6–10 μm thick.

Kricheldorf's group [223] prepared a series of chiral PEIs by polycondensation of acid chloride of 4-aminocinnamic acid trimellitimide with various chiral diols at low or moderate temperature (0–60°C) in the presence of Py as HCl acceptor. They also synthesized [224] several cholesteric PEIs from (S)-pentyloxyterephthalic acid or (S,S)-2,5-bispentyloxyterephthalic acid and N-(4′-hydroxyphenyl)-4-hydroxyphthalimide. 2,5-bis(dodecyloxy)terephthalic acid and 2-(4′-chlorophenoxy) terephthalic acid were used as comonomer.

2.7. Poly(amide-ester-imide)s

A series of optically active poly(amide-ester-imide)s (PAEI)s based on bis(p-aminobezoic acid)-N-trimellitylimido-S-valine or L-isoleucine were prepared via polyesterification reaction of synthetic chiral diacids and different aromatic diols using TsCl/Py/(DMF) as a condensing agent by Mallakpour and coworkers (Figure 22) [225, 226]. The effect of the amount of DMF, aging time, reaction temperature, and reaction time was studied on the reaction yields and polymer viscosities. The resulting novel optically active PAEIs with inherent viscosities ranging 0.10–0.71 dL/g were obtained in high yield.
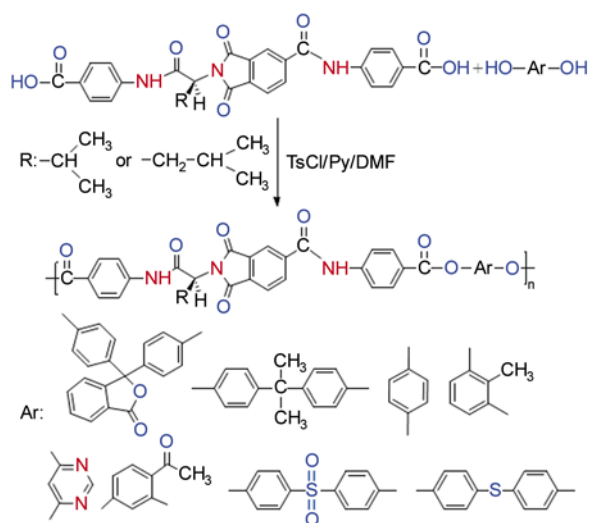
Figure 22. Preparation of optically active PAEIs [225, 226]

Li *et al*. [227] prepared PAEIs from amino acid (4-aminobenzoic acid, 3-aminobenzoic acid, or 6-aminohexanoic acid) and N-(4-hydroxyphenyl) phthalimide-4-carboxylic acid, N-(3-hydroxyphenyl) phthalimide-4-carboxylic acid, or N-(2-methyl-4-hydroxyphenyl) phthalimide-4-carboxylic acid in the presence of diphenylchlorophosphate and Py as direct condensation agents. The inherent viscosities of PAEIs were in the range of 0.13–0.95 dl/g. Thermotropic liquid crystalline behavior of these polymers was examined by DSC and optical polarizing microscopy. These PAEIs showed thermotropic liquid crystalline behavior in the range of 190–426°C.

2.8. Polyurethanes

Polyurethanes (PU)s, having a relatively short history, of slightly more than 65 years, became one of the most dynamic groups of polymers, and their use covers practically all the fields of polymer applications such as foams, elastomers, thermoplastics, thermorigids, adhesives, coatings, sealants, fibres and so on. PUs are used in nearly every aspect of daily life, changing the quality of human life. Furniture, bedding, seating for cars, shoe soles, thermoinsulation for refrigerators and buildings, wood substitutes, packaging, and coatings, are only a few common examples of PU use in every day life [228]. Because of importace of PUs and optically active polymers, many studies have been performed in the synthesis of optically active PUs by researchers. Chen *et al*. [229] synthesized an optically active PU by the step-growth polymerization of (2R,3R)-(+)-diethyl L-tartrate, MDI and polyethylene glycol (PEG) with various molecular weights at 60°C in DMSO. Chirackal Varkey and Sreekumar [230] prepared the TDI based optically active PUs consist of chiral units (diethyl-(2R,3R)(+)-tartrate) and donor-acceptor building blocks in the main chain with a helical conformation in the macromolecular chain by using DBTDL catalyst by incorporating the amido diols which were obtained by the aminolysis of ε-caprolactone by using the diamines, diaminoethane, diaminobutane, and diaminohexane, respectively. The effect of incorporation of the chiral molecule diethyl-(2R,3R)-(+)-tartrate on the properties of PUs was studied by changing the chromophores and also by varying the chiral-chromophore composition. An azobenzene PU containing chiral units with high thermal stability was synthesized by Qiu *et al*. [231] via step-growth polymerization of a chiral diol derived from diethyl-(2R,3R)-(+)-tartrate and 4-(4′-nitrophenylazo) phenylamine with TDI in the presence of the catalyst T-12 (Figure 23). It was a levopolymer whose optical rotation and melting point were –18.06 and 302°C, respectively. They investigated optical parameters, including the refractive index (n) and thermo-optic coefficient (dn/dT); the dielectric constant (ε) and its variation with temperature; and the thermal volume expansion coefficient and its variation with temperature of PU. These parameters are of great significance for the optical application of the material, particularly for the development of optical materials because of the control of their n values. The results indicated that the PU could be used in the design of high-performance thermo-optic polymer devices. Nagai *et al*. [232]
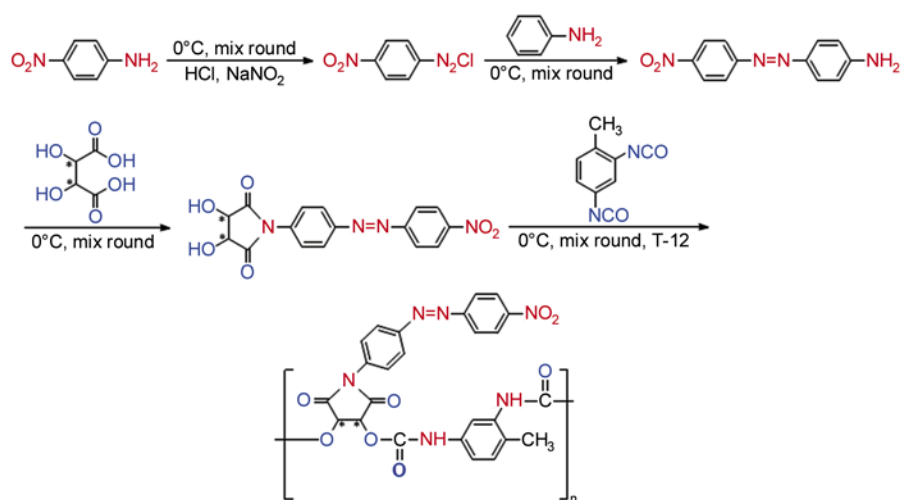
Figure 23. Synthesis of the chiral azobenzene PU containing [231]

reported on the synthesis and self-step-growth polymerization of optically active monomers having both isocyanate and hydroxyl groups derived from tyrosine. The resulting PUs had specific head-to-tail structures and some regulated, higher order structures such as helical conformation because of its asymmetric carbon. A series of optically active PUs were prepared by Chen *et al*. [233] from step-growth polymerization of chiral 1,1′-binaphthyl and TDI and the high-intensity ultrasonic was applied to the preparation of PU/TiO$_2$ nanocomposites. TGA studies indicated that thermal stability of the nanocomposites has improved with increasing nanoparticles content. Infrared emissivity study showed that the nanocomposites possessed lower emissivity value than those of PU and TiO$_2$, respectively. The ultrasonic method is a simple and inexpensive route to synthesize the polymer/nanoparticles, which can be extended to prepare a novel low infrared emissivity material. Zhou's group [234] also described the synthesis and the properties of novel optically active PUs based on chiral binaphthol via direct step-growth polymerization. The effect of optical purity on the specific rotation of the polymers was studied and results showed that the specific rotation of the polymer kept increasing with the optical purity, it may be explained that the increment of the optical purity caused a bigger chiral groups density. The resulting polymers displayed low infrared emissivity, which were expected to have potential application in the field of steals materials.

2.9. Polyureas

Diamines are frequently used to cure diisocyanates, especially isocyanate prepolymers, to give polyureas. The reaction has the advantages that no by-products are produced and that it can be carried out at low tempratures. Optically active polyureas have been reported to be prepared from optically active diisocyanate (L-lysinediisocyanatemethyl ester) and optically inactive linear diamine $H_2N(CH_2)_n$, where $n = 2$–6 and 9. Polymerization reaction was carried out by step-growth polymerization method [235]. The values of optical rotation of obtained polyureas were dependent on the methylene number of diamines. Asymmetric selective polyaddition of L-lysinediisocyanatemethylester for racemic 1,2-diaminopropane was unsuccessful.

A series of chiral polyureas having chiral diamine unity as part of the backbone were synthesized via step-growth polymerization of two chiral diamines and several aromatic and aliphatic diisocyanates by Dunjic *et al*. [236]. The resulting polymers were complexed with rhodium and used as catalysts in asymmetric hydride transfer C=O bond reduction.

2.10. Poly(imide-urethane)s

A series of poly(imide-urethane)s (PIU)s derived from N,N′-(pyromellitoyl)-bis-(L-leucine) diisocyanate and aromatic diols were synthesized via solution polycondensation by Mallakpour and Shahmohammadi [237]. Polymers were obtained in good yield and moderate inherent viscosity in the range 0.18–0.28 dl/g. The resulting PIUs have potential to be used as packing materials in column chromatography. Wang *et al*. [238] reported on the synthesis and characterization of optically active helical PIU with optical activity based on R-1,1′-binaphthyl-2′,2-diol and racemic PIU based on racemic 1,1′-binaphthyl-2′,2-diol. The thermal stability of R-PUI was higher than that of racemic-PUI due to the higher degree of hydrogen bond for R-PUI. In another study, this group prepared [239] helical PIU@attapulgite composite based on the surface modification of attapulgite. The results indicated that helical PIU has been grafted onto the surfaces of the modified attapulgite without destroying the original crystalline structure of attapulgite. The infrared emissivity of result composite was also investigated. The infrared emissivity value of PIU@attapulgite composite (0.628) was lower than that of bare attapulgite (0.934) due to the interfacial interactions between organics and inorganics. This work opened up a possibility for the preparation of infrared low-emissive materials.

2.11. Poly(urea-urethane)s

The synthesis and characterization of five new optically active poly(urea-urethane)s (PUU)s by solution step-growth polymerization of (1S,2S)-(+)-2-amino-3-methoxy-1-phenyl-1-propanol with diisocyanates (MDI, TDI, HDI, IPDI, *m*-xylylene diisocyanate) was reported by Chen and Tseng [240]. The conformation of the polymers in film state was studied by CD spectra, by comparison with the corresponding model compounds which

were synthesized from (1S,2S)-(+)-2-amino-3-methoxy-1-phenyl-1-propanol and phenyl isocyanate or propyl isocyanate. Polymers derived from aromatic diisocyanates formed as ordered conformation in the film state, while those from aliphatic diisocyanates did not. After packing as chiral stationary phases of HPLC, the polymers showed selective resolution to trans-stilbene oxide and trans-1,2-cyclopentanedicarboxanilide. Wang *et al.* [241] prepared several helical R/S- PUUs with R/S-1,1′-binaphthyl-2′,2-diol, TDI, and 1,4-diaminobenzene by a simple step-growth polymerization reaction. R-PUU and S-PUU were two enantiomorphs with wonderful mirror-image symmetry. The optical rotation values were +54.7 and –60.7°, respectively. The left-handed rotation structure was more stimulative for thermal stability than the righthanded rotation below 250°C because of both conformation and interchain hydrogen bonds, and they were reversed above 250°C; this can be attributed to the breaking of hydrogen bonds. The crystallizability of S-PUU was better than that of R-PUU because of the more orderly hydrogen bonds resulting in the interchain effects of S-PUU. The interchain hydrogen bonds were the plane-bifurcated structures, which are more stable and inlocked to the helical structures. In another study, this group also synthesized an optically active helical PUU with single-handed helical conformation by step-growth polymerization of chiral binaphthyl compound with MDI [242]. The interchain hydrogen bonds were controlled and changed in the synthesized progress, and they were affected by the helical conformation and the optical activity.

2.12. Poly(amide-imide-urethane)s

A series of optically active poly(amide-imide-urethane)s (PAIUs) based on PEG and MDI were prepared by Mallakpour's group [243–247] by the chain extension reaction of NCO terminated oligoamide prepared from the reaction of a chiral amino acid based dicarboxylic acid having a preformed imide ring according to diisocyanate route, with different M_W of PEG polyols by the two-step methods. The synthetic procedure referred to as two-step method, is effective for the synthesis of the multiblock copolymers having high structural regularity. Systematic study of PAIUs based PEG-MDI obtained in the presence of different solvents

and catalysts under different reaction time and temperatures demonstrated the influence of reaction condition on the efficiency of the polymer chain growth, viscosity, solubility and therefore porocessability of PAIUs. Best condition for the preparation of these optically active PAIUs was NMP as a solvent in the absence of any catalyst. They also synthesized [248] a new class of optically active PAIUs via a two-step diisocyanate route. In the first step, MDI was reacted with different diacids to produce an isocyanate-terminated oligo(amide imide). The chain extension of the previous hard segment with PEG with a M_W of 400 dalton was the second step for furnishing a series of new PAIUs. N-Trimellitylimido-L-leucine was used as a diacid monomer for polycondensation reactions. Polymerization reactions were performed without any catalyst or with Py or DBTDL as a catalyst. The optimized reaction conditions were used for the reaction of N-trimellitylimidoisoleucine, N-trimellitylimidomethionine, N-trimellitylimido-S-valine, and N-trimellitylimidophenyl-alanine as diacid monomers with MDI. In another study by Mallakpour *et al*. [249], a new series of optically active PAIUs were synthesized via two-step reactions. In the first step, MDI reacted with several PEGs such as PEG-400, PEG-600, PEG-2000, PEG-4000, and PEG-6000 to produce the soft segment parts. On the other hand, 4,4′-(hexafluoroisopropylidene)-N,N′-bis(phthaloylleucine-p-amidobenzoic acid) was prepared from the reaction of 4,4-(hexafluoroisopropylidene)-N,N′-bis(phthaloylleucine) diacid chloride with p-aminobenzoic acid to produce hard segment part. The chain extension of the above soft segment with the amide-imide is the second step to give a homologue series of PAIUs.

2.13. Poly(amide-imide-ether-urethane)s

Mallakpour's researcher group [250] used mathematical method for the optimization of some of the reaction parameters, that can influence viscosity and polymer chain growth of thermally stable optically active poly(amide-imide-ether-urethane)s (PAIEU)s based on a reaction component, bis(p-amidobenzoic acid)-N-trimellitylimidoleucine. It was shown that, the temperature of 85ºC and the reaction time of 2 h gives the highest viscosity for any PEG M_W. It means that, in spite of what they assumed, the constructed correlation in this study

showed there was no significant difference between the viscosities of polymers based on different M_W of PEGs. Another series of optically active PAIEUs based on polytetrahydrofuran (PTHF), of number-average molecular weights (M_n) = 1000 dalton as soft segment were synthesized by Mallakpour and Rafiemanzelat [251]. These copolymers were prepared via direct polycondensation reaction of an aromatic diacid based on L-leucine with preformed imide ring, MDI and PTHF-1000. The effect of the introduction of bis(p-amidobenzoic acid)-N-trimellitylimidoleucine (BPABTL) into PU back-bone on their properties was also studied. It was shown that BPABTL is an interesting candidate to incorporate amide, imide and amino acid moieties into segmented PUs and prepare them with more thermal stability, induced more crystallinity as well as good solubility.

2.14. Poly(amide-imide-ether-urea)s

Mallakpour and Seyedjamali [252] have also investigated the synthesis and characterization of a new multifunctional diamine containing L-leucine moieties in the structure and its polymerization with various diisocyanates to afford corresponding optically active poly(amide-imide-ether-urea)s. These components supplied several functional groups which showed some regulation effects on the properties of final polymers. The incorporation of stiff functions (imide, amide and urea groups) and flexible functions (aliphatic and ether moieties) made polymer chains flexible enough to be soluble in the common aprotic organic solvents as well as preservation of good thermal stability especially when aromatic diisocyanates were employed. The existence of isobutyl moieties in the structure of L-leucine may be the source of the increase of the free inter-chain volumes, suppressing the usual attraction of polymer chains as well as inducing the asymmetric character.

3. Synthesis of optically active polymers by Suzuki-Miyaura coupling reaction

The palladium-catalyzed cross-coupling reaction between organoboron compounds and organic halides or triflates provides a powerful and general methodology for the formation of carbon-carbon bonds. Recently, this reaction has been called the Suzuki coupling, Suzuki reaction, or Suzuki-Miyaura coupling [253]. Lately, many optically active conjugated polymers were synthesized by this reaction. Hu *et al*. [254] synthesized an optically active conjugated poly(arylenevinylene). They selected 1,1′-bi-2-naphthol, and its derivatives as building blocks in the construction of main chain chiral polymers because of their outstanding asymmetric differentiation properties. This polymer was soluble in common organic solvents and could be cast into self-standing films. This researcher group also prepared [255] an optically active polyarylene from the palladium-catalyzed Suzuki cross-coupling of an optically active binaphthyl molecule, 2′-bis(hexyloxy)-1,1′-binaphthyl-6,6′-diboronic acid, with 1,4-dibromobenzene. GPC analysis of this
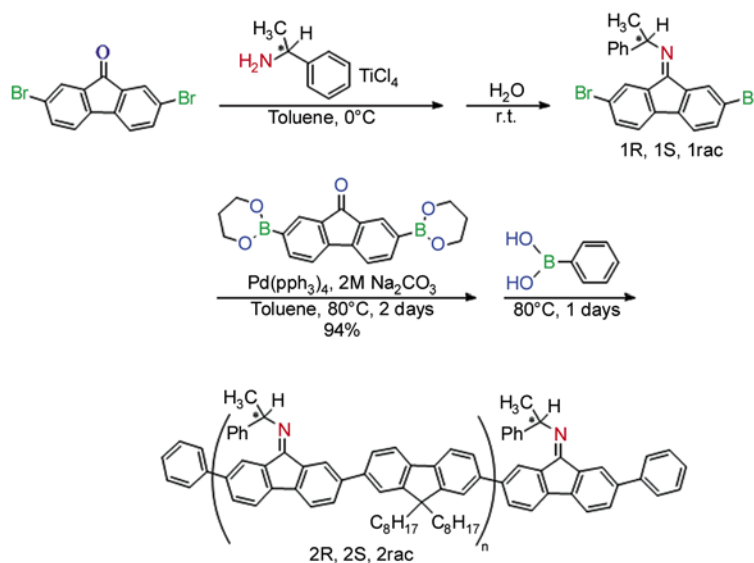
Figure 24. Synthesis of optically active polyfluorenes with chiral Schiff bases in the side chain by the palla-dium-catalyzed Suzuki-Miyaura coupling polymerization [258]

polymer showed $M_W = 41\,000$ and $M_n = 20\,000$. The specific optical rotation of resulting polymer was –289.4°. In another study Pu's group [256] synthesized a series of binaphthyl-based chiral poly(aryleneethynylene)s with different M_W by Suzuki coupling rection of an optically active binaphthyl molecule, (R)-2,2′-bis(octadecyloxy)-6,6′-diethynyl-1,1′-binaphthyl, with 1,4-diiodobenzene in the presence of tetrakis(triphenylphosphine)palladium(0) and cuprous iodide catalysts. The synthesis of the first optically active 1,1′-bi-2-naphthol and 2,2′-bis(diphenylphosphino)-1,1′-binaphthyl copolymer by Suzuki coupling reaction was reported by Yu *et al*. [257]. The resulting polymer showed $M_W = 11\,600$ dalton and $M_n = 7500$ dalton as was measured by GPC relative to polystyrene standards. They utilized this polymer in a tandem catalytic asymmetric diethylzinc addition and asymmetric hydrogenation of p-acetylbenzaldehyde to generate a chiral diol.

The synthesis of optically active poly(fluorene-alt-chiral iminofluorene)s using 1-phenylethylamine as a chiral auxiliary was described by Asai *et al*. [258]. Optically active polyfluorenes were synthesized by the palladium-catalyzed Suzuki-Miyaura coupling polymerization of 9,9′-dioctylfluorene-2,7-bis(trimethyleneborate) with a chiral Schiff base monomer (imino group modified-fluorene) (Figure 24). The obtained polymers showed intense green emission with high quantum efficiency.

4. Synthesis of optically active polymers by Sonogashira reaction
In 1975, Sonoghashira *et al.* reported [259] for the first time a coupling reaction of terminal alkynes with aryl or vinyl halides. Recently, this reaction has been used for the synthesis of different optically active polymers. Block and Hecht [260] used this reaction for the synthesis of a series of block copolymers composed of a highly isotactic and non-racemic poly(propylene oxide) segment joined to a poly(phenylene ethynylene) segment, with either meta or para connectivity. Two regioregular poly(p-phenyleneethynylene-alter-mphenyleneethynylene)s bearing (–)-trans-myrtanoxyl side groups with different substitution patterns were designed and synthesized by Li *et al*. [261] via Sonogashira reaction. These two polymers have the same chemical com-

ponent and main chain structure, but the substitution pattern of the chiral groups was different from each other. The effects of annealing temperature and time on the properties of the films were investigated by ultraviolet-visible absorption, fluorescence and CD spectra. The observations indicated that the substitution pattern of the chiral side groups had significant effect on the chiroptical properties of chirally substituted conjugated polymers.

5. Conclusions
In this paper, synthesis of various optically active condensation polymers was reviewed. There is currently intense interest in the synthesis and control of optically active polymers. Many of the condensation polymers reviewed here are prepared by polycondensation reaction of chiral monomers, which is more versatile, inexpensive and generally poor in control than addition polymerization. Optically active polymers often play important roles as key fundamental materials for welldefined polymers with specific secondary and/or tertiary structures. Optically active polymers have stimulated wide interest from synthetic, structural, and functional viewpoints. They have been extensively studied aiming at the application in optoelectronic devices and chiral recognition materials including asymmetric catalyst, chiral stationary phase in HPLC, enantioselective permeation membrane, chiral adsorbent for separation of racemates and in liquid crystals. Nature uses chirality as one of the key structural factors to perform a series of complicated functionalities such as molecular recognition and catalytic activities and can be saying that chirality is important for life.

References
[1] Okamoto Y.: Chiral polymers. Progress in Polymer Science, **25**, 159–162 (2000).
DOI: 10.1016/S0079-6700(99)00034-9

[2] Nakano T.: Optically active synthetic polymers as chiral stationary phases in HPLC. Journal of Chromatography A, **906**, 205–225 (2001).
DOI: 10.1016/S0021-9673(00)00944-4

[3] Okamoto Y.: Chiral polymers for resolution of enantiomers. Journal of Polymer Science Part A: Polymer Chemistry, **47**, 1731–1739 (2009).
DOI: 10.1002/pola.23215

[4] Fujiki M.: Optically active polysilylenes: State-of-the-art chiroptical polymers. Macromolecular Rapid Communications, **22**, 539–563 (2001).
DOI: 10.1002/1521-3927(20010501)22:8<539::AID-MARC539>3.0.CO;2-K

[5] Takata T., Furusho Y., Murakawa K. I., Endo T., Matsuoka H., Hirasa T., Matsuo J., Sisido M.: Optically active poly(aryl carbonates) consisting of axially chiral units. Chiral binaphthyl group induced helical polymer. Journal of the American Chemical Society, **120**, 4530–4531 (1998).
DOI: 10.1021/ja9743371

[6] Abdul Rahim E., Sanda F., Masuda T.: Synthesis and properties of optically active amino acid based polyacetylenes bearing eugenol and fluorene moieties. Journal of Polymer Science Part A: Polymer Chemistry, **44**, 810–819 (2006).
DOI: 10.1002/pola.21215

[7] Lee H. S., Hong J.: Chiral and electrokinetic separation of amino acids using polypyrrole-coated adsorbents. Journal of Chromatography A, **868**, 189–196 (2000).
DOI: 10.1016/S0021-9673(99)01246-7

[8] Guo H. S., Knobler C. M., Kaner R. B.: A chiral recognition polymer based on polyaniline. Synthetic Metals, **101**, 44–47 (1999).
DOI: 10.1016/S0379-6779(98)00301-4

[9] Hoffmann P., Wagner H., Weber G., Lanz M., Caslavska J., Thormann W.: Separation and purification of methadone enantiomers by continuous- and interval-flow electrophoresis. Analytical Chemistry, **71**, 1840–1850 (1999).
DOI: 10.1021/ac981178v

[10] Lemaire M., Delabouglise D., Garreau R., Guy A., Roncali J.: Enantioselective chiral poly(thiophenes). Journal of the Chemical Society, Chemical Communications, 658–661 (1988).
DOI: 10.1039/C39880000658

[11] Chen Z., Takei Y., Deore B. A., Nagaoka T.: Enantioselective uptake of amino acid with overoxidized polypyrrole colloid templated with L-lactate. Analyst, **125**, 2249–2254 (2000).
DOI: 10.1039/b005745m

[12] Kane-Maguire L. A. P., Norris I. D., Wallace G. G.: Properties of chiral polyaniline in various oxidation states. Synthetic Metals, **101**, 817–818 (1999).
DOI: 10.1016/S0379-6779(98)01117-5

[13] Pu L.: The study of chiral conjugated polymers. Acta Polymerica, **48**, 116–141 (1997).
DOI: 10.1002/actp.1997.010480402

[14] Kozlovsky M. V.: Chiral polymers with photoaffected phase behaviour for photo-optical and optoelectronic applications. Synthetic Metals, **127**, 67–70 (2002).
DOI: 10.1016/S0379-6779(01)00595-1

[15] Wulff G.: Main-chain chirality and optical activity in polymers consisting of C–C chains. Angewandte Chemie International Edition, **28**, 21–37 (1989).
DOI: 10.1002/anie.198900211

[16] Liaw D. J., Liaw B. Y., Kang E. T.: Synthesis and characterization of new cardo polyamide-imides containing ether and tricyclo[5.2.1.0^{2,6}]decane groups. Macromolecular Chemistry and Physics, **200**, 2402–2406 (1999).
DOI: 10.1002/(SICI)1521-3935(19991001)200:10<2402::AID-MACP2402>3.0.CO;2-C

[17] Feng L., Hu J., Liu Z., Zhao F., Liu G.: Preparation and properties of optically active poly(*N*-methacryloyl L-leucine methyl ester). Polymer, **48**, 3616–3623 (2007).
DOI: 10.1016/j.polymer.2007.04.064

[18] Sanda F., Yukawa Y., Masuda T.: Synthesis and properties of optically active substituted polyacetylenes having carboxyl and/or amino groups. Polymer, **45**, 849–854 (2004).
DOI: 10.1016/j.polymer.2003.11.044

[19] Takei F., Yanai K., Onitsuka K., Takahashi S.: Screw-sense-selective polymerization of isocyanides by dinuclear *μ*-ethynediyl complexes. Angewandte Chemie International Edition, **35**, 1554–1556 (1996).
DOI: 10.1002/anie.199615541

[20] Ute K., Hirose K., Kashimoto H., Hatada K., Vogl O.: Haloaldehyde polymers. 51. Helix-sense reversal of isotactic chloral oligomers in solution. Journal of American Chemical Society, **113**, 6305–6306 (1991).
DOI: 10.1021/ja00016a076

[21] Okamoto Y., Suzuki K., Ohta K., Hatada K., Yuki H.: Optically active poly(triphenylmethyl methacrylate) with one-handed helical conformation. Journal of the American Chemical Society, **101**, 4763–4765 (1979).
DOI: 10.1021/ja00510a072

[22] Chen L., Chen Y., Yao K., Zhou W., Li F., Chen L., Hu R., Tang B. Z.: A novel type of optically active helical liquid crystalline polymers: Synthesis and characterization of poly(*p*-phenylene)s containing terphenyl mesogen with different terminal groups. Journal of Polymer Science Part A: Polymer Chemistry, **47**, 4723–4735 (2009).
DOI: 10.1002/pola.23526

[23] Bouman M. M., Meijer E. W.: Stereomutation in optically active regioregular polythiophenes. Advanced Materials, **7**, 385–387 (1995).
DOI: 10.1002/adma.19950070408

[24] Suzuki Y., Shiotsuki M., Sanda F., Masuda T.: Chiral 1-methylpropargyl alcohol: A simple and powerful helical source for substituted polyacetylenes. Macromolecules, **40**, 1864–1867 (2007).
DOI: 10.1021/ma0629642

[25] Aoki T., Kaneko T., Maruyama N., Sumi A., Takahashi M., Sato T., Teraguchi M.: Helix-sense-selective polymerization of phenylacetylene having two hydroxy groups using a chiral catalytic system. Journal of the American Chemical Society, **125**, 6346–6347 (2003).
DOI: 10.1021/ja021233o

[26] Li B. S., Cheuk K. K. L., Ling L., Chen J., Xiao X., Bai C., Tang B. Z.: Synthesis and hierarchical structures of amphiphilic polyphenylacetylenes carrying L-valine pendants. Macromolecules, **36**, 77–85 (2003).
DOI: 10.1021/ma0213091

[27] Cheuk K. K. L., Lam J. W. Y., Chen J., Lai L. M., Tang B. Z.: Amino acid-containing polyacetylenes: Synthesis, hydrogen bonding, chirality transcription, and chain helicity of amphiphilic poly(phenylacetylene)s carrying L-leucine pendants. Macromolecules, **36**, 5947–5959 (2003).
DOI: 10.1021/ma0344543

[28] Lam J. W. Y., Tang B. Z.: Functional polyacetylenes. Accounts of Chemical Research, **38**, 745–754 (2005).
DOI: 10.1021/ar040012f

[29] Okoshi K., Sakurai S. I., Ohsawa S., Kumaki J., Yashima E.: Control of main-chain stiffness of a helical poly(phenylacetylene) by switching on and off the intramolecular hydrogen bonding through macromolecular helicity inversion. Angewandte Chemie International Edition, **48**, 8173–8176 (2006).
DOI: 10.1002/anie.200603663

[30] Wu S., Yang N., Yang L., Cao J., Liu J.: A novel type of optically active helical polymers: Synthesis and characterization of poly(α,β-unsaturated ketone). Journal of Polymer Science Part A: Polymer Chemistry, **48**, 1441–1448 (2010).
DOI: 10.1002/pola.23915

[31] Torma V., Gyenes T., Szakács Z., Noszál B., Némethy A., Zrínyi M.: Novel amino acid-based polymers for pharmaceutical applications. Polymer Bulletin, **59**, 311–318 (2007).
DOI: 10.1007/s00289-007-0774-9

[32] Sogawa H., Terada K., Masuda T., Sanda F.: Synthesis and properties of amino acid-derived optically active photo-responsive polymers. Polymer Bulletin, **63**, 803–813 (2009).
DOI: 10.1007/s00289-009-0121-4

[33] Terada K., Sanda F., Masuda, T.: Polycondensation of diketopiperazine-based dicarboxylic acids with diamines and dibromoxylenes. Journal of Macromolecular Science Part A: Pure and Applied Chemistry, **44**, 789–794 (2007).
DOI: 10.1080/10601320701406971

[34] Chankvetadze B., Yamamoto C., Kamigaito M., Tanaka N., Nakanishi K., Okamoto Y.: High-performance liquid chromatographic enantioseparations on capillary columns containing monolithic silica modified with amylose tris(3,5-dimethylphenylcarbamate). Journal of Chromatography A, **1110**, 46–52 (2006).
DOI: 10.1016/j.chroma.2006.01.076

[35] Okamoto Y., Yashima E., Hatada K., Mislow K.: Chromatographic resolution of perchlorotriphenylamine on (+)-poly(triphenylmethyl methacrylate). Journal of Organic Chemistry, **49**, 557–558 (1984).
DOI: 10.1021/jo00177a037

[36] Zheng J., Bragg W., Hou J., Lin N., Chandrasekaran S., Shamsi S. A.: Sulfated and sulfonated polysaccharide as chiral stationary phases for capillary electrochromatography and capillary electrochromatography-mass spectrometry. Journal of Chromatography A, **1216**, 857–872 (2009).
DOI: 10.1016/j.chroma.2008.11.082

[37] Lao W., Gan J.: High-performance liquid chromatographic separation of imidazolinone herbicide enantiomers and their methyl derivatives on polysaccharide-coated chiral stationary phases. Journal of Chromatography A, **1117**, 184–193 (2006).
DOI: 10.1016/j.chroma.2006.03.094

[38] Zhong Q., Han X., He L., Beesley T. E., Trahanovsky W. S., Armstrong D. W.: Chromatographic evaluation of poly (*trans*-1,2-cyclohexanediyl-bis acrylamide) as a chiral stationary phase for HPLC. Journal of Chromatography A, **1066**, 55–70 (2005).
DOI: 10.1016/j.chroma.2004.12.088

[39] Corley L. S., Vogl O.: Optically active polychloral. Polymer Bulletin, **3**, 211–217 (1980).
DOI: 10.1007/BF00291959

[40] Chiellini E., Senatori L., Solaro R.: A new chiral poly(alkyl vinyl ether): Synthesis and chiroptical properties. Polymer Bulletin, **20**, 215–220 (1988).
DOI: 10.1007/BF00261971

[41] Miyabe T., Hase Y., Iida H., Maeda K., Yashima E.: Synthesis of functional poly(phenyl isocyanide)s with macromolecular helicity memory and their use as asymmetric organocatalysts. Chirality, **21**, 44–50 (2009).
DOI: 10.1002/chir.20604

[42] Cao J., Yang N-F., Wang P-D., Yang L-W.: Optically active polyethers from chiral terminal epoxides with bulky group. Polymer International, **57**, 530–537 (2008).
DOI: 10.1002/pi.2380

[43] Pino P., Ciardelli F., Lorenzi G. P., Natta G.: Optically active vinyl polymers. VI. chromatographic resolution of linear polymers of (R)(S)-4-methyl-1-hexene. Journal of the American Chemical Society, **84**, 1487–1488 (1962).
DOI: 10.1021/ja00867a028

[44] Marvel C. S., Overberger C. G.: An optically active styrene derivative and its polymer. Journal of the American Chemical Society, **66**, 475–477 (1944).
DOI: 10.1021/ja01231a051

[45] Bailey W. J., Yates E. T.: Polymers. III. Synthesis of optically active stereoregular polyolefins. Journal of Organic Chemistry, **25**, 1800–1804 (1960).
DOI: 10.1021/jo01080a033

[46] Rogers M. E., Long T. E.: Synthetic methods in step-growth polymers. Wiley, New Jersey (2003).
DOI: 10.1002/0471220523

[47] Selegny E.: Optically active polymers. Springer, Dordrecht (1979).

[48] Morikawa A., Kakimoto M-A., Imai Y.: Preparation and properties of optically active aromatic polyamides derived from newly prepared chiral phenylindanediamine. High Performance Polymers, **7**, 149–156 (1995).
DOI: 10.1088/0954-0083/7/2/002

[49] Iribarren I., Alemán C., Bou J. J., Muñoz-Guerra S.: Crystal structures of optically active polyamides derived from di-*O*-methyl-l-tartaric acid and 1,*n*-alkanediamines: A study combining energy calculations, diffraction analysis, and modeling simulations. Macromolecules, **29**, 4397–4405 (1996).
DOI: 10.1021/ma951394v

[50] Bueno M., Zamora F., Molina I., Orgueira H. A., Varela O., Galbis J. A.: Synthesis and characterization of optically active polyamides derived from carbohydrate-based monomers. Journal of Polymer Science Part A: Polymer Chemistry, **35**, 3645–3653 (1997).
DOI: 10.1002/(SICI)1099-0518(199712)35:17<3645::AID-POLA4>3.0.CO;2-R

[51] Varela O., Orgueira H. A.: Synthesis of chiral polymides from carbohydrate-derived monomers. Advances in Carbohydrate Chemistry and Biochemistry, **55**, 137–174 (2000).
DOI: 10.1016/S0065-2318(00)55005-7

[52] Orgueira H. A., Erra-Balsells R., Nonami H., Varela P.: Synthesis of chiral polyhydroxy polyamides having chains of defined regio and stereoregularity. Macromolecules, **334**, 687–695 (2001).
DOI: 10.1021/ma000016+

[53] Orgueira H. A., Varela O.: Stereocontrolled synthesis of stereoregular, chiral analogs of nylon 5,5 and nylon 5,6. Tetrahedron: Asymmetry, **8**, 1383–1389 (1997).
DOI: 10.1016/S0957-4166(97)00121-3

[54] Orgueira H. A., Bueno M., Funes J. L., Galbis J. A., Varela O.: Synthesis and characterization of chiral polyamides derived from glycine and (S)-5-amino-4-methoxypentanoic acid. Journal of Polymer Science Part A: Polymer Chemistry, **36**, 2741–2748 (1998).
DOI: 10.1002/(SICI)1099-0518(19981115)36:15<2741::AID-POLA10>3.0.CO;2-E

[55] de Gracia García-Martín M., De Paz Báñez M. V., Galbis J. A.: Preparation of 3-amino-3-deoxy-2,4,5,6-tetra-o-methyl-D-altronic acid hydrochloride, a precursor in the preparation of a chiral *β*-polyamide (nylon 3 analog). Journal of Polymer Science Part A: Polymer Chemistry, **19**, 805–815 (2000).
DOI: 10.1080/07328300008544119

[56] Overberger C. G., Shimokawa Y.: Synthesis and optical properties of asymmetric polyamides derived from optically active cyclic dicarboxylic acids. Macromolecules, **4**, 718–725 (1971).
DOI: 10.1021/ma60024a010

[57] Overberger C. G., Okamoto Y., Bulacovschi V.: Synthesis and optical properties of asymmetric polyamides derived from optically active dicarboxylic acids and spirodiamine. Macromolecules, **8**, 31–36 (1975).
DOI: 10.1021/ma60043a007

[58] Lu C. X., Ji A., Overberger C. G.: Synthesis of polyamide containing optically active thymine derivative as a grafted pendant. Journal of Polymer Science Part A: Polymer Chemistry, **24**, 269–278 (1986).
DOI: 10.1002/pola.1986.080240206

[59] Overberger C. G., Lu C. X., Chen C. C.: Syntheses of stereoregular and optically active polyamides from active 4-chloro-1-benzotriazolyl diesters and diamines. Journal of Polymer Science Part A: Polymer Chemistry, **24**, 75–85 (1986).
DOI: 10.1002/pola.1986.080240106

[60] Li B., Yang X., Yang K., Fu E.: Synthesis of novel chiral macrocyclic polyamides derived from L-/D-tartaric acid. Synthetic Communications, **35**, 2603–2608 (2005).
DOI: 10.1080/00397910500214235

[61] Marqués M. S., Regaño C., Nyugen J., Aidanpa L., Muñoz-Guerra S.: Hydrolytic and fungal degradation of polyamides derived from tartaric acid and hexamethylenediamine. Polymer, **41**, 2765–2772 (2000).
DOI: 10.1016/S0032-3861(99)00422-X

[62] Esquivel D., Bou J. J., Muñoz-Guerra S.: Synthesis, characterization and degradability of polyamides derived from tartaric acid and diaminoethers. Polymer, **44**, 6169–6177 (2003).
DOI: 10.1016/S0032-3861(03)00651-7

[63] Bou J. J., Rodriguez-Galan A., Muñoz-Guerra S.: Optically active polyamides derived from L-tartaric acid. Macromolecules, **26**, 5664–5670 (1993).
DOI: 10.1021/ma00073a020

[64] Majó M. A., Alla A., Bou J. J., Herranz C., Muñoz-Guerra S.: Synthesis and characterization of polyamides obtained from tartaric acid and L-lysine. European Polymer Journal, **40**, 2699–2708 (2004).
DOI: 10.1016/j.eurpolymj.2004.07.020

[65] Alla A., Oxelbark J., Rodriguez-Galan A., Muñoz-Guerra S.: Acylated and hydroxylated polyamides derived from L-tartaric acid. Polymer, **46**, 2854–2861 (2005).
DOI: 10.1016/j.polymer.2005.02.046

[66] Cianga L.: Synthesis and characterization of optically active polymers containing azo groups and (L)-α-amino acid moieties. European Polymer Journal, **39**, 2271–2282 (2003).
DOI: 10.1016/S0014-3057(03)00140-X

[67] Carlini C., Fissi A., Galletti A. M. R., Sbrana G.: Optically active polymers bearing side-chain photochromic moieties: synthesis and chiroptical properties of methacrylic homopolymers with pendant *trans*-azobenzene chromophores bound through L-leucine, L-valine and L-proline amino acid spacers. Macromolecular Chemistry and Physics, **201**, 1540–1551 (2000).
DOI: 10.1002/1521-3935(20000801)201:13<1540:: AID-MACP1540>3.0.CO;2-8

[68] Wang L., Wang Y., Cao D.: Synthesis and characterization of novel biodegradable polyamides containing α-amino acid. Journal of Macromolecular Science Part A: Pure and Applied Chemistry, **46**, 312–320 (2009).
DOI: 10.1080/10601320802637441

[69] Ikeuchi Y., Nakagawa M., Yoshikawa M., Yoshida H., Sakurai S.: Chiral polyamides consisting of N-α-benzoyl-L-glutamic acid as a diacid component. Journal of Polymer Science Part A: Polymer Chemistry, **47**, 2530–2538 (2009).
DOI: 10.1002/pola.23335

[70] Nakagawa M., Ikeuchi Y., Yoshikawa M.: Chiral separation of racemic amino acids with novel polyamides having *N*-α-acetyl-L-glutamyl residue as a diacid component. Polymer, **49**, 4612–4619 (2008).
DOI: 10.1016/j.polymer.2008.08.018

[71] Katasarava R., Kharadze D., Kirmelashvili L., Medzmariashvili N., Goguadze T., Tsitlanadze G.: Polyamides from 2,2′-*p*-phenylenebis(Δ^2-5-oxazolone)s and *N,N*′-bistrimethylsilylated diamines. Synthesis of polyamides containing dipeptide links in the main chains. Die Makromolekulare Chemie, **194**, 143–150 (1993).
DOI: 10.1002/macp.1993.021940111

[72] Mansour M. E., Kandil S. H., Hassan H. H. A. M., Shaban M. A. E.: Synthesis of carbohydrate-containing polyamides and study of their properties. European Polymer Journal, **26**, 267–276 (1990).
DOI: 10.1016/0014-3057(90)90240-5

[73] Bachmann F., Thiem J.: Synthesis of hydrophilic carbohydrate-derived polyamides. Journal of Polymer Science Part A: Polymer Chemistry, **30**, 2059–2062 (1992).
DOI: 10.1002/pola.1992.080300934

[74] Zamora F., Bueno M., Molina I., Orgueira H. A., Varela O., Galbis J. A.: Synthesis of carbohydrate-based monomers that are precursors for the preparation of stereoregular polyamides. Tetrahedron: Asymmetry, **7**, 1811–1818 (1996).
DOI: 10.1016/0957-4166(96)00216-9

[75] Mancera M., Roffé I., Al-Kass S. S. J., Rivas M., Galbis J. A.: Synthesis and characterization of new stereoregular AABB-type polyamides from carbohydrate-based monomers having D-*manno* and L-*ido* configurations. Macromolecules, **36**, 1089–1097 (2003).
DOI: 10.1021/ma021307g

[76] Zamora F., Bueno M., Molina I., Iribarren J. I., Muñoz-Guerra S., Galbis J. A.: Stereoregular copolyamides derived from D-xylose and L-arabinose. Macromolecules, **33**, 2030–2038 (2000).
DOI: 10.1021/ma9916436

[77] Fernández C. E., Bermúdez M., Alla A., Mancera M., Garcia-Martín M. G., Benito E., Roffe I., Galbis J. A., Muñoz-Guerra S.: Crystallization studies on linear aliphatic polyamides derived from naturally occurring carbohydrates. Journal of Applied Polymer Science, **116**, 2515–2525 (2010).
DOI: 10.1002/app.31759

[78] Mallakpour S., Dinari M.: Microwave step-growth polymerization of 5-(4-methyl-2-phthalimidylpentanoylamino)isophthalic acid with different diisocyanates. Polymers for Advanced Technologies, **19**, 1334–1342 (2008).
DOI: 10.1002/pat.1142

[79] Mallakpour S., Taghavi M.: A facile, microwave-assisted synthesis of novel optically active polyamides derived from 5-(3-methyl-2-phthalimidylpentanoylamino)isophthalic acid and different diisocyanates. European Polymer Journal, **44**, 87–97 (2008).
DOI: 10.1016/j.eurpolymj.2007.10.027

[80] Mallakpour S., Sepehri S.: Preparation of new optically active polyamides containing a L-phenylalanine, phthalimide side-chain via the diisocyanate route by microwave energy: Comparison with conventional heating. Designed Monomers and Polymers, **11**, 535–546 (2008).
DOI: 10.1163/156855508X363825

[81] Mallakpour S., Dinari M.: Soluble new optically active polyamides derived from 5-(4-methyl-2-phthalimidylpentanoylamino)isophthalic acid and different diisocyanates under microwave irradiation in molten ionic liquid. Journal of Applied Polymer Science, **112**, 244–253 (2009).
DOI: 10.1002/app.29410

[82] Mallakpour S., Sepehri S.: Polycondensation of new optically active diacid with diisocyanates in the presence of tetrabutylammonium bromide as a green media under microwave heating. Reactive and Functional Polymers, **68**, 1459–1466 (2008).
DOI: 10.1016/j.reactfunctpolym.2008.07.004

[83] Mallakpour S., Taghavi M.: Efficient and rapid synthesis of optically active polyamides in the presence of tetrabutylammonium bromide as ionic liquids under microwave irradiation. Journal of Applied Polymer Science, **109**, 3603–3612 (2008).
DOI: 10.1002/app.28263

[84] Mallakpour S., Zadehnazari A.: Fast synthesis, using microwave induction heating in ionic liquid and characterization of optically active aromatic polyamides. Journal of Macromolecular Science Part A: Pure and Applied Chemistry, **46**, 783–789 (2009).
DOI: 10.1080/10601320903004541

[85] Mallakpour S., Taghavi M.: Direct polyamidation in green media: Studies on thermal degradation of novel organosoluble and optically active flame retardant polyamides. Reactive and Functional Polymers, **69**, 206–215 (2009).
DOI: 10.1016/j.reactfunctpolym.2008.12.023

[86] Mallakpour S., Rafiee Z.: Expeditious synthesis of novel aromatic polyamides from 5-[3-phenyl-2-(9,10-dihydro-9,10-ethanoanthracene-11,12-dicarboximido) propanoylamino]isophthalic acid and various diamines using microwave-assisted polycondensation. Reactive and Functional Polymers, **69**, 252–258 (2009).
DOI: 10.1016/j.reactfunctpolym.2009.01.003

[87] Mallakpour S., Taghavi M.: Microwave heating coupled with ionic liquids: Synthesis and properties of novel optically active polyamides, thermal degradation and electrochemical stability on multi-walled carbon nanotubes electrode. Polymer, **49**, 3239–3249 (2008).
DOI: 10.1016/j.polymer.2008.06.001

[88] Liu Y., Hua J., Sang W.: Dielectric properties in ferroelectric optically active polyamides. Journal of Macromolecular Science Part B: Physics, **39**, 349–358 (2000).
DOI: 10.1081/MB-100100390

[89] Chen Y., Siago K., Yonezawa N., Tachibana K., Hasegawa M.: Optically active polyamides having (−)-anti head-to-head coumarin dimer component. 3. Chiral recognition ability. Bulletin of the Chemical Society of Japan, **60**, 3341–3345 (1987).
DOI: 10.1246/bcsj.60.3341

[90] Liou G-S., Maruyama M., Kakimoto M-A., Imai Y.: Preparation and properties of aromatic polyamides from 2,2′-bis(*p*-aminophenoxy) biphenyl or 2,2′-bis(p-aminophenoxy)-1,1′-binaphthyl and aromatic dicarboxylic acids. Journal of Polymer Science Part A: Polymer Chemistry, **31**, 2499–2506 (1993).
DOI: 10.1002/pola.1993.080311010

[91] Liou G-S., Kakimoto M-A., Imai Y.: Preparation and properties of aromatic polyamides from 2,2′-bis(p-carboxyphenoxy) biphenyl or 2,2′-bis(*p*-carboxyphenoxy)-1,1′-binaphthyl and aromatic diamines. Journal of Polymer Science Part A: Polymer Chemistry, **31**, 3265–3272 (1993).
DOI: 10.1002/pola.1993.080311314

[92] Nozaki K., Terakawa T., Takaya H., Hiyama T.: Cyclic polyamides consisting of 1,1′-binaphthyls. 'Chiral twist' of glycine residues. Tetrahedron: Asymmetry, **8**, 3431–3436 (1997).
DOI: 10.1016/S0957-4166(97)00460-6

[93] Hsiao S-H., Yang C-P., Tsai C-Y., Liou G-S.: A novel class of organosoluble and light-colored fluorinated polyamides derived from 2,2′-bis(4-amino-2-trifluoromethylphenoxy)biphenyl or 2,2′-bis(4-amino-2-trifluoromethylphenoxy)-1,1′-binaphthyl. European Polymer Journal, **40**, 1081–1094 (2004).
DOI: 10.1016/j.eurpolymj.2004.01.001

[94] Agata Y., Kobayashi M., Kimura H., Takeishi M.: Synthesis and photoinduced transformation of helical aromatic polyamides containing atropisomeric biphenylene units and azobenzene segments in the main chain. Polymer International, **54**, 260–266 (2005).
DOI: 10.1002/pi.1664

[95] Liou G-S., Fang Y-K., Yen H-J.: Synthesis and properties of noncoplanar rigid-rod aromatic polyamides containing phenyl or naphthyl substituents. Journal of Polymer Research, **14**, 147–155 (2007).
DOI: 10.1007/s10965-006-9094-2

[96] Korshak V. V., Rogozhin S. V., Davankov V. A., Davidovich Y. A., Makarova T. A.: Advances in the synthesis of polypeptides. Russian Chemical Reviews, **34**, 329–366 (1965).
DOI: 10.1070/RC1965v034n05ABEH001449

[97] Dickinson H. R., Hiltner A.: Biodegradation of a poly-(*α*-amino acid) hydrogel. II. *In vitro*. Journal of Biomedical Materials Research, **15**, 591–603 (1981).
DOI: 10.1002/jbm.820150413

[98] Deming T. J.: Synthetic polypeptides for biomedical applications. Progress in Polymer Science, **32**, 858–875 (2007).
DOI: 10.1016/j.progpolymsci.2007.05.010

[99] Yang D. J., Li C., Nikiforow S., Gretzer M. B., Kuang L-R., Lopez M. S., Vargas K., Wallace S.: Diagnostic and therapeutic potential of poly(benzyl L-glutamate). Journal of Pharmaceutical Sciences, **83**, 328–331 (1994).
DOI: 10.1002/jps.2600830312

[100] Anson M. L., Edsall J. T., Bailey K.: Advances in protein chemistry, Volume 6. Academic Press, New York (1951).

[101] Frankel M., Neufeld O., Katchalski E.: Carbamates of *α*-amino-acid esters and their polycondensation. Nature, **144**, 832–833 (1939).
DOI: 10.1038/144832b0

[102] Frankel M., Katchalski E.: Poly-condensation of *α*-amino acid esters. I. Poly-condensation of glycine esters. Journal of the American Chemical Society, **64**, 2264–2268 (1942).
DOI: 10.1021/ja01262a011

[103] Frankel M., Katchalski E.: Poly-condensation of *α*-amino acid esters. II. Poly-condensation of alanine ethyl ester. Journal of the American Chemical Society, **64**, 2268–2271 (1942).
DOI: 10.1021/ja01262a012

[104] Katchalski E., Grossfeld I., Frankel M.: Poly-condensation of α-amino acid derivatives. III. Poly-lysine. Journal of the American Chemical Society, **70**, 2094–2101 (1948).
DOI: 10.1021/ja01186a032

[105] Frankel M., Berger A.: Synthesis of poly-aspartic acid. Nature, **163**, 213–214 (1949).
DOI: 10.1038/163213b0

[106] Fasman G. D., Blout E. R.: The synthesis and the conformation of poly-L-serine and poly-O-acetyl-L-serine. Journal of the American Chemical Society, **82**, 2262–2267 (1960).
DOI: 10.1021/ja01494a041

[107] Kim J-H., Son C. M., Jeon Y. S., Choe W-S.: Synthesis and characterization of poly(aspartic acid) derivatives conjugated with various amino acids. Journal of Polymer Research, in press, (2010).
DOI: 10.1007/s10965-010-9485-2

[108] Yuki H., Okamoto Y., Kobayashi Y.: Poly(β-amino acids). VI. Synthesis and conformational properties of poly[(r)-3-pyrrolidinecarboxylic acid]. Journal of Polymer Science: Polymer Chemistry Edition, **17**, 3867–3878 (1979).
DOI: 10.1002/pol.1979.170171207

[109] Mittal K. L.: Polyimides and other high temperature polymers: Synthesis, charactherization and applications, Volume 2. VSP, Utrecht (2003).

[110] Barikani M.: Polyimides derived from diisocyanates. Iranian Polymer Journal, **11**, 215–236 (2002).

[111] Mi Q., Gao L., Ding M.: The synthesis of a 1,1′-bi-2-naphthol-based bis(ether anhydride) and aromatic polyimides derived therefrom. Polymer, **38**, 3663–3668 (1997).
DOI: 10.1016/S0032-3861(96)00912-3

[112] Gao C., Zhang S., Gao L., Ding M.: Syntheses of biphenyl polyimides via nickel-catalyzed coupling polymerization of bis(chlorophthalimide)s. Macromolecules, **36**, 5559–5565 (2003).
DOI: 10.1021/ma034036y

[113] Yan J., Liu C., Wang Z., Xing W., Ding M.: Water resistant sulfonated polyimides based on 4,4′-binaphthyl-1,1′,8,8′-tetracarboxylic dianhydride (BNTDA) for proton exchange membranes. Polymer, **48**, 6210–6214 (2007).
DOI: 10.1016/j.polymer.2007.07.026

[114] Mi Q., Gao L., Ding M.: Optically active aromatic polyimides having axially dissymmetric 1,1′-binaphthalene-2,2′-diyl units. Macromolecules, **29**, 5758–5759 (1996).
DOI: 10.1021/ma9606667

[115] Mi Q., Ma Y., Gao L., Ding M.: New optically active aromatic polyimides II: Synthesis and properties of optically active aromatic polyimides based on (R)-(+)-2,2′-bis(trifluoro-4-aminophenoxy)-1,1′-binaphtyl. Chinese Journal of Polymer Science, **17**, 87–90 (1999).

[116] Mi Q., Ma Y., Gao L., Ding M.: Synthesis and characterization of optically active aromatic polyimides derived from 2,2′-bis(2-trifluoro- 4-aminophenoxy)-1,1′-binaphthyl and aromatic tetracarboxylic dianhydrides. Journal of Polymer Science Part A: Polymer Chemistry, **37**, 4536–4540 (1999).
DOI: 10.1002/(SICI)1099-0518(19991215)37:24< 4536 ::AID-POLA10>3.0.CO;2-Y

[117] Liou G-S.: Synthesis and properties of soluble aromatic polyimides from 2,2′-bis(3,4-dicarboxyphenoxy)-1,1′-binaphthyl dianhydride and aromatic diamines. Journal of Polymer Science Part A: Polymer Chemistry, **36**, 1937–1943 (1998).
DOI: 10.1002/(SICI)1099-0518(199808)36:11<1937:: AID-POLA29>3.0.CO;2-E

[118] Yigit M., Seçkin T., Koytepe S., Çetinkaya E.: Synthesis and characterization of polyimides prepared from optically active (R,R) and (S,S)-1,3-bis(p-N,N′-dimethylaminobenzyl)-perhydrobenzimidazol-2-thion. Turkish Journal of Chemistry, **31**, 113–124 (2007).

[119] Kudo K., Li J., Nonokawa D., Yoshizawa T., Kishida Y., Takayama T., Shiraishi S.: Synthesis and properties of structurally ordered alicyclic polyimides. Journal of Photopolymer Science and Technology, **15**, 215–218 (2002).

[120] Kudo K., Nonokawa D., Li J., Shiraishi S.: Synthesis of optically active alicyclic polyimides from a chiral, nonracemic dianhydride. Journal of Polymer Science Part A: Polymer Chemistry, **40**, 4038–4044 (2002).
DOI: 10.1002/pola.10497

[121] Li J., Kudo K., Shiraishi S.: Synthesis and properties of novel soluble polyimides having an unsymmetric spiro tricyclic dianhydride unit. Macromolecular Chemistry and Physics, **201**, 2289–2297 (2000).
DOI: 10.1002/1521-3935(20001101)201:17<2289:: AID-MACP2289>3.0.CO;2-F

[122] Kudo K., Yoshizawa T., Hamada T., Li J., Sakamoto S., Shiraishi S.: One-pot synthesis of an alternating copolyimide based on regioselective reaction of a non-symmetrical alicyclic dianhydride. Macromolecular Rapid Communications, **27**, 1430–1436 (2006).
DOI: 10.1002/marc.200600319

[123] Li J., Kudo K., Shiraishi S.: A study on the effect of spirocyclic structures in the main chain on the physical properties of copolyimides. Macromolecular Rapid Communications, **21**, 1166–1170 (2000).
DOI: 10.1002/1521-3927(20001101)21:16<1166:: AID-MARC1166>3.0.CO;2-M

[124] Barikani M., Mehdipour-Ataei S., Yeganeh H.: Synthesis and properties of novel optically active polyimides. Journal of Polymer Science Part A: Polymer Chemistry, **39**, 514–518 (2001).
DOI: 10.1002/1099-0518(20010215)39:4<514::AID-POLA1020>3.0.CO;2-4

[125] Yeganeh H., Tamami B., Ghazi I.: Synthesis and properties of novel diisocyanate based optically active polyimides. European Polymer Journal, **38**, 2179–2185 (2002).
DOI: 10.1016/S0014-3057(02)00115-5

[126] Yeganeh H., Tamami B., Ghazi I.: Synthesis and properties of novel optically active and soluble aromatic/aliphatic polyimides via reaction of dianhydrides and diisocyanates. Iranian Polymer Journal, **14**, 277–285 (2005).

[127] Mallakpour S., Kolahdoozan M.: Synthesis and properties of thermally stable and optically active novel wholly aromatic polyesters containing a chiral pendent group. European Polymer Journal, **43**, 3344–3354 (2007).
DOI: 10.1016/j.eurpolymj.2007.06.006

[128] Mallakpour S., Seyedjamali H.: Synthesis and characterization of novel organosoluble and optically active aromatic polyesters containing L-methionine and phthalimide pendent groups. Amino Acids, **34**, 531–538 (2008).
DOI: 10.1007/s00726-007-0005-6

[129] Mallakpour S., Rafiee Z.: Synthesis and characterization of novel organosoluble, thermal stable and optically active polyesters derived from 5-(2-phthalimidiylpropanoylamino)isophthalic acid. Polymer Journal, **39**, 1185–1192 (2007).
DOI: 10.1295/polymj.PJ2007061

[130] Mallakpour S., Sepehri S.: Synthesis and characterization of new optically active polyesters by step-growth polymerization of novel aromatic (2S)-4-[(4-methyl-2-phthalimidyl-pentanoylamino)benzoylamino]isophthalic acid with aromatic diols. Journal of Applied Polymer Science, **110**, 2942–2949 (2008).
DOI: 10.1002/app.28897

[131] Mallakpour S., Tirgir F.: Preparation and characterization of new thermally stable and optically active polyesters by direct polycondensation reaction promoted by Vilsmeier adduct. e-Polymers, no.108, 1–10 (2009).

[132] Mallakpour S., Hashemi E.: Synthesis and characterization of novel optically active and photoactive aromatic polyesters containing 1,8-naphthalimidyl pendant group by step-growth polymerization. Polymer Bulletin, **65**, 551–563 (2010).
DOI: 10.1007/s00289-009-0226-9

[133] Fujishiro K., Lenz R. W.: Main-chain cholesteric liquid crystalline polyesters with chiral pendant groups. 2. Cholesteric copolyesters containing chiral and achiral substituted hydroquinones. Macromolecules, **25**, 88–95 (1992).
DOI: 10.1021/ma00027a015

[134] Schwarz G., Kricheldorf H. R.: New polymer synthesis. LXXXIII. Synthesis of chiral and cholesteric polyesters from silylated 'sugar diols'. Journal of Polymer Science Part A: Polymer Chemistry, **34**, 603–611 (1996).
DOI: 10.1002/(SICI)1099-0518(199603)34:4<603::AID-POLA6>3.0.CO;2-R

[135] Stumpe J., Ziegler A., Berghahn M., Kricheldorf H. R.: Photoreactive cholesteric polyesters derived from 4-carboxycinnamic acid and novel chiral spacers. Macromolecules, **28**, 5306–5311 (1995).
DOI: 10.1021/ma00119a021

[136] Kricheldorf H. R., Wulff D. F.: Layer structures 12. Chiral sanidic polyesters derived from 2,5-bis(hexadecyloxy)terephthalic acid, 2,5-bis((S)-2-methylbutoxy)terephthalic acid and 4,4′-dihydroxybiphenyl. Polymer, **39**, 2683–2692 (1996).
DOI: 10.1016/S0032-3861(97)00580-6

[137] Kricheldorf H. R., Wulff D. F., Wutz C.: Layer structures, 13. Chiral sanidic polyesters derived from 2,5-bis(alkylthio)terephthalic acids. Macromolecular Chemistry and Physics, **200**, 799–809 (1999).
DOI: 10.1002/(SICI)1521-3935(19990401)200:4<799::AID-MACP799>3.0.CO;2-S

[138] Bahulayan D., Sreekumar K.: Chiral polyesters with azobenzene moieties in the main chain, synthesis and evaluation of nonlinear optical properties. Journal of Materials Chemistry, **9**, 1425–1429 (1999).
DOI: 10.1039/a900567f

[139] Philip B., Sreekumar K.: Second-harmonic response of a series of chiral polyesters: A joint experimental and theoretical study. Journal of Polymer Science Part A: Polymer Chemistry, **40**, 2868–2877 (2002).
DOI: 10.1002/pola.10371

[140] Philip B., Sreekumar K.: Studies on second harmonic generation efficiency by a series of chiral polyesters. Journal of Applied Polymer Science, **89**, 2468–2473 (2003).
DOI: 10.1002/app.12477

[141] Philip B., Sreekumar K.: Synthesis and characterization of chiral main chain polyesters with polar segments tailored for second harmonic generation. Journal of Materials Science, **38**, 1573–1577 (2003).
DOI: 10.1023/A:1022949320834

[142] Nemoto N., Miyata F., Nagase Y., Abe J., Hasegawa M., Shirai Y.: Novel types of polyesters containing second-order nonlinear optically active chromophores with high density. Macromolecules, **29**, 2365–2371 (1996).
DOI: 10.1021/ma951032n

[143] Mehl G. H., Valvo F., Lacey D., Goodby J. W., DasGupta D. K.: Properties of side chain liquid crystal polyesters containing chiral groups in the main chain. Polymer Engineering and Science, **36**, 2921–2931 (1996).
DOI: 10.1002/pen.10693

[144] Nagata M., Kono Y., Sakai W., Tsutsumi N.: Preparation and characterization of novel biodegradable optically active network polyesters from malic acid. Macromolecules, **32**, 7762–7767 (1999).
DOI: 10.1021/ma990907l

[145] Bai F., Chien L-C., Li C. Y., Cheng S. Z. D., Petschek R.: Synthesis and characterization of isoregic chiral smectic polyesters. Chemistry of Materials, **11**, 1666–1671 (1999).
DOI: 10.1021/cm990159e

[146] Srinivasan R., Radhakrishnan G.: Synthesis and characterization of liquid-crystalline polyesters with chiral and achiral twin spacers. Journal of Polymer Science Part A: Polymer Chemistry, **39**, 1743–1752 (2001).
DOI: 10.1002/pola.1152

[147] Lin Q., Pasatta J., Long T. E.: Synthesis and characterization of chiral liquid-crystalline polyesters containing sugar-based diols via melt polymerization. Journal of Polymer Science Part A: Polymer Chemistry, **41**, 2512–2520 (2003).
DOI: 10.1002/pola.10787

[148] Hilker I., Rabani G., Verzijl G. K. M., Palmans A. R. A., Heise A.: Chiral polyesters by dynamic kinetic resolution polymerization. Angewandte Chemie International Edition, **45**, 2130–2132 (2006).
DOI: 10.1002/anie.200503496

[149] Van As B. A. C., Buijtenen J. V., Mes T., Palmans A. R. A., Meijer E. W.: Iterative tandem catalysis of secondary diols and diesters to chiral polyesters. Chemistry-A European Journal, **13**, 8325–8332 (2007).
DOI: 10.1002/chem.200700818

[150] Gómez R., Segura J. L., Martín N.: Synthesis of an optically active electron-acceptor tetracyanoanthraquinodimethane (TCAQ) main-chain polyester. Tetrahedron Letters, **47**, 6445–6448 (2006).
DOI: 10.1016/j.tetlet.2006.06.112

[151] Mallakpour S. E., Hajipour A. R., Roohipour-fard R.: Direct polycondensation of *N*-trimellitylimido-L-leucine with aromatic diamines. European Polymer Journal, **36**, 2455–2462 (2000).
DOI: 10.1016/S0014-3057(00)00018-5

[152] Mallakpour S. E., Hajipour A-R., Shahmohammadi M. H.: Direct polycondensation of *N*-trimellitylimido-L-isoleucine with aromatic diamines. Journal of Applied Polymer Science, **89**, 116–122 (2003).
DOI: 10.1002/app.12075

[153] Mallakpour S. E., Hajipour A-R., Habibi S.: Synthesis of novel poly(amide-imide)s containing trimellitylimido-DL/L-alanine moieties via direct polycondensation. Journal of Applied Polymer Science, **80**, 1312–1318 (2001).
DOI: 10.1002/app.1218

[154] Mallakpour S. E., Hajipour A. R., Habibi S.: Synthesis of new poly(amide–imide)s derived from trimellitylimido-L-phenylalanine. Polymer International, **50**, 331–337 (2001).
DOI: 10.1002/pi.633

[155] Mallakpour S., Rafiemanzelat F.: Diisocyanate route as a convenient method for the preparation of novel optically active poly(amide–imide)s based on *N*-trimellitylimido-*S*-valine. European Polymer Journal, **41**, 2945–2955 (2005).
DOI: 10.1016/j.eurpolymj.2005.05.037

[156] Mallakpour S., Khani M.: Novel optically active poly(amide-imide)s derived from N-trimellitylimidol-L-isoleucine and different diisocyanates. Polymer Bulletin, **59**, 587–596 (2007).
DOI: 10.1007/s00289-007-0802-9

[157] Mallakpour S. E., Hajipour A. R., Habibi S.: Facile synthesis of new optically active poly(amide–imide)s derived from *N*,*N*′-(pyromellitoyl)-bis-L-leucine diacid chloride and aromatic diamines under microwave irradiation. European Polymer Journal, **37**, 2435–2442 (2001).
DOI: 10.1016/S0014-3057(01)00151-3

[158] Mallakpour S., Shahmohammadi M. H.: Microwave-promoted rapid synthesis of new optically active poly(amide imide)s derived from *N*,*N*′-(pyromellitoyl)-bis-L-isoleucine diacid chloride and aromatic diamines. Journal of Applied Polymer Science, **92**, 951–959 (2004).
DOI: 10.1002/app.13720

[159] Mallakpour S., Shahmohammadi M. H.: Synthesis of new optically active poly(amide-imide)s derived from *N*,*N*′-(pyromellitoyl)-bis-*S*-valine diacid chloride and aromatic diamines under microwave irradiation and classical heating. Iranian Polymer Journal, **14**, 473–483 (2005).

[160] Mallakpour S. E., Hajipour A-R., Zamanlou M. R.: Novel optically active poly(amide–imide)s from *N*,*N*′-(4,4′-carbonyldiphthaloyl)-bis-L-phenylalanine diacid chloride and aromatic diamines by microwave irradiation. European Polymer Journal, **38**, 475–485 (2002).
DOI: 10.1016/S0014-3057(01)00199-9

[161] Mallakpour S. E., Hajipour A-R., Faghihi K.: Microwave-assisted synthesis of optically active poly(amide–imide)s with benzophenone and L-alanine linkages. European Polymer Journal, **37**, 119–124 (2001).
DOI: 10.1016/S0014-3057(00)00097-5

[162] Mallakpour S. E., Hajipour A-R., Zamanlou M. R.: Synthesis of optically active poly(amide-imide)s derived from *N*,*N*′-(4,4′-carbonyldiphthaloyl)-bis-L-leucine diacid chloride and aromatic diamines by microwave radiation. Journal of Polymer Science Part A: Polymer Chemistry, **39**, 177–186 (2001).
DOI: 10.1002/1099-0518(20010101)39:1<177::AID-POLA200>3.0.CO;2-L

[163] Mallakpour S. E., Dabbagh A. H., Faghihi K.: Synthesis of novel optically active poly(amide-imide)s with benzophenone and L-alanine moieties. Iranian Polymer Journal, **9**, 41–48 (2000).

[164] Mallakpour S., Kowsari E.: Thermally stable and optically active poly(amide-imide)s derived from 4,4′-(hexafluoroisopropylidene)-*N*,*N*′-bis-(phthaloyl-L-methionine) diacid chloride and various aromatic diamines: synthesis and characterization. Polymer Bulletin, **57**, 169–178 (2006).
DOI: 10.1007/s00289-006-0549-8

[165] Mallakpour S. E., Hajipour A-R., Khoee S.: Synthesis and characterization of novel optically active poly (amide-imide)s. Polymer International, **48**, 1133–1140 (1999).
DOI: 10.1002/(SICI)1097-0126(199911)48:11<1133::AID-PI275>3.0.CO;2-#

[166] Mallakpour S., Moghadam E.: Direct polyamidation of *N*,*N*′-(4,4′-hexafluoroisopropy-lidendiphthaloyl)-bis-L-isoleucine with different aromatic diamines via vilsmeier adduct derived from tosyl chloride and *N*,*N*-dimethylformamide. Polymer Bulletin, **56**, 339–347 (2006).
DOI: 10.1007/s00289-006-0504-8

[167] Mallakpour S. E., Hajipour A. R., Khoee S.: Rapid synthesis of optically active poly(amide–imide)s by direct polycondensation of aromatic dicarboxylic acid with aromatic diamines. European Polymer Journal, **38**, 2011–2016 (2002).
DOI: 10.1016/S0014-3057(02)00099-X

[168] Mallakpour S., Kowsari E.: Synthesis and properties of novel soluble and thermally stable optically active poly(amide-imide)s from *N*,*N*′-(4,4′-oxydiphthaloyl)-bis-L-phenylalanine diacid chloride and aromatic diamines. Polymer Bulletin, **54**, 147–155 (2005).
DOI: 10.1007/s00289-005-0374-5

[169] Mallakpour S., Kowsari E.: Ionic liquids as novel solvents and catalysts for the direct polycondensation of *N*,*N*′-(4,4′-oxydiphthaloyl)-bis-L-phenylalanine diacid with various aromatic diamines. Journal of Polymer Science Part A: Polymer Chemistry, **43**, 6545–6553 (2005).
DOI: 10.1002/pola.21100

[170] Mallakpour S., Kowsari E.: Soluble novel optically active poly(amide–imide)s derived from *N*,*N*′-(4,4′-oxydiphthaloyl)-bis-L-leucine diacid chloride and various aromatic diamines: Synthesis and characterization. Journal of Applied Polymer Science, **96**, 435–442 (2005).
DOI: 10.1002/app.21462

[171] Mallakpour S., Kowsari E.: Polycondensation reaction of *N*,*N*′-(4,4′-oxydiphthaloyl)-bis-l-methionine diacid chloride with aromatic diamines: Synthesis and properties. Journal of Applied Polymer Science, **99**, 1038–1044 (2006).
DOI: 10.1002/app.22616

[172] Mallakpour S., Kowsari E.: Preparation and characterization of new optically active poly(amide-imide)s derived from *N*,*N*-(4,4′-Oxydiphthaloyl)-bis-(s)-(+)-valine diacid chloride and aromatic diamines. Polymer Engineering and Science, **46**, 558–565 (2006).
DOI: 10.1002/pen.20490

[173] Mallakpour S., Rafiemanzelat F.: Microwave-assisted and classical heating polycondensation reaction of bis(p-amido benzoic acid)-*N*-trimellitylimido-*L*-leucine with diisocyanates as a new method for preparation of optically active poly(amide imide)s. Journal of Applied Polymer Science, **93**, 1647–1659 (2004).
DOI: 10.1002/app.20603

[174] Mallakpour S., Hajipour A-R., Vahabi R.: Synthesis and characterization of novel poly(amide imide)s based on bis(*p*-amidobenzoic acid)-*n*-trimellitylimido-L-leucine. Journal of Applied Polymer Science, **84**, 35–43 (2002).
DOI: 10.1002/app.10181

[175] Mallakpour S., Kolahdoozan M.: Preparation of new poly(amide–imide)s with chiral architectures via direct polyamidation reaction. Journal of Applied Polymer Science, **104**, 1248–1254 (2007).
DOI: 10.1002/app.25747

[176] Mallakpour S., Kowsari E.: Preparation and characterization of new optically active poly(amide imide)s derived from *N*,*N*′-(4,4′-sulphonediphthaloyl)-bis-(s)-(+)-valine diacid chloride and aromatic diamines under microwave irradiation. Polymer Bulletin, **53**, 169–180 (2005).
DOI: 10.1007/s00289-004-0331-8

[177] Mallakpour S., Kowsari E.: Synthesis and characterization of novel, optically active poly(amide-imide)s from *N*,*N*′-(4,4′-sulfonediphthaloyl)-bis-L-phenylalanine diacid chloride and aromatic diamines under microwave irradiation. Journal of Applied Polymer Science, **41**, 3974–3988 (2003).
DOI: 10.1002/pola.10998

[178] Mallakpour S., Kowsari E.: Microwave-assisted and conventional polycondensation reaction of optically active *N*,*N*′-(4,4′-sulphonediphthaloyl)-bis-L-leucine diacid chloride with aromatic diamines. Journal of Applied Polymer Science, **91**, 2992–3000 (2004).
DOI: 10.1002/app.13515

[179] Mallakpour S., Kowsari E.: Preparation and characterization of optically active and organosoluble poly(amide-imide)s from polycondensation reaction of *N*,*N*′-(4,4′-sulphonediphthaloyl)-bis-L-isoleucine diacid with aromatic diamines. Polymers for Advanced Technologies, **16**, 466–472 (2005).
DOI: 10.1002/pat.603

[180] Mallakpour S. E., Hajipour A-R., Faghihi K., Foroughifar N., Bagheri J.: Novel optically active poly(amide-imide)s with tetrahydropyrimidinone and tetrahydro-2-thioxopyrimidine moieties by microwave-assisted polycondensation. Journal of Applied Polymer Science, **80**, 2416–2421 (2001).
DOI: 10.1002/app.1348

[181] Mallakpour S., Kowsari E.: Application of microwave irradiation for synthesis of novel optically active poly(amide imides) derived from diacid chloride containing epiclon and L-isoleucine with aromatic diamines. Journal of Applied Polymer Science, **93**, 2218–2229 (2004).
DOI: 10.1002/app.20738

[182] Mallakpour S. E., Hajipour A-R., Zamanlou M. R.: Microwave-assisted synthesis of optically active poly(amide imide)s derived from diacid chloride containing epiclon and L-leucine with aromatic diamines. Journal of Polymer Science Part A: Polymer Chemistry, **41**, 1077–1090 (2003).
DOI: 10.1002/pola.10652

[183] Mallakpour S., Kowsari E.: Synthesis and characterization of new optically active poly(amide-imide)s containing epiclon and L-methionine moieties in the main chain. Polymers for Advanced Technologies, **16**, 732–737 (2005).
DOI: 10.1002/pat.648

[184] Mallakpour S., Zamanlou M. R.: Synthesis of new optically active poly(amide-imide)s containing EPI-CLON and L-phenylalanine in the main chain by microwave irradiation and classical heating. Journal of Applied Polymer Science, **91**, 3281–3291 (2004).
DOI: 10.1002/app.13517

[185] Mallakpour S., Kowsari E.: Synthesis and properties of organosoluble and optically active poly(amide-imide)s based on epiclon and (S)-(+)-valine under microwave irradiation. Iranian Polymer Journal, **14**, 81–90 (2005).

[186] Faghihi K., Zamani K., Mallakpour S. E.: Synthesis and characterization of optically active poly(amide-imide)s with hydantoin and thiohydantoin derivatives in the main chain. Iranian Polymer Journal, **11**, 339–347 (2002).

[187] Faghihi K., Foroughifar N., Mallakpour S. E.: Facile synthesis of novel optically active poly(amide-imide)s derived from *N,N*-(pyromellitoyl)-bis-*l*-alanine diacid chloride, tetrahydropyrimidinone and tetrahydro-2-thioxopyrimidine by microwave-assisted polycondensation. Iranian Polymer Journal, **13**, 93–99 (2004).

[188] Faghihi K., Zamani K., Mirsamie A., Mallakpour S. E.: Facile synthesis of novel optically active poly(amide-imide)s containing *N,N′*-(pyromellitoyl)-bis-l-phenylalanine diacid chloride and 5,5-disubstituted hydantoin derivatives under microwave irradiation. Journal of Applied Polymer Science, **91**, 516–524 (2004).
DOI: 10.1002/app.13161

[189] Song N., Gao L., Ding M.: Optically active poly(amide–imide)s containing axially dissymmetric 1,1′-binaphthyl moieties. Journal of Polymer Science Part A: Polymer Chemistry, **37**, 3147–3154 (1999).
DOI: 10.1002/(SICI)1099-0518(19990815)37:16< 3147::AID-POLA12>3.3.CO;2-Q

[190] Atkins K. M., Lopez D., Knight D. K., Mequanint K., Gillies E. R.: A versatile approach for the syntheses of poly(ester amide)s with pendant functional groups. Journal of Polymer Science Part A: Polymer Chemistry, **47**, 3757–3772 (2009).
DOI: 10.1002/pola.23429

[191] Shi R., Chen D., Liu Q., Wu Y., Xu X., Zhang L., Tian W.: Recent advances in synthetic bioelastomers. International Journal of Molecular Sciences, **10**, 4223–4256 (2009).
DOI: 10.3390/ijms10104223

[192] Okada M., Tsunoda K., Tachikawa K., Aoi K.: Biodegradable polymers based on renewable resources. IV. Enzymatic degradation of polyesters composed of 1,4:3.6-dianhydro-D-glucitol and aliphatic dicarboxylic acid moieties. Journal of Applied Polymer Science, **77**, 338–346 (2000).
DOI: 10.1002/(SICI)1097-4628(20000711)77:2<338:: AID-APP9>3.0.CO;2-C

[193] Armelin E., Paracuellos N., Rodríguez-Galán A., Puiggalí J.: Study on the degradability of poly(ester amide)s derived from the α-amino acids glycine, and L-alanine containing a variable amide/ester ratio. Polymer, **42**, 7923–7932 (2001).
DOI: 10.1016/S0032-3861(01)00315-9

[194] Pinilla I. M., Bueno Martinez M., Perez J. A. G.: Synthesis of a stereoregular poly(ester amide) derived from L-arabinose. Macromolecules, **28**, 3766–3770 (1995).
DOI: 10.1021/ma00115a003

[195] Fan X-H., Zhou J-L., Chen X-F., Wan X-H., Zhou Q-F.: Synthesis, characterization of chiral poly(ester amide)s derived from L-isoleucine. Chinese Journal of Polymer Science, **22**, 497–500 (2004).

[196] Fan Y., Kobayashi M., Kise H.: Synthesis and specific biodegradation of novel polyesteramides containing amino acid residues. Journal of Polymer Science Part A: Polymer Chemistry, **39**, 1318–1328 (2001).
DOI: 10.1002/pola.1109

[197] Nagata M.: Synthesis and enzymatic degradation of poly(ester-amide) stereocopolymers derived from alanine. Macromolecular Chemistry and Physics, **200**, 2059–2064 (1999).
DOI: 10.1002/(SICI)1521-3935(19990901)200:9< 2059::AID-MACP2059>3.0.CO;2-N

[198] Philip B., Sreekumar K.: Optically active poly(ester-amide)s: Synthesis and characterization. Polymer International, **50**, 1318–1323 (2001).
DOI: 10.1002/pi.777

[199] Asín L., Armelin E., Montané J., Rodríguez-Galán A., Puiggalí J.: Sequential poly(ester amide)s based on glycine, diols, and dicarboxylic acids: Thermal polyesterification versus interfacial polyamidation. Characterization of polymers containing stiff units. Journal of Polymer Science Part A: Polymer Chemistry, **39**, 4283–4293 (2001).
DOI: 10.1002/pola.10082

[200] Paredes N., Rodríguez-Galán A., Puiggalí J., Peraire C.: Studies on the biodegradation and biocompatibility of a new poly(ester amide) derived from L-alanine. Journal of Applied Polymer Science, **69**, 1537–1549 (1998).
DOI: 10.1002/(SICI)1097-4628(19980822)69:8<1537::AID-APP8>3.0.CO;2-D

[201] Koyama E., Sanda F., Endo T.: Polycondensations of dicarboxylic acids and diols derived from optically active amino alcohols. Journal of Polymer Science Part A: Polymer Chemistry, **35**, 2925–2934 (1997).
DOI: 10.1002/(SICI)1099-0518(199710)35:14<2925::AID-POLA13>3.0.CO;2-L

[202] Bettinger C. J., Bruggeman J. P., Borenstein J. T., Langer R. S.: Amino alcohol-based degradable poly(ester amide) elastomers. Biomaterials, **29**, 2315–2325 (2008).
DOI: 10.1016/j.biomaterials.2008.01.029

[203] Kobayashi T., Kakimoto M. A., Imai Y.: Synthesis and properties of optically active polyester-amides from ester-containing chiral dicarboxylic acid and aromatic diamines. Polymer Journal, **25**, 65–73 (1993).

[204] Gomurashvili Z., Kricheldorf H. R., Katsarava R.: Amino acid based bioanalogous polymers. synthesis and study of new poly(ester amide)s composed of hydrophobic *α*-amino acids and dianhydrohexitoles. Journal of Macromolecular Science Part A: Pure and Applied Chemistry, **37**, 215–227 (2000).
DOI: 10.1081/MA-100101089

[205] Yue Ying H. E., Xiao M.: Synthesis and properties of lactic acid-based cross-linked poly(ester-amide). Chinese Chemical Letters, **17**, 645–648 (2006).

[206] Agrawal A. K., Bhalla R.: Advances in the production of poly(lactic acid) fibers. A review. Journal of Macromolecular Science Part C: Polymer Reviews, **43**, 479–503 (2003).
DOI: 10.1081/MC-120025975

[207] De Wit M. A., Wang Z., Atkins K. M., Mequanint K., Gillies E. R.: Syntheses, characterization, and functionalization of poly(ester amide)s with pendant amine functional groups. Journal of Polymer Science Part A: Polymer Chemistry, **46**, 6376–6392 (2008).
DOI: 10.1002/pola.22915

[208] Mallakpour S. E., Hajipour A-R., Habibi S.: Microwave-assisted synthesis of new optically active poly(ester-imide)s containing *N,N′*-(pyromellitoyl)-bis-*L*-phenylalanine moieties. Journal of Applied Polymer Science, **86**, 2211–2216 (2002).
DOI: 10.1002/app.11219

[209] Mallakpour S., Habibi S.: Microwave-promoted synthesis of new optically active poly(ester-imide)s derived from *N,N′*-(pyromellitoyl)-bis-L-leucine diacid chloride and aromatic diols. European Polymer Journal, **39**, 1823–1829 (2003).
DOI: 10.1016/S0014-3057(03)00079-X

[210] Mallakpour S. E., Hajipour A-R., Khoee S.: Microwave-assisted polycondensation of 4,4′-(hexafluoroisopropylidene)-*N,N′*-bis(phthaloyl-L-leucine) diacid chloride with aromatic diols. Journal of Applied Polymer Science, **77**, 3003–3009 (2000).
DOI: 10.1002/1097-4628(20000923)77:13<3003::AID-APP26>3.0.CO;2-6

[211] Mallakpour S., Kowsari E.: Preparation and characterization of new thermally stable and optically active poly(ester-imide)s by direct polycondensation with thionyl chloride in pyridine. Polymers for Advanced Technologies, **17**, 174–179 (2006).
DOI: 10.1002/pat.711

[212] Mallakpour S., Kowsari E.: Synthesis of novel optically active poly(ester imide)s by direct polycondensation reaction promoted by tosyl chloride in pyridine in the presence of *N,N*-dimethyformamide. Journal of Applied Polymer Science, **101**, 455–460 (2006).
DOI: 10.1002/app.23289

[213] Mallakpour S., Moghaddam E.: Preparation of new poly(ester-imide)s from N,N′-(4,4′-hexafluoroisopropylidendiphthaloyl)-bis-isoleucine and aromatic diols with TsCl/Py/DMF as a condensing agent. Iranian Polymer Journal, **15**, 547–554 (2006).

[214] Mallakpour S., Kowsari E.: Direct polycondensations of *N,N′*-(4,4′-oxydiphthaloyl)-bis-L-leucine diacid by use of tosyl chloride in the presence of *N,N*-dimethylformamide. Polymers for Advanced Technologies, **16**, 795–799 (2005).
DOI: 10.1002/pat.654

[215] Mallakpour S., Kowsari E.: Thionyl chloride/pyridine system as a condensing agent for the polyesterification reaction of *N,N′*-(4,4′-oxydiphthaloyl)-bis-*L*-leucine and aromatic diols. Iranian Polymer Journal, **15**, 457–465 (2006).

[216] Mallakpour S., Kowsari E.: Synthesis of organosoluble and optically active poly(ester-imide)s by direct polycondensation with tosyl chloride in pyridine and dimethylformamide. Polymer Bulletin, **55**, 51–59 (2005).
DOI: 10.1007/s00289-005-0416-z

[217] Mallakpour S. E., Hajipour A-R., Zamanlou M-R.: New optically active poly(ester-imide)s derived from *N,N′*-(4,4′-carbonyldiphthaloyl)-bis-L-phenylalanine diacid chloride. Journal of Applied Polymer Science, **85**, 315–320 (2002).
DOI: 10.1002/app.10630

[218] Mallakpour S. E., Hajipour A-R., Faghihi K.: Synthesis of novel optically active poly(ester-imide)s with benzophenone linkages by microwave-assisted polycondensation. Polymer International, **49**, 1383–1388 (2000).
DOI: 10.1002/1097-0126(200011)49:11<1383::AID-PI502>3.0.CO;2-D

[219] Mallakpour S., Shahmohammadi M. H.: Direct poly-condensation of *N*-trimellitylimido-*L*-isoleucine with aromatic diols. Iranian Polymer Journal, **14**, 974–981 (2005).

[220] Mallakpour S., Meratian S. H.: Synthesis and characterization of organosoluble optically active poly(ester-imide)s derived from trimellitic anhydride, L-methionine and bisphenols. High Performance Polymers, **20**, 3–18 (2008).
DOI: 10.1177/0954008307078385

[221] Mallakpour S., Asadi P.: Novel chiral poly(ester-imide)s with different natural amino acids in the main chain as well as in the side chain: Synthesis and characterization. Colloid and Polymer Science, **288**, 1341–1349 (2010).
DOI: 10.1007/s00396-010-2269-8

[222] Song N., Qi W., Qiu X., Gao L., Ding M.: Synthesis and chirooptical properties of optically active poly (ester imide)s based on axially asymmetric 1,1′-binaphthyls. Journal of Polymer Science Part A: Polymer Chemistry, **42**, 4318–4326 (2004).
DOI: 10.1002/pola.20297

[223] Kricheldorf H. R., Probst N., Gurau M., Berghahn M.: Liquid-crystalline polyimides. 20. Photoreactive and cholesteric poly(ester-imide)s based on 4-aminocinnamic acid trimellitimide and chiral sulfide spacers. Macromolecules, **28**, 6565–6570 (1995).
DOI: 10.1021/ma00123a025

[224] Kricheldorf H. R., Wulff D. F.: LC polyimides. XXVII. Cholesteric poly(ester-imide)s derived from chiral *i*-pentyloxyterephthalic acids. Journal of Polymer Science Part A: Polymer Chemistry, **34**, 3511–3518 (1996).
DOI: 10.1002/(SICI)1099-0518(199612)34:17<3511::AID-POLA5>3.0.CO;2-X

[225] Mallakpour S., Kolahdoozan M.: Preparation and characterization of novel optically active poly(amide-ester-imide)s based on bis(p-aminobezoic acid)-*N*-trimellitylimido-*S*-valine via direct polyesterification. Iranian Polymer Journal, **15**, 307–315 (2006).

[226] Mallakpour S. E., Hajipour A. R., Vahabi R.: Synthesis and characterization of novel poly(amide-ester-imide)s based on bis(p-amidobenzoyl chloride) ntrirnellitylimido-leucine. Iranian Polymer Journal, **10**, 321–330 (2001).

[227] Li C-H., Jung A., Liang A-L., Chang T-C.: Studies on the synthesis and properties of thermotropic liquid crystalline copoly(amide-ester-imide) derived from *N*-(hydroxyphenyl)phthalimide-4-carboxylic acid with amino acid. Journal of Applied Polymer Science, **56**, 1661–1666 (1995).
DOI: 10.1002/app.1995.070561217

[228] Ionescu M.: Chemistry and technology of polyols for polyurethanes. Rapra, Shawbury (2005).

[229] Chen C. F., Su Q., Chen Y. M., Xi F.: A new optically active polyurethane derived from chiral (2R,3R)(+)-diethyl L-tartrate and diisocyanate. Chinese Journal of Polymer Science, **17**, 371–373 (1999).

[230] Varkey E. C., Sreekumar K.: Optical and thermal properties of diethyl-(2R, 3R) (+)-tartrate based chiral polyurethanes with main chain amido chromophores. Journal of Applied Polymer Science, **119**, 111–119 (2010).
DOI: 10.1002/app.32593

[231] Qiu F., Zhang W., Yang D., Zhao M., Cao G., Li P.: Synthesis, characterization, and thermo-optical properties of azobenzene polyurethane containing chiral units. Journal of Applied Polymer Science, **115**, 146–151 (2010).
DOI: 10.1002/app.30948

[232] Nagai A., Ishikawa J., Kudo H., Endo T.: Synthesis of optically active polyurethanes by self-polyaddition of tyrosine-based monomers. Journal of Polymer Science Part A: Polymer Chemistry, **42**, 1143–1153 (2004).
DOI: 10.1002/pola.11047

[233] Chen J., Zhou Y., Nan Q., Ye X., Sun Y., Zhang F., Wang Z.: Preparation and properties of optically active polyurethane/TiO$_2$ nanocomposites derived from optically pure 1,1′-binaphthyl. European Polymer Journal, **43**, 4151–4159 (2007).
DOI: 10.1016/j.eurpolymj.2007.07.006

[234] Chen J., Nan Q., Guo L., Sun Y., Zhou Y.: Preparation and characterization of novel optically active polyurethanes containing 1,1′-binaphthol. Journal of Applied Polymer Science, **115**, 2190–2196 (2010).
DOI: 10.1002/app.31355

[235] Yasuzawa T., Yamaguchi H., Minoura Y.: Synthesis and properties of optically active polyurea by interfacial polyaddition. Journal of Polymer Science: Polymer Chemistry Edition, **17**, 3387–3396 (1979).
DOI: 10.1002/pol.1979.170171027

[236] Dunjic B., Gamez P., Fache F., Lemaire M.: Synthesis and characterization of a new chiral polyurea-based catalyst. Journal of Applied Polymer Science, **59**, 1255–1262 (1996).
DOI: 10.1002/(SICI)1097-4628(19960222)59:8<1255::AID-APP8>3.0.CO;2-B

[237] Mallakpour S., Shahmohammadi M. H.: Synthesis and characterization of novel optically active poly (imide–urethane)s derived from *N,N*′-(pyromellitoyl)-bis-(L-leucine) diisocyanate and aromatic diols. Polymer International, **53**, 184–190 (2004).
DOI: 10.1002/pi.1416

[238] Wang Z., Zhou Y., Sun Y.: Helical polyurethane-imide with optical activity based on binaphthyl units: Preparation, characterization, and study of interchain hydrogen bonds. Polymer Bulletin, **63**, 699–708 (2009).
DOI: 10.1007/s00289-009-0153-9

[239] Wang Z., Zhou Y., Sun Y.: Helical polyurethane-imide@attapulgite composite: Preparation, characterization and infrared emissivity study. Materials Letters, **64**, 908–911 (2010).
DOI: 10.1016/j.matlet.2010.01.055

[240] Chen Y., Tseng H-H.: Synthesis, characterization, and chiroptical property of optically active poly (urea-urethane)s. Journal of Polymer Science Part A: Polymer Chemistry, **31**, 1719–1727 (1993).
DOI: 10.1002/pola.1993.080310710

[241] Wang Z-Q., Zhou Y-M., Ye X-Y., Chen J., Sun Y-Q.: Synthesis and characterization of novel optically active poly(urethane urea)s: Effect of left/right rotation conformation. Journal of Applied Polymer Science, **111**, 2134–2140 (2009).
DOI: 10.1002/app.29220

[242] Wang Z. Q., Zhou Y., Sun Y., Yao Q.: Optically active helical polyurethane-urea with single-handed conformation for infrared low emissivity. Macromolecules, **42**, 4972–4976 (2009).
DOI: 10.1021/ma900763r

[243] Mallakpour S., Rafiemanzelat F.: Synthesis and characterization of new optically active poly(amide–imide–urethane) thermoplastic elastomers, derived from bis(*p*-amido benzoic acid)-*N*-trimellitylimido-L-leucine and polyoxyethylene-MDI. Reactive and Functional Polymers, **62**, 153–167 (2005).
DOI: 10.1016/j.reactfunctpolym.2004.11.005

[244] Mallakpour S., Rafiemanzelat F.: New optically active poly(amide-imide-urethane) thermoplastic elastomers derived from poly(ethylene glycol diols), 4,4′-methylene-bis(4-phenylisocyanate), and a diacid based on an amino acid by a two-step method under microwave irradiation. Journal of Applied Polymer Science, **98**, 1781–1792 (2005).
DOI: 10.1002/app.22363

[245] Mallakpour S., Rafiemanzelat F.: Synthesis and characterization of novel optically active poly(ether-urethane)s modified by copoly(amide-imide) segments based on amino acid through diisocyanate route: Influence of reaction parameters. Iranian Polymer Journal, **15**, 79–90 (2006).

[246] Mallakpour S., Rafiemanzelat F.: Facile and rapid synthesis of novel optically active poly(amide-imide-urethane)s derived from bis(p-amido benzoic acid)-N-trimellitylimido- L-leucine and polyoxyethylene-MDI under microwave irradiation. Iranian Polymer Journal, **14**, 909–919 (2005).

[247] Mallakpour S., Rafiemanzelat F.: Synthesis and properties of novel optically active poly(amide imide urethane) thermoplastic elastomers by the reaction of a L-leucine based diacid chain extender and PEG-terminated MDI. Iranian Polymer Journal, **14**, 169–180 (2005).

[248] Mallakpour S., Khani M., Rafiemanzelat F.: Synthesis and characterization of new optically active segmented poly(amide imide urethane)s based on different diacids via an isocyanate route. Journal of Applied Polymer Science, **108**, 2975–2982 (2008).
DOI: 10.1002/app.27925

[249] Mallakpour S., Khoee S.: Synthesis and characterization of new optically active poly(amide-imide-urethane) thermoplastic elastomers, derived from 4,4′-(hexafluoroisopropylidene)-*N*,*N*′-bis(phthaloyl-L-leucine-*p*-aminobenzoic acid) and PEG-MDI. Journal of Applied Polymer Science, **91**, 2288–2294 (2004).
DOI: 10.1002/app.13361

[250] Mallakpour S., Esteki M., Rafiemanzelat F., Khayamian T.: Application of factorial design method for the optimization of reaction conditions influencing viscosity of poly(amide-imide-ether-urethane)s based PEG and L-leucine. Iranian Polymer Journal, **16**, 21–29 (2007).

[251] Mallakpour S., Rafiemanzelat F.: Preparation and Properties of new copoly(amide-imide-ether-urethane)s based on bis(*p*-amido benzoic acid)-*N*-trimellitylimido-*L*-leucine by two different polymerization methods. Polymer Bulletin, **58**, 339–350 (2007).
DOI: 10.1007/s00289-006-0674-4

[252] Mallakpour S., Seyedjamali H.: Design and synthesis of novel organosoluble chiral poly(amide-ether-imide-urea) containing L-leucine moieties in the main chain. Colloid and Polymer Science, **288**, 703–710 (2010).
DOI: 10.1007/s00396-010-2202-1

[253] Suzuki A.: Recent advances in the cross-coupling reactions of organoboron derivatives with organic electrophiles, 1995–1998. Journal of Organometallic Chemistry, **576**, 147–168 (1999).
DOI: 10.1016/S0022-328X(98)01055-9

[254] Hu Q-S., Vitharana D., Liu G-Y., Jain V., Wagaman M. W., Zhang L., Lee T. R., Pu L.: Conjugated polymers with main chain chirality. 1. Synthesis of an optically active poly(arylenevinylene). Macromolecules, **29**, 1082–1084 (1996).
DOI: 10.1021/ma951414t

[255] Hu Q-S., Vitharana D., Liu G., Jain V., Pu L.: Conjugated polymers with main chain chirality. 2. Synthesis of optically active polyarylenes. Macromolecules, **29**, 5075–5082 (1996).
DOI: 10.1021/ma960249u

[256] Ma L., Hu Q-S., Musick K. Y., Vitharana D., Wu C., Kwan C. M. S., Pu L.: Conjugated polymers with main chain chirality. 3. Synthesis of optically active poly(aryleneethynylene)s. Macromolecules, **29**, 5083–5090 (1996).
DOI: 10.1021/ma960250t

[257] Yu H-B., Hu Q-S., Pu L.: The first optically active BINOL-BINAP copolymer catalyst: Highly stereoselective tandem asymmetric reactions. Journal of American Chemical Society, **122**, 6500–6501 (2000).
DOI: 10.1021/ja000778k

[258] Asai K., Konishi G., Sumi K., Kawauchi S.: Synthesis of optically active green fluorescent π-conjugated fluorene polymers having chiral Schiff bases in the side chain. Polymer Chemistry, **1**, 321–325 (2010).
DOI: 10.1039/b9py00268e

[259] Sonogashira K., Tohda Y., Hagihara N.: A convenient synthesis of acetylenes: Catalytic substitutions of acetylenic hydrogen with bromoalkenes, iodoarenes and bromopyridines. Tetrahedron Letters, **16**, 4467–4470 (1975).
DOI: 10.1016/S0040-4039(00)91094-3

[260] Block M. A. B., Hecht S.: Poly(propylene oxide)-poly(phenylene ethynylene) block and graft copolymers. Macromolecules, **41**, 3219–3227 (2008).
DOI: 10.1021/ma702844w

[261] Li X., Li C., Lu J., Liang H.: Designed synthesis and chiroptical properties of regioregular poly(*p*-phenyleneethynylene-alter-m-phenyleneethynylene) bearing (−)-trans-myrtanoxyl side groups. Frontiers of Chemistry in China, **4**, 93–103 (2009).
DOI: 10.1007/s11458-009-0018-7

Coaxial electrospun polyurethane core-shell nanofibers for shape memory and antibacterial nanomaterials

H. T. Zhuo, J. L. Hu[*], S. J. Chen

Institute of Textiles and Clothing, The Hong Kong Polytechnic University, Hung Hom, Kowloon, Hong Kong, China

Abstract. A novel kind of shape memory polyurethane (SMPU) nanofibers with core-shell nanostructure is fabricated using coaxial electrospinning. Transmission electron microscopy (TEM) and scanning electron microscopy (SEM) results show that nanofibers with core-shell structure or bead-on-string structure can be electrospun successfully from the core solution of polycaprolactone based SMPU (CLSMPU) and shell solution of pyridine containing polyurethane (PySMPU). In addition to the excellent shape memory effect with good shape fixity, excellent antibacterial activity against both gram-negative bacteria and gram-positive bacteria are achieved in the CLSMPU-PySMPU core-shell nanofiber. Finally, it is proposed that the antibacterial mechanism should be resulted from the PySMPU shell materials containing amido group in γ position and the high surface area per unit mass of nanofibers. Thus, the CLSMPU-PySMPU core shell nanofibers can be used as both shape memory nanomaterials and antibacterial nanomaterials.

Keywords: nanomaterials, smart polymers, electrospinning, shape memory, antibacterial

1. Introduction

Smart polymer ultrafine fibers have gained much attention due to their great potential applications, such as textiles, filtration, catalysis, reinforcement and biomedical use [1–3]. Particularly, polymeric micro/nanofibers with core-shell structure have been attractive in the past decades [4, 5]. Co-axial electrospinning provides an effective and versatile way to fabricate core-shell micro/nanofibers [4, 6, 7]. This technique can not only be used to spin the unspinnable polymers into ultrafine fiber, but also be used to keep the functionalizing agents like biomolecules and antibacterial agents in the core-shell nanofibers. For example, Liu *et al.* [8] had developed core-shell nanofibrous mats with a controllable drug-releasing capability for the tissue engineering scaffold. Jiang *et al.* [9] encapsulated BSA and lysozyme in polycaprolactone (PCL) nanofibers and found the released lysozyme main-

tained its structure and bioactivity. Therefore, it is desirable to achieve various functionalizations in the core-shell micro/nanofibers using the coaxial electrospinning.

In addition, shape memory polymers (SMPs) in particular shape memory polyurethanes (SMPUs) were widely studied in the past decades [10–12]. In addition to the excellent shape memory effect, the SMPUs demonstrate functional biocompatibility and had been used in various medical interventions such as vascular stents [13]. Recently, antibacterial activity was reported in the SMPU ionomers by Zhu *et al.* [14]. Most recently, Chen *et al.* [15–17] had also synthesized one novel kind of supramolecular SMPUs containing pyridine moieties. Not only thermal-induced shape memory effect (SME) [17], but moisture-sensitive shape memory effect are also achieved in the pyridine containing SMPUs (PySMPUs) [16]. A preliminary investigation sug-

gests that the nanofibers based on the PySMPUs exhibits antibacterial activity. However, it is difficult to spin the pure PySMPU/dimethylformamide (DMF) solution into fibers with the conventional electrospinning.

Therefore, the coaxial electrospinning is introduced to fabricate antibacterial nanofiber with core-shell structure in this experiment. The PCL based SMPUs (CLSMPU) or the elastic polyurethanes (TPUs) are designed to provide the certain mechanical properties as the core materials while the PySMPU is introduced as the sheath to exhibit additional properties including antibacterial activity. The preparation and antibacterial activity of SMPU-PySMPU core-shell nanofibers are reported in this communication.

2. Experimental section
2.1. Materials
DMF bought from Sigma-Aldrich Corporation (U.S.A) was used without any treatment. CLSMPU containing 75% soft segment content was synthesized by bulk polymerization in our lab according to the literature procedure [18, 19]. The PySMPU containing various contents of pyridine moieties was synthesized by solution polymerization in our lab according to the literature procedure [15]. For comparison study, TPU based on polytetramethylene glycol with glass transition temperature of –30°C are selected in this study. CLSMPU (M_n = 180 000), TPU (M_n = 200 000, bought from Hong Kong HI-Tec Enterprises Limited), PySMPU containing 53wt% pyridine moieties (named PUPy53, M_n = 40 000) and PySMPU containing 35wt% pyridine moieties and 35wt% hard segment (named PUPyMDI35, M_n = 70 000), were prepared to 10wt% DMF solutions for electrospinning.

2.2. Coaxial electrospinning
In this experiment, for comparison, the CLSMPU-PUPy53 and TPU-PUPyMDI53 core-shell nanofibers were prepared using the co-axial electrospinning. The experimental setup for coaxial electrospinning is shown in Figure 1. Both the shell solution and core solution were fed independently with a programmable syringe pump. The feed rates are both set at 0.015 ml/min. A collecting plate was placed on a rotating drum controlled by a stepping motor. The applied voltage was 20 kV.
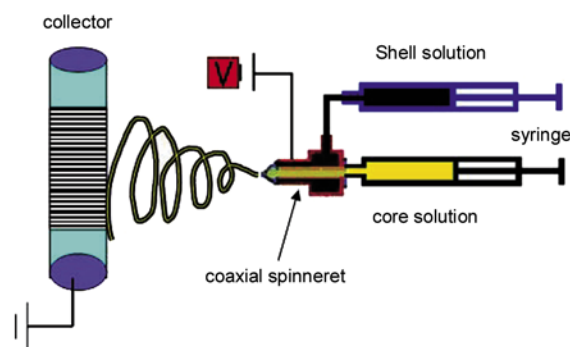

Figure 1. Experimental setup for coaxial electrospinning

2.3. Characterization
The surface morphology was observed using a scanning electron microscopy (SEM, S-4700 Hitachi, Japan) with an accelerating voltage of 20.0 kV. The core-shell structure was characterized using a transmission electron microscopy (TEM, Tecnai G2 F20 Philips, The Netherlands).

Antibacterial activity against gram-positive bacteria *Staphylococcus aureus* (*S.aureus*, ATCC6538) and gram-negative bacteria *Klebsiella pneumoniae* (*K.pneumoniae*, ATCC31488) was evaluated qualitatively according to the AATCC test method AATCC147 [14]. In this test, the specimens including corresponding untreated controls of the same material were placed in intimate contact with growth agar which had been previously streaked with test organism. After incubation, a clear area of interrupted growth underneath and along the sides of the test material indicated the antibacterial activity of the specimen. The size of the zone of inhibition and the narrowing of the streaks caused by the presence of the antibacterial agent permitted an estimate of the antibacterial activity.

Thermal-induced shape memory behaviors were characterized with cyclic tensile test method according to the literature method [17]. The test specimens with a width of 5.0 mm and length of 4.0 mm for cyclic tensile test are cut directly from the nanofibrous mat. The low temperature (T_{low}) for specimen stretching is about 45°C while the high temperature (T_{high}) for recovering is about 70°C.The test was done using an Instron 4466 apparatus with a temperature-controlled chamber; and a personal computer was used to control and record all data. The shape fixity and shape recovery were calculated from the recorded cyclic strain-stress curves [17].

3. Results and discussion

3.1. Structure and morphology

Figure 2 shows the SEM images of CLSMPU-PUPy53 and TPU-PUPyMDI35 core-shell nanofibers; and Figure 3 shows their TEM images. It is found in Figure 2 that uniform nanofibers with a diameter ranging from 600 to 1000 nm are fabricated in the CLSMPU-PUPy53 nanofiber. The TEM images confirm that the resultant CLSMPU-PUPy53 nanofibers have core-shell structure. The diameter of CLSMPU core nanofiber is changed from 250 to 320 nm while the sheath has a diameter of more than 600 nm. The interface between core material and sheath materials is clear since they are spun from different polymer. However, when the core material is spun from TPU/DMF solution and the shell material is spun from PUPyMDI35 materials, the resultant nanofibers not only form core-shell structure, but beads with average diameters of 1.5 μm are also observed on the core nanofibers. The distance within one bead is changed from 2.5 to 3.5 μm. It is also observed in Figure 2b. that clear interface is formed between the bead and the continuous core fiber. The core fiber threads the beads like a string. In this system, the core material is TPU while the shell material is PUPyMDI35. Thus, the beads should be formed by the PUPyMDI35 material due to their bad spinnability. Therefore, the coaxial electrospinning method can be used to fabricate core-shell micro/nanofibers and beads-on-string micro/nanofibers by adjusting the composition of core materials and shell materials. Comparing with the bulk film, the surface area per unit
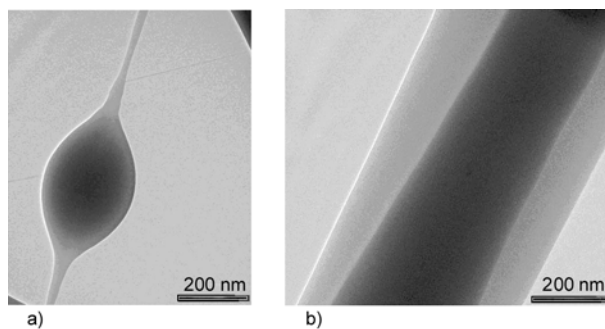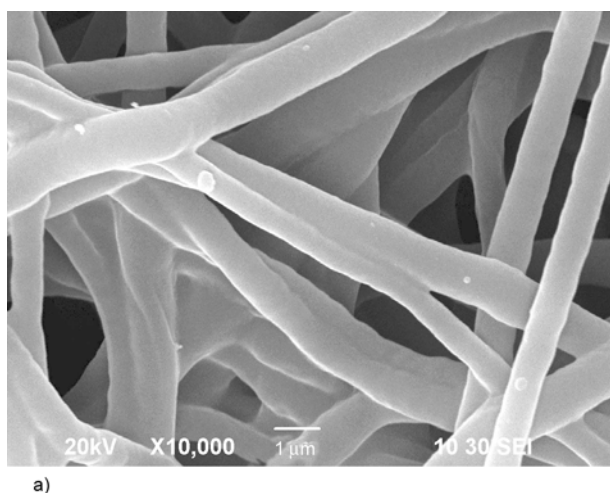

Figure 3. TEM images of (a) SMPU-PUPy53 and (b) TPU-PUPyMDI35 core-shell nanofiber

mass is improved greatly in both core-shell structure and bead-on-string structure nanofibers.

3.2. Thermal-induced shape memory properties

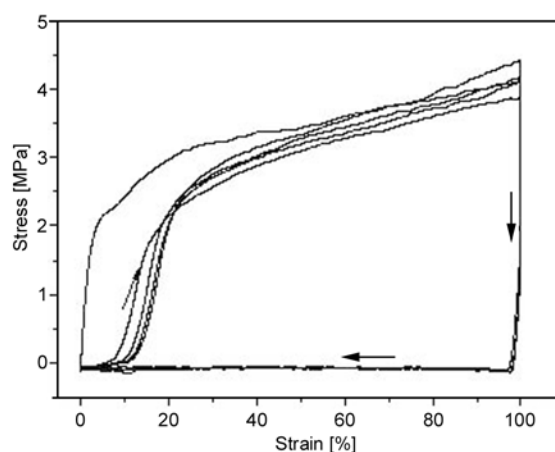Figure 4 shows the cyclic strain-stress curve of CLSMPU-PUPy53 core-shell nanofibrous mat. It

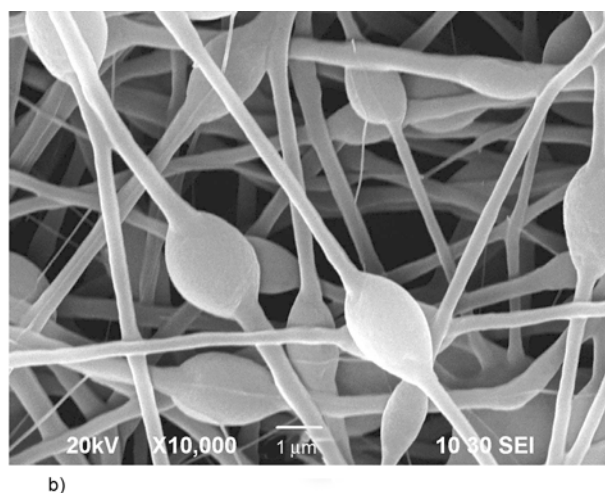**Figure 4.** Stress-strain curve of CLSMPU/PUPy53 core-shell microfibrous mat

Figure 2. SEM images of (a) SMPU-PUPy53 and (b) TPU-PUPyMDI35 core-shell nanofiber

was reported that the transition temperature of CLSMPU nanofiber is about 46.83°Cwhile the transition temperature of PUPy53 is about 56°C [17]. The CLSMPU nanofiber usually shows unsatisfying shape fixity, less than 80% [20, 21]. However, when the CLSMPU nanofiber is coaxial electrospun into core-shell nanofibers with the sheath of PUPy53, the shape fixity is increased significantly to above 95% as shown in Figure 4. The shape recovery at the first cycle is still beyond 90% in the CLSMPU-PUPy53 core-shell nanofiber under the recovery temperature of 70°C. This behavior is very similar to the thermal-induced shape memory behavior of PUPy53 bulk film, which exhibits not only high shape fixity, but also good shape recovery [17]. This is due to the fact that the PUPy53 polymer has much high glassy modulus as reported by Chen *et al.* [17]. The PUPy53 sheath plays key role on the thermal-induced SME in this CLSMPU-PUPy53 core-shell nanofiber mat.

3.3. Antibacterial activity

Table 1 summarizes the result of antibacterial activity of CLSMPU-PUPy53 core-shell nanofibrous mat as compared with the pure CLSMPU nanofibrous mat and the PUPy53 bulk film. It is found that no growth of *S. aureus* and *K. pneumoniae* bacteria is observed directly underneath the CLSMPU-PUPy53 core-shell nanofibrous mat. However, growth of *S. aureus* and *K. pneumoniae* bacteria is observed directly underneath the PUPy53 bulk film and the pure CLSMPU nanofibrous mat. Additionally, 0 mm clear zone of inhibition is observed in the CLSMPU-PUPy53 core-shell nanofibrous mat. This observation suggests that the CLSMPU-PUPy53 core-shell nanofibrous mat has the acceptable antibacterial activity against both gram-positive and gram-negative bacteria while the CLSMPU

nanofibrous mat and PUPy53 bulk polymer show unacceptable antibacterial activity. Moreover, there is no detectable diffusion of antibacterial agent from the CLSMPU-PUPy53 core-shell fibrous mat, *i.e.* the coaxial electrospinning provides a versatile method to encapsulate immobilized antibacterial agents in the core-shell micro/nanofibers. The antibacterial mechanism of this new kind of core-shell nanofibers may be different from the mechanism of Ag-doped antibacterial nanofibers [22, 23]. One reason is that the PySMPU like PUPy53 and PUPyMDI35 contains large fraction of BINA unit which have an amido group in γ position, and has important anti-tubercular, anti-pyretic and antibacterial properties [24]. Moreover, the microorganism contact surface area has been improved greatly after the PySMPU was electrospun into micro/nanofibers with core-shell structure or beads-on-string structure.

4. Conclusions

Novel core-shell micro/nanofibers are fabricated from the SMPU/DMF core solution and PySMPU/DMF shell solution using the coaxial electrospinning method in this experiment. Results show that both core-shell structure and bead-on-string structure can be formed in the core-shell micro/nanofiber by adjusting the core solution and shell solution. In addition to the excellent shape memory behaviors with good shape fixity, the CLSMPU-PySMPU core-shell nanofibrous mat is tested to show excellent antibacterial activity against both gram-negative bacteria and gram-positive bacteria. The antibacterial mechanism should be resulted from the PySMPU shell materials and the high surface area per unit mass of nanofibers. Thus, the CLSMPU-PySMPU core shell nanofibers are proposed for both shape memory nanomaterials and antibacterial nanomaterials.

Table 1. Antibacterial activity testing result using AATCC 147-2004

Test microorganism	Antibacterial activity		
	PUPy53 bulk film	CLSMPU nanofiber mat	CLSMPU-PUPy53 core-shell nanofiber mat
Staphylococcus aureus	**Growth** was observed directly underneath the tested specimen	**Growth** was observed directly underneath the tested specimen	**No growth** was observed directly underneath the tested specimen with 0 mm clear zone
Klebsiella pneumoniae	**Growth** was observed directly underneath the tested specimen	**Growth** was observed directly underneath the tested specimen	**No growth** was observed directly underneath the tested specimen with 0 mm clear zone

Acknowledgements

References

[1] Danno T., Matsumoto H., Nasir M., Shimizu S., Minagawa M., Kawaguchi J., Horibe H., Tanioka A.: Fine structure of PVDF nanofiber fabricated by electrospray deposition. Journal of Polymer Science Part B: Polymer Physics, **46**, 558–563 (2008).
DOI: 10.1002/polb.21391

[2] Greiner A., Wendorff J. H.: Electrospinning: A fascinating method for the preparation of ultrathin fibers. Angewandte Chemie, International Edition, **46**, 5670–5703 (2007).
DOI: 10.1002/anie.200604646

[3] Huang Z-M., Zhang Y-Z., Kotaki M., Ramakrishna S.: A review on polymer nanofibers by electrospinning and their applications in nanocomposites. Composites Science and Technology, **63**, 2223–2253 (2003).
DOI: 10.1016/S0266-3538(03)00178-7

[4] Zhang J-F., Yang D-Z., Xu F., Zhang Z-P., Yin R-X., Nie J.: Electrospun core-shell structure nanofibers from homogeneous solution of poly(ethylene oxide)/chitosan. Macromolecules, **42**, 5278–5284 (2009).
DOI: 10.1021/ma900657y

[5] Li W., Liu C., Zhou Y. X., Bai Y., Feng X., Yang Z. H., Lu L. H., Lu X. H., Chan K. Y.: Enhanced photocatalytic activity in anatase/TiO$_2$(B) core-shell nanofiber. Journal of Physical Chemistry C, **112**, 20539–20545 (2008).
DOI: 10.1021/jp808183q

[6] Sun Z. C., Zussman E., Yarin A. L., Wendorff J. H., Greiner A.: Compound core–shell polymer nanofibers by co-electrospinning. Advanced Materials, **15**, 1929–1932 (2003).
DOI: 10.1002/adma.200305136

[7] Moghe A. K., Gupta B. S.: Co-axial electrospinning for nanofiber structures: Preparation and applications. Polymer Reviews, **48**, 353–377 (2008).
DOI: 10.1080/15583720802022257

[8] Liu S. P., Li X. Q., Su Y., Tan L. J., Zhang Y., Chen Y. M.: Study of electrospun PLLACL nanofibrous mats for drug delivery system. Materials Science Forum, Materials Research, **610–613**, 1319– 1322 (2009).
DOI: 10.4028/www.scientific.net/MSF.610-613.1319

[9] Jiang H. L., Hu Y. Q., Li Y., Zhao P. C., Zhu K. J., Chen W. L.: A facile technique to prepare biodegradable coaxial electrospun nanofibers for controlled release of bioactive agents. Journal of Controlled Release, **108**, 237–243 (2005).
DOI: 10.1016/j.jconrel.2005.08.006

[10] Gunes I. S., Jana S. C.: Shape memory polymers and their nanocomposites: A review of science and technology of new multifunctional materials. Journal of Nanoscience and Nanotechnology, **8**, 1616–1637 (2008).
DOI: 10.1166/jnn.2008.038

[11] Liu C., Qin H., Mather P. T.: Review of progress in shape-memory polymers. Journal of Materials Chemistry, **17**, 1543–1558 (2007).
DOI: 10.1039/B615954K

[12] Ratna D., Karger-Kocsis J.: Recent advances in shape memory polymers and composites: A review. Journal of Materials Science, **43**, 254–269 (2008).
DOI: 10.1007/s10853-007-2176-7

[13] Cabanlit M., Maitland D., Wilson T., Simon S., Wun T., Gershwin M. E., Van de Water J.: Polyurethane shape-memory polymers demonstrate functional biocompatibility in vitro. Macromolecular Bioscience, **7**, 48–55 (2007).
DOI: 10.1002/mabi.200600177

[14] Zhu Y., Hu J., Yeung K.: Effect of soft segment crystallization and hard segment physical crosslink on shape memory function in antibacterial segmented polyurethane ionomers. Acta Biomaterialia, **5**, 3346–3357 (2009).
DOI: 10.1016/j.actbio.2009.05.014

[15] Chen S. J., Hu J. L., Yuen C-W., Chan L. K.: Supramolecular polyurethane networks containing pyridine moieties for shape memory materials. Materials Letters, **63**, 1462–1464 (2009).
DOI: 10.1016/j.matlet.2009.03.028

[16] Chen S., Hu J., Yuen C-W., Chan L.: Novel moisture-sensitive shape memory polyurethanes containing pyridine moieties. Polymer, **50**, 4424–4428 (2009).
DOI: 10.1016/j.polymer.2009.07.031

[17] Chen S., Hu J., Zhuo H., Yuen C., Chan L.: Study on the thermal-induced shape memory effect of pyridine containing supramolecular polyurethane. Polymer, **51**, 240–248 (2010).
DOI: 10.1016/j.polymer.2009.11.034

[18] Chen S., Hu J., Liu Y., Liem H., Zhu Y., Liu Y.: Effect of SSL and HSC on morphology and properties of PHA based SMPU synthesized by bulk polymerization method. Journal of Polymer Science Part B: Polymer Physics, **45**, 444–454 (2007).
DOI: 10.1002/polb.21046

[19] Chen S. J., Hu J. L., Liu Y. Q., Liem H. M., Zhu Y., Meng Q. H.: Effect of molecular weight on shape memory behavior in polyurethane films. Polymer International, **56**, 1128–1134 (2007).
DOI: 10.1002/pi.2248

[20] Zhuo H. T., Hu J. L., Chen S. J., Yeung L. P.: Preparation of polyurethane nanofibers by electrospinning. Journal of Applied Polymer Science, **109**, 406–411 (2008).
DOI: 10.1002/app.28067

[21] Zhuo H. T., Hu J. L., Chen S. J.: Electrospun polyurethane nanofibres having shape memory effect. Materials Letters, **62**, 2074–2076 (2008). DOI: 10.1016/j.matlet.2007.11.018

[22] Yuan J., Geng J., Xing Z., Shen J., Kang I-K., Byun H.: Electrospinning of antibacterial poly(vinylidene fluoride) nanofibers containing silver nanoparticles. Journal of Applied Polymer Science, **116**, 668–672 (2010). DOI: 10.1002/app.31632

[23] Son B., Yeom B-Y., Song S. H., Lee C-S., Hwang T. S.: Antibacterial electrospun chitosan/poly(vinyl alcohol) nanofibers containing silver nitrate and titanium dioxide. Journal of Applied Polymer Science, **111**, 2892–2899 (2009). DOI: 10.1002/app.29233

[24] Akalin E., Yilmaz A., Akyuz S.: Vibrational analysis of isonicotinamide. Journal of Molecular Structure, **744–747**, 881–886 (2005). DOI: 10.1016/j.molstruc.2004.11.077

On the morphology and potential application of polydimethylsiloxane-silica-titania composites

M. Alexandru[1*], *M. Cazacu*[1], *F. Doroftei*[1], *M. Ignat*[2], *D. Timpu*[1], *C. V. Grigoras*[1], *B. C. Simionescu*[1,3]

[1]'Petru Poni' Institute of Macromolecular Chemistry, Aleea Gr. Ghica Voda 41 A, 700487 Iasi, Romania
[2]National Institute for Research and Development in Electrical Engineering ICPE-CA, Splaiul Unirii 313, 030138 Bucharest, Romania
[3]Department of Natural and Synthetic Polymers, 'Gh. Asachi' Technical University of Iasi, 700050 Iasi, Romania

Abstract. Polydimethylsiloxane-α,ω-diol was used as matrix for the preparation of polysiloxane-SiO_2-TiO_2 composites through *in situ* incorporation of silica and titania using a solvent-free sol-gel procedure. For this purpose, oxide precursors tetraethyl-orthosilicate and tetrabutyl-orthotitanate, and a proper condensation catalyst, *viz.* dibuthyltin dilaurate, were added in pre-established amounts to the polymer. The hydrolysis and condensation reactions take place under mild conditions, with the formation of silicon and titanium oxide networks and polymer crosslinking. The effect of SiO_2 and TiO_2 mass ratio on the morphology of the composites was investigated by scanning electron microscopy (SEM) and X-rays diffraction (XRD), and interpreted in correlation with differential scanning calorimetry (DSC) and energy-dispersive X-ray spectroscopy (EDX) data. The film samples were tested as active elements in actuation devices.

Keywords: polymer composites, reinforcements, materials testing

1. Introduction

Silicones possess many excellent properties (thermal stability over a large temperature range, low surface tension, low dielectric constant, high hydrophobicity and a high degree of water-repellency, etc.). The condensed polysiloxanes have special mechanical properties compared to most organic polymers at moderate temperatures [1]. The extremely high mobility of the siloxane chain leads to a low glass-transition temperature [2], and this is why polydimethylsiloxanes remain fluid and silicone elastomers remain flexible at low temperatures [2]. In order to develop materials with useful properties, high molecular weights, chemical crosslinking and reinforcement are required.

The incorporation of different inorganic components into siloxane-based structures is carried out in order to improve the mechanical, thermal, electrical and optical properties and the dimensional stability or to obtain new properties derived from the hybrid nature of the material [3–5]. Therefore, due to their potential for large gains in mechanical and morphological properties, polymer/inorganic particle composites have received considerable interest. Silica, in the form of silica fume or aerogel with particle sizes in the nanometric range is the most preferred filler for silicones, although carbon black has been also used [6]. Other components can be added as well to achieve the desired properties. Thus, ferric oxide, titanium dioxide and organometallic compounds are added as heat stabilizers or pigments [7]. Titanium dioxide is one of the most important fillers used for obtaining composites designed for engineering applications [8]. Polymer-TiO_2 com-

*Corresponding author, e-mail: amihaela@icmpp.ro

posites have been successfully prepared by using different polymer matrices – silicone elastomers [9], polyacrylates [10], poly(methyl methacrylate) [11], polyamide 6 [12], polyimides [13], polystyrene [14], polycarbonates [15], epoxies [16], unsaturated polyesters [17], and dental composites [18].

Titanium dioxide confers optical, photocatalytic and bactericide properties to the materials incorporating it. It has the advantage of a high chemical and thermal stability and non-toxicity [19]. Titania is transparent to visible light and possesses a high refractive index ($n = 2.7$). Optical silicones have excellent properties but their applications are limited due to the small value of the refractive index ($n \sim 1.5$). The increase of their refractive index has a major impact in a range of applications, including optical devices for space environments and optical encapsulants [8]. Titanium dioxide has become a usual photocatalyst for both air and water purification [20]. Titania has a high dielectric constant ($\varepsilon \sim 89$) being of real interest as an active filler in the modification of the dielectric properties of silicones as well as of other polymers [21, 22].

TiO_2-SiO_2 composites have received much attention as raw materials in the production of low thermal expansion glasses, photonic crystals, dispersed phases of electrorheological fluids, catalysts for the removal of sulfur from fuel oil, ethylene terephthalate polycondensation, hydration of carbon monoxide, and selective liquid-phase oxidation of organics by peroxides. Anatase-phase titania has attracted extensive attention during the last few decades due to its excellent photocatalytic properties [23–25]. When SiO_2-TiO_2 composites are used as photocatalysts, titania is the more active component. However, titania alone has poor mechanical properties and a reduced specific surface area, its structural and sorption characteristics are less thermally stable, and titania suspensions are less stable with respect to coagulation. In some reactions, SiO_2-TiO_2 composites show even higher catalytic activity in comparison with TiO_2 due to the higher concentration of catalytically active centers owing to the interaction between their components [26].

Taking into account those above presented, this paper is concerned with the generation of TiO_2-SiO_2 oxide mixtures using different ratios between the two components in a polydimethylsiloxane matrix according to an already reported solvent-free sol-gel procedure [27] The use of this alternative was imposed by the difficulty to find an efficient solvent for the whole system when this contains a relatively high molecular weight polysiloxane. In addition, the process we approached is economical and environmentally friendly because no solvents are required. The resulting materials were investigated for their morphology and tested as active elements in actuation devices.

2. Experimental
2.1. Materials

Polydimethylsiloxane-α,ω-diol, PDMS, ($\overline{M_v} = 48\,000$) was prepared according to a procedure described in previous papers [27, 28]. Tetraethylorthosilicate (TEOS) was purchased from Fluka (Steinheim, Germany). Tetrabutyl-orthotitanate (TBT) was purchased from Merck-Schuchardt (Hohenbrunn, Germany). Dibuthyltin dilaurate (DBTDL) was received from Merck-Schuchardt (Hohenbrunn, Germany). All of these materials were used as received.

Composites based on polydimethylsiloxane reinforced with silica and titania were prepared [27] by mixing polydimethylsiloxane with proper oxides precursors, TEOS and TBT, in different ratios, in the presence of DBTDL as a catalyst. PDMS was introduced in a Teflon dish and mixed with pre-established amounts of TEOS and TBT, according to Table 1. After 10 min of stirring, about 0.2 g of DBTDL was added and the stirring was continued for another 10 min. The mixture was poured on a Teflon foil and vacuumed for 10 min to eliminate the incorporated air. The investigations were performed after the samples were kept in the laboratory for about 2 months. The tests revealed that this

Table 1. The recipes used to prepare PDMS-SiO_2-TiO_2 composites [27]

Sample	Inorganic		Organic	Catalyst
	TEOS [wt.%]	TBT [wt.%]	PDMS [wt.%]	DBTDL [wt.%]
T0	35.0	0.0	65	0.165
T5	32.5	2.5	65	0.196
T7.5	31.0	4.0	65	0.245
T10	30.0	5.0	65	0.222
T15	28.0	7.0	65	0.132
T20	26.0	9.0	65	0.166
Tr	0.0	35.0	65	0.080

period of time was sufficient to stabilize the mass of the samples.

2.2. Equipments

Crystallization and melting processes of PDMS based composites were followed using a Pyris Diamond DSC (Perkin Elmer USA) instrument. The samples were cooled from room temperature to –150°C, at a rate of 10°C/min, and then heated up to room temperature at a rate of 10°C/min. Helium was purged through the cells at a rate of 20 ml/min to insure an inert atmosphere and good thermal conductivity. Before the measurements, the instrument was calibrated for temperature and energy scales using n-hexane and pure water, according to the recommended standards for LN2 range of DSC analysis.

WAXD – Wide Angle X-rays Diffraction was performed on a Bruker-AXS D8 ADVANCE diffractometer, with Bragg–Brentano parafocusing goniometer. Scans were recorded in step mode using Ni-filtered Cu K_{α} radiation ($\lambda = 0.1541$ nm). The working conditions were 40 kV and 30 mA tube power. All diffractograms were collected in the range of 4–40°, 2θ [°], at +24, –80, –110 and +24°C. The cooling/heating rate (between isothermal registering data) was 20°C/min. A MRI-WRTC temperature chamber (with purged nitrogen atmosphere) and a MRI-TCPU1 temperature control power unit were used. The Bruker computer softwares Eva 11 and Topaz 3.1 were used to plot and process the data.

Microscopic investigation was performed on an Environmental Scanning Electron Microscope (ESEM) type Quanta 200 coupled with an Energy Dispersive of X-ray System. The SEM micrographs and corresponding EDX spectrum were recorded at 25 kV with secondary electrons in low vacuum mode. The energy-dispersive X-ray system (EDX) coupled with the scanning electron microscope permitted to perform the elemental analysis on film surface.

The linear micro- and nano-displacements of polymeric membranes were determined using an experimental setup for linear measurements, based on a Michelson-type interferometer using an Agilent 5529A system. This interferometric system has a 2 nm resolution for linear displacement. The nano-

actuation experiments were performed at a constant force of 22.5 cN.

3. Results and discussion

A series of polydimethylsiloxane-silica-titania composites with different mass ratios between organic and inorganic parts (Table 1) were prepared, processed as films, and subsequently investigated by different techniques. A polydimethylsiloxane-α,ω-diol was used as matrix for obtain composite materials with SiO_2 and TiO_2, by adapting a solvent-free sol-gel procedure already described [27]. TEOS and TBT oxide precursors were added in pre-established amounts to the polymer and DBTDL was added as catalyst. After vigorous stirring of the reactants and removing of the formed gas, the obtained mixtures were processed as films. The hydrolysis of the corresponding precursors took place under the influence of atmospheric humidity and it was followed by catalytic condensation with the formation of silicon and titanium oxides networks [29], several days being required to complete the process. As a result of the reactions between the alkoxydes and their hydrolysates with Si–OH PDMS end groups, the crosslinking of PDMS occurred. White opaque films (of about 0.2–0.9 mm thickness), easily detachable (peeled) from the substrate were obtained. The sum of SiO_2 and TiO_2 is considered as the inorganic part, while PDMS is considered to represent the organic part of the composites. The SiO_2/TiO_2 ratio was varied, but their cumulated amounts remained constant, as previously reported by other authors [30].

3.1. Differential scanning calorimetry

Different from the procedure previously reported [27], the present approach consisted of cooling and heating the samples at a controlled rate of 10°C/min. As a consequence, the transitions are better evidenced and can be correlated with the XRD data also obtained under controlled heating-cooling conditions (Figure 1). Both cooling and heating curves shown slight changes in both melting and crystallization processes depending on the filler content. The main data of the DSC curves (T_{peak}, ΔH) are summarized in Table 2. For all compositions, it can be observed that, while the peak temperatures (T_c, T_m) remain almost constant (max-
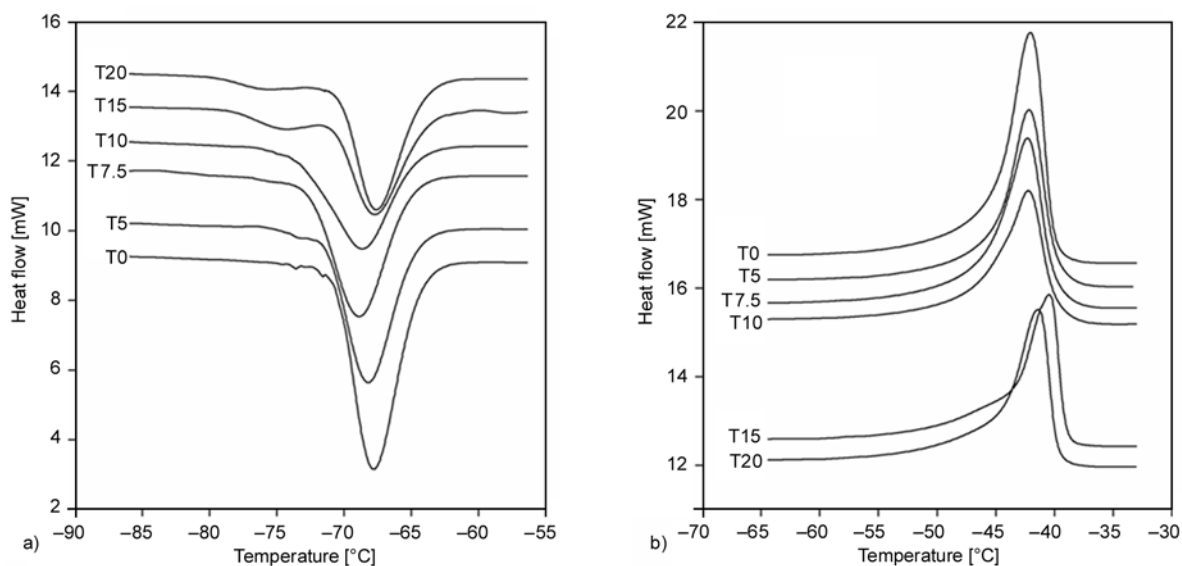
Figure 1. Crystallization processes (a) and melting endotherms (b) in PDMS/SiO$_2$/TiO$_2$ composites

imum 1 degree), the enthalpy is affected, its values lowering in the presence of the titania. The nucleation processes occurring on cooling are restricted by the presence of fillers, so the decreasing of crystallization enthalpy is related to the development of a less crystalline fraction within the matrix. In the heating curves, this behavior is also observed by the decrease of the melting enthalpy of samples due to a less crystalline phase developed in the cooling process. The presence of TiO$_2$ limits the quantity of crystals developed in the PDMS matrix.

The XRD diffractograms (Figures 2 and 3), reveal that the crystals have the same organization (peaks XRD), which can be related to same values for T_c or

T_m for all the components. In order to estimate the ΔH_c value, we considered that the crystallization process is completed after the lower exotherm appeared as a shoulder on the curves corresponding to the samples containing more than 10% titania. It is possible that a higher TiO$_2$ content, can lead to the development of a separate morphology. However, a more elaborate study is needed to test this hypothesis but this is not the aim of this study.

3.2. WAXD – wide angle X-Rays diffraction

Crystallisable polymers tend to develop a certain level of crystallinity when heated above glass transition temperature. Semicrystalline polymers typi-
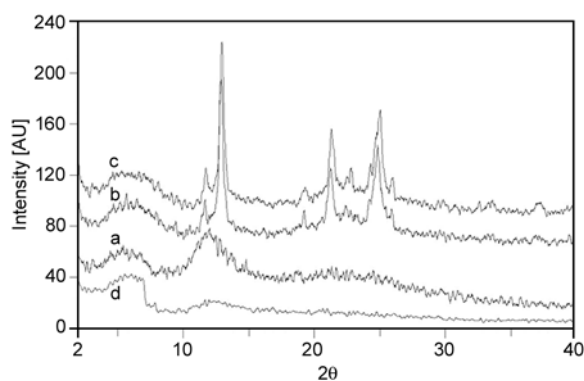

Figure 2. Diffractograms of sample T7.5 at a) +24°C, b) –80°C, c) –110°C, d) +24°C
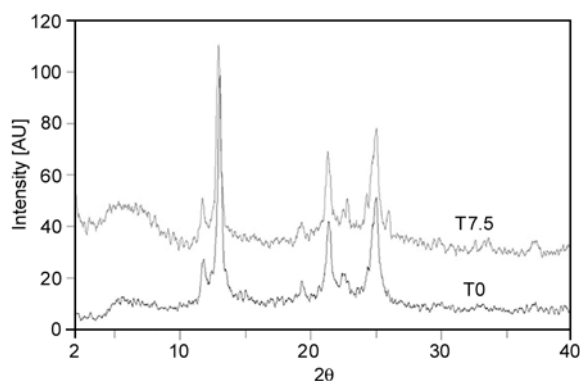

Figure 3. Diffractograms of samples T0 and T7.5 registered at –110°C

Table 2. Cooling and heating enthalpies normalized in relation to PDMS amount for the composites

Sample		T0	T5	T7.5	T10	T15	T20
ΔH_{norm} [J/g]	Cooling	−16.50	−13.40	−13.95	−12.00	−11.34	−12.23
T_{peak}		−67.80	−68.24	−68.89	−68.63	−67.75	−67.58
ΔH_{norm} [J/g]	Heating	−16.57	−13.50	−13.32	−11.04	−11.85	−11.45
T_{peak}		−42.04	−42.18	−42.28	−42.24	−40.45	−41.42

cally show a distinct lamellar morphology consisting of stacks of laminar crystals intercalated by amorphous, less ordered regions. Taking into account the DSC data, for the studied materials the crystallization can occur, at least for a fraction of the polymer, when slow cooling below –40 ºC takes place. However, the cooling rate should be low enough to allow chains to form crystalline structures.

The X-ray diffractograms registered at different temperatures (+24, –80, –110, +24°C) show an amorphous state at room temperature both initially and after a cooling-heating cycle for all used SiO_2/TiO_2 ratios. On the other hand, when cooling the samples at –80 and –110°C all composites show a high crystallization degree (Figure 2). This behavior is due to the cold crystallization process that, according to DSC data, takes place around –68°C.
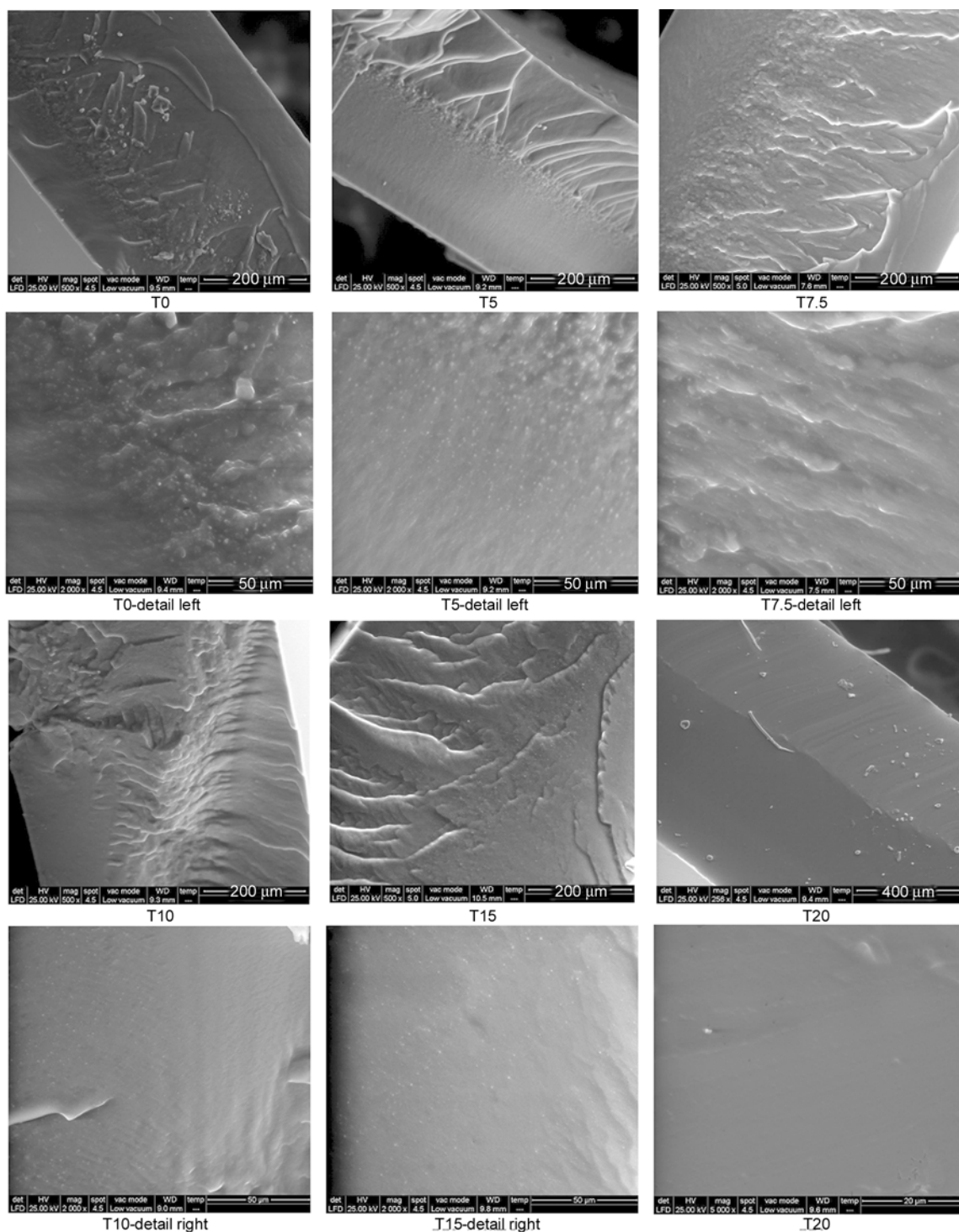
Figure 4. SEM micrographs of the broken surfaces deposed on Al supports and coated with Au

Because the crystallization seems to end at –75°C, the diffractograms at –80 and –110°C show almost the same pattern (Figure 2b, 2c). At room temperature, the samples are above the melting point of the polymeric chains (about –40°C) showing as a result an amorphous state.

At first glance, at a certain temperature the samples show similar diffractogram patterns regardless the composition, suggesting that the morphology is dictated mainly by the polydimethylsiloxane matrix. A comparison between the diffractograms of the samples T0 and T7.5 at –110°C is provided as an example in Figure 3.

However, a deeper analysis of the diffractograms registered for different samples at the same temperature allows the observation of a decrease in the degree of crystallinity in the composite with the increase of TiO$_2$ content. It is to presume that TiO$_2$, structurally different from PDMS, acts as a disruptive agent during the crystallization of the polymeric chains. At the same time, the amount of titania is low and doesn't meet the conditions to develop and impose its own ordering.

3.3. Scanning electron microscopy

SEM micrographs of the cross section of the prepared film composites are displayed in Figure 4. A globular texture concentrated toward the center section can be observed, while the outward surface appears to be smooth. The natural tendency of polydimethylsiloxane chains to migrate to the surface determines this stratification phenomenon. As globular domains can be seen in the sample T0 without titania, these are attributed to the silica. With increasing titania content, these domains become scarce and the surface becomes smoother, and in the case of sample T20 which has the lowest silica content, the globular domains are almost absent.

The EDX analyses, performed to identify the nature of the atoms present in the samples at a depth of 100–1000 nm from the surface, proved the presence of all expected elements (C, O, Si, and Ti) (Figure 5).

The well-known tendency of segregation to the surface of polysiloxane confer hydrophobicity as well as very low porosity (BET surface: 6.6–17 m^2/g) [27] which make such composites not suitable for photocatalysis. In this respect, our attempts aimed to decompose Bromothymol blue in aqueous solu-
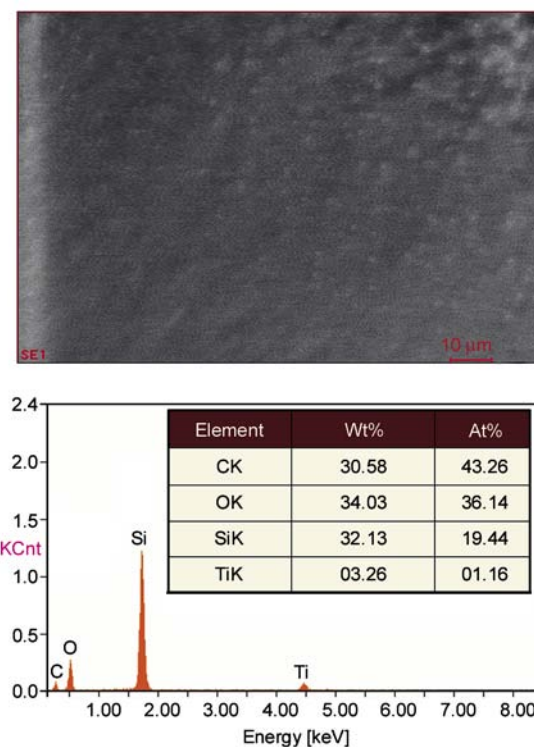

Element	Wt%	At%
CK	30.58	43.26
OK	34.03	36.14
SiK	32.13	19.44
TiK	03.26	01.16

Figure 5. EDX analysis of T5 composite

tion failed. Thus, the UV spectrum of a solution containing 0.0048 wt.% bromothymol blue in water remained unmodified after immersion of a piece of composite film sample and irradiation for different time periods with an UV lamp of 250 W.

3.4. Nano-actuation measurements

Due to their interesting properties such as elasticity, insulating ability and easy processing, silicones are used in microelectromechanical systems (MEMS) where they play a structural role as protective layers, encapsulating elements, valves and diaphragms. However, by using active fillers, the dielectric properties of silicones can be modified [21, 22]. Films containing TiO$_2$ have been often used in microelectronic devices, e.g. in capacitors, or as a dielectric gate in metal-dielectric-semiconductor devices [19]. The composites processed as films have been tested for actuation effect. The microelectromechanical actuation experiments have been performed by using the Agilent 5529A interferometric method. The measurements of the film nano-displacements were carried out using the time operation module of the Agilent system that can determine the position, velocity and acceleration as a function of time. For this, a voltage was applied by using thin electrodes that ensure a good electric contact with the polymer
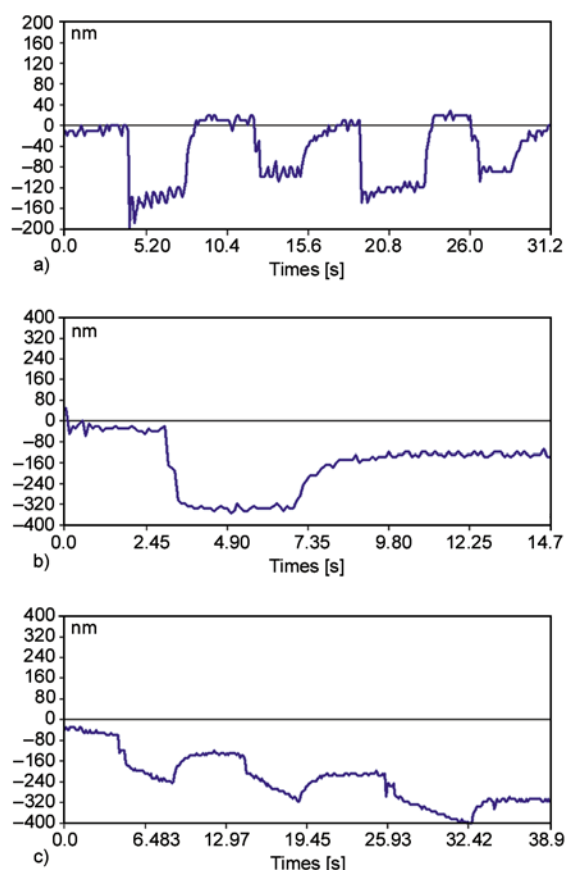
Figure 6. Nanometric displacements of the composite films at 400 V: a) T10; b) T20; c) Tr

Table 3. Actuation parameters

Sample	Voltage U [V]	Maximum displacement (actuation) d [nm]	Actuation sensitivity S [nm·V^{-1}]
T10	400	180	0.45
T20	400	360	0.90
Tr	400	400	1.00

stant increases by several units, which would be a prerequisite for improving the actuation properties, taking into account the silicone's low modulus and low flexibility. Indeed, the samples proved to be able for actuation, a better behavior being observed for sample Tr, which contains a high percent of TiO_2 (without silica): 400 nm displacement at 400 V (Figure 6). The sensitivity values S (the ratio between maximum displacement and the applied voltage) – a significant parameter for actuation – also increase by rising titania content in the material in the order T10 < T20 < Tr (Table 2), the sample Tr containing about 35% titania.

4. Conclusions

A series of composites have been prepared by partial replacement of SiO_2 in a PDMS-silica composite with TiO_2 (both generated in-situ by a sol-gel process). The introduction of titania proved to have the following effects: crystallization and melting temperatures values changed as compared to the blank sample, while the crystallization degree slightly decreased as titania content increased. The tendency to form particles agglomeration on the surface is reduced as silica is partially replaced with titania in the composite. The prepared composites showed good values for the main parameters in microelectromechanical actuation tests (displacement, sensitivity, and response time), which recommends them for planar or multilayer actuators. This behavior improves with increasing the titanium dioxide content.

Acknowledgements

film and good mechanical roughness at the contact with the retroreflector. The experiments were performed using a manual switch to control the continuum electric field (DC). The signals shown in Figure 6 represent the film actuation responses to a DC electric field.

Nano-electromechanical noise appears due to the dielectric membrane effects. The local dielectric parameters (conductivity, permittivity and dielectric loss angle) are changed in the electric field, this effect causing an unstable response. It is considered that the nano-actuation has an electrostriction character. The mechanical forces arising in a dielectric, in this case the polymeric composite film, under the action of an electric field tend to deform the membrane [31].

The specific actuation parameters of the experiments performed on polymer composites films are summarized in Table 3.

A previous study [27] reported that by incorporating TiO_2 in a PDMS-silica matrix the dielectric con-

References

[1] Ames J.: Silicones and their applications. Journal of Scientific Instruments, **35**, 1–7 (1958). DOI: 10.1088/0950-7671/35/1/302

[2] Dollase T., Spiess H. W., Gottlieb M., Yerushalmi-Rozen R.: Crystallization of PDMS: The effect of physical and chemical crosslinks. Europhysics Letters, **60**, 390–396 (2002).
DOI: 10.1209/epl/i2002-00276-4

[3] Yamada N., Yoshinaga I., Katayama S.: Formation behavior and optical properties of transparent inorganic-organic hybrids prepared from metal alkoxides and polydimethylsiloxane. Journal of Sol-Gel Science and Technology, **17**, 123–130 (2000).
DOI: 10.1023/A:1008787200364

[4] Rojas-Cervantes M. L., López-Peinado A. J., Martín-Aranda R. M., Gómez-Serrano V.: Synthesis and characterisation of xTiO2·$(1−x)$SiO$_2$–carbon composites. Carbon, **41**, 79–86 (2003).
DOI: 10.1016/S0008-6223(02)00273-7

[5] Pêna-Alonso R., Téllez L., Rubio J., Rubio F.: Surface chemical and physical properties of TEOS-TBOT-PDMS hybrid materials. Journal of Sol-Gel Science and Technology, **38**, 133–145 (2006).
DOI: 10.1007/s10971-006-7116-6

[6] Akinci A.: Mechanical and morphological properties of basalt filled polymer matrix composites. Archives of Materials Science and Engineering, **35**, 29–32 (2009).

[7] Wang X. X., Wang H. T., Song X. M., Wang G. Q., Du Q. G., Chen Q. T.: Photocatalytic polymerization induced by a transparent anatase titania aqueous sol and fabrication of polymer composites. Express Polymer Letters, **4**, 373–381 (2010).
DOI: 10.3144/expresspolymlett.2010.47

[8] Monson T. C., Huber D. L: High refractive index TiO$_2$ nanoparticle silicone composites. in 'Physical, chemical, and nano sciences center research briefs 2008' Sandia National Laboratories Albuquerque (2008).

[9] Mirabedini S. M., Mohseni M., PazokiFard Sh., Esfandeh M.: Effect of TiO$_2$ on the mechanical and adhesion properties of RTV silicone elastomer coatings. Colloids and Surfaces A: Physicochemical and Engineering Aspects, **317**, 80–86 (2008).
DOI: 10.1016/j.colsurfa.2007.09.044

[10] Chen Y., Lin A., Gan F.: Improvement of polyacrylate coating by filling modified nano-TiO$_2$. Applied Surface Science, **252**, 8635–8640 (2006).
DOI: 10.1016/j.apsusc.2005.11.083

[11] Yang M., Dan Y.: Preparation and characterization of poly(methyl methacrylate)/titanium oxide composite particles. Colloid and Polymer Science, **284**, 243–250 (2005).
DOI: 10.1007/s00396-005-1356-8

[12] Zhu M., Xing Q., He H., Zhang Y., Chen Y., Pötschke P., Adler H-J.: Preparation of PA6/nano titanium dioxide (TiO$_2$) composites and their spinnability. Macromolecular Symposia, **210**, 251–261 (2004).
DOI: 10.1002/masy.200450629

[13] Tsai M-H., Liu S-J., Chiang P-C.: Synthesis and characteristics of polyimide/titania nano hybrid films. Thin Solid Films, **515**, 1126–1131 (2006).
DOI: 10.1016/j.tsf.2006.07.092

[14] Rong Y., Chen H-Z., Li H-Y., Wang M.: Encapsulation of titanium dioxide particles by polystyrene via radical polymerization. Colloids and Surfaces A: Physicochemical and Engineering Aspects, **253**, 193–197 (2005).
DOI: 10.1016/j.colsurfa.2004.11.018

[15] Hwang D. K., Moon J. H., Shul Y. G., Jung K. T., Lim D. H., Lee D. W.: Scratch resistant and transparent UV-protective coating on polycarbonate. Journal of Sol-Gel Science and Technology, **26**, 783–787 (2003).
DOI: 10.1023/A:1020774927773

[16] Wetzel B., Rosso P., Haupert F., Friedrich K.: Epoxy nanocomposites- Fracture and toughening mechanisms. Engineering Fracture Mechanics, **73**, 2375–2398 (2006).
DOI: 10.1016/j.engfracmech.2006.05.018

[17] Xiao Y., Wang X., Yang X., Lu L.: Nanometre-sized TiO$_2$ as applied to the modification of unsaturated polyester resin. Materials Chemistry and Physics, **77**, 609–611 (2002).
DOI: 10.1016/S0254-0584(02)00114-1

[18] Yoshida K., Tanagawa M., Atsuta M.: Effects of filler composition and surface treatment on the characteristics of opaque resin composites. Journal of Biomedical Materials Research Part B: Applied Biomaterials, **58**, 525–530 (2001).
DOI: 10.1002/jbm.1050

[19] Răileanu M., Crişan M., Drăgan N., Crişan D., Galtayries A., Brăileanu A., Ianculescu A., Teodorescu V. S., Niţoi I., Anastasescu M.: Sol–gel doped TiO$_2$ nanomaterials: A comparative study. Journal of Sol-Gel Science and Technology, **51**, 315–329 (2009).
DOI: 10.1007/s10971-009-2017-z

[20] Bokobza L., Diop A. L.: Reinforcement of poly (dimethylsiloxane) by sol-gel *in situ* generated silica and titania particles. Express Polymer Letters, **4**, 355–363 (2010).
DOI: 10.3144/expresspolymlett.2010.45

[21] Cazacu M., Ignat M., Racles C., Vlad A., Alexandru M., Zarnescu G.: Polydimethylsiloxane/silica composites incorporating pyrite powders for actuation elements. Polymer International, **58**, 745–751 (2009).
DOI: 10.1002/pi.2586

[22] Cazacu M., Ignat M., Vlad A., Alexandru M., Zarnescu G.: Heat-cured silicone rubber incorporating pyrite powders for actuation elements. Optoelectronics Advanced Materials Rapid Communication, **4**, 349–351 (2010).

[23] Yu J-G., Yu H-G., Cheng B., Zhao X-J., Yu J. C., Ho W-K.: The effect of calcinations temperature on the surface microstructure and photocatalytic activity of TiO_2 thin films prepared by liquid phase deposition. Journal of Physical Chemistry B, **107**, 13871–13879 (2003).
DOI: 10.1021/jp036158y

[24] Petkowicz D. I., Pergher S. B. C., Silva da Silva C. D., da Rocha Z. N., dos Santos J. H. Z.: Catalytic photodegradation of dyes by in situ zeolite-supported titania. Chemical Engineering Journal, **158**, 505–512 (2010).
DOI: 10.1016/j.cej.2010.01.039

[25] Alem A., Sarpoolaky H., Keshmiri M.: Sol–gel preparation of titania multilayer membrane for photocatalytic applications. Ceramics International, **35**, 1837–1843 (2009).
DOI: 10.1016/j.ceramint.2008.10.034

[26] Murashkevich A. N., Lavitskaya A. S., Alisienok O. A. Zharskii I. M.: Fabrication and properties of SiO_2/TiO_2 composites. Inorganic Materials, **45**, 1146–1152 (2009).
DOI: 10.1134/S0020168509100124

[27] Alexandru M., Cazacu M., Nistor A., Musteata V. E., Stoica I., Grigoras C., Simionescu B. C.: Polydimethylsiloxane/silica/titania composites prepared by solvent-free sol–gel technique. Journal of Sol-Gel Science and Technology, **56**, 310–319 (2010).
DOI: 10.1007/s10971-010-2307-5

[28] Cazacu M., Marcu M.: Silicone rubbers IX. Contributions to polydimethylsiloxane-α,ω-diols synthesis by heterogeneous catalysis. Journal of Macromolecular Science Part A: Pure and Applied Chemistry, **32**, 1019–1029 (1995).
DOI: 10.1080/10601329508019142

[29] Rubio F., Rubio J., Oteo J. L.: Effect of TiO_2 on the pore structure of SiO_2-PDMS ormosils. Journal of Sol-Gel Science and Technology, **18**, 105–113 (2000).
DOI: 10.1023/A:1008704701204

[30] Diré S., Babonneau F., Sanchez C., Livage J.: Sol–gel synthesis of siloxane–oxide hybrid coatings $[Si(CH_3)_2O \cdot MO_x$: M = Si, Ti, Zr, Al] with luminescent properties. Journal of Materials Chemistry, **2**, 239–244 (1992).
DOI: 10.1039/JM9920200239

[31] Tareev B.: Physics of dielectric materials. Mir Publishers, Moscow (1975).

Study of the PVA hydrogel behaviour in 1-butyl-3-methylimidazolium tetrafluoroborate ionic liquid

S. Paţachia[1], Chr. Friedrich[2], C. Florea[1], C. Croitoru[1]*

[1]Department of Chemistry, 'Transilvania' University of Brasov, 29 Eroilor Street, 500036 Braşov, Romania
[2]Freiburg Materials Reserch Center (FMF), 'Albert Ludwigs' University Freiburg, Stefan-Meier-Str. 21, 79104 Germany

Abstract. The present paper aims at studying the behaviour of the poly(vinyl alcohol) [PVA] cryogel in the presence of 1-butyl-3-methylimidazolium tetrafluoroborate ($[BMIM]^+[BF_4]^-$) aqueous solutions with various concentrations. The gravimetric method showed that the swollen PVA cryogels exhibit mechanically active behaviour. PVA cryogels showed shrinking in the presence of ionic liquid, (IL), and re-swelling in the presence of distilled water. The re-swelling is not completely reversible, due to the influence of the IL ions on the gel morphology. The Fourier transform infrared (FTIR) spectra have indicated no chemical interaction between the PVA and the studied IL, but highlighted the gel crystallinity change as a function of IL concentration, as well as changes in the bound water amount. Rheological analyses showed dominating plastifying effect of the cation at a lower IL concentration and dominating kosmotropic effect of the anion at a higher IL concentration. A phenomenological kinetic equation that takes into account both fluxes of matters, in and out of the gel, is proposed, explaining the alteration of the gel properties when it comes in contact with $BMIMBF_4$ solutions.

Keywords: polymer gels, rheology, ionic liquids, poly (vinyl alcohol), 1-butyl-3 methylimidazolium tetrafluoroborate

1. Introduction
The main properties of hydrogels, such as density, sorption and diffusion capacity, mechanical, optical and electrical properties are determined by their water content [1–5]. Hydrogels exhibit a high degree of swelling in aqueous environment. In the presence of organic solvents as well as of ionic aqueous solutions or liquid ionic compounds, the hydrogels could shrink or swell, modifying their water content and, as a consequence, all other properties of the gels [6–10].
The determination of swelling behaviour of hydrogels in different environments is very important due to their very broad areas of application where hydrogels come in contact with organic or inorganic ionic substances, such as: wound dressing, drugs and protein delivery, artificial tissues, muscles or other organs, separation processes by sorption or diffusion, sensors design etc. [11, 12, 33, 34].
The behaviour of hydrogels with different compositions, in the presence of different ionic substances has been studied [13, 18, 23–25, 32].
PVA is a widely used polymer, due to its exceptional properties such as non-toxicity, non-carcinogenity, water solubility, biodegradability, biocompatibility, good mechanical and optical properties that could generate hydrogels by physical and chemical ways. Loaded with ionic substances, PVA could be a suitable matrix for electrolytes that could be used in electrochemical systems [14–17].
The electrical stability of these systems is affected by the water (solvent) volatility. The replacement of aqueous or organic solvents of electrolytes that imbibe the PVA hydrogels with room temperature

ionic liquids (RTIL-s) could be a promising way to obtain solid-like electrolyte materials.

Ionic liquids are ionic substances which contain generally organic cations and inorganic or organic anions, with almost no volatility, high conductivity and exhibit a large electrochemical window. Their non-volatility decreases the electrochemical instability risks caused by the solvent evaporation and also protect the atmosphere, being considered a green solvent.

The development of hydrophilic air-stable imidazolium based RTIL-s have attracted the researchers' interest and studies on the behaviour of some hydrogels in the presence of these RTIL-s have been reported [17].

There are no studies concerning PVA cryogels and imidazolium based RTIL aqueous solutions interaction.

The main goal of this paper is to monitor and to understand the swelling/deswelling behaviour of the PVA cryogels in the presence of $[BMIM]^+[BF_4]^-$ and water and to study its effect on the rheological properties of this ternary system.

2. Materials and methods
2.1. Materials
Poly(vinyl alcohol) with a polymerization degree of 900, a hydrolysis degree of 98% and industrial grades was purchased from the Chemical Plant Râşnov (Romania) and used for the preparation of cryogels without being submitted to any purification processes.

1-butyl-3-methylimidazolium tetrafluoroborate ($[BMIM]^+[BF_4]^-$) ionic liquid was purchased from Sigma-Aldrich (Germany). $[BMIM]^+[BF_4]^-$ has been used for the preparation of solutions with a concentration ranging from 5% to 100%. Distilled water has been used for the preparation of all ionic liquid solutions.

2.2. Methods
2.2.1. PVA hydrogel preparation
The PVA hydrogels were prepared by repeated freezing and thawing cycles. The hydrogel sample preparation has been started from a 12% PVA solution obtained by mixing a specific amount of PVA powder in a corresponding volume of distilled water, under continuous magnetic stirring, for

3 hours, at a temperature of 80ºC. The obtained PVA solution has been chilled to the room temperature and filtered before further usage. Then, it has been molded in a Petri dish and submitted to 3 repeated cycles of freezing at –20ºC for 12 hours, and thawing at room temperature for another 12 hours.

The obtained white and opaque PVA cryogel has been immersed in distilled water for 7 days, at room temperature (25°C), in order to allow the swelling of the prepared samples until reaching their swelling equilibrium. The initially obtained PVA hydrogel has a solid matter (dried polymer) content (CS) of 9.78 w%. Each sample has a content of the dried polymer mx, calculated as $m_{gel}*CS/100$ (m_{gel} is the mass of the sample balanced in water).

2.2.2. Gravimetric study upon shrinking of PVA hydrogels
The completely swollen PVA hydrogel has been cut into circular samples, pre-weighed, immersed in aqueous solutions of $[BMIM]^+[BF_4]^-$ with various concentrations (12, 50, 75% and respectively 100%), and stored at room temperature. The ratio polymer: storage solution was 1:100 (mass/vol). At the predetermined period of time (*t*), the PVA hydrogels have been taken out of the ionic liquid solutions, gently wiped between two filter papers and weighed (m_t) using a Kern ABJ (Germany) balance with a precision of 10^{-5} g. After each weighing process, the PVA hydrogel samples have been immersed back into the same bath. The weighing procedure for the PVA samples and their mass monitoring has been repeated until reaching the shrinking equilibrium.

2.2.3. Re-swelling process study by gravimetric method
The re-swelling capacity of the shrunk PVA hydrogels has been monitored by using the gravimetric methods described in 2.2.2. The PVA hydrogels shrunk in $[BMIM]^+[BF_4]^-$ ionic liquid with different concentrations have been immersed in distilled water and weighed at a predetermined time. The weighing procedure has been repeated until the re-swelling equilibrium of the PVA samples has been reached.

2.2.4. Release of [BMIM]⁺[BF4]⁻ monitoring

PVA hydrogels initially collapsed in the solution of [BMIM]$^+$[BF$_4$]$^-$ with concentrations between 12 and 100% have been immersed in distilled water in order to determine the absolute conductivity of the obtained solutions, due to the ionic liquid release from the studied samples. The conductivity measurements have been performed at room temperature, at predetermined time, using a Radelkis OK-112 (Hungary) conductometer. For a set of the studied PVA hydrogels, the conductivity measurements have been performed without refreshing the storage distilled water, while for another set of samples, the distilled water has been replaced periodically, after each measurement, to avoid the contact of the hydrogel with released ions and to ensure the total IL release.

2.2.5. Gels analysis by Fourier transform infrared spectroscopy [FTIR]

The swollen, shrunk and the re-swollen PVA hydrogels (in the same storage water and in the refreshed storage water as we described in 2.2.4) have been subjected to FTIR spectroscopy in the range of 4000 and 600 cm^{-1}, using a Perkin-Elmer spectrophotometer with ATR device. Prior to the measurement, the samples have been vacuum dried overnight, at 40°C, until the constant weight.

The FTIR analysis gave information about the cryogel crystallinity based on the band intensity ratio of 1141 cm^{-1}:1096 cm^{-1} [19].

The ratio of absorption band intensities of the 1141 and 1096 cm^{-1} band has been determined for the shrunk PVA hydrogels and the PVA hydrogels re-swollen in non-refreshed and refreshed storage water (as we described in 2.2.4).

2.2.6. Rheological measurements

The rheological measurements have been performed on a Paar Physica UDS200 rheometer, equipped with 25 mm diameter steel plates. The average sample thickness was 1.5 mm. The storage and loss moduli of the collapsed PVA hydrogels have been measured at a constant temperature of 25ºC. The samples were stable under shear conditions ($v = 1.0$ Hz and $\gamma = 1.0\%$) on a time scale up to 1000 sec. The experiments with deformation amplitude of about 1% were, for all gels, within the linear viscoelastic regime. The immersion solutions

had the following concentrations: 5, 15, 25, 50, 70 and 100%.

3. Results and discussion
3.1. Gels mass monitoring during their immersion in BMIMBF₄ aqueous solutions

By immersing the PVA HG-s, initially balanced in water, in BMIMBF$_4$ aqueous solutions it could be noticed that the gels shrink. The shrinkage is influenced by the IL concentration (correlated with the water activity) and the contact time.

Figure 1 shows that higher IL concentration and contact time, results in higher hydrogel mass loss and rate of shrinking, as well as in longer time of swelling equilibrium reaching has been noted.

The PVA gel collapse could be explained by the water elimination from the mass of the gels, due to the high osmotic pressure created by IL ions from the contact solution.

The sigmoidal shape of the curve describing the shrinking process for PVA gels immersed in 12% BMIMBF$_4$ aqueous solution suggests that there are in fact two simultaneous fluxes of matters in the system: one is that of the water leaving the initially swollen gel and the second one is that of the IL ions that diffuse into the gel.

Firstly, due to the osmotic pressure exerted by IL ions outside the gel, the water molecules, more mobile, will diffuse from the gel, determining its mass loss. Later, IL ions, bigger and less mobile, will penetrate the gel network, determining the mass increase.
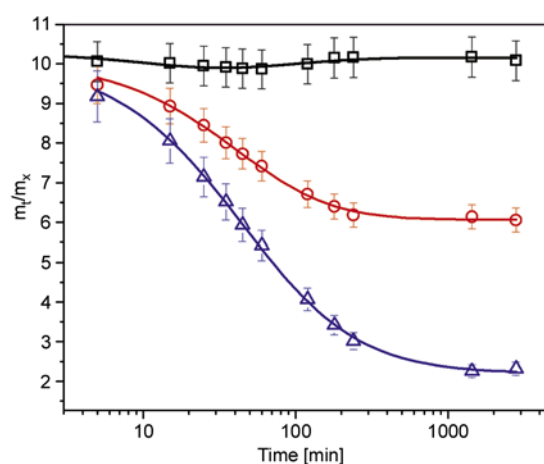

Figure 1. Shrinking process- PVA hydrogel normalized mass dependency as a function of time and concentration of [BMIM]$^+$[BF$_4$]$^-$ aqueous solution: (□) 12%; (○) 50% and (Δ) 100% of IL

Once the ionic liquid concentration inside the gel is zero, the osmotic pressure will govern the water release process.

For more concentrated BMIMBF$_4$ solutions, the higher osmotic pressure within the gel determines a higher and more rapid water release, emphasized by a higher mass loss of the gel. The sorption of IL ions into the gel will diminish, due to the decrease of gel porosity, as a consequence of its collapse. Also, the tendency of IL ions to agglomerate at a higher concentration than 50% [20] could be a cause of their sorption decrease. In this case, the simultaneous processes are less visible on the gravimetric kinetic curves, the IL sorption being negligible by comparison to the water release.

To prove this, PVA HG samples, initially immersed into aqueous solutions of BMIMBF$_4$, were dried and weighed. The experiments were performed seven times.

3.2. Determination of BMIMBF$_4$ mass sorbed into the PVA gel

Taking into account the very low volatility of ionic liquids, the amount of BMIMBF$_4$ sorbed into the gel has been determined as the difference between the mass of the dried gel balanced into the IL solution ($m_{gel,eq,inIL}$) and the mass of the polymer (m_x), calculated taking into account the solid content of the PVA gel balanced in water (Equation (1)):

$$\frac{m_{IL}}{m_x} = \frac{m_{gel,eq,inIL} - m_x}{m_x} \tag{1}$$

It could be noted that the retained amount of BMIMBF$_4$ decreases when the contact solution concentration increases (Table 1).

In case of the contact between the gel and pure BMIMBF$_4$, a small negative value for the absorbed

Table 1. BMIMBF$_4$ mass absorbed into the PVA gel as a function of the IL solution concentration

c_{IL} [%]	m_{IL}/1 g xerogel [g]
0	0
12	0.975649
50	0.702873
75	0.17515
100	–0.01515

IL mass was obtained. This suggests that the usual drying conditions for hydrogels (110°C at normal pressure) are not sufficient to eliminate the bonded water from the gel.

It seems that BF$_4^-$ behaves as a kosmotropic ion, interacting with water molecules by H-bondings and structuring them around it. The interaction between BF$_4^-$ and water molecules has been reported in the literature by various authors [21]; even other authors calculated the B Jones Dole's coefficient for much diluted solutions and classified this anion as chaotropic [22]. BMIM$^+$, is an organic cation, with a hydrophobic chain, and behaves as a chaotropic ion, breaking the H-bondings between water molecules and PVA-water molecules, transforming initially bonded water in free water. The last one could be easily released from the gel during the drying process. In different papers, it was reported that cation BMIM$^+$ behaves as a chaotropic ion while in other situations, it was classified as kosmotropic, due to the possible hydrophobic hydration.

Figure 2. presents the scheme of the processes that take place when PVA HG is in contact with BMIMBF$_4$.

We could assume that BMIMBF$_4$ acts as a dehydrating agent for the swollen PVA hydrogels.

This behaviour does not seem to be unique, as similar phenomena have been noted and reported also
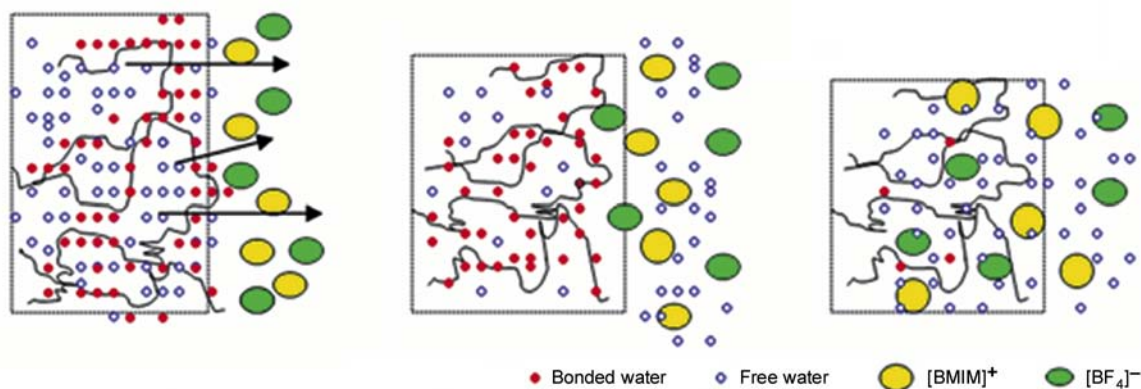

Figure 2. Scheme of the processes that occur at PVAHG contact with BMIMBF$_4$

for chitosan hydrogels, when in contact with BMIMBF$_4$ [24]. So, in case the practical interest is to load the PVA hydrogel with BMIMBF$_4$, we have to use more highly diluted IL solution for the gel immersion. When the hydrogel drying is the goal, it has to be immersed into pure BMIMBF$_4$.

In Figure 2, we made an attempt to show the mechanism of PVA hydrogel collapse due to the double fluxes of matters in/from the hydrogel. After equilibrium is reached, the collapsed hydrogel contains IL ions embedded into the polymeric network. PVA chains could stronger interact by H bonding between their own OH groups, due to the removal of the bonded water molecules. As a consequence, it is expected that the collapsed gels exhibit a higher modulus.

When the amount of the absorbed IL ions is higher, the effect of the cations on the gel plasticizing has to be more evident. This is valid for the diluted IL solution used for PVA HG immersion.

When the solution concentration is higher, the IL sorption diminishes and the polymer-polymer interaction becomes more dominant. The obtained collapsed gel has to be more rigid.

To prove this assumption, the PVA hydrogels balanced in BMIMBF$_4$ solutions with different concentrations (Figure 1), have been studied rheologically.

3.3. Rheological analysis of the PVA/BMIMBF$_4$ gels

Experimental data show, as we assumed, that the PVA hydrogel shrinking in the presence of ionic liquids and the absorption of the ions into the gel matrix strongly influence their rheological properties.

Figure 3 shows that the values of the storage modulus, G', are higher than that of the loss modulus, G'', evidencing a solid-like behaviour of the collapsed PVA hydrogels. The plateau modulus, G_p, (determined as the storage modulus at a frequency of 1 Hz), is lower in comparison to the G_p-value of the non-collapsed PVA cryogel, if the concentration of the IL immersion solution is lower than 50% (Figure 4). This behaviour could be correlated with the plasticizing effect of the absorbed cations that is predominant at lower values of the IL concentration, while, at the same time, the volume of the
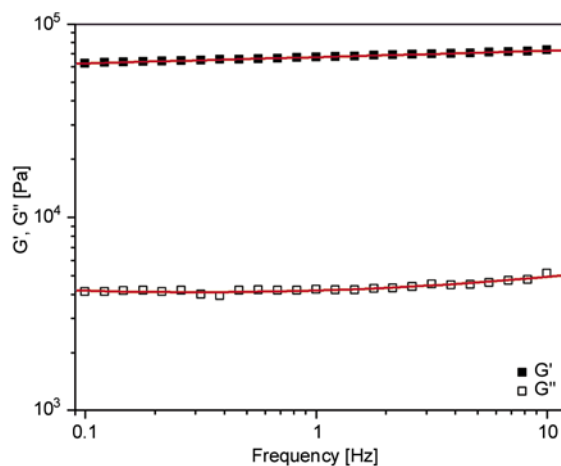

Figure 3. Dependency of the rheological parameters on the frequency, for the PVA hydrogels shrunk in pure [BMIM]$^+$[BF$_4$]$^-$
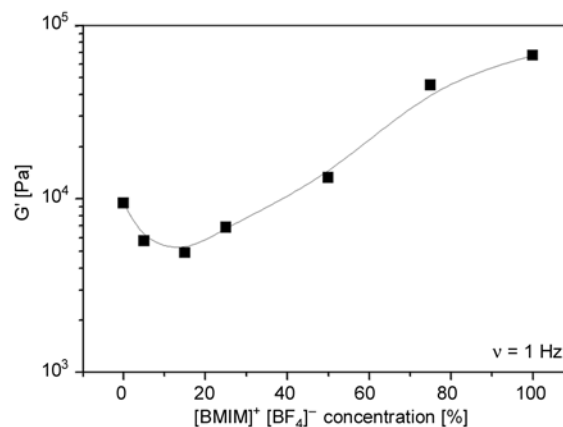

Figure 4. Dependency of the plateau modulus G_p [G' (1 Hz)] on the IL solution concentration

sample is not shrinking significantly in this concentration range.

In the presence of IL having the concentration value between 12% and 50%, the storage modulus of the collapsed PVA hydrogels begins to increase, but its value is still lower than the G_p value corresponding to the initial PVA hydrogel. This behaviour could be correlated to the tendency of IL ions to agglomerate, decreasing the concentration of the free cations [19]. The lower the concentration of the free cations in solution, the lower the cations absorbed and the lower the plasticizing effect marked out.

At a concentration of the IL solution higher than 50%, the storage modulus of the shrunk PVA hydrogels becomes higher than the value of the neat PVA hydrogel. This behaviour could be explained by the increase of the cation agglomeration, which induces the decrease of their absorption and, consequently,
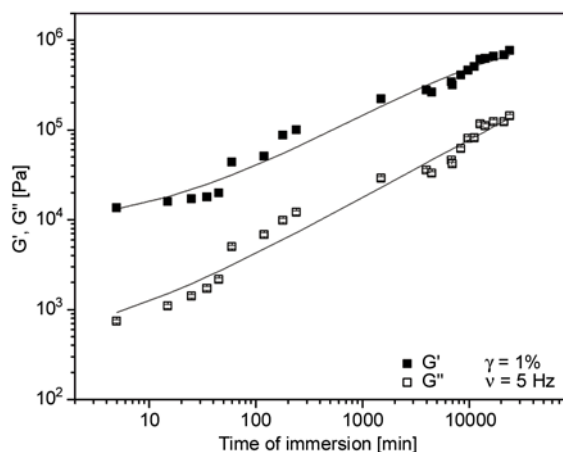
Figure 5. *G'* and *G"* in dependency as a function of the imersion time of the PVA hydrogels in 100% [BMIM]$^+$[BF4]$^-$

Figure 6. Conductance of the water in which the initially shrunk PVA hydrogels are immersed, as a function of time and of the initial concentration of the IL immersion solution: (■) 12%; (○) 50% and (Δ) 100%

a decrease of the plasticizing effect; additionally, the ions, placed at the interface of the swollen PVA chains, determine a stronger collapse of the studied hydrogel. The PVA hydrogel shrinking is determined by the capacity of the IL ions to extract the water molecules from the hydrogel, expressed by the kosmotropic character of the anions. The elimination of the water molecules from the gel and the higher interaction between the chains of the polymer determines the increase of the gel rigidity.

Dynamic moduli *G'* and *G"* of the PVA gels, measured after different periods of their immersion in pure IL, allowed, indirectly, to monitor the sample shrinking (Figure 5).

The variation of the hydrogel rheological properties as a function of the imersion time is consistent with the variation in time of the gel mass, at the sample contact with IL solutions, confirming both matter fluxes: *G'*, *G"* and viscosity increase simultaneously with the gel mass decrease in the first moments after their immersion in [BMIM]$^+$[BF$_4$]$^-$ solutions. At higher contact times, a relative independence of the rheological parameters on time indicates that the collapse equilibrium is reached.

To check the type of interaction between PVA and BMIMBF$_4$ the following aspects have been monitored: ILs ions release from the gel, the shrunk hydrogel capacity to re-swell in water and FTIR spectra alteration after gels contact with ILs solutions.
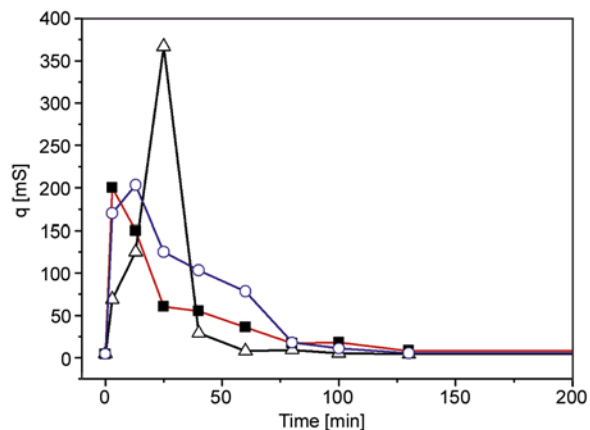
3.4. Monitoring of the BMIMBF$_4$ release from the gel

The conductometric analysis of the distilled water in which the PVA gels, initially collapsed in IL solutions, have been immersed, shows that the entire amount of sorbed IL is released (Figure 6). This fact emphasized that no chemical interaction between PVA and IL ions occurs.

Also, it could be noted that the diffusion of the ions from the higher collapsed gels is more difficult, the maximum of ions release is being shifted to higher times.

3.5. Monitoring of the gels shrinking reversibility

The recovery capacity of the shrunk PVA hydrogels during the re-immersion into distilled water is confirmed by the increase of their mass. We used refreshed and non-refreshed water to monitor the shrinking reversibility and the results were similar, meaning that the necessary concentration gradient for complete IL removal was ensured.

During the re-swelling process, the samples immersed in 12% IL solution reabsorb water until reaching 99% of the initial PVA hydrogel matrix mass. On the other hand, the PVA hydrogels immersed in pure IL reabsorb water until reaching only approximately 70% of the initial mass of the hydrogels (Figure 7).
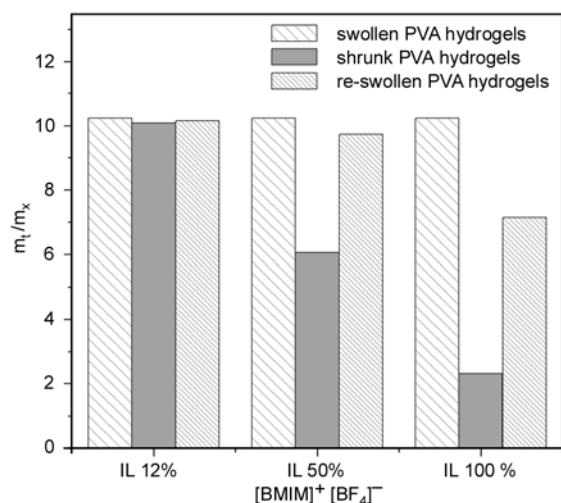
Figure 7. Comparative analysis of the normalized mass of the PVA hydrogels at their initial swollen state, shrunk state and re-swollen state as a function of the IL concentration

Figure 8. FTIR Spectra of PVA cryogel and PVA cryogels collapsed in IL solutions with different concentrations: 0% IL (—), 12% IL (—), 50% IL(—) and 100% IL (—)

The maintenance of the shrunk state of the hydrogels initially immersed in highly concentrated IL solutions evidences a higher interaction between the PVA macromolecular chains by H-bondings. This result is in agreement with the above mentioned data showing that the removal of the bonded water molecules allows stronger interaction between the OH groups of the PVA. That interaction does not seem to be reversible.

3.6. FTIR spectra of PVA/BMIMBF$_4$ gels

FTIR spectra have been measured in order to clarify the cause of the PVA hydrogel re-swelling limits when they are immersed in water. The absorption bands have been identified [19, 20].

It can be noticed that no new absorption bands appeared in the FTIR spectra, emphasizing that no chemical interaction occurs between PVA and [BMIM]$^+$[BF$_4$]$^-$, (Figure 8).

The presence of the IL ions in the gel matrix, proportional to the concentration of the ionic liquid solution, indicates the capacity of the PVA cryogels to retain ions. FTIR spectra of PVA/IL gels evidence the alteration of some absorption bands, both due to the interaction between the components and to changing system composition.

The absorption band from 3270 cm^{-1} could be attributed not only to the O–H bondings from PVA, but also to those from the bonded water remained into the system after a gel's partial 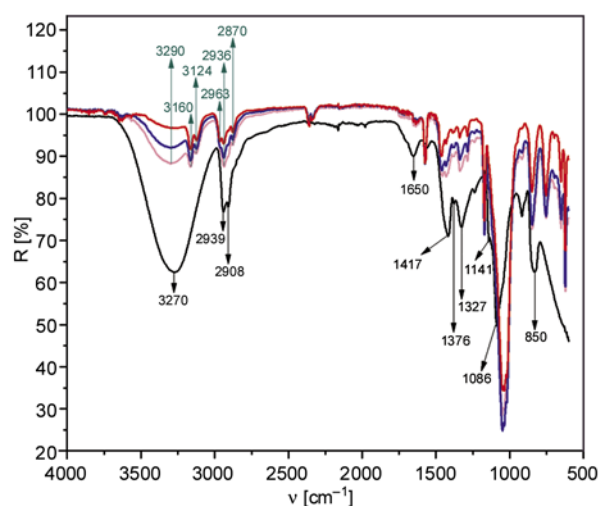drying. A decrease of the OH band intensity, when the IL concentration into the contact solution increases, was noted. This means that IL ions extract the bonded water molecules from the PVA cryogel matrix. The ratio between the intensity of the bands from 3270 and 2939 cm^{-1} demonstrates this. The following values were obtained for this ratio: 2.1 (for PVA cryogel), 0.97 (for PVA cryogel immersed in 12% IL solution), 0.68 (for PVA cryogel immersed in 50% IL solution) and 0.44 (for PVA cryogel immersed in 100% IL). The decrease of the mentioned ratio could be attributed simultaneously to the decrease of the bonded water amount but also to the increase of the C–H groups' number into the gel, by BMIM$^+$ ions sorption.

The intensity and the width diminution of the band from 3270 cm^{-1}, and its shifting to 3290 cm^{-1}, mean the decrease of the amount of associated OH groups, by H bondings. The shifting of this band could be correlated to the chaotropic character of BMIM$^+$ ions, diffused into the matrix, according to the literature [26]. This is consistent with the presence in the FTIR spectra of the shrunk gels, of small absorption bands at 3593 and 3531 cm^{-1}, characteristic for OH free groups [27]. In addition, the characteristic band for [BF$_4$]$^-$ from 1060 cm^{-1} [27] is split into three peaks and shifted to 1048, 1034 and 1017 cm^{-1} showing the lowering of B-F vibration symmetry, due to the F atom involving within H bonds with water molecules. Also the skeletal and C–O stretching band from 830 cm^{-1} from the PVA FTIR spectrum is shifted in the PVA/IL gels spectra

to 844 and respectively 848 cm^{-1}, showing a stiffening of the polymeric chain as a consequence of the interaction by H bondings between OH groups of PVA.

To come to a conclusion, FTIR spectra demonstrate the diffusion of BMIM$^+$ and BF$_4^-$ ions into the gel and the decrease of the amount of bonded water molecules into the gel as a consequence of the absorbed IL ions that compete for the water molecules binding with PVA.

After re-swelling, the characteristic absorption bands of IL ions disappeared, emphasizing their total release from the gel matrix, in agreement with the conductometric results.

FTIR spectra allow monitoring the PVA crystallinity changes. Figure 9 illustrates the decrease of the PVA cryogel crystallinity when being immersed in ionic liquid solutions. This behaviour could be explained by the strong kosmotropic character of the studied IL that determines the rapid extraction of the water from the gel, and, consequently, leads to the precipitation of the PVA chains in amorphous phase.

The PVA-based cryogel re-swelling leads to the increase of its crystallinity due to the slower release of the IL ions from the matrix and to the kosmotropic effect of the IL ions that structure the water molecules around them; both phenomena allow the macromolecules to organize and to interact by H bonding, determining the increase of the degree of crystallinity.
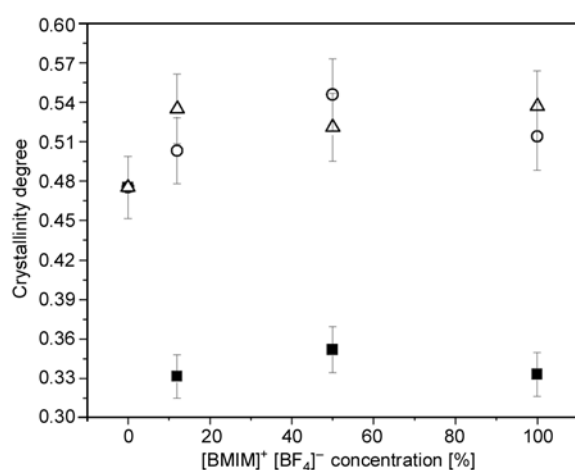

Figure 9. The crystallinity variation of the shrunk and re-swollen PVA cryogels as a function of the initial concentration of the immersion solution: (■) shrunk PVA hydrogels; (○) PVA hydrogels swollen in non-refreshed storage water; (Δ) PVA hydrogels swollen in refreshed storage water

If we consider that the gels density is not significantly affected by the swelling/shrinking processes, and is close to 1 g/cm^3, it could be noted that after PVA gels immersion in the 50% IL solution, the crystallinity of the gel decreased by approximately 30% while the gels volume decreased by 40%. As a consequence, the increase by approximately 7% of the crystallites concentration/ gel's volume unit has to determine the increase of the shrunk gel modulus. The experimental data show that the modulus increased by 40%. These results evidenced that the amorphous part of the hydrogels plays an important role in the alteration of the PVA hydrogel mechanical properties. In this phase, the PVA chains strongly interact by H bondings as a consequence of the bonded water release, participating in the increase of gel's modulus.

The decrease of the modulus in case of the hydrogels immersed in diluted IL solutions could be determined not only by the plasticizing effect of the BMIM$^+$, but also by the possible stronger decrease of the gels crystallinity as compared to its volume decrease.

3.7. Kinetic study of the PVA hydrogels swelling/deswelling

All the above mentioned PVA gel modifications occur during its contact with BMIMBF$_4$ solutions. Generally, the swelling processes of the gels are described from the kinetic point of view by the Peppas equation [28–31] (Equation (2)):

$$\frac{m_t}{m_x} = k \cdot t^n \qquad (2)$$

This equation allows to calculate the exponent n that indicates the water (or other species) diffusion mechanism (Fickian or non-Fickian) and the diffusion constant *k*. This equation is not applicable in our case, due to the complexity of the process and changing gel morphology. If we still try to apply this equation, we get very low n-values, which do not correspond to the diffusion mechanism.

So, in order to characterize from the kinetic point of view the behaviour of PVA hydrogels in contact with BMIMBF$_4$ aqueous solutions we propose a phenomenological equation (Equation (3)) that takes into consideration both fluxes of matters. This equation fits very well the experimental data, for both gel collapse and re-swelling.

$$y(t) = \frac{y_0}{\left(1 + \dfrac{t}{t_0}\right)^p} + y_1 \frac{\left(\dfrac{t}{t_1}\right)^p}{\left(1 + \dfrac{t}{t_1}\right)^p} \tag{3}$$

where $y(t)$ is m_t/m_x, t is time expressed in minutes, the values related to the water flux are represented by index 0 and those of the second flux of IL into the gel by index 1, t_0 and t_1 are the characteristic time for which a significant mass change has been noted due to the water or IL flux, respectively, and p is a power law exponent. R is the correlation coefficient.

y_0 shows the swelling equilibrium of the initial gel that is approximately the same for all the samples.

Higher t_0 values for more concentrated IL solutions pointed out that the water release, monitored in the first moments by the osmotic pressure, is counterbalanced by the IL ions sorption on the surface of the gels, leading to an apparent time lag of mass change, determined by gravimetric methods. The higher IL solution concentration is, the greater apparent time lag is, because of the increased amount of the sorbed IL ions.

The increase of t_1 parameter with the IL solution concentration increase shows the extension of the IL sorption to the higher contact times of the IL solution with the PVA cryogel, diminishing the gel weight loss determined by water release. y_1 parameter represents the value of shrinking equilibrium, showing an increase with the IL solution concentration decrease.
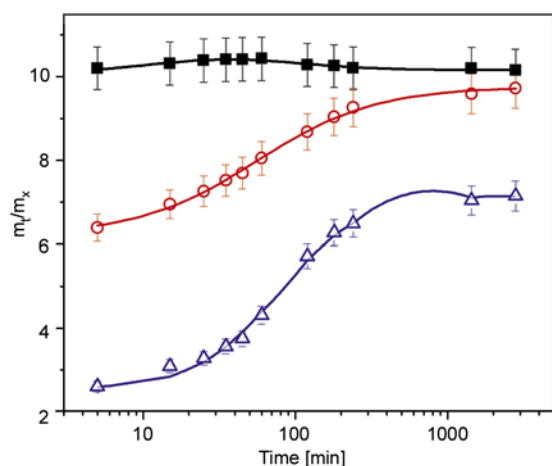

Figure 10. Re-swelling process - variation of the normalized mass of the shrunk PVA hydrogels as a function of time, in distilled water: (■) 12%; (○) 50% and (△) 100%

These simultaneous processes emphasized the complexity of the gel collapse in the presence of ionic liquids. The behaviour (mass change as a function of time) of the shrunk PVA hydrogels when they are in contact with distilled water is illustrated in Figure 10.

Experimental data have been fitted by Equation (1). It can be noted that t_0 or/and t_1 increase means more intense simultaneous processes that determine the lowering of the gel mass changing in the first period of the contact time. The higher the IL solution concentration is, the more compact gel result and the lower diffusion rate of the IL ions is observed. As a consequence, higher 'apparent time lag' on the re-swelling kinetic curve will be emphasized.

y_0 indicates the initial shrinking equilibrium of the gel and y_1 could be correlated to the equilibrium of the gels in the swollen state.

Although this equation is of entirely phenomenological nature, it allows capturing all details of the shrinking and swelling process qualitatively and it allows a quantitative intepretation of the complex processes going on during the uptake and release of IL.

4. Conclusions

The behaviour of PVA cryogels in the presence of [BMIM]$^+$[BF$_4$]$^-$ has been studied using a series of analytical techniques. All of them led to the same conclusions, as follows.

In the presence of [BMIM]$^+$[BF$_4$]$^-$, the swollen PVA cryogels shrink. The higher IL aqueous solution concentration is, the higher shrinking of the PVA gel is. The contact of the PVA gels with lower concentrated IL solutions favored the IL ions sorption. This determines the PVA gels plastisizing, both by their crystallinity decrease and by the dominating chaotropic effect of [BMIM]$^+$.

At higher IL solutions concentration, the strong collapse of the PVA cryogels determines the decrease of the IL's ions sorption. In this case, the dominating effect is that of the kosmotropic [BF$_4$]$^-$ ions. They determine the transformation of the bonded water molecules in free water molecules, making easier the water release from the gel during the heating. Removing of bonded water determines also a higher interaction between the polymeric chains and as consequence the increase of the gel rigidity.

An equation has been proposed to describe the mass change during the collapse/swelling of the hydrogels in contact with IL solutions and distilled water, respectively, along the entire time domain, until equilibrium is attained. This equation takes into account both fluxes of matters in/from the gel: water flux and IL flux. It emphasizes the swelling and collapse equilibria and the apparent time lag of the gel mass modifying as a function of IL solution concentration. Based on the kinetic curve of shrinking, a mechanism of shrinking/swelling process is proposed.

Acknowledgements

References

[1] Peppas N. A., Bures P., Leobandung W., Ichikawa H.: Hydrogels in pharmaceutical formulations. European Journal of Pharmaceutics and Biopharmaceutics, **50**, 27–46 (2000).
DOI: 10.1016/S0939-6411(00)00090-4

[2] Hennink W. E., van Nostrum C. F.: Novel crosslinking methods to design hydrogels. Advanced Drug Delivery Reviews, **54**, 13–36 (2002).
DOI: 10.1016/S0169-409X(01)00240-X

[3] Paţachia S.: Blends based on poly(vinyl alcohol) and the products based on this polymer. in: 'Handbook of polymer blends and composites' (eds.: Vasile C., Kulshreshtha A. K.) Rapra, Shawbury, Vol 4A, 288–365 (2003).

[4] Paţachia S., Rînja M., Friedrich C.: Correlation between poly(vinyl alcohol) cryogel swelling capacity and synthesis parameters. in 'Recent advances in research on biodegradable polymers and sustainable composites' (eds.: Jimenez A., Zaikov G. E.) Nova, New York, Vol 3, 121–134 (2008).

[5] Hassan C. M., Peppas N. A.: Structure and applications of poly(vinyl alcohol) hydrogels produced by conventional crosslinking or by freezing/thawing methods. Advances in Polymer Science, **153**, 37–65 (2000).
DOI: 10.1007/3-540-46414-X_2

[6] Lozinsky V. I., Domotenko L. V., Zumbov A. L., Simenel I. A.: Study of cryostructuration of polymer systems. XII. Poly(vinyl alcohol) cryogels: Influence of low-molecular electrolytes. Journal of Applied Polymer Science, **31**, 1991–1998 (1996).
DOI: 10.1002/(SICI)1097-4628(19960912)61:11<1991::AID-APP13>3.0.CO;2-2

[7] Zhang Y., Cremer P. S.: Interactions between macromolecules and ions: The Hofmeister series. Current Opinion in Chemical Biology, **10**, 658–663 (2006).
DOI: 10.1016/j.cbpa.2006.09.020

[8] Shaheen S. M., Ukai K., Dai L., Yamaura K.: Properties of hydrogels of atactic poly(vinyl alcohol)/NaCl/H_2O system and their application to drug release. Polymer International, **51**, 1390–1397 (2002).
DOI: 10.1002/pi.1061

[9] Paţachia S., Baciu Florea C.: Poly(vinyl alcohol) hydrogels interaction with electrolytes in aqueous solution. Revue Roumaine de Chimie, **52**, 1145–1149 (2007).

[10] Paţachia S., Valente A. J. M., Baciu C.: Effect of non associated electrolytes on the behaviour of poly(vinyl alcohol) based hydrogels. European Polymer Journal, **43**, 460–467 (2007).

[11] Lozinsky V. I., Zubov A. L., Titova E. F.: Swelling behavior of poly(vinyl alcohol) cryogels employed as matrices for cell immobilization. Enzyme and Microbial Technology, **18**, 561–569 (1996).
DOI: 10.1016/0141-0229(95)00148-4

[12] Lozinsky V. I., Plieva F M.: Poly(vinyl alcohol) cryogels employed as matrices for cell immobilization. 3. Overview of recent research and developments. Enzyme and Microbial Technology, **23**, 227–242 (1998).
DOI: 10.1016/S0141-0229(98)00036-2

[13] Paţachia S., Florea C., Friedrich C., Thomann Y.: Tailoring of poly(vinyl alcohol) cryogels properties by salts addition. Express Polymer Letters, **3**, 320–331 (2009).
DOI: 10.3144/expresspolymlett.2009.40

[14] Agrawal S. L., Awadhia A.: DSC and conductivity studies on PVA based proton conducting gel electrolytes. Bulletin of Materials Science, **27**, 523–527 (2004).
DOI: 10.1007/BF02707280

[15] Hashim M. A., Majid S. R., Ibrahim Z. A., Arof A. K.: Electrochemical double layer capacitor based on cellulose-PVA hybrid electrolyte. Ionics, **11**, 464–467 (2005).
DOI: 10.1007/BF02430268

[16] Rajendran S., Mahendran O.: Experimental investigations on plasticized PMMA/PVA polymer blend electrolytes. Ionics, **7**, 463–468 (2001).
DOI: 10.1007/BF02373585

[17] Yang C. C., Lin S. J.: Preparation of alkaline PVA-based polymer electrolytes for Ni-MH and Zn-air batteries. Journal of Applied Electrochemistry, **33**, 777–784 (2003).
DOI: 10.1023/A:1025514620869

[18] Lu J., Yan F., Texter J.: Advanced applications of ionic liquids in polymer science. Progress in Polymer Science, **34**, 431–448 (2009).
DOI: 10.1016/j.progpolymsci.2008.12.001

[19] Mansur H. S., Sadahira C. M., Souza A., Mansur A. A. P.: FTIR spectroscopy characterization of poly (vinyl alcohol) hydrogel with different hydrolysis degree and chemically crosslinked with glutaraldehyde. Material Science and Engineering C: Biomimetic and Supramolecular Systems, **28**, 539–548 (2008).
DOI: 10.1016/j.msec.2007.10.088

[20] Liu W., Zhao T., Zhang Y., Wang H., Yu M.: The physical properties of aqueous solutions of the ionic liquid [BMIM][BF$_4$]. Journal of Solution Chemistry, **35**, 1337–1346 (2006).
DOI: 10.1007/s10953-006-9064-7

[21] Paţachia S., Croitoru C., Friedrich C.: Computational study of 1-butyl-3-methylimidazolium tetrafluoroborate ionic liquid–water system. in 'Recent Advances in Mathematical and Computational Methods in Science and Engineering. (MACMESE'08) Bucharest, Romania' PART II, 469–472 (2008).

[22] Danten Y., Cabaçao M. I., Besnard M.: Interaction of water highly diluted in 1-alkyl-3-methyl imidazolium ionic liquids with the PF$_6^-$ and BF$_4^-$ anions. Journal of Physical Chemistry A, **113**, 2873–2889 (2009).
DOI: 10.1021/jp8108368

[23] Zhao H.: Are ionic liquids kosmotropic or chaotropic? An evaluation of available thermodynamic parameters for quantifying the ion kosmotropicity of ionic liquids. Journal of Chemical Technology and Biotechnology, **81**, 877–891 (2006).
DOI: 10.1002/jctb.1628

[24] Spinks G. M., Lee C. K., Wallance G. G., Kim S. I., Kim S. J.: Swelling behavior of chitosan hydrogels in ionic liquid−water binary systems. Langmuir, **22**, 9375–9379 (2006).
DOI: 10.1021/la061586r

[25] Rogers R. D., Seddon K. R., Volkov S.: Green industrial applications of ionic liquids. Kluwer, Dordrecht (2003).

[26] Bridges N. J., Gutowski K. E., Rogers R. D.: Investigation of aqueous biphasic systems formed from solutions of chaotropic salts with kosmotropic salts (salt-salt ABS). Green Chemistry, **9**, 77–183 (2007).

[27] Martens C. F., Schenning A. P. H. J., Feiters M. C., Heck J., Beurskens G., Beurskens P. T., Steinwender E., Nolte R. J. M.: Structure determination, spectroscopic characterization, and magnetic properties of a novel dinuclear copper(II) crown ether bipyridine complex. Inorganic Chemistry, **32**, 3029–3033 (1993).
DOI: 10.1021/ic00066a012

[28] Bashir A., Bashir S., Nisa S-U., Huglin M. B.: Chemically crosslinked N-vinyl-2-pyrrolidone/2-hydroxyethyl methacrylate (VP/HEMA) Copolymer for the controlled release of cyclic oligopeptide. Turkish Journal of Chemistry, **28**, 279–285 (2004).

[29] Peppas N. A., Khare A. R.: Preparation, structure and diffusional behavior of hydrogels in controlled release. Advance Drug Delivery Reviews, **11**, 1–35 (1993).
DOI: 10.1016/0169-409X(93)90025-Y

[30] Kim B., La Flamme K., Peppas N. A.: Dynamic swelling behavior of pH-sensitive anionic hydrogels used for protein delivery. Journal of Applied Polymer Science, **89**, 1606–1613 (2003).
DOI: 10.1002/app.12337

[31] Ji S., Ding J.: The wetting process of a dry polymeric hydrogel. Polymer Journal, **34**, 267–270 (2002).
DOI: 10.1295/polymj.34.267

[32] Shi J., Guo Z-X., Zhan B., Luo H., Li Y., Zhu D.: Actuator based on MWNT/PVA hydrogels. Journal of Physical Chemistry B, **109**, 14789–14791 (2005).
DOI: 10.1021/jp052677k

[33] Murali Mohan Y., Keshava Murthy P. S., Sreeramulu J., Mohana Raju K.: Swelling behavior of semi-interpenetrating polymer network hydrogels composed of poly(vinyl alcohol) and poly(acrylamide-co-sodium methacrylate). Journal of Applied Polymer Science, **98**, 302–314 (2005).
DOI: 10.1002/app.21849

[34] Sambasivudu K., John P. S., Keshava Murthy P. S., Mani Y., Murali Mohan Y., Sreeramulu J., Mohana Raju K.: Poly(vinyl alcohol) based pH responsive semi-IPN hydrogels: A comparative swelling investigation. International Journal of Polymeric Materials, **56**, 1099–1111 (2007).
DOI: 10.1080/00914030701283030